The University Of Sheffield.

Department of Animal and Plant Sciences

"Quantitative resistance to clubroot in Brassica crops"

Sarah Sommer

A thesis submitted in partial fulfilment of the requirements for the degree of
Doctor of Philosophy

September 2018

ABSTRACT

Clubroot is a plant disease caused by the eukaryotic biotrophic pathogen *Plasmodiophora brassicae* in vegetables and crop plants within the *Brassicaceae* family. Infected plants develop large galls in the root system while the aerial plant body is dwarfed and stressed (e.g. wilting, chlorosis, premature senescence). Symptoms result from changes of the host's primary and secondary metabolism, alterations in host stem cell maintenance and differentiation, and perturbations of vascular development. Clubroot disease is a worldwide problem and cannot be controlled effectively. Existing resistance is monogenic, unstable due to the genetic variability of the pathogen, and has already been broken down in the field. This project aims to identify robust, quantitative measures of disease development that could be exploited in breeding programmes to develop plants with durable, polygenic quantitative resistance to clubroot infection. It utilised a panel of Brassica plants (ASSYST panel) that represent the majority of genetic diversity in current Brassica crops. Initial experiments indicated that changes in above-ground plant development might act as a non-invasive measure of below-ground disease development. A large-scale phenomics screen was initiated but was unsuccessful as variation in environmental conditions within the phenomics facility resulted in highly variable symptom development. Smaller scale screens were then used to examine alternative approaches. A combination of above and below-ground biomass measurements, coupled with qRT-PCR assays of pathogen content, provided precise measurements of disease development. Of particular note was the observation that plants with visually similar gall development varied markedly in pathogen development and root-shoot ratio, indicating the presence of multiple underlying mechanisms. Metabolomics methods were also used to identify metabolic signatures of disease development in leaves and roots of susceptible and resistant cultivars. Together, these approaches have the potential to act as non-destructive measures of disease development for use in clubroot resistance breeding programmes.

Table of Contents

ACKNOWLEDGEMENTS

CHAPTER 1: GENERAL INTRODUCTION

1.1. CHALLENGES OF MODERN AGRICULTURE

In a world with a steadily-growing population, today's challenge is food and energy sustainability with limited available areas for agricultural expansion, and productivity-inhibiting biotic and abiotic factors [1][2]. Biotic factors include plant damage through parasitic weeds, plant/leaf consumption by herbivores/folivore (i.e. invertebrates, mammals, birds), or plant diseases caused by pathogenic microorganisms. Abiotic factors include drought, salinity, nutrient scarcity, extreme temperatures, or high/low irradiance. Both biotic and abiotic factors reduce productivity due to smaller yields (quantitative loss) or reduction in market quality because of aesthetics (e.g. pigmentation) or toxic contamination (e.g. mycotoxin) (qualitative loss) [1]. Estimates of crop losses range between 25-30% [3]. Pre-harvest crop protection schemes (e.g. soil management, crop rotation, chemical treatment) and marker-assisted breeding of high-yielding cultivars that are resistant or tolerant to biotic and abiotic stresses, and adapted to various climate and soil conditions [2], are the two main options for preventing crop loss.

Marker-assisted breeding requires information about the approximate location of genes that confer resistance. Information thereof can be acquired through resistance screens using a whole population of different genotypes. However, regardless of the design of resistance screens, the basics of resistance frequently lie within the plant immune system.

1.2. THE PLANT IMMUNE SYSTEM

1.2.1. THE ZIG-ZAG MODEL – CO-EVOLUTION OF AVIRULENCE AND RESISTANCE GENES

Plants have evolved mechanisms to defend themselves against attacks by microbial pathogens, herbivores, and pests. Some defence mechanisms are constitutively present, such as mechanical barriers (i.e. thorns or wax) or chemical compounds with antimicrobial activity (i.e. phytoanticipin) [4]. However, some plant defence mechanisms are activated only after perception of an attacker. These inducible defence mechanisms are coordinated by the innate immune system, which works as two-branched system. The first branch responds to pathogen-specific compounds, termed pathogen-associated molecular patterns (PAMPs). PAMPS are recognised by the host's transmembrane pattern recognition receptors (PRRs), which induce PAMP-triggered immunity (PTI). In most cases PTI prevents pathogen invasion, for example through cell alkalisation via Ca^{2+} influx or ROS production. It is therefore known as non-host or basal resistance. The second branch of the immune system responds to pathogen virulence factors (effectors). They are recognised within the cell by polymorphic nucleotide binding-leucine rich repeat (NB-LRR) proteins, and elicit effector-triggered immunity (ETI), which often

includes the hypersensitive response (HR). Recognition of effectors can be direct or indirect. If pathogen effectors are not recognised by the plant's NB-LRR proteins, they induce effector-triggered susceptibility (ETS). Effectors and NB-LRR proteins are products of a constant arms race between pathogen and plant. Effectors evolved in some pathogen strains to overcome PTI, and NB-LRR proteins co-evolved in plants to counteract effectors. The underlying genes are avirulence (Avr) genes in pathogens, and disease resistance (R) genes in plants. One R gene only confers resistance against a pathogen strain that contains the "matching" Avr gene. The relationship between an R gene and a corresponding Avr gene is known as gene-for-gene resistance, but only works for biotrophic pathogens. The arms race is still on-going, and described by the "zig-zag model" [5] (figure 1.1).
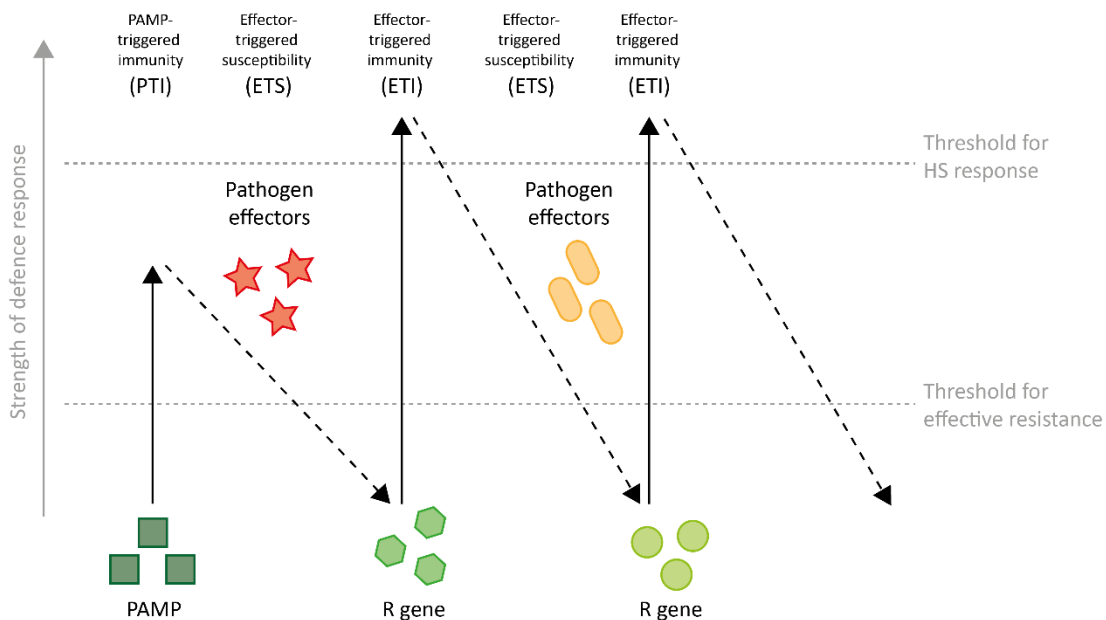
Figure 1.1: Zig-Zag-model of the co-evolution between plants and biotrophic pathogens (see main text for details, figure re-created after [5])

1.2.2. DEFENCE SIGNALLING

Induction of defence responses is mediated by a complex, interconnected hormone signalling network, consisting mainly of salicylic acid (SA), jasmonic acid (JA), and ethylene (ET), but also abscicic acid (ABA), auxin (IAA), gibberellic acid (GA), cytokinin (CK), brassinosteroids (BR), and peptide hormones. However, involvement of IAA, GA, CK, BR, and peptide hormones in defence signalling is less well understood [6].

Cross-talk between SA and JA/ET

Pathogens can be classified broadly as either necrotrophic or biotrophic intruders. The former kills the host, and obtains its nutrients. The latter keeps the host alive whilst securing host nutrient supply. Depending on the type of microbial intruder, there are different combinations of hormones that induce defence responses (figure 1.2). JA and ET are important for the defence against necrotrophic pathogens, and operate synergistically. In contrast, SA plays a crucial role in defence responses against biotrophic pathogens, but also during the establishment of systemic acquired resistance (SAR). Therefore, JA/ET and SA mediated defence pathways are generally antagonistic, and rely on negative cross-talk to coordinate responses against multiple attackers [5][6]. Interestingly, microbial pathogens not only evolved effectors to overcome host-defence, but also the ability to manipulate the defence-related signalling network of the plant by producing hormone-mimics [6].
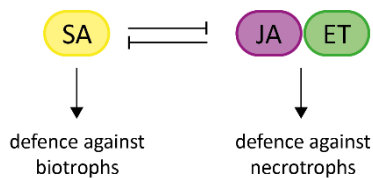
Figure 1.2: Simplified cross-talk between SA and JA/ET during attack of biotrophic and necrotrophic pathogens.

SA = Salicylic acid, JA = Jasmonic acid, ET = Ethylene

1.2.3. QUALITATIVE AND QUANTITATIVE RESISTANCE

Plant disease resistance contains a phenotypic and genetic aspect, each divided into qualitative and quantitative resistance. The phenotypic aspect refers to how successfully pathogen reproduction was inhibited (i.e. partial or impeded reproduction), and the genetic aspect to gene numbers and effect thereof (i.e. monogenic with a major gene or polygenic with minor genes). This results in 4 categories as seen in table 1.1. Therefore, qualitative resistance summarises phenotypically complete resistance that is based on one gene with major effect on plant defence. In contrast, quantitative resistance is defined as phenotypically incomplete resistance that is based on the joined effect of several genes with minor effects, each contributing quantitatively to plant defence [7].

Table 1.1: Four categories of resistance

	Genetically qualitative	Genetically quantitative
Phenotypically qualitative	Complete resistance [monogenic, major gene]	Complete resistance [polygenic, minor genes]
Phenotypically quantitative	Incomplete resistance [monogenic, major gene]	Incomplete resistance [polygenic, minor genes]

1.3. THE *BRASSICACEAE* FAMILY & THE IMPORTANCE OF BRASSICA CROPS

The *Brassicaceae* family is one of the biggest families of the Angiosperms. It contains the genus *Brassica* with the agriculturally important species *Brassica napus* (i.e. oilseed rape, or swede), *Brassica oleracea* (i.e. kale, broccoli, cauliflower, Brussels sprout, cabbage, or kohlrabi) and *Brassica rapa* (i.e. Chinese cabbage, or turnip). As Brassica crops produce food and oil, they are widely cultivated to address the challenges of food and energy sustainability as a consequence of a steadily growing world population and climate change. However, the *Brassicaceae* family is susceptible to many plant diseases, for example leaf spot, powdery mildew, downy mildew, black leg, or clubroot. The latter is the most devastating disease in Brassica crops [8].

1.4. CLUBROOT DISEASE

Clubroot infection is a universal problem, and assessed as the main contributor to disease-induced Brassica crop loss. It is found in more than 60 countries (mild, temperate, and moist regions) with yield losses typically between 10-15%. Clubroot disease is caused by the eukaryotic obligate biotrophic pathogen *Plasmodiophora brassicae* (*P. brassicae*), a member of the super-group Rhizaria within the Protista kingdom [9][10]. Due to genetic variability, numerous strains with different pathogenicity (pathotypes) can be found globally [3]. Infection occurs in all members of the *Brassicaceae* family. This includes the genera *Brassica*, but also *Raphanus*, and *Arabidopsis* [8].

1.4.1. DISEASE SYMPTOMS – SUSCEPTIBILITY AND PATHOGENICITY

Clubroot infected plants show typical above- and below-ground disease symptoms. Those increase with disease severity, and lead to death in the most severe cases. Infected plants develop large galls in the root system as a consequence of extensive cell divisions (hyperplasia) and expansion (hypertrophy), whilst above-ground symptoms include wilting, stunting, chlorosis, and premature senescence. Occasionally, early flowering is initiated, and physical instability might occur. Agriculturally, this means loss in yield, seed number and seed/oil quality [11]. Symptoms result from changes in the host's primary and secondary metabolism, alterations in host stem cell maintenance and differentiation, and perturbations of vascular development with reduction in xylogenesis [12]. Clubroot disease symptoms depend on host resistance and the pathogenicity of P. *brassicae*. Symptoms are either time-shifted or differ in intensities. The fact that it is not uncommon to find different pathotypes on a field, or even within the same plant gall [13], adds more complexity to disease symptoms. The variation in host responses to different clubroot pathotypes is exploited by the European Clubroot Differential (ECD) classification system. The ECD is an internationally accepted system for classification of clubroot pathotypes to enable comparisons of research results [3]. It is based on the relative susceptibility of a definite number of plant genotypes, each of *Brassica rapa*, *Brassica napus*, and *Brassica oleracea*. Many pathotypes are represented by an ECD triplet code (i.e. ECD 16/2/12).

1.4.2. LIFE CYCLE OF P. BRASSICAE – PRIMARY AND SECONDARY INFECTION

The generally accepted life history of *P. brassicae* describes a two phase life cycle [14][15]. The life cycle consist of a primary root hair phase (= primary infection) and a secondary cortical phase (= secondary infection) as reviewed in [16][17] (figure 1.3). Throughout the whole pathogen life cycle various different appearances of *P. brassicae* can be observed, starting and terminating the life cycle as a resting spore in the soil. The resting spores have a half-life time of 3.6 years, and are not detectable after 17.3 years [18].

Resting spores differ in age, and can be roughly categorized into young and mature spores. All are haploid. Spores are 2.8 - 3.8 µm in diameter, and sub-spherical to spherical shaped [16]. The surface of young spores is covered with fibrous material, while mature spores have spines [17]. Germination, which marks the first step in the life cycle, depends on the maturation level. Mature spores have a higher germinability compared to young spores [19]. Young spore germination is triggered by release of calcium ions. Mature spores require environmental and biological factors instead, such as pH, humidity, temperature, and other inorganic ions. Resting spore germination is enhanced at 24°C, and between pH 6.0 and pH 7.0 [8][17][20]. Different studies suggest plant root exudates of hosts (i.e. oilseed rape), non-cruciferous hosts (i.e. *lolium*/ryegrass), and non-host plants (i.e. wheat) to function as additional trigger for resting spore germination. However, due to various experimental conditions (laboratory or field/greenhouse) contradictory results occurred. Results of field experiments were inconsistent, and only a minimal effect of root exudates on spore germinability was observed [21]. Under controlled laboratory conditions root exudates from hosts and non-cruciferous host increased germination rates [22][23][24]. Suzuki et al [19] identified a chemical element within some root exudates of Crucifers and non-Crucifers, that functions as a putative germination-stimulating factor (GSF). However, it was suggested not to be related to clubroot susceptibility since it was also found in clubroot resistant cultivars. On the *P. brassicae* genome, a single-copy gene (*Pro1*) was found with upregulated gene expression during spore germination. It encodes a serine protease which stimulates the germination of the resting spore through proteolytic activity. The enzyme exhibits high activity at 25°C and pH 6.0 - 6.4 (lowest activity at pH 7.6 - 8.0) [25], which correlates with optimal field conditions for clubroot infection [8]. It is therefore believed to play a role in pathogenicity.

During the germination of resting spores, short-living primary zoospores are released in the soil. They are 2.8 - 5.9 µm in diameter, and spindle- or pyriform-shaped with 2 flagella (biflagellate) of unequal length and shape. The short flagellum has a blunt end, while the long flagellum ends with a whiplash or tail piece [16]. At the root hair, these primary zoospores encyst. During the process, the flagella gets absorbed, the body rounds up, and a tube-shaped structure develops

6

(Rohr) containing a sharply pointed projectile-like rod (Stachel). With this Stachel, the primary zoospore can attach to the host's cell wall, and inject its protoplasm (i.e. ribosomes, lipids, mitochondria, and vesicles) into the cell [26][3]. The injection is physical without enzyme involvement, and termed primary clubroot infection.

Within the cytoplasm of root hairs, primary zoospores appear as small spherical amoeba, which develop to primary multinucleate plasmodia. Through synchronous cruciform nuclear divisions and cleaving, zoosporangia are produced and form clusters. Zoosporangia contain secondary zoospores [26]. Each zoosporangium can release between 4 and 16 secondary zoospores both into the rhizosphere via exit pores or at the base of the root hair lumen [16][14].

In the rhizosphere they can re-infect healthy root hairs and epidermal cells [27]. Secondary zoospores develop into secondary binucleate plasmodia (myxamoeba), which then actively move between host cells and invade cortical cells [28]. This is termed secondary infection. In cortical cells, a sequence of nuclear divisions, cleavage, and meiosis occur during which secondary binucleate plasmodia turn into secondary multinucleate plasmodia, and thereafter into numerous resting spores [14][26]. Sexual recombination of *P. brassicae* was discussed as reason for its genetic variability, but could not be detected through restriction fragment length polymorphism, and electrophoretic karyotyping using a mix of 2 single-spore isolates. However, chromosomal re-arrangement was indicated [29]. Resting spores are released into the soil as soon as the root tissue disintegrates.

Several studies have been conducted to study the range of host plants. Thereby, primary clubroot infection was found in other plant families, such as *Papaveraceae* (poppy family), *Rosaceae* (rose family), and *Poaceae* (true grasses) [8][20][30][31]. Further studies revealed secondary infection of non-cruciferous plants without gall formation [32][33]. Secondary zoospores [33] and resting spores [32] could be extracted with the capability to infect Brassica cultivars - gall formation was observed. It is therefore assumed that *P. brassicae* uses primary infection as strategy for survival in case it fails to overcome plant defence. Furthermore, *P. brassicae* could proliferate through repetitive cycles in root hairs prior to secondary infection to increase the chance of successful cortical invasion.

For life cycle completion, *P. brassicae* depends on host nutrients, such as carbohydrates, amino acids, and lipids. The supply of those host resources is induced by a plethora of physiological and molecular changes. The former includes rearrangement of the root vasculature to transform the root into a strong sink. The latter summarises gradual changes in primary and secondary host metabolism, and alterations in hormone homeostasis mediating the plant's metabolism (= growth and defence).
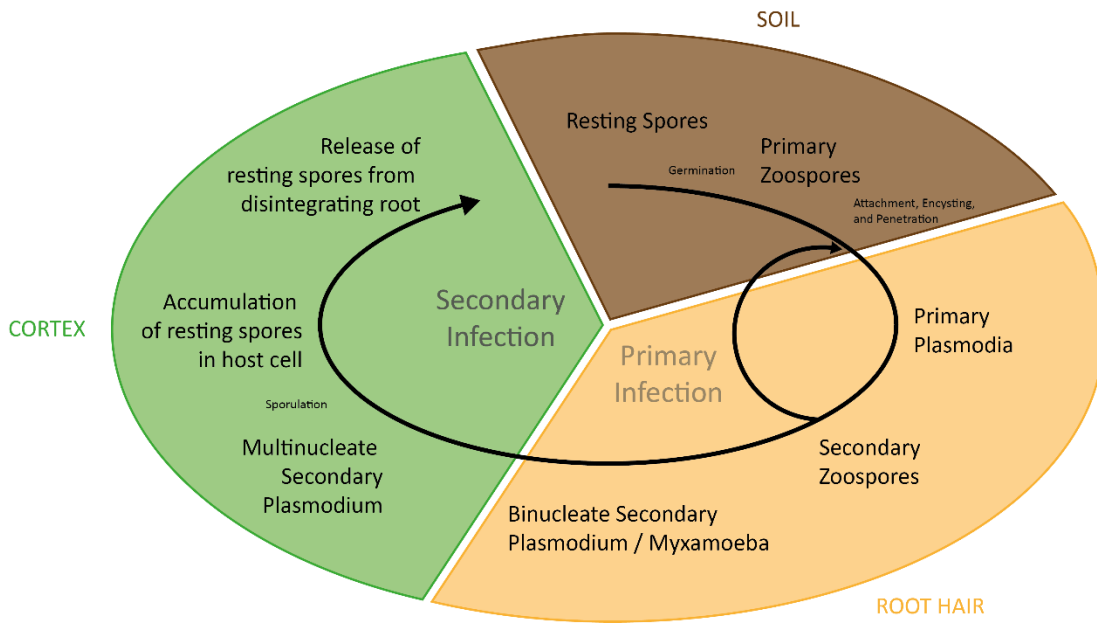
Figure 1.3: Life-cycle of *P. brassicae* in a Brassica host plant

(see main text for details)

1.4.3. METABOLIC HOST-PATHOGEN INTERACTION: AUXIN AND INDOLE-GLUCOSINOLATES

Auxin is a crucial phytohormone throughout the life cycle of plants since it coordinates many developmental and growth processes, including cell division and expansion. The most important active member of the auxin family is indole-3-acetic acid (IAA). IAA is present in all parts of the plant, but in different concentrations. The concentration of IAA is the key to orchestrate growth-related processes, and each concentration signals different developmental information. Therefore, IAA biosynthesis, metabolism, transport, and signalling are tightly regulated [34][35].

Clubroot infection alters IAA homeostasis. Researchers found elevated IAA concentrations in clubroot infected root tissue compared to their controls. Initially, *P. brassicae* was suspected to synthesise IAA, but the idea was discarded due to a lack of evidence [36][32][37]. Therefore, subsequent investigations focussed on IAA regulation in host plants, and manipulation thereof.

IAA biosynthesis and connection to indolic-glucosinolates

IAA biosynthesis is either Trp-dependent or Trp-independent. The latter is important during normal plant growth and utilizes a Trp-precursor (i.e. indole). The former is assumed to be stress-induced when more IAA is needed [35]. Three interconnected pathways for Trp-dependent IAA biosynthesis in plants are widely accepted [34][38]: IAOx, IPA, and IAM. The former is largely restricted to the *Brassicaceae* family. All pathways are displayed in figure 1.4 A with information about abbreviations.

Pathways containing the intermediate IAOx are interconnected to the synthesis of indolic-glucosinolates (indolic-GLSs). Indolic-GLSs belong to a group of secondary metabolites termed glucosinolates (GLSs). GLSs derive from glucose and a modified amino acid. They contain sulphur and nitrogen. Biochemically, there are 3 different types of GLSs depending on which amino acid-derivate (8 in total) was used for synthesis: aliphatic- (Ala, Leu, Ile, Met, or Val), aromatic- (Phe or Tyr), and the above mentioned indolic-GLSs (Trp). Hydrolysis products of GLSs are diverse. Some are toxic (i.e. thiocyanate, isothiocyanate), and play a role in pathogen defence mechanisms. Others, such as indole-3-methyl glucosinolates, are involved in IAA synthesis. The responsible enzyme is myrosinase (figure 1.4). Usually, it is spatially separated from GLSs, but released upon cell damage [39].

Studies on clubroot disease found increased amounts of IAOx, IAN, and indole-3-methyl glucosinolates in *A. thaliana* [37], upregulated myrosinase and nitrilase activity in *A. thaliana* and *B. rapa* [40][41][42], and increased transcript levels for nitrilase during gall formation in *A. thaliana* [43]. Therefore, it was assumed that indolic-GLSs were responsible for elevated concentrations of IAA in galls. However, experiments with *A. thaliana* mutant lines refuted the

hypothesis. A double mutant in the enzyme cytochrome P450 (CYP79B2 and CYP79B3) showed no differences in gall formation [44], and nitrilase mutant lines (*NIT*-genes) only showed clubroot tolerance (*nit1*) or delayed gall development (*nit2*), but no clubroot resistant phenotype [43].

IAA inactivation

IAA can be stored as indole-3-acetic acid (IBA) or IAA-conjugates. The latter encompasses IAA ester-linked to sugars or IAA amide-linked to amino acids or peptides. Both types of conjugates are also involved in transport, protection, and excess IAA detoxification/ degradation. Synthesis of IAA-conjugates is performed by auxin amino acid conjugate synthetases, which belong to the GH3 family, in particular GH3.5 [45]. However, it is a reversible process, and conducted upon peroxisomal β-oxidation for IBA, and hydrolyses for IAA conjugates [35].

During late stages of clubroot infection, a strong increase of IAA-conjugates was observed in *B. rapa* [46], and studies on *A. thaliana* revealed upregulated genes that encode enzymes for IAA conjugation (i.e. GH3.5) [47]. The latter was interpreted as the plants attempt to control disease symptoms [48]. In 2016, it was postulated that *P. brassicae* might contain a protein with strong homology to an indole-3-acetic acid synthetase being able to conjugate IAA [49].

IAA-transport and modulation through flavonoids

Most plant cells can synthesise IAA. However transport of IAA-conjugates to distant sites of the plant body is required for normal development. There is long distance transport through the vasculature based on mass-flow, and short distance transport. IAA is transported from cell to cell via auxin influx (*AUX*) and efflux (*PIN*) carrier, which are located in specific pattern. This facilitates directional and polar transport of IAA, but also allows the plant to control IAA concentrations in cells [35]. Flavonoids have been shown to alter IAA transport activity by modulating PIN proteins. They are a large group of secondary metabolites with diverse functions (i.e. UV protection, plant defence, and plant-microbe interactions), and are synthesised via the phenylpropanoid pathway [50]. Studies on clubroot in *A. thaliana* revealed the importance of flavonoids as PIN modulators during gall formation. Investigations showed accumulation of 3 flavonoids and their glycosides in galls (naringenin, quercetin, and kaempferol), upregulated transcripts of genes involved in flavonoid synthesis (i.e. chalcone synthase and isomerase during early and late stages), and mild clubroot tolerance in mutant lines with deficiencies in flavonoid synthesis [51].

IAA signalling

IAA signalling is initiated by the co-receptor TIR1/AFB (transport inhibitor response 1/ auxin signalling F-box protein) upon the perception of auxin. TIR1/AFB is localised in the nucleus, where the transcription of auxin-responsive genes is negatively controlled by the repressor Aux/IAA (Auxin/Indole-3-acetic acid). With low auxin levels, it blocks ARFs (auxin response factors) together with the co-repressor TPL (TOPLESS), and therefore inhibits transcription of auxin-responsive genes. However, upon perception of auxin, the co-receptors TIR1/AFB interact with the repressor Aux/IAA. They form an E3 ubiquitin ligase SCF$^{TIR1/AFB}$ complex designated for degradation via the ubiquitin/26S proteasome pathway. This allows ARF activation. In their role as transcription factors, they bind to the promotor through AuxREs (Auxin response elements), and initiate the transcription of auxin-responsive genes (figure 1.4 B). Amongst those auxin-responsive genes are modulators for auxin homeostasis, for example Aux/IAA and the GH3 family (= negative feedback loop) [52][53]. GH3 proteins can conjugate IAA (i.e. auxin amino acid conjugate synthetases), but also respond to biotic (i.e. plant-pathogen interactions) and abiotic stress [45][54]. For example, the enzyme GH3.5 also conjugates SA, which leads to SA inactivation. GH3.5 is also involved in the synthesis of the phytoalexin camalexin [55].

Microarray data obtained from clubroot infected *A. thaliana*, revealed upregulation of TIR1 and AFB1 transcripts, alongside enzymes of the GH3 family (i.e. GH3.5) [47]. Differential expression of enzymes belonging to the GH3 family could give insights on host defence and manipulation thereof. Thereby, upregulated GH3.5 might explain the accumulation of both camalexin and inactive IAA-conjugates. The former was discarded as contributing factor for clubroot disease development in a different study, the latter might be the plant's attempt of detoxification [48].
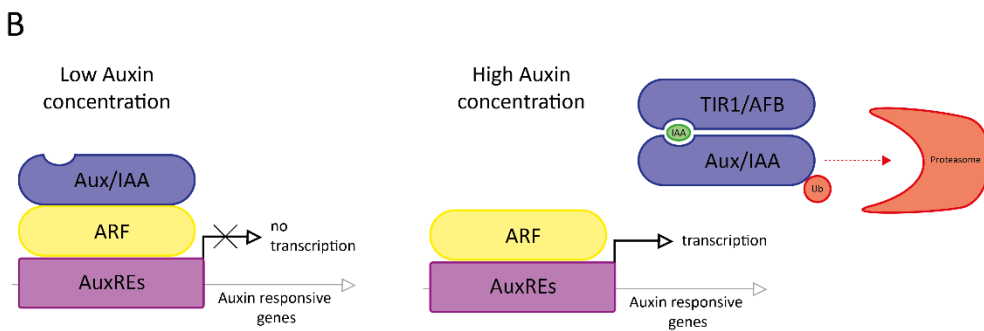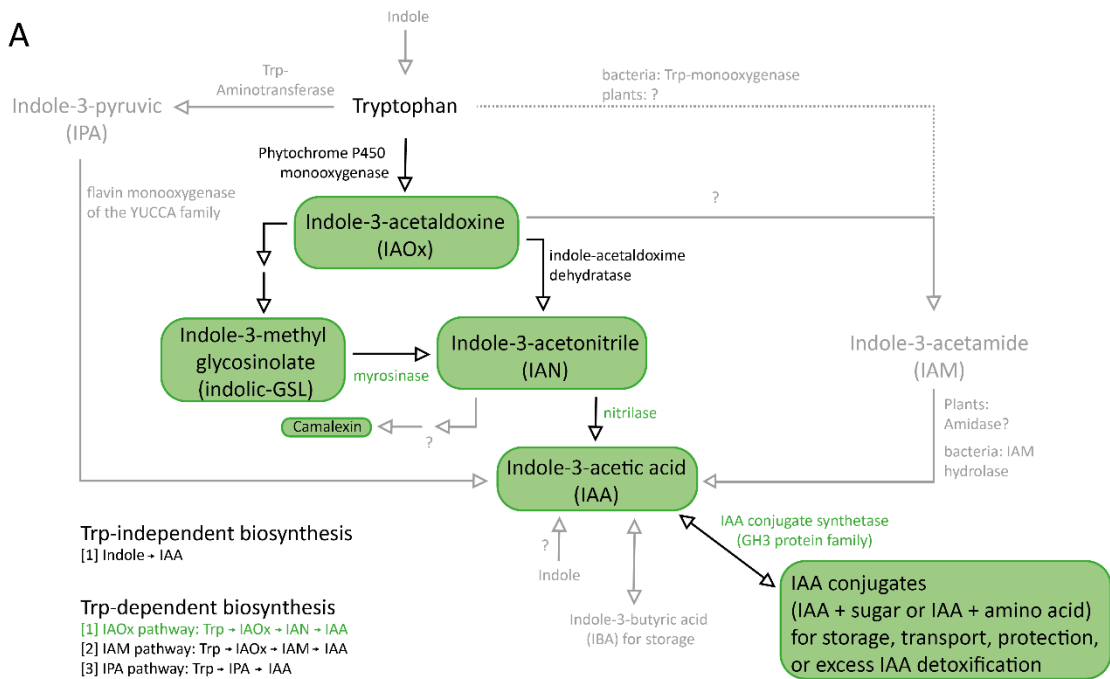
Figure 1.4: IAA biosynthesis and signalling in plants

|A| Trp-dependent and Trp-independent biosynthesis of IAA in plants. Solid black arrows indicate *Brassicaceae*-specific IAA synthesis of IAA, while solid grey arrows show IAA pathways also found in other plants. Question marks highlight that underlying enzymes are unknown or known to be in bacteria (dashed line), but assumed to be present in plants since intermediates of biochemical reactions have been found. IAA-intermediates, enzymes, and secondary metabolites in green are found in higher concentrations during clubroot infection (information from [37][38]) |B| Simplified IAA signalling in plants (see main text for details)

1.4.4. METABOLIC HOST-PATHOGEN INTERACTION: CYTOKININ

Cytokinin (CK) is a crucial signalling molecule since it affects many developmental and growth processes, including cell division (mitosis), shoot growth, leaf senescence (delay thereof), and nutrient movement by creating a new sink-source relationship. It is also important for plant-pathogen interactions [56].

CK-biosynthesis in A. thaliana

Cytokinin is synthesised in root tips and then transported to the aerial plant body. Naturally occurring cytokinins derive from the nucleotide adenine and contain a distinct substitute at the N^6-position of the adenine ring. The most abundant cytokinin in *A. thaliana* is zeatin. It contains an isoprenoid side chains, and exists as *trans*-zeatin (tZ) and *cis*-zeatin (cZ). The former is the active form, the latter shows only limited activity. Other forms of zeatin are zeatin-riboside (ribose attached to N^9-position of zeatin) and zeatin-ribotide (ribose with phosphate-group attached to N^9-position of zeatin). Biosynthesis of both *trans-* and *cis*-zeatin occurs through plastidic MEP (methylerythritol phosphate) and cytosolic MVA (mevalonate) pathways. The former pathway is mostly used in *A. thaliana*. Product of both pathways is the isoprenoid precursor DMAPP (dimethylallyl pyrophosphate). For the synthesis of *trans*-zeatin, DMAPP is first enzymatically converted to iPRTP (isopentenyladenosine-5'-triphosphate), iPRDP (isopentenyladenosine-5'-diphosphate), or iPRMP (isopentenyladenosine-5'-monophosphate) using ATP, ADP or AMP. The conversion is mediated by isopentenyltransferases (*IPT*-genes). Subsequently, iPRTP and iPRDP are hydroxylated to the ribotides tZRTP (*trans*-zeatin-riboside triphosphate), and tZRDP (*trans*-zeatin-riboside diphosphate) through cytokinin trans-hydroxylase (CYP735A). iPRMP can either be converted to tZRMP (*trans*-zeatin-riboside monophosphate) through the same enzyme, or to the cytokinin iP (isopentenyl-adenine). The conversion of tZRTP, tZRDP, and tZRMP to *trans*-zeatin is catalysed by LOG-enzymes (LONELY GUY) [57]. Synthesis of *cis*-zeatin occurs through the use of tRNA as alternative adenine donor, and is mediated by the enzyme tRNA-IPT (figure 1.5 A).

CK-storage in plants

The concentrations of active zeatin-isomers is controlled through irreversible cleavage (i.e. cytokinin oxidase/ dehydrogenase), or through conjugation to glucose (i.e. glucosyltransferase). Thereby, conjugation can be conducted as irreversible N-glycosylation (i.e. N-glycosylzeatin) or reversible O-glycosylation (i.e. O-glycosylzeatin). O-glycosylzeatin is used for storage, and can be converted back via β-glucosidase activity [56][57] (figure 1.5 A).

CK-signalling in plants

Cytokinin signal transduction in plants uses a multistep phosphorelay pathway, which is a more complex version of prokaryotic two-component response systems. It involves receptors, phosphotransfer proteins, and response regulators. Cytokinin is perceived via an ER-membrane-bound hybrid histidine sensor kinase receptor (*AHK* gene family). The receptor consists of an extracellular input domain, a transmembrane transmitter domain, and an intracellular receiver domain, allowing signal input and output. Perception of cytokinin activates auto-phosphorylation of the kinase, which is then transferred to histidine-containing phosphotransfer proteins (*AHP* gene family). AHP-proteins shuttle between cytoplasm and nucleus. In the nucleus, they transfer phosphate to Type A and B response regulators of the *ARR* gene family. The latter consist of a receiver and output domain, and positively regulate transcription of many target genes. The former are responsible for feedback-regulation, and inhibit CK signalling [57] (figure 1.5 B).

CK-biosynthesis by P. brassicae

Clubroot studies hypothesised that *P. brassicae* synthesises cytokinin which is then released into the host cytoplasm to trigger cell division [58]. Further studies postulated that *P. brassicae* requires CK for its development [59]. Studies showed elevated cytokinin levels in Chinese cabbage (not distinguished between isomers) [59] and *A. thaliana* (zeatin and iP) [60] during early stages of infection, and decreased concentrations of cytokinin in Chinese cabbage [59] alongside decreased expression of the host cytokinin oxidase gene [61] and type-A ARRs during late infection stages [12]. Recent sequence completion of the *P. brassicae* genome [49][62], revealed the capacity of CK biosynthesis (i.e. isopentenyl-diphosphate-delta-isomerase), and found two IPT-related gene copies (*PbIPT* and *PbIPT2*) encoding isopentenyltransferases [49][62]. RNAseq data from clubroot-infected *A. thaliana*, showed expression of pathogen *IPT*-genes alongside strong downregulation of host genes involved in CK biosynthesis at the onset and late stages of gall formation. The only host upregulated genes were O-glycosyl-transferases [12] (figure 1.5 C). Subsequent *A. thaliana* mutant analysis (*ipt1, 3, 5, 7*) confirmed impeded development by plasmodia when host CK synthesis is strongly inhibited (e.g. delayed resting spore formation). However, it also showed that pathogen CK has only little impact on host plants. A wildtype-like expression of cytokinin responsive genes was observed in the clubroot infected quadruple mutant, but the phenotype could not be restored [12].
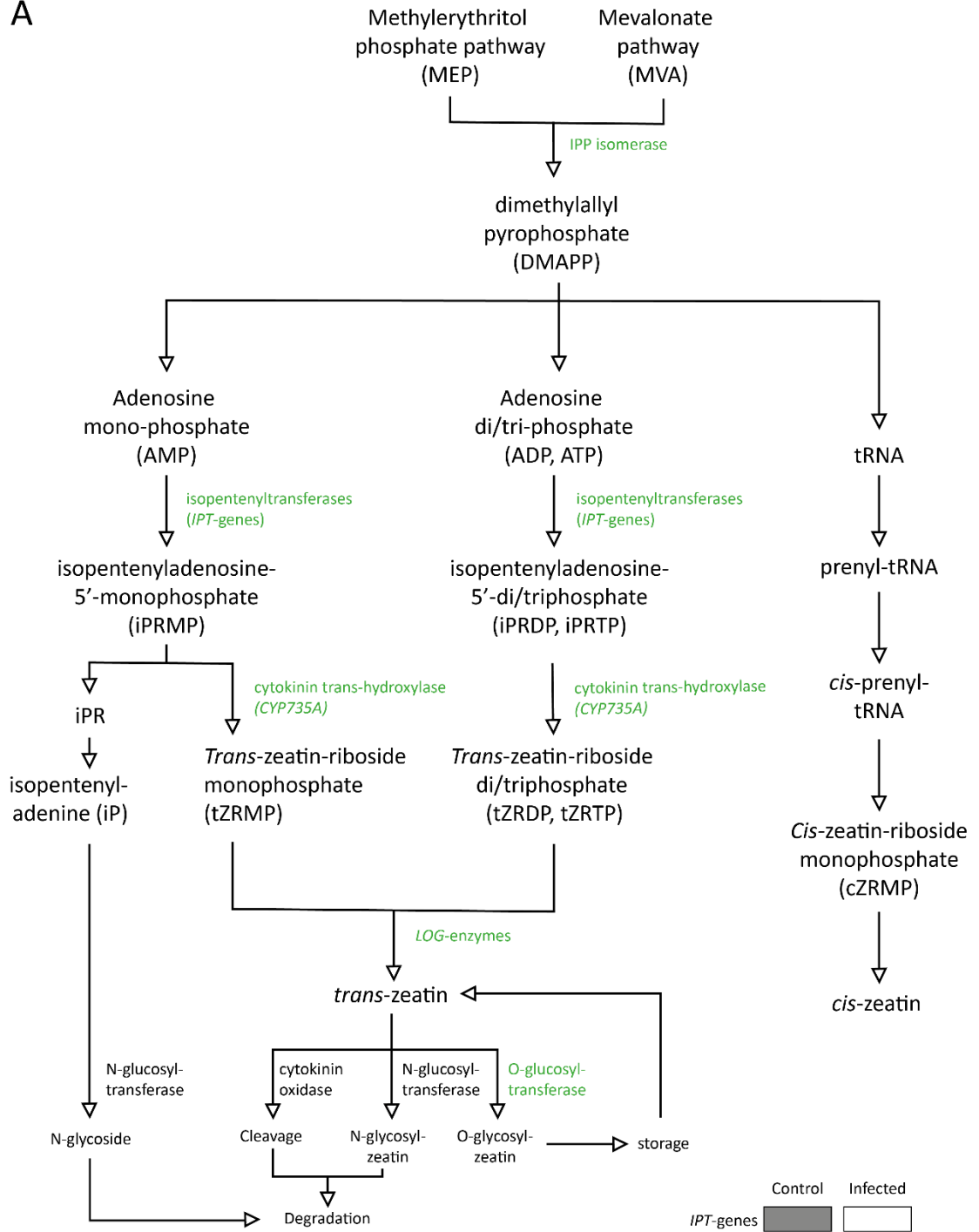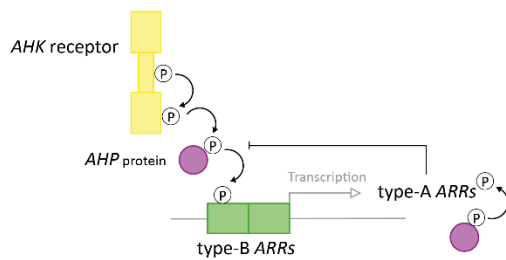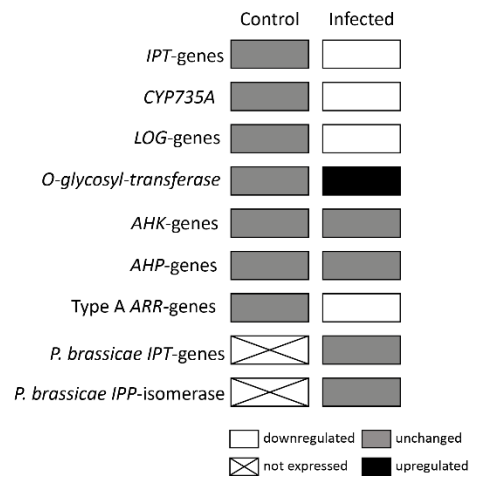
Figure 1.5: Cytokinin biosynthesis and signalling [Legend on next page]

[Legend to figure 1.5]

|A| Simplified biosynthesis and inactivation/degradation of *trans*-zeatin in plants. Underlying enzymes involved in clubroot disease development are highlighted in green |B| Simplified CK signalling in plants |C| Differential gene-expression with focus in CK synthesis, inactivation, and signalling during clubroot infection. Data obtained from [12]

1.4.5. METABOLIC HOST-PATHOGEN INTERACTION: CARBOHYDRATE METABOLISM

Plant growth and the ability to react to changing environmental conditions depends highly on photosynthesis, and allocation of photosynthates. The latter is mediated by the vascular system. The vascular system of higher plants can be defined as distribution network for water, nutrients, and photosynthates between source and sink tissues. Source tissues are photosynthetic organs such as mature leaves, and sink tissues either non-photosynthetic organs (i.e. roots) or organs with high demand in carbohydrates but low productivity rates (i.e. immature leaves) [63].

In healthy plants, fixed carbon (end-product of Calvin cycle and driven by photosynthesis) from source tissues is first stored in chloroplasts (insoluble starch) and vacuoles (soluble sucrose), and then mobilised as sucrose for transport over short- and long-distances through the phloem into sink tissues (translocation) [63]. Thereby, phloem loading and unloading is performed by sugar permeases transporters of the SWEET gene family. In sink tissues, received carbohydrates are hydrolysed by invertases or sucrose synthases. Products of this hydrolysis reaction are hexose monomers and UDP-glucose/fructose, respectively [64]. They are either used to drive metabolic processes promoting both growth and development (e.g. glycolysis), or stored for future needs (e.g. starch storage in amyloplasts) [63] (figure 1.6 A).

Translocation of carbohydrates from source to sink organs is an important factor for sink metabolism. It underlines the importance of source activity for plant performance. However, not all source organs equally supply all sink organs. Instead, a preferential supply is apparent. Differential distribution of carbohydrate (assimilate partitioning) is driven by proximity (relative distance and vascular connection) between sink and source organs, and competition between multiple sinks. The latter is defined as sink strength, and describes the capacity of sink structures (size and carbohydrate-storing activity) to compete for receiving photosynthates. However, the carbohydrate supply is slowed down when a strong sink is not able to metabolise carbohydrates quickly enough (sink limitation). These synchronised source-sink activities result in a balance between shoot and root growth (shoot-root ratios). Synchronisation relies on communication, which includes physical (e.g. turgor pressure in the phloem) and chemical signals (e.g. phytohormones and carbohydrates). Those signals have an impact on photosynthetic activity [63] (figure 1.6 B).

Photosynthesis is a tightly regulated process responsive to changing environmental conditions and variable needs of sink organs during growth. Adjustments include increase or repression of photosynthetic activity. They can be short- or long-term, and rely on sink-mediated feedback. Short-term feedback control of photosynthesis is biochemical. It includes the redox control of key components of the photosynthetic apparatus (i.e. PSII and PSI transcription), and the rate of

triose phosphate[1] utilisation during sucrose and starch synthesis. If a sink has a higher demand in carbohydrates, photosynthesis will increase in the responsible source organ. This mediates enhanced translocation of photosynthates. Long-term feedback control of photosynthesis is based on genetic regulation. Many photosynthesis genes (including Rubisco) are responsive to sugar depletion and abundance. The regulation of their expression follows a feast-or-famine model [65]: Enhanced sink demands causes reduced sugar levels in source organs, which respond with the up-regulation of famine-genes. Subsequent sugar abundance in sink tissues activates feast-genes. This promotes enhanced use of sugars. Phytohormones (i.e. Cytokinins, or Auxin) stimulate or inhibit of photosynthates partitioning (i.e. genes for loading or unloading the vasculature) [63][66].
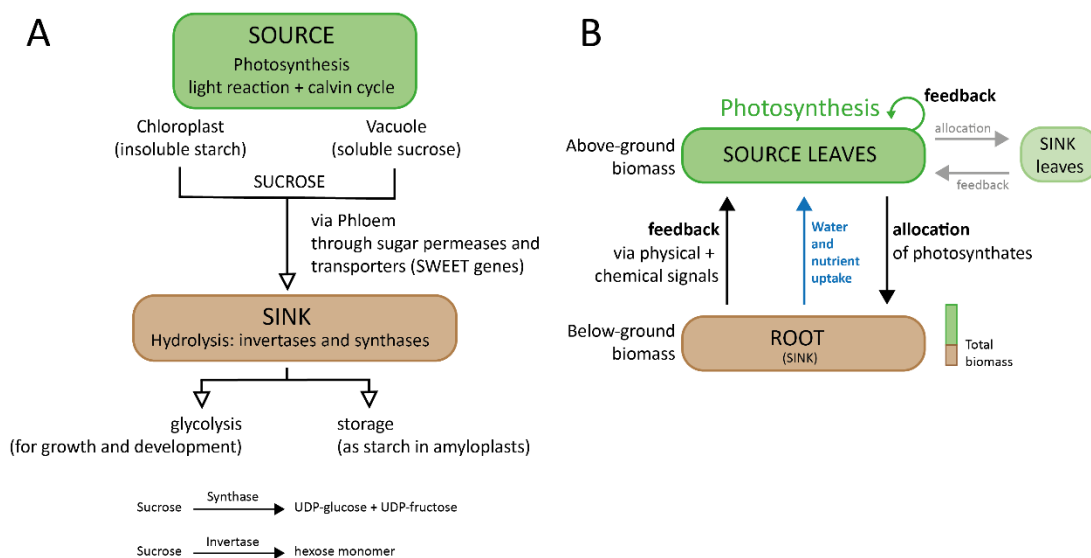
Figure 1.6: Overview of sugar allocation and source-sink equilibrium

|A| Overview of sugar allocation from source to sink tissue in healthy plants

|B| Overview of feedback-controlled source-sink balance in healthy plants – a model of the interrelationship between photosynthesis and plant growth

---

[1] Starch and sucrose synthesis are competing processes. Triose-phosphate is the photosynthetic end-product of the Calvin cycle, and used for starch and sucrose synthesis. The former takes place in the cytosol, the latter inside the chloroplast. Triose-phosphate incorporates inorganic phosphate, which needs to be recycled to the reactions of photosynthesis. Inorganic phosphate is released during starch and sucrose synthesis, and accumulates in chloroplasts and cytosol. A phosphate/ triose-phosphate translocator (stoichiometric antiporter) in the membrane ensures the export of triose-phosphate into the cytosol and import of inorganic phosphate into the chloroplast. Increased photosynthesis causes excessive accumulation of triose phosphate in chloroplasts with difficulties to export those quickly into the cytosol. Starch synthesis is therefore enhanced while sucrose synthesis remains the same. As a result, leaf starch content rises. This is re-mobilised during the night, and ensures on-going carbohydrate allocation.

Distorted source-sink balance in clubroot-infected plants

P. brassicae completely depends on the host for nutritional purposes. To ensure a reliable supply of host resources, the pathogen transforms the root into a metabolic sink for carbohydrates [67]. Clubroot infected host plants (i.e. *A. thaliana* and *B. rapa*) exhibit altered carbohydrate metabolism and partitioning [68][69]. Studies showed an increased rate of carbohydrate translocation from leaves to roots/galls [69], reduced sugar (sucrose, glucose, and fructose) and starch content in leaves [69][70], and increased concentrations of glucose and fructose in roots [70]. The rate of photosynthesis and stomatal conductance was found to be reduced in *A. thaliana* with unchanged maximum capacity of photosynthesis [69]. Molecular studies using clubroot infected root tissue of *A. thaliana* revealed upregulated gene expression for sucrose and starch synthesis (e.g. sucrose synthase) [61][71] and extracellular invertases [72][71]. Furthermore, it could be shown that many SWEET genes are differentially expressed during clubroot infection. In *A. thaliana*, increased levels of *SWEET 11* and *12* (sugar permease for bidirectional transport of sucrose and hexose) was observed in phloem cells of hypocotyls, which leads to local distribution of sugars towards the pathogen [71]. Studies in *B. rapa* showed the upregulation of 6, 7 and 3 SWEET genes in roots, hypocotyls, and leaves, respectively [70]. Observations of altered sugar translocation are in line with histological examinations of clubroot infected hypocotyl/root tissues of *A. thaliana*. Those examinations elucidated increased phloem formation during the proliferate stage of gall formation, increased phloem bundle complexity with the number of phloem bundles unchanged, alongside increased meristematic activity of the vascular cambium and reduction of xylogenesis [73].

Different studies found the disaccharide trehalose to be synthesised by *P. brassicae* using the enzyme trehalose-6-phosphate synthase (TPS) [74]. Recent sequence completion of the pathogen's genome [49][62] revealed the existence of 3 TPS genes (*PbTPS1-3*) and one single gene encoding trehalose phosphate phosphatase [49]. *PbTPS1* was upregulated during gall formation. Initially, it was thought, that accumulating trehalose might be exported/released from the pathogen into plant cells to interfere with the host's sugar signalling pathways. But no effect on sugar metabolism could be observed. Only trehalase activity (plant enzyme to hydrolyse trehalose) was increased in infected root tissue [74].

1.4.6. METABOLIC HOST-PATHOGEN INTERACTION: SALICYLIC ACID

Salicylic acid (2-hydroxybenzoicacid, SA) is a crucial phytohormone for the activation of defence responses upon attack of biotrophic pathogens. It is a phenolic compound, and synthesised in chloroplasts via 2 pathways with chorismic acid and the amino acid phenylalanine as starting points. Subsequently, SA is transported in to the cytosol, where it undergoes several modifications. Modifications generally inactivate cytosolic SA, reducing the level of active SA when immune signalling is not required. Glycosylation performed by SA-glucosyltransferase generates SA 2-O-β-D-glucoside (SAG), and methylation through the activity of SA-methyltransferases creates volatile methyl-SA (MeSA). MeSA is extremely phloem-mobile due to its hydrophobicity, and during plant defence used to signal pathogen attacks from the side of infection to more distant plant areas. In those distant areas, it triggers systemic acquired resistance (SAR) when converted back into SA by MeSA-esterases [75].

SA-methyltransferases in plants belong to the class II SABATH protein family – a unique family only found in the plant kingdom [76]. In *A. thaliana*, SA-methyltransferases are encoded by the gene AtBSMT1. Recent findings [77] indicated, that *P. brassicae* possesses a SA-methyltransferase, structurally unrelated to those of plants, but with SABATH-like activity. It is encoded by the gene PbBSMT. During clubroot-mediated gall formation in *A. thaliana*, accumulation of SA and MeSA could be detected in both leaves and root. The former contained the highest level. Experiments demonstrated that MeSA in leaves originated from the root, and suggested that *P. brassicae* affects MeSA movement from the root to leaves. Therefore, it was hypothesised that *P. brassicae* secretes its SA-methyltransferase into the host cell, where it turns the plant defence signal SA into MeSA. Unable to initiate plant defence mechanisms, MeSA is then transported into leaves. In leaves, MeSA gets either emitted or converted back to SA.

The hypothesis of failed activation of defence responses could potentially explain earlier microarray findings. The analysis showed that the majority of defence-related genes were not differentially expressed, and the ones that showed different expression levels were mostly downregulated [61]. A different study showed that the susceptible *A. thaliana* wildtype Col-0 induced large JA and weak SA responses during clubroot disease, and that exogenous application of SA reduced clubroot disease symptoms. Subsequently, synergistic effects between SA and JA pathways were suggested [78].

1.4.7. METABOLIC HOST-PATHOGEN INTERACTION: JASMONIC ACID

Jasmonic acid (JA) is a crucial phytohormone for the activation of defence responses upon attack of necrotrophic pathogens. It originates from α-linoleic acid, which itself derives from galactolipids of chloroplast membranes. Synthesis follows the octadecanoid pathway, starting in chloroplasts, and terminating in peroxisomes. The final step in JA biosynthesis is catalysed by the enzyme JAR1 (jasmonic acid amino synthetase) [79]. JAR1 is a member of the auxin-induced GH3 family, in particular GH3.11, and activates JA upon conjugation to JA-Ile [80]. During clubroot infection in *A. thaliana*, transcripts for GH3.11 were down-regulated [61][47][81], and the *A. thaliana* mutant line *jar1* showed increased susceptibility [82].

1.4.8. METABOLIC HOST-PATHOGEN INTERACTION: BRASSINOSTEROIDS (BRS)

BRs are a group of phytohormones essential for plant growth and development. This includes maintenance of meristem sizes, cell division and elongation, vascular differentiation (i.e. xylogenesis, and phloem genesis), or transport and partitioning of carbohydrates [83][84][85]. Therefore, BRs are involved in functions overlapping with auxin.

BR biosynthesis and inactivation

BR biosynthesis is complex, and involves 3 interconnected pathways with campesterol (CR) as primary precursor (figure 1.7 A). Campesterol can be converted to campestanol (CN), and via castasterone (CS) to brassinolide (BL) – the most active members of BRs. Two parallel pathways operate between CS and BL, termed early and late C6 oxidation pathway. They are usually summarised as CN-dependent BR biosynthesis. CN-independent BR biosynthesis is performed by the C22 hydroxylation pathway, whose final intermediate gets fed into the late C6 oxidation pathway. Key enzymes of all 3 pathways are DET2 (DE-ETIOLATED 2), and several cytochrome P450 enzymes, such as CPD (CONSTITUTIVE PHOTOMORPHOGENESIS AND DWARFISM), DWF4 (DWARF 4), ROT3 (ROTUNDIFOLIA3, or CYP90C1), CYP90D1, BR6ox1 (BRASSINOSTEROID-6-OXIDASE 1), and BR6ox2. BR biosynthesis is controlled through a feedback-loop and auxin. While elevated auxin stimulates BR biosynthesis (i.e. *DWF4*), high levels of BR inhibit transcription genes involved in BR biosynthesis (i.e. *DWF4*) [83][85].

BR can be inactivated enzymatically through hydroxylation by hydroxylase BAS1 (PHYB ACTIVATION-TAGGED SUPPRESSOR1), sulfonation by sulfotransferase BNST3 (BRASSICA NAPUS SULFOTRANSFERASE 3), glycosylation by glycosyltransferase UGT73C5, and acylation by acyltransferases DRL1 (DWARF AND ROUND LEAF-1), BEN1 (bri1-5 ENHANCED1) and BIA1 (BRASSINOSTEROID INACTIVATOR1) [83][85].

BR signalling

BRs are perceived by the main receptor BRI1 (Brassinosteroid-insensitive 1) and its paralogs BRL1 (BRI1-like1) and BRL3 (BRI1-like3). All three belong to the group of LRR-RLK (LEUCINE-RICH REPEAT RECEPTOR-LIKE KINASE) receptors. After BR binds to the extracellular domain of BRI1, the cytoplasmatic kinase domain phosphorylates BKI1 (BRI1 KINASE INHIBITOR 1). BKI1 then dissociates from the plasma membrane, and thereby allows BRI1 to recruit its co-receptor BAK1 (BRI1-ASSOCIATED RECEPTOR KINASE 1) – a member of the SERKs (SOMATIC EMBRYOGENESIS RECEPTOR KINASES) subfamily of LRR-RLKs. Activated BAK1 phosphorylates RLCKs (membrane-bound receptor-like cytoplasmic kinases), such as BSK1 (BR-SIGNALING KINASE 1) and CDG1 (CONSTITUTIVE DIFFERENTIAL GROWTH 1), which then activate BSU1 (BRI1-SUPPRESSOR 1). Thereafter, BSU1 inactivates the negative regulator BIN2 (BRASSINOSTEROID-INSENSITIVE 2) through dephosphorylation, which results in accumulation of the previously inhibited transcription factors BZR1 (BRASSINAZOLE-RESISTANT 1) and BES1 (BRI1-EMS-SUPPRESSOR 1, or BZR2). Both BZR1 and BES1 can then induce or repress the transcription of target genes [83][85] (figure 1.7 B).

BRs and clubroot

Alterations in BR homeostasis contribute to gall formation during clubroot infection. Reduced gall formation could be observed in clubroot-infected *A. thaliana* mutant lines *bri1-6* and *det2* [82][81], as well as in the infected wildtype after treatment with an inhibitor of BR biosynthesis [81]. Laser microdissection coupled with microarray analysis of individual enlarged root cells harbouring defined developmental stages of *P. brassicae* (i.e. small and big plasmodia in enlarged cells of inner and outer cortex layer, respectively) could detect plasmodia-mediated transcriptional changes of genes involved in BR synthesis and signalling [81]. A summary of differential gene expression obtained from this study (single-cell analysis technique instead of the common bulk tissue technique) [81] is displayed in figure 1.7 C and D. However, it must be stated that technical difficulties limited replication in the study.
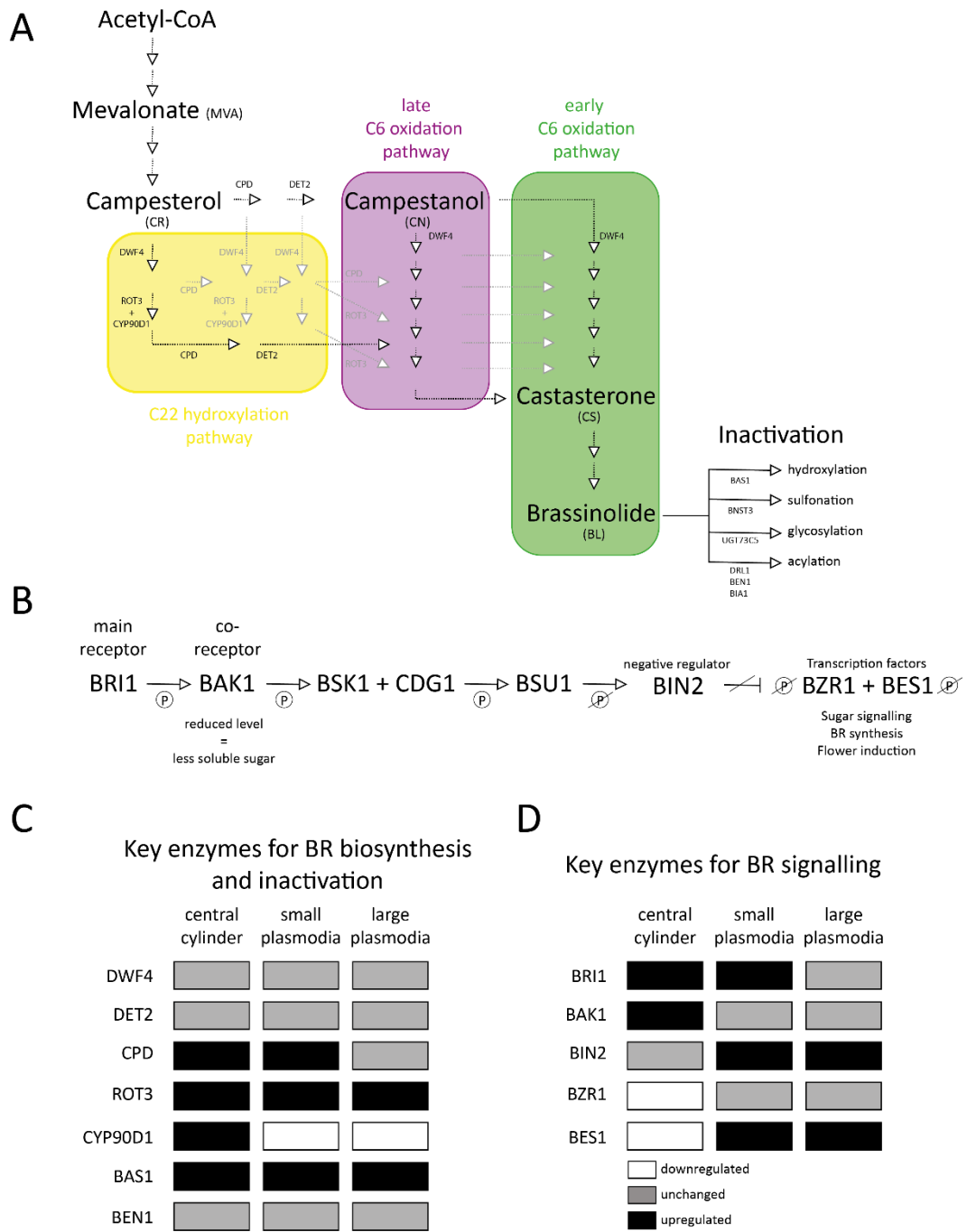
Figure 1.7: BR biosynthesis and signalling pathways with selected root transcriptome results for clubroot infected *A. thaliana* [Legend on next page]

[Legend to figure 1.7]:

|A| Simplified BR biosynthesis pathways. Black arrows show main routes of CN-dependent (early and late C6 oxidation), and CN-independent pathways (C22 hydroxylation); grey arrows their interconnection. For simplicity, only a selection of intermediates with catalysing enzymes are indicated |B| Simplified BR signalling pathway, which relies on a cascade of phosphorylation and dephosphorylation mediated by several kinases. Enzyme activity is indicated with the letter "P" |C| Transcriptome results of selected enzymes involved in BR synthesis and inactivation that are differentially expressed during clubroot infection in *A. thaliana*. Information obtained from [81] |D| Transcriptome results of selected enzymes involved in BR signalling that are differentially expressed during clubroot infection in *A. thaliana*. Information obtained from [81]

1.4.9. DISEASE CONTROL

Several strategies can been applied to tackle clubroot disease. Soil management strategies are the most common ones. Applications of lime, calcium, boron, and some nitrogenous fertiliser (e.g. nitrate-nitrogen, calcium cyanamide) aiming to increase soil alkalinity (low concentration of hydrogen ions). For the mineral soil constituents calcium and boron, studies showed a retarding effect on primary zoospores to reach root hair, and to mature within them [3][86][87][88]. Additionally, boron is suspected to be somewhere involved in the inhibition of secondary infection [3][86]. A more direct control measure for clubroot is the application of agro-chemicals (i.e. epoxydon) [3]. However, the use of most agro-chemicals is generally restricted due to environmental legislations. Indirect biological control of clubroot offers typical husbandry methods such as crop rotation with non-host cultivars, and intercropping with trap plants (i.e. Raphanus sativus) [89], but also improved sanitisation of field machinery [88]. But despite all scientific efforts, most field approaches to tackle clubroot are time-consuming, prohibitively expensive when applied on larger scale, and not always effective. In fact, they never eliminate clubroot, and once infestation is established, it immediately diminishes the value of land [8]. Growth of clubroot resistant Brassica cultivars on fields is the most successful and sustainable strategy to prevent accumulation of *P. brassicae* in soil [90].

1.4.10. CLUBROOT RESISTANCE GENES

Three ecotypes of *A. thaliana* (*Ze-0*, *Tsu-0* and *Ta-0*) showed hypersensitive responses in roots after infection with a single spore inoculum containing the clubroot pathotype "e". Thereby, necrotic boundaries around infected cells inhibited invasion of *P. brassicae*. Genetic examinations revealed alleles of a dominant single nuclear gene termed RPB1 (REACTION TO PLASMODIOPHORA BRASSICAE 1), which is localized on chromosome 1 [91]. Later, other regions were detected on the chromosomes 1 (*Pb-At1*), 4 (*Pb-At4*), and 5 (*Pb-At5.1* and *Pb-At5.2*) conferring clubroot resistance [92]. However, necrosis of neighbouring cells to prevent secondary infection was never observed in resistant Brassica cultivars. Only deposition of callose at the penetration side of *P. brassicae* was visible to inhibit primary clubroot infection [93].

Genetic resistance in Brassica cultivars

Brassica cultivars have a complex genome. According to "the theory of U" [94], interspecific breeding of the diploid species *B. rapa* (genome AA), *B. nigra* (genome BB), and *B. oleracea* (genome CC) allowed the creation of 3 new Brassica species with tetraploid genomes. These species include *B. juncea* (genome AABB), *B. napus* (genome AACC), and *B. carinata* (genome BBCC). Today, as a result of constant hybridisation of Brassica species with occurring polyploidy, there is a huge genetic and morphological diversity. To unravel the genetic make-up of Brassica

plants, genetic maps have been constructed. They are known as genetic linkage maps, since they link specific phenotypes (quantitative traits, QT) to a section on the genome that correlates with those phenotypes (quantitative trait loci, QTL). QTLs are used for plant breeding before the actual underlying genes are identified and sequenced. Therefore, QTLs can contain single or multiple genes with strong or weak effects [7].

Most clubroot resistance genes or QTLs were found in European fodder turnips (*B. rapa* ssp. *rapifera*), particularly in the lines "Gelria R", "Siloga", "Milan White", and "Debra". These genes or QTLs were then used as source for breeding clubroot resistance into *B. rapa* ssp. *pekinensis* (i.e. Chinese Cabbage), *B. napus* (i.e. oilseed rape) and *B. oleracea* (i.e. cabbage, kale) [90]. Due to advances in genetic analysis, those progeny species (i.e. complex back-crosses of inbred and DH lines) can be compared to genetic linkage maps of *B. rapa* to find other clubroot resistance genes (for example in [95]). *B. rapa* and *B. napus* fodder types usually contain dominant and pathotype-specific genes. Those dominant genes are strong in *B. rapa* and weak in *B. napus.* In contrast, *B. oleracea* offers recessive but mainly unspecific genes giving resistance to a broad spectrum of pathotypes [96]. Table 1.2 displays a selection of QTLs for pathotype-specific clubroot resistance, which were found in *B. rapa* or their progenies. In all cases the underlying molecular defence mechanism is unknown.

"Mendel" resistance

The most popular resistance gene is "Mendel", and named after the hybrid cultivar *B. napus* "Mendel". In 2000, "Mendel" was successfully introduced to the European Seed Market – the first winter oilseed rape resistant to clubroot. "Mendel" is a progeny of the crossing *B. rapa* ECD-04 x *B. oleracea* ECD-15 inter-crossed with the high yielding *B. napus* "Falcon". Genetically, it contains one dominant, pathotype-specific gene and two recessive genes [97]. However, the defence mechanism is unknown to the general scientific community (Elke Diederichsen, personal communication). Cultivation of "Mendel" was treated as valuable strategy to tackle clubroot disease. It is resistant to a broad spectrum of pathotypes, but due to the existence of compatible clubroot pathotypes, it was only recommended for severely infested soil [90]. Over the years, the "Mendel" gene was bred into other plant lines with the intention to cultivate them as last resort (i.e. winter oilseed rape "Cracker"). Reports emerged (especially from Canada), stating that monogenic "Mendel" resistance starts to break down due to genetic variability of the pathogen [98]. Therefore, novel sources of qualitative and quantitative clubroot resistance is required.

Table 1.2: Selected QTLs found in *B. rapa* or progenies thereof [99][100][101][102][103][104][95][105]

QTL Name	Linkage group	Gene			Resistance to	Reference
		number	name	structure		
Crr1	A08	2	Crr1a (major) Crr1b (minor)	TIR-NBS-LRR	Ano-01 and Wakayama-01	Subawe et al., 2003, 2006
Crr2	A01				Ano-01 and Wakayama-01	Subawe et al., 2003, 2006
Crr3	A03				Ano-01	Hirai et al., 2004
Crr4	A06				Ano-01 and Wakayama-01	Subawe et al., 2006
CRa	A03			TIR-NBS-LRR	Pb2	Matsumoto et al., 1998
CRb	A03				Pb4	Piao et al., 2004
CRc	A02				M85 and K04	Sakamoto et al., 2008
CRd	A03	4	Bra001160, Bra001161, Bra001162, Bra001175		Pb4	Pang et al., 2018
CRk	A03				M85 and K04	Sakamoto et al., 2008
PbBa1.1	A01				Pb2, Pb7	Chen et al., 2013
PbBa3.1	A03				Pb2, Pb7	Chen et al., 2013
PbBa3.2	A03				Pb10	Chen et al., 2013
PbBa3.3	A03				Pb7	Chen et al., 2013
PbBa8.1	A08				Pb4	Chen et al., 2013
Rcr4	A03	6	Bra012541, Bra019413, Bra019412, Bra019410, Bra019409, Bra019273	TIR-NBS-LRR	Pb2, 3, 5, 6 and 8	Yu et al., 2017
Rcr8	A02	4	Bra022069, Bra022071, Bra026556, Bra032996	TIR-NBS-LRR	canadian pathotype 5x	Yu et al., 2017
Rcr9	A08	2	Bra020936, Bra020861	TIR-NBS-LRR	canadian pathotype 5x	Yu et al., 2017

1.5. SCOPE OF PHD THESIS – AIMS AND OBJECTIVES

The PhD project's overall aim was to find ways to measure quantitative resistance in order to generate new generations of crop plants with durable polygenic clubroot resistance. The project followed up physiological and molecular methods with destructive and non-destructive approaches, which were applied to both below- and above-ground plant material of a population of different Brassica cultivars inoculated with known concentrations of *P. brassicae*.

Chapter 1 (general introduction) gives an overview of the topic, while chapter 2 (materials and methods) explains the methods and lists the materials used during the PhD project.

Chapter 3 is focussing on physiological methods performed at two different phenomic platforms to (1) quantify early and for the human eye not visible above-ground plant responses to below-ground clubroot disease, and to (2) link clubroot resistant/tolerant phenotypes (physiology and morphology) with resistance genes (genotype) eventually. Plant development, growth, and performance was monitored by frequent application of non-destructive imaging and weighing techniques.

Chapter 4 describes an end-point screen, involving biomass measurements, gall scoring, and total disease quantification based on qRT-PCR. The former was conducted to extract information about source-sink distortions within a population of plants showing different disease phenotypes. The latter was performed to test depth and accuracy of a molecular clubroot assay. For the assay, gene copy numbers of *P. brassicae* in DNA samples of clubroot infected Brassica cultivars were calculated. At the end, the results of all 3 measurements were compared.

Chapter 5 explores the potential of metabolomics approaches to understand resistance and susceptibility in host plants during clubroot infection. The analysis was focussed on key stages of clubroot disease (i.e. primary, early secondary, and late secondary infection) using leaf and root material. Both tissue types, all time points, and 2 genotypes were compared.

A summary of all findings together with technical limitations is discussed in chapter 4 (general discussion).

CHAPTER 2: MATERIALS AND METHODS

2.1. BIOLOGICAL MATERIAL

2.1.1. CLUBROOT PATHOTYPE

Resting spores of *Plasmodiophora brassicae* were originally isolated from galls of infected *Brassica oleracea* in Penyrheol (South Wales) and classified as 16/2/12 [12] according to the European Clubroot Definition (ECD) [106]. The universally susceptible Chinese Cabbage Wong Bok was used as host plant in Sheffield. Galls were collected at 56 days after inoculation with 50 ml of 10^6 spores/ml, and stored at -20°C until required.

2.1.2. PATHOGEN EXTRACTION

Clubroot spore preparation was performed following Mithen and Magrath (1992) [28]. Galls of infected Chinese Cabbage Wong Bok were homogenized in dH_2O, filtered through 3 layers of muslin, and centrifuged (30 min, 7750 x g, 4°C). Soil, starch and plant tissue were removed from the pellet with a spatula, and the remaining spores re-suspended in dH_2O. The centrifugation step was repeated to remove additional soil, starch and plant tissue. The inoculum was stored at 4°C until required with a maximum storage time of 4 weeks. For each experiment a new inoculum was prepared.

2.1.3. DETERMINATION OF SPORE CONCENTRATION

For the determination of spore concentration, a staining solution [107] containing 9.5 µl ethidium bromide (50 µg/ml) and 0.5 µl calcofluor white (100 µg/ml) was prepared, mixed with 10 µl of a 100-fold diluted spore stock (10 µl spore stock + 990 µl dH_2O), and 10 µl loaded onto a haemocytometer. Spore density was determined via fluorescence microscopy (BX51 Olympus) using excitation at 400 nm and detecting emission at 455 nm. Walls of active spores showed intense blue fluorescence as calcofluor white binds chitin. Non-viable spores could be identified through red fluorescence as ethidium bromide was not excluded from the spore and stained DNA red. Living spores were counted in 4 squares (1 square = 0.004 mm^3), and the average number of spores calculated. Spores per ml were determined with the equation: average x 250 x 1000 x 100.

2.1.4. BRASSICA GENOTYPES

Seeds of different Brassica cultivars were kindly provided by the universities of Nottingham and York (table 2.1). Both sets contained genotypes used for associative transcriptomics by Ian Bancroft, published in [108]. Amongst the listed cultivars was Winter Oilseed Rape Cracker. Cracker is a descendant of the *B. napus* genotype Mendel, and therefore genetically equipped

with the dominant "Mendel" resistance gene. However, due to a natural consequence of breeding procedures, 10-30% of each "Cracker-batch" did not contain the clubroot resistance gene (Elke Diederichsen, personal communication). As a results, the majority of experiments were carried out as time-course experiments.

Table 2.1: List of Brassica cultivars

Plant Name	Species	BnASSYST number	Source	Experiment
Cauliflower	Brassica oleracea	NA	Enza Zaden	Phenomics Trial 3
Chinese Cabbage Wong Bok	Brassica rapa	NA	Seedaholic, Ireland	Phenomics preliminary series 1+2, Trial 1, Trial 3
Kohlrabi	Brassica oleracea	NA	Enza Zaden	Phenomics Trial 3
Winter Oilseed Rape Cracker	Brassica napus	NA	Scotland	Phenomics Trial 1-3, End-point screen, Metabolomics
Oilseed Rape Apex	Brassica napus	BnASSYST-040	University of Nottingham + York	Phenomics Trial 2 set 1, End-point screen
Winter Oilseed Rape Bravour	Brassica napus	BnASSYST-048	University of Nottingham + York	Phenomics Trial 2 set 1, End-point screen
Oilseed Rape Verona	Brassica napus	BnASSYST-053	University of Nottingham + York	Phenomics Trial 2 set 1, End-point screen
Winter Oilseed Rape Tapidor	Brassica napus	BnASSYST-099	University of Nottingham + York	Phenomics Trial 2 set 1, End-point screen
Oilseed Rape Eurol	Brassica napus	BnASSYST-101	University of Nottingham + York	Phenomics Trial 2 set 1, End-point screen
Oilseed Rape Lembkes Malchower	Brassica napus	BnASSYST-108	University of Nottingham + York	Phenomics Trial 2 set 1, End-point screen
Oilseed Rape Jet Neuf	Brassica napus	BnASSYST-121	University of Nottingham + York	Phenomics Trial 2 set 1, End-point screen
Winter Oilseed Rape Baltia	Brassica napus	BnASSYST-133	University of Nottingham + York	Phenomics Trial 2 set 1, End-point screen
Oilseed Rape Coriander	Brassica napus	BnASSYST-137	University of Nottingham + York	Phenomics Trial 2 set 1, End-point screen
Oilseed Rape Dippes	Brassica napus	BnASSYST-139	University of Nottingham + York	Phenomics Trial 2 set 1, End-point screen
Winter Oilseed Rape Ramses	Brassica napus	BnASSYST-168	University of Nottingham + York	Phenomics Trial 2 set 1, End-point screen
Oilseed Rape Moana	Brassica napus	BnASSYST-186	University of Nottingham + York	Phenomics Trial 2 set 1, End-point screen
Oilseed Rape Q100	Brassica napus	BnASSYST-204	University of Nottingham + York	Phenomics Trial 2 set 1, End-point screen
Ragged Jack Kale	Brassica napus	BnASSYST-209	University of Nottingham + York	Phenomics preliminary series 1+2, Trial 1, Trial 3
Siberian Kale	Brassica napus	BnASSYST-211	University of Nottingham	Phenomics Trial 1
Oilseed Rape Westar 10	Brassica napus	BnASSYST-240	University of Nottingham	Phenomics Trial 2 set 2 End-point screen
Oilseed Rape Karoo-057	Brassica napus	BnASSYST-256	University of Nottingham	Phenomics Trial 2 set 2 End-point screen
Spring Oilseed Rape Monty-028	Brassica napus	BnASSYST-257	University of Nottingham	Phenomics Trial 2 set 2 End-point screen
Oilseed Rape N01D-1330	Brassica napus	BnASSYST-258	University of Nottingham	Phenomics Trial 2 set 2 End-point screen

Plant Name	Species	BnASSYST number	Source	Experiment
Spring Oilseed Rape Monty-028	Brassica napus	BnASSYST-257	University of Nottingham	Phenomics Trial 2 set 2 End-point screen
Oilseed Rape N01D-1330	Brassica napus	BnASSYST-258	University of Nottingham	Phenomics Trial 2 set 2 End-point screen
Oilseed Rape N02D-1952	Brassica napus	BnASSYST-259	University of Nottingham	Phenomics Trial 2 set 2 End-point screen
Spring Oilseed Rape Erglu	Brassica napus	BnASSYST-263	University of Nottingham	Phenomics Trial 2 set 2 End-point screen
Winter Oilseed Rape Bronowski	Brassica napus	BnASSYST-273	University of Nottingham	Phenomics Trial 2 set 2 End-point screen
Oilseed Rape Ceska	Brassica napus	BnASSYST-274	University of Nottingham	Phenomics Trial 2 set 2 End-point screen
Oilseed Rape Duplo	Brassica napus	BnASSYST-275	University of Nottingham	Phenomics Trial 2 set 2 End-point screen
Winter Oilseed Rape Topas	Brassica napus	BnASSYST-283	University of Nottingham	Phenomics Trial 2 set 2 End-point screen
Swede Vige	Brassica napus	BnASSYST-401	University of Nottingham	Phenomics Trial 2 set 2 End-point screen
Swede Huguenot	Brassica napus	BnASSYST-410	University of Nottingham	Phenomics Trial 2 set 2 End-point screen
Swede Tina	Brassica napus	BnASSYST-436	University of Nottingham	Phenomics Trial 2 set 2 End-point screen
Winter Oilseed Rape Temple	Brassica napus	BnASSYST-527	Elsoms Seed	all

2.1.5. PLANT GERMINATION

Brassica seeds of different cultivars (supplementary table 1, Appendix) were placed on moistened filter paper in aluminium foil-covered Petri dishes in a growth chamber for 3 days (20 ± 2°C day/ 18 ± 2°C night).

2.1.6. TRANSPLANTATION AND INOCULATION OF HOST PLANTS

Germinated seedlings were transplanted into well-watered compost (one seedling per plant pot), and inoculated with a spore -solution of a defined concentration or mock inoculated with water. Control and inoculated seedlings were then transferred into a greenhouse (AWEC or IBERS) or phyto chamber, and bottom watered in trays for the first 2-3 weeks to allow disease establishment.

2.2. PLANT HARVEST AND VISUAL ASSESSMENT OF DISEASE SEVERITY

2.2.1. DESTRUCTIVE HARVEST

Unless stated, all experiments were terminated with a destructive harvest at 51 dpi. This included root excavation with subsequent root washing under tap water. Plants were visually assessed (photographs of root and shoot) and scored for above- and below-ground clubroot symptoms. Gall size scoring was performed following the clubroot classification system, where roots are rated on a scale between 0 and 3 [109] (table 2.2). For molecular measurements of infection, leaf and/or root tissue was collected, divided into 200-400 mg subsamples, snap-frozen in liquid nitrogen, and stored at -80°C until required. The remaining above- and below-ground material was collected and placed in a drying oven (5 days at 65°C) for biomass measurements.

2.2.2. DISEASE SCORING

Gall size scoring was performed following the clubroot classification system, where roots are rated on a scale between 0 and 3 [109]. Typical pictures and scores of galls were taken from chapter 4, and shown below for different oilseed rape varieties.

Table 2.2: Clubroot classification system

Cracker	Apex	N01D-1330	Q100
0	1	2	3
No gall formation and other clubroot disease symptoms	A few small and separate globular or spindle-shaped clubs on main root or side roots	Intermediate sized clubs	Severe clubs on main root including side roots; affects more than half of the root system

2.3. EXPERIMENTAL OUTLINE

2.3.1. PHENOMICS

Four phenomics screens were performed at two different locations: AWEC at the University of Sheffield, and IBERS at the University of Aberystwyth in Wales. For phenomics screens at IBERS, an automated Lemnatech conveyor system was used to monitor plant phenotype parameters non-destructively at specific time points throughout the experiment. A phenomics screen at AWEC was conducted without a scanner system. Table 2.3 gives an overview of the experimental outline and environmental condition.

2.3.2. METABOLOMICS

Two metabolomics screens were performed. All screens followed the same experimental outline and identical environmental conditions in a controlled environment chamber (see table 2.4 for details). Metabolomics experiment 1 was performed with destructive harvest using one oilseed rape genotype at 3 different time points: 11 dpi (TP1), 35 dpi (TP2), and 50 dpi (TP3). Time points were picked to represent primary and secondary (early, late) infection. During each destructive harvest leaf and root material was collected, immediately snap-frozen in liquid nitrogen, and stored at -80°C until required. Metabolomics experiment 2 was conducted as a time-course experiment. Leaf material was taken at 11 and 35 dpi, and destructive harvest performed at 50 dpi by collecting both leaf and root material.

2.3.3. END-POINT DISEASE SCREEN

Two end-point disease screens were conducted in semi-controlled greenhouse conditions (AWEC at the University of Sheffield) (see table 2.5 for details). The former was destructively harvested on two days with immediate sampling (harvest and sampling on same day), the latter was subdivided into 5 sets of 6 oilseed rape varieties. Seedlings were transplanted and inoculated with 1 day difference (i.e. set 1 on day 1, set 2 on day 2, etc.), and harvested at 51 dpi. This staggered planting procedure allowed all samples to be processed on the same timescale.

Table: 2.3: Experimental outline for phenomics

Experiment	Genotype	Treatment	Soil Type	Pot size	Environmental Conditions	Watering	Measurements
AWECs *preliminary series 1 + 2* Winter	3 (3 biological replicates)	- Control (H₂O) - Dilution series: 6.25 x 10¹ - 6.25 x 10⁵ spores/ml - 100 ml	- Levington M3 compost - 1100 grams/ pot	Medium: 9.5 x 9.5 x 11.5 cm	- Semi-controlled greenhouse - 20 ± 2°C day/ 18 ± 2°C night - 12h photoperiod - 40-55% day/night humidity - 200 µmol PAR m⁻² x s⁻¹ irradiance tungsten light bulbs, sodium halide with winter spectrum	- Manual - 0-20 dpi: bottom - 21-51 dpi: alternated	- Start: 51 dpi (end-point) - Visual scoring of above- and below-ground symptoms - Photographs of phenotype - Root sampling for DNA assay (control, low spore (6.25 x 10²) and high spore (6.25 x 10⁵ spores/ml), primary and secondary root)
AWEC *Trial 3* Winter	6 (6 biological replicates)	- Control (H₂O) - Low spore (6.25 x 10² spores/ ml) - High Spore (6.25 x 10⁵ spores/ml) - 100 ml			- Semi-controlled greenhouse - 16 ± 2°C day/ 14 ± 2°C night - 10h photoperiod - approx. 40% day/night humidity - 150 µmol PAR m⁻² x s⁻¹ irradiance Tungsten light bulbs, metal halide with early summer spectrum		- Start: 9 dpi until end (51 dpi) - Water use (pot weight) - Biomass (end-point) - Visual scoring (end-point)
IBERS *Trial 1* Summer	5 (4 biological replicates)	- Control (H₂O) - Low spore (6.25 x 10² spores/ ml) - High Spore (6.25 x 10⁵ spores/ml) - 70 ml	- Levington M2:M3 compost mix - ratio 1:2 - 1100 grams/ pot	15 x 15 x 20 cm with slightly tapered base	- unregulated greenhouse - Humidity: 60 ± 10 % - Temperature: 20 ± 2°C day	- Automated with manual - correction - Top	- Start: 14 dpi until end (51 dpi) - Water use (pot weight), daily - Transpiration via thermal imaging at 29 dpi, 43 dpi, and 50 dpi - Area and height of plant by taking RGB pictures at 90° and 180° angles - Biomass (end-point) - Visual scoring (end-point)
IBERS *Trial 2 set 1* *Early autumn*	14 (3 biological replicates)	- Control (H₂O) - Low spore (6.25 x 10² spores/ ml) - High Spore (6.25 x 10⁵ spores/ml) - 50 ml			- unregulated greenhouse - Humidity: 50 ± 10 % - Temperature Aug-Sept.: 20 ± 6°C day - Temperature Oct.: 18 ± 3°C day	- Automated - Bottom - Corrected for biomass increase	- Start: 20 dpi until end (51 dpi) - Water use (pot weight), daily - Transpiration via thermal imaging at 28, 39, 42, 45, 47, and 49 dpi for set 1 - Area and height of plant by taking RGB pictures at 45°, 90°, 180° angles - Visual scoring (end-point)
IBERS *Trial 2 set 2* *Late autumn*	15 (3 biological replicates)				- unregulated greenhouse - Humidity: 50 ± 10 % - Temperature Sept.: 20 ± 6°C day - Temperature Oct.-Nov.: 18 ± 2°C day	- Automated - Alternated - Corrected for biomass increase	

Table 2.4: Experimental outline for metabolomics and transcriptomics

Experiment	Genotype	Treatment	Soil Type	Pot size	Environmental Conditions	Watering	Harvest + Sampling
Metabolomics experiment 1	1 (3 biological replicates)	- Control (H_2O) - 6.25 x 10^5 spores/ml - 50 ml	- Levington M3 compost - 1100 grams/ pot	Medium: 9.5 x 9.5 x 11.5 cm	- Phyto chamber - 20 ± 2°C day/ 18 ± 2°C night - 16h photoperiod - 40-55% day/night humidity - 300-400 µmol PAR m-² x s-¹ irradiance	- Manual - 0-20 dpi: bottom - 21-51 dpi: alternated	- Destructive harvest for TP1 (11 dpi), TP2 (35 dpi), and TP3 (50 dpi) - Leaf discs of 10 mm diameter - Root sampling (< 0.2 g)
Metabolomics experiment 2	2 (3 biological replicates)						- Collection of leaf material for TP1 (11 dpi), and TP2 (35 dpi) without uprooting - Destructive harvest for TP3 (50 dpi) with collection of leaf and root material - Leaf discs of 10 mm diameter - Root sampling (< 0.2 g) - Visual scoring for TP3

Table 2.5: Experimental outline for end-point disease screens

Experiment	Genotype	Treatment	Soil Type	Pot size	Environmental Conditions	Watering	Harvest + Sampling
End-point screen 1	33 (3 biological replicates)	- Control (H_2O) - 6.25 x 10^5 spores/ml - 50 ml	- Levington M3 compost - 1100 grams/ pot	Medium: 9.5 x 9.5 x 11.5 cm	- Semi-controlled greenhouse - 20 ± 2°C day/ 18 ± 2°C night - 18h photoperiod - 40-55% day/night humidity - 200-400 µmol PAR m-² x s-¹ irradiance	- Manual - 0-20 dpi: bottom - 21-51 dpi: alternated	- Destructive harvest at 51 dpi - Visual scoring (end-point) - Photographs of end-point phenotype - Root sampling (< 0.2 g) - Biomass (end-point)
End-point screen 2	30 (3 biological replicates)						- Destructive harvest at 51 dpi - Visual scoring (end-point) - Photographs of end-point phenotype - Root sampling (< 0.2 g) - Biomass (end-point)

2.4. PHENOMICS

2.4.1. THERMAL IMAGING – PROCEDURE, DATA ACQUISITION, AND ANALYSIS

A heated screen (Bio Green Heating Mat (HMT-A 60 x 120 cm, 140 W) with black and corrugated polythene sheeting from Jewsons) was placed 1 m behind the conveyor belt in the greenhouse. Plants passed by individually on the conveyor in front of the uniformly heated background (approx. 25-30°C), and thermal images were taken using either a VarioCAM HiRes 640x480 (Jenoptik AG, Germany, spectral range 7.5- 14 μm) or a ThermaCAM SC660 Wes (FLIR Systems AB) camera in a 45° angle.

Two methods were used to extract leaf temperature data from the images: an automated (figure 2.1 A) and a manual approach (figure 2.1 B). For the automated approach (threshold method), plant positions were estimated (horizontal black line) and a temperature threshold set. The former was used to remove all pixel values corresponding to pot + conveyor at the picture bottom, the latter to segment plant pixel values from the heated background. For the manual approach (spot method), 25 equally sized regions of interest (ROI) were manually placed on leaf images, and the average temperatures calculated. The automated approach was more rapid, but excluded data from leaves that were positioned below the horizontal black line. R studio was used for data analysis. The work-flow is displayed in figure 2.2.

For comparison of camera performances, thermal images of winter oilseed rape Temple from both thermal cameras were analysed according to the spot method (see chapter 3). The output data is seen in figure 2.1 C. The results showed a good correlation (93.7%), and regression analysis gave a slope close to 1 with an intercept of +1.2. The VarioCAM HiRes was used for further experiments.
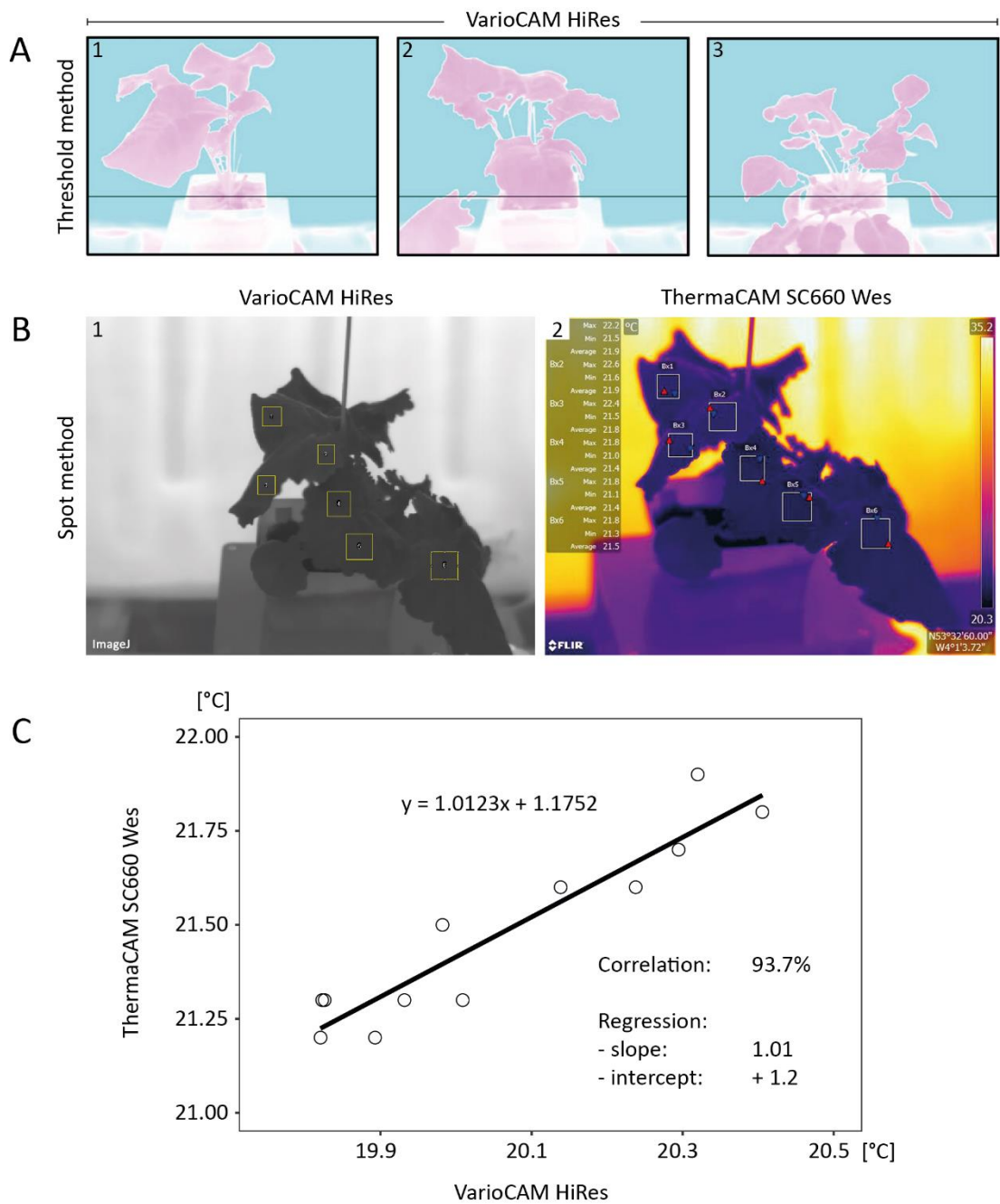
Figure 2.1: Approaches of thermal data extraction and comparison of camera models
|A| Three images of oilseed rape plants with varying leaf positions imaged using VarioCAM HiRes and the baseline position for automated thermal data extraction shown as solid black line |B| Image of oilseed rape plants with regions of interests for manual thermal data extraction using ImageJ and FLIR software |C| Linear regression of spot measurement results from images using VarioCAM HiRes and ThermaCAM SC660 Wes.
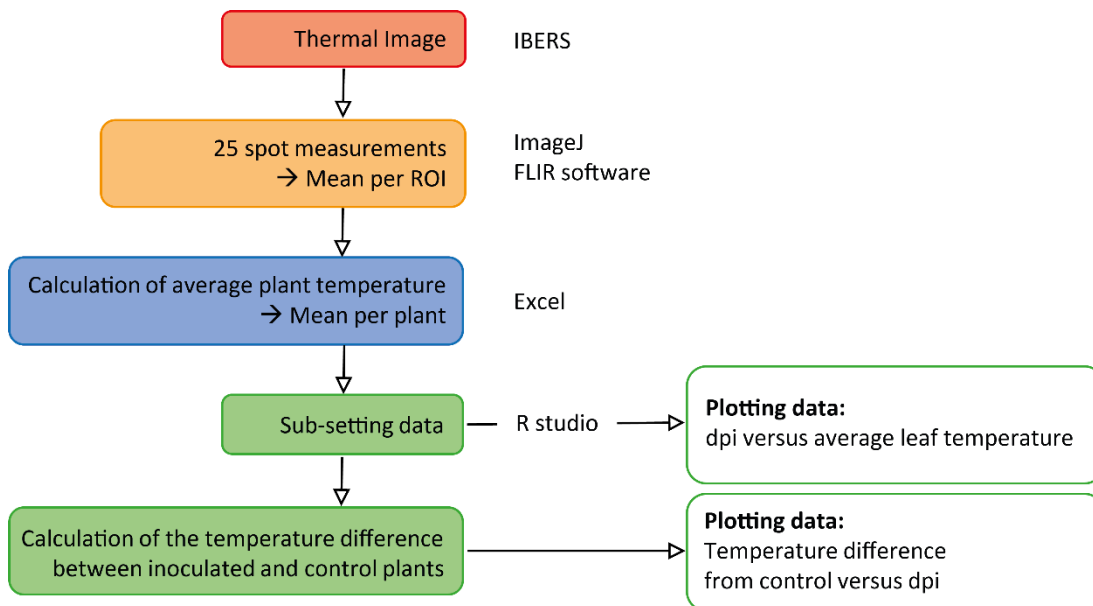
Figure 2.2: Work-flow of thermal image analysis following the manual spot method

2.4.2. PLANT WATER USE DURING DISEASE DEVELOPMENT

2.4.2.1. AUTOMATED APPROACH - DATA ACQUISITION AND ANALYSIS

Plant water use at IBERS was monitored daily using an automated pot weighing system. For system calibration, plant pots were filled with 1100 grams of compost, and watered until 100% saturate. The weight corresponding to 80% saturation was then calculated, and used as reference value for automated watering. The watering system could water from above, below (into a tray) or both.

Plant pots with seedlings were weighed daily before and after watering with water use calculated as the difference between the two values on consecutive days (figure 2.3 A) Water was then added to return the total pot weight to the reference value (figure 2.3 B). The approach turned out to be problematic since the use of a fixed reference point did not account for increasing plant biomass during the experiment. As the biomass increased, the soil moisture content decreased. To compensate for this, the biomass increase over time was estimated based on area and height data, and the watering reference point modified to adapt to plant growth (figure 2.3 C). Water evaporation from the soil was measured using soil-only pots evenly distributed in the greenhouse.

Water use data was analysed in R studio. Daily water use measurements were smoothed using a rolling average with a central 7 day window to remove noise and decrease data complexity. The maximum use was calculated as the average of the 6 largest values. The time taken to reach this maximum was determined when water use approached 90% of the maximum value (figure 2.4 A). Cumulative water use was also calculated (figure 2.4 B). Figure 2.5 summarizes the work-flow.
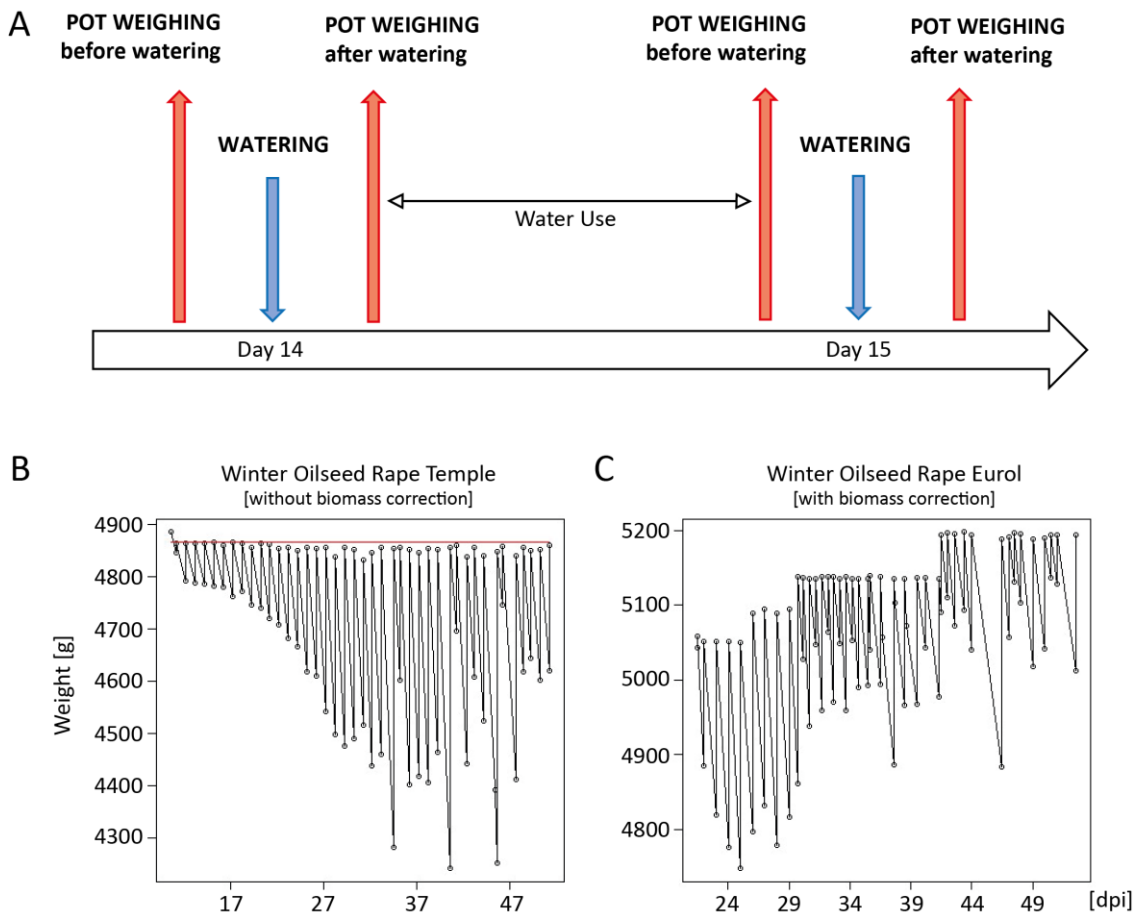
Figure 2.3: Automated watering at IBERS

|A| Watering scheme at IBERS |B| Watering RAW data shows repetitive procedure of pot weight before and after watering, always returning to a fixed reference value (solid red line) |C| Watering RAW data with reference value adjusted to increased plant biomass during the experiment.
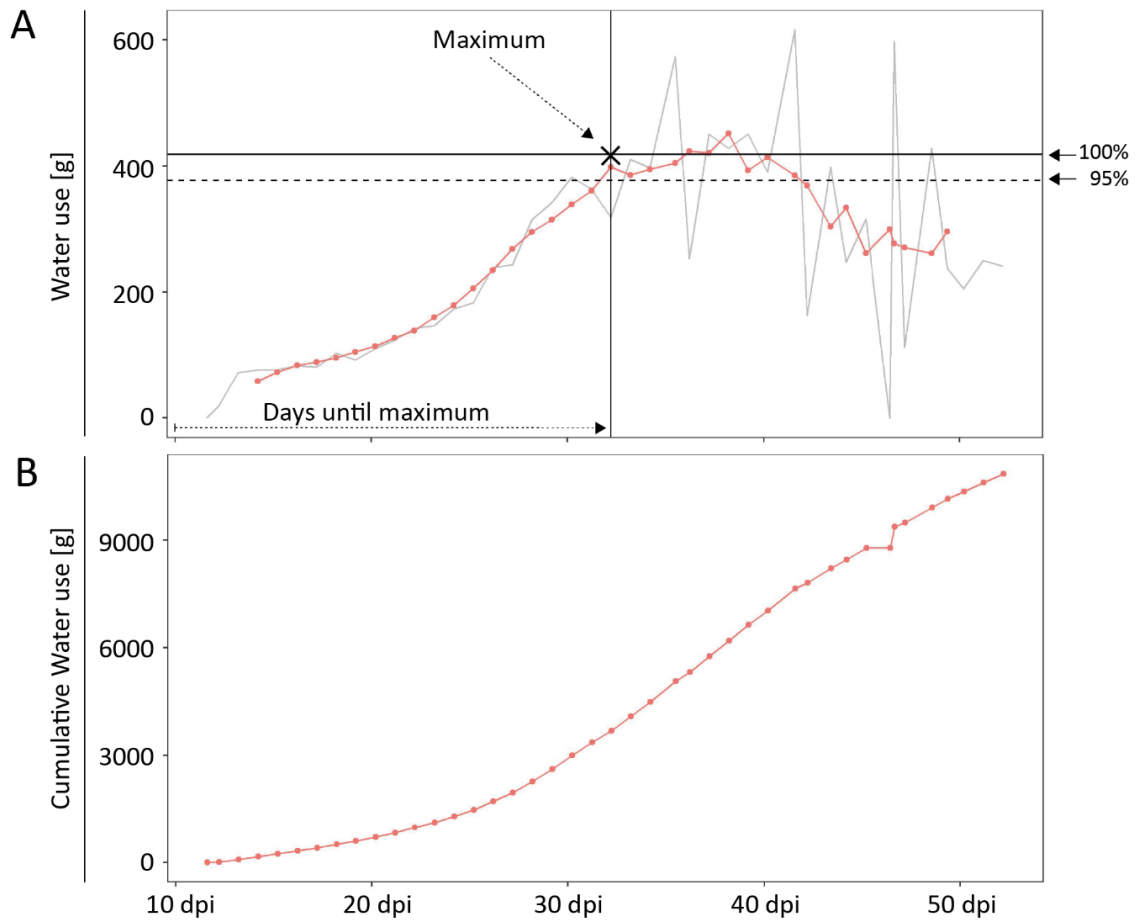
Figure 2.4: Example for water use analysis

|A| Water use of oilseed rape Temple (uninfected) measured using the automated watering system (grey line). A rolling average (central 7 day window) is shown as connected red dots, the maximum value with 10% tolerance as solid and dashed horizontal black lines, and the time taken to reach the maximum as solid vertical black line |B| Cumulative water use
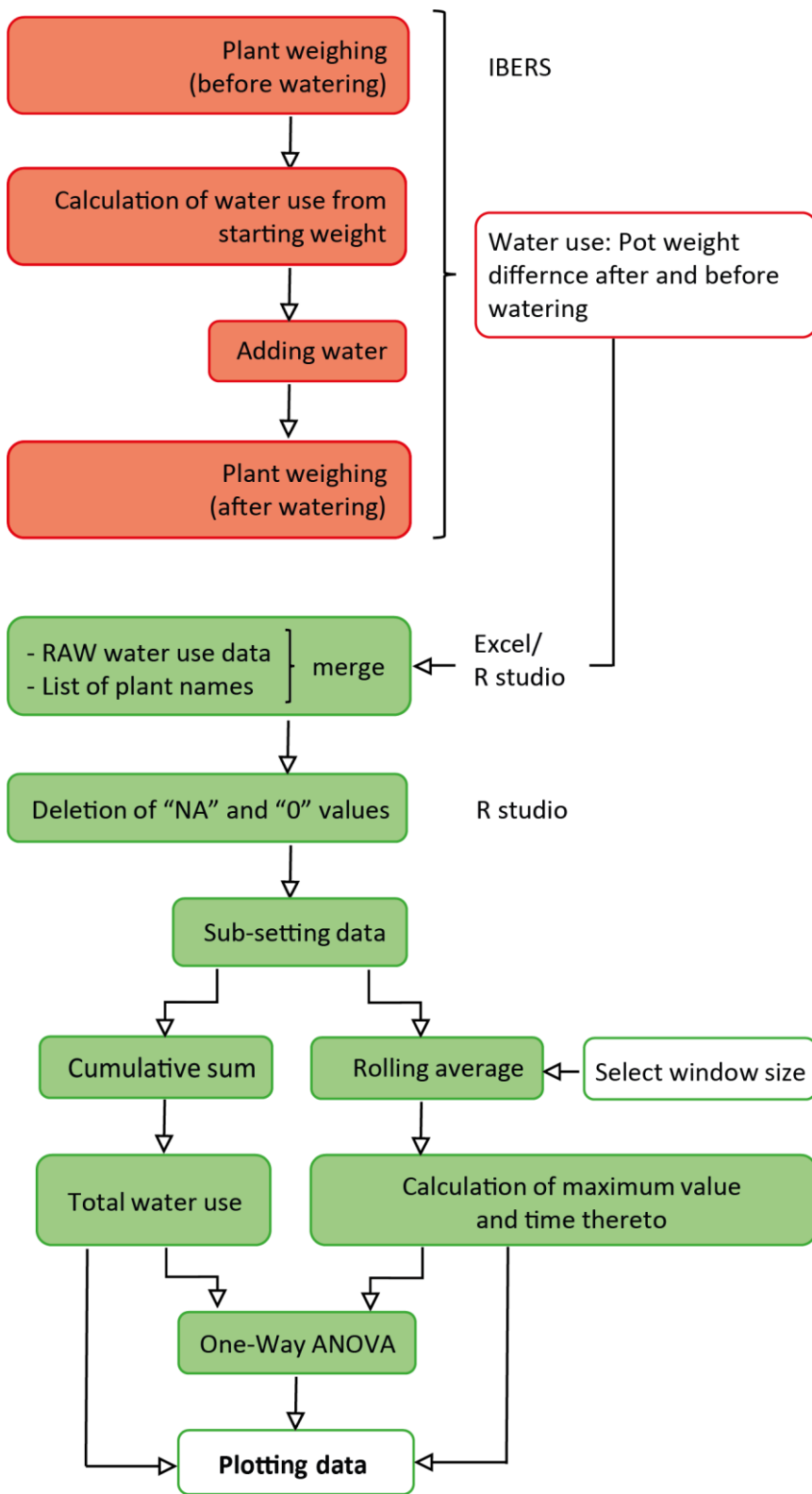
Figure 2.5: Work-flow for water use analysis (IBERS)

2.4.2.2. MANUAL APPROACH - DATA ACQUISITION AND ANALYSIS

Pots were saturated with water by standing in a tray for 60 min. Excess water was then allowed to drain for 30 min. The pots were weighed to give the saturated soil + pot + plant weight. Pots were weighed again after 24 h (water + soil + pot + plant weight) and the difference taken as the water use (figure 2.6). The plant biomass gain in this period was negligible.

Data was investigated in R studio by calculating end-point and cumulative water use, and testing for statistical significance.
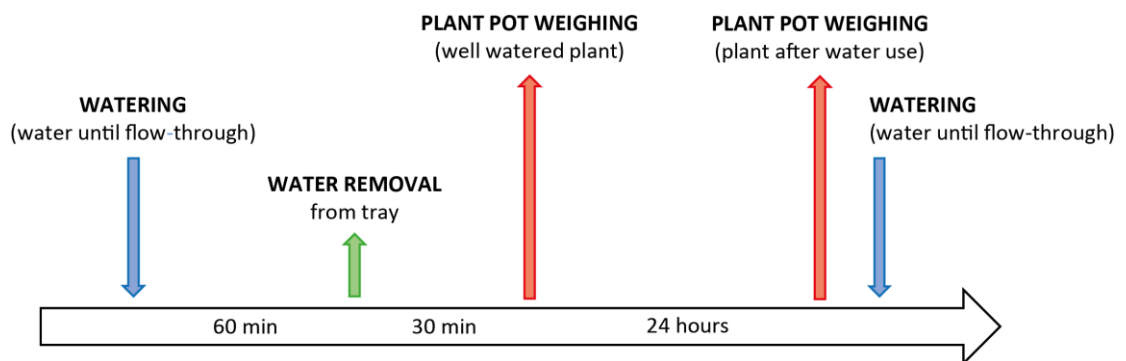
Figure 2.6: Manual watering scheme (AWEC)

2.4.3. PLANT AREA AND HEIGHT MEASUREMENTS –

PROCEDURE, DATA ACQUISITION, AND ANALYSIS

RGB pictures were taken daily from two angles (see table 2.2) of each plant, and both the plant height and average area measured. A rolling average, maximum value and time to reach the maximum value were calculated as described in section 2.4.2. In most cases the area reached a maximum and then declined. If the plants were still growing at the end of the experiment, the final area value was used as the maximum value (figure 2.7). One-way-ANOVA was implemented to compare the impact of treatment on different cultivars. Figure 2.8 shows the work-flow.
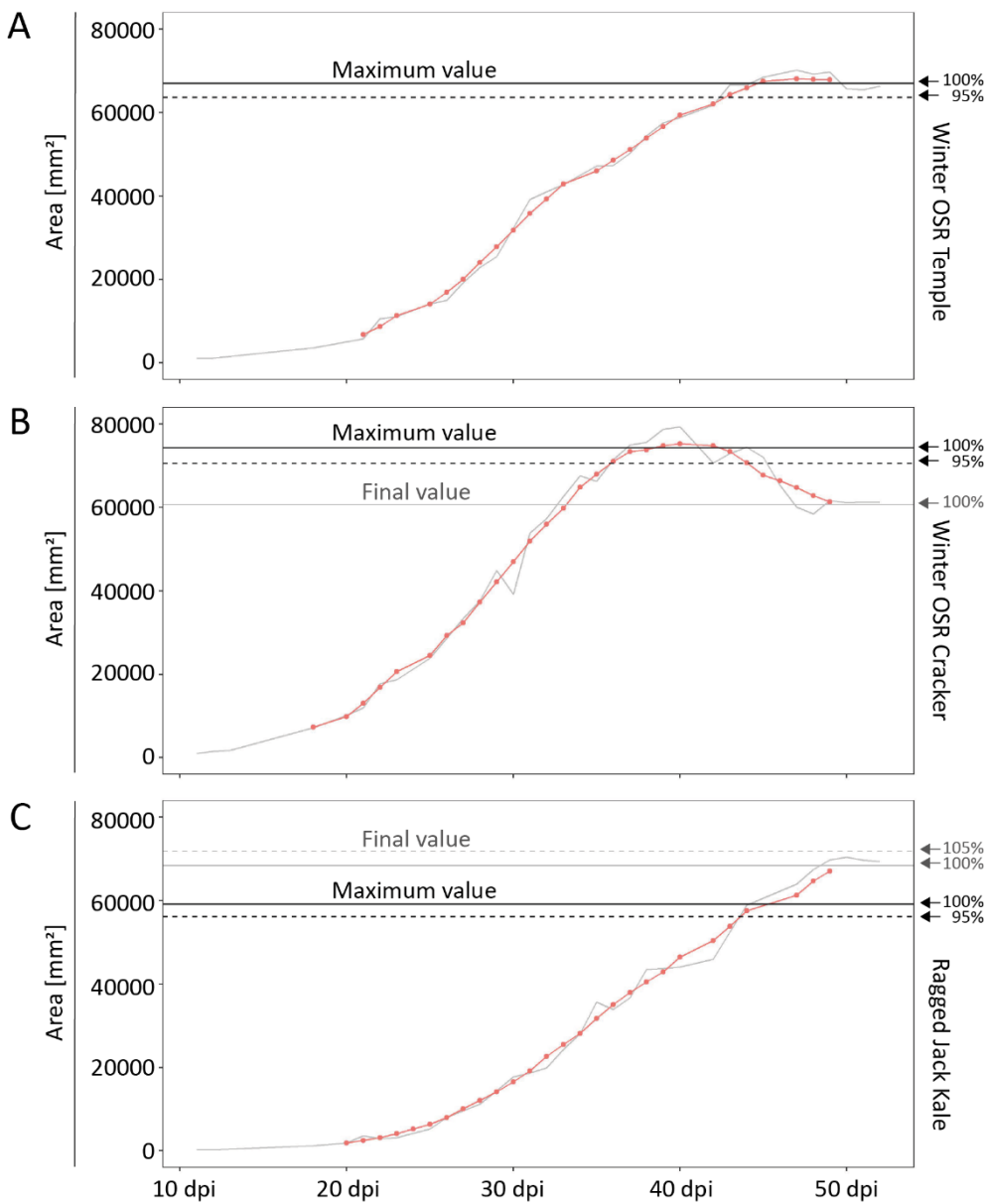
Figure 2.7: Example for area data analysis [Legend on next page]

[Legend to figure 2.7]

|A|-|C| Area data of two oilseed rape varieties and one Kale cultivar (grey line) measured using RGB images. A rolling average (central 7 day window) is shown as connected red dots. Final and maximum value are indicated as solid horizontal lines of grey and black colour, respectively. Dashed horizontal lines represent the area when values approached 95% of the maximum value (black), or when values were 1-5% bigger than the final value (grey). Final and maximum area data was picked individually for each plant depending on the growth status on harvest day.

|A| Area data of oilseed rape Temple (uninfected). RAW data shows a curve with plateau due to stop in plant growth at the end of the experiment: maximum value = final value. The maximum value was used for statistical analysis |B| Area data of oilseed rape Cracker (uninfected). RAW data displays a plateau with subsequent decrease due to natural leaf wilting before the end of the experiment: maximum value > final value. The maximum value was used for statistical analysis. |C| Area data of Ragged Jack Kale (uninfected). RAW data illustrates a continuing area increase without plateau due to ongoing plant growth on harvest day: maximum value < final value. The final value was used for statistical analysis.
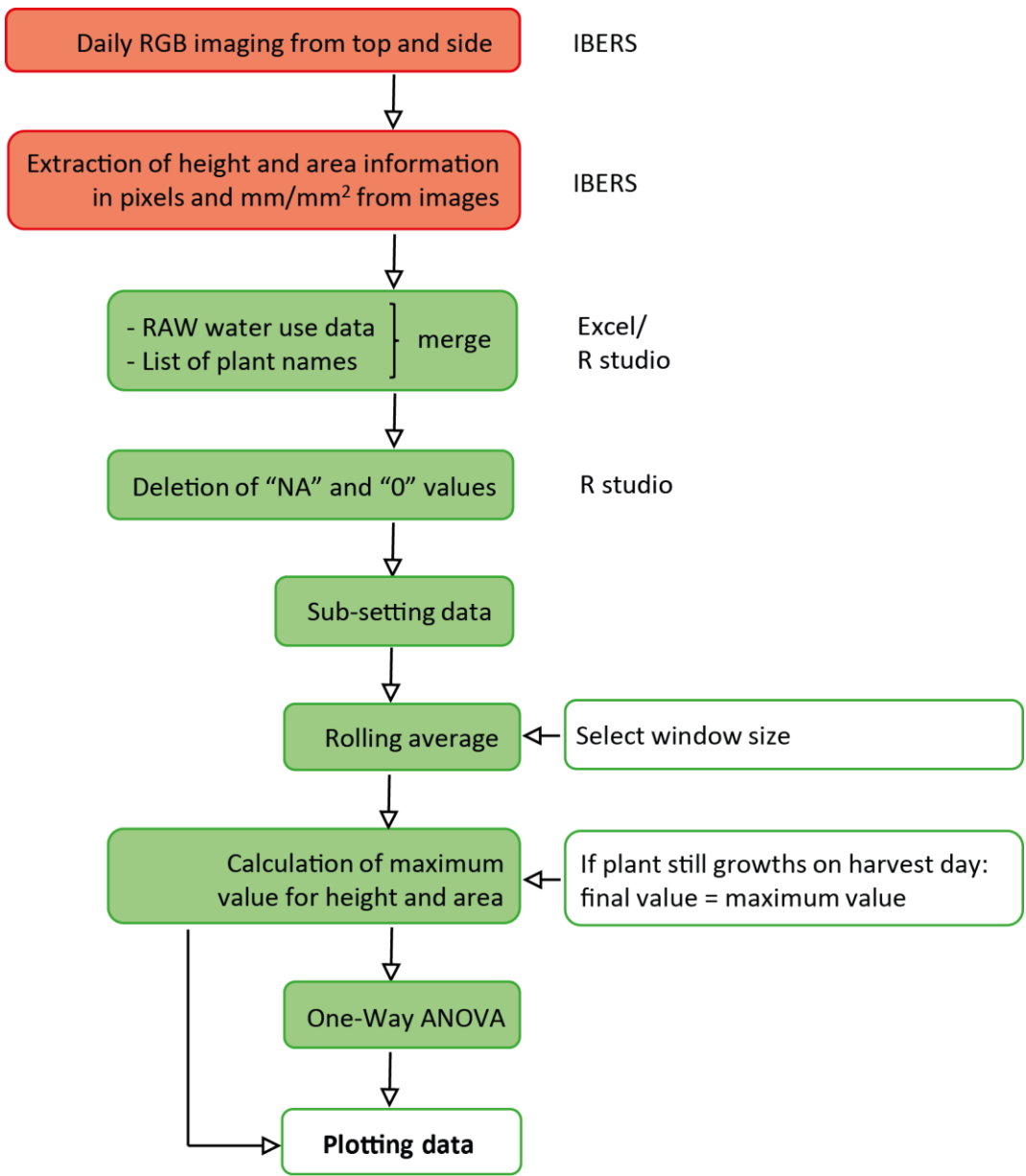
Figure 2.8: Work-flow for area and height data analysis (IBERS)

2.5. END-POINT DISEASE SCREENS

2.5.1. SAMPLE HOMOGENISATION AND DNA EXTRACTION

Mortar and pestle versus bead-beater homogenisation with 2 stainless-steel beads (3 mm diameter, Atlas ball + bearing CO. LTD.) was tested for optimal sample pulverization prior to DNA extraction. Five μl of DNA extracts were confirmed by gel electrophoresis on 1% agarose gels stained with ethidium bromide (figure 2.9). Bead-beater QIAGEN TissueLyser II yielded little or no genomic DNA (figure 2.9 A) compared to grindings using mortar and pestle (figure 2.9 B). As molecular analysis required large numbers of samples to be processed, further development of the bead-beater method was tried. Using a different model (MP FastPrep-24™ 5G), genomic DNA could be obtained from both freeze-dried (figure 2.9 C) and snap-frozen (figure 2.9 D) plant material. However, samples with reduced water content pulverised quicker and better.

DNA extraction was performed using a modified CTAB-based protocol originally published in [110]. Unless stated, all centrifugation steps were performed for 10 minutes at 12,000 x g and 4°C (SANYO HAWK 15/05 Refrigerated), and all chemicals purchased from Sigma-Aldrich and Fisher Scientific. For DNA extraction, the homogenate was mixed with 1.0 ml pre-cooled CTAB-free buffer[2] and 30 μl 2-Mercaptoethanol, then incubated on ice (10 min) and centrifuged. After centrifugation the supernatant was discarded, and the pellet mixed with 800 μl pre-heated (65°C) CTAB-buffer[3], 24 μl 2-Mercaptoethanol, and 6 μl RNase (30U/mg). Subsequently, the mixture was incubated in a heating block for 50 minutes at 65°C, with sample inversion every 10 minutes. After centrifugation, the supernatant was transferred into a new reaction tube, mixed with an equal volume of chloroform: isoamyl alcohol (24:1) via shaker incubation (10 minutes, room temperature) (Vortex-Genie 2, MO BIO Laboratories, Inc.), and centrifuged again. The upper aqueous phase was then transferred into a new reaction tube to repeat the chloroform: isoamyl alcohol (24:1) treatment. Thereafter, 2/3 volume pre-cooled isopropanol was added to the upper aqueous phase for DNA precipitation over-night (-20°C). After precipitation all samples were centrifuged, and the pellet washed with 3 ethanol washing steps (100%, 75%, and 70% Ethanol). DNA was then dried at room temperature and dissolved in 50 μl 1x TE-buffer[4] or nuclease free water.

---

[2] 2% Polyvinylpyrollidone (w/v), 0.25M NaCl (v/v), 0.2M Tris-HCl (v/v), 0.05M EDTA (v/v), pH 8.0
[3] 2% Polyvinylpyrollidone (w/v), 1.4M NaCl (v/v), 0.1M Tris-HCl (v/v), 0.02M EDTA (v/v), 2% CTAB (w/v), pH 8.0
[4] 0.01M Tris (v/v), 0.001M EDTA (v/v), pH 8.0

Figure 2.9: Sample homogenisation methods

|A|-|D| 1% agarose gel pictures of 5 µl genomic DNA after application of different homogenisation methods: |A| Homogenisation of snap-frozen root samples using bead-beater model QIAGEN TissueLyser II at 27 Hertz for 2 x 15 minutes prior to DNA extraction. No genomic DNA is visible |B| Homogenisation of snap-frozen root samples using mortar and pestle achieved good results |C| Homogenisation of freeze-dried root samples using bead-beater model MP FastPrep-24™ 5G at 10 meter per second for 2x 30 seconds prior to DNA extraction obtained genomic DNA |D| Homogenisation of snap-frozen root samples using the same bead-beater model and program achieved similar results.

2.5.2. DETERMINATION OF DNA CONCENTRATION

DNA concentration was measured using Quant-iT Pico Green dsDNA quantitation reagent (Molecular probes by life technologies), and fluorometry with excitation at 485 nm and emission at 545 nm (Fluorimeter BMG FLUOstar optima). Two µl of undiluted DNA samples were mixed with 98 µl 1x TE buffer pH 7.5 and 100 µl of a 200-fold diluted Pico Green solution. A calibration standard (0, 10, 25, 50, 75, and 100 ng/µl) was prepared from herring sperm DNA (Sigma-Aldrich), and quantified via photo-spectrometry. After quantification, all DNA samples were diluted to 10 ng/µl and stored at -20°C until required.

2.5.3. PB-PRIMER DESIGN

Quantification of *P. brassicae* by quantitative real-time polymerase chain reaction (qRT-PCR) required a primer pair that amplified a unique sequence conserved in the genome of *P. brassicae* not present in Brassicas or contaminating microbes. Ribosomal RNA genes were considered as a suitable amplicon (high sequence stability and specificity) to distinguish between pathogen *P. brassicae* and Brassica host plant. Eukaryotes contain 80S ribosomes which consist of a small (40S) and a large (60S) subunit. While the small subunit is composed of an 18S RNA-gene (1900 nucleotides) and 33 proteins, the large subunit contains a 5.8S RNA- (160 nucleotides), a 28S RNA- (4700 nucleotides), 5S RNA-gene (120 nucleotides) and 46 proteins. The genes of both subunits except for the 5S rRNA are organized in a cluster with intergenic spacer (IGS): one external transcribed spacer (ETS) at the cluster's starting point, and two internal transcribed spacer (ITS) in between (ITS1, ITS2). Each cluster is a tandem repeat, and separated by non-transcribed cluster (NTS) (figure 2.10).

All published *P. brassicae* rRNA gene cluster sequences were identified using the NCBI database, aligned with the program MEGA6.06, and checked for areas with little sequence variation. The longest and most complete sequence (Japanese GenBank Accession Number AB526843) was eventually taken as reference for primer design using the online program Primer3Plus. The designed primer pair covers the 5.8S rRNA gene of *P. brassicae* flanked with partial ITS1 and ITS2, and amplifies a product of 216 bp length (figure 2.10) Each primer contains one positional sequence variation (IUPAC code) to ensure the application for several pathotypes without losing much specificity. Primer and product sequence were aligned using BLASTN against the NCBI database – no matches with available Brassica genomes and other *P. brassicae* sequences were found. Recently (2 years after primer design), the GenBank Accession Number AB526843 was removed from the NCBI data base due to its chimeric nature. It was found, that approximately 75% of the large ribosomal subunit contained another Cercozoan sequence, most likely derived from non-parasitic Glissomonadida [111]. However, Pb-primer and amplicon sequences still

aligned correctly with the 5.8S rRNA sequences of *P. brassicae* in the NCBI data base (i.e. 100% match with KX430467-3).

2.5.4. PB-PRIMER TEST

The annealing temperature of Pb-ITS1-F and Pb-ITS2-R were obtained from a gradient PCR ranging from 56°C to 60°C. Subsequently, the primer pair was tested for specificity in a conventional 3-step-PCR. For both PCRs, 3 µl of DNA extracts of clubroot infected Chinese Cabbage Wong Bok [5] were amplified using the PCR kit from Bioline. The reaction contained 2.5 U/µl Taq-polymerase, supplier PCR buffer (1x final concentration), 2.5 mM $MgCl_2$, 0.2 mM dNTPs, and 0.2 µmol of each primer in a total volume of 50 µl. PCRs were performed with an initial incubation at 95°C for 5 minutes, then 30 cycles of 95°C, 60-56°C/ 59°C, and 72°C each for 30 seconds with a final extension step of 5 minutes at 72°C. PCR products (5 µl) were confirmed by gel electrophoresis on 2% agarose gels stained with ethidium bromide (figure 2.11).

---

[5] Cultivar from preliminary phenomics experiment at AWEC described in chapter 3. Manual homogenisation and CTAB-DNA extraction according to section 2.5.1.
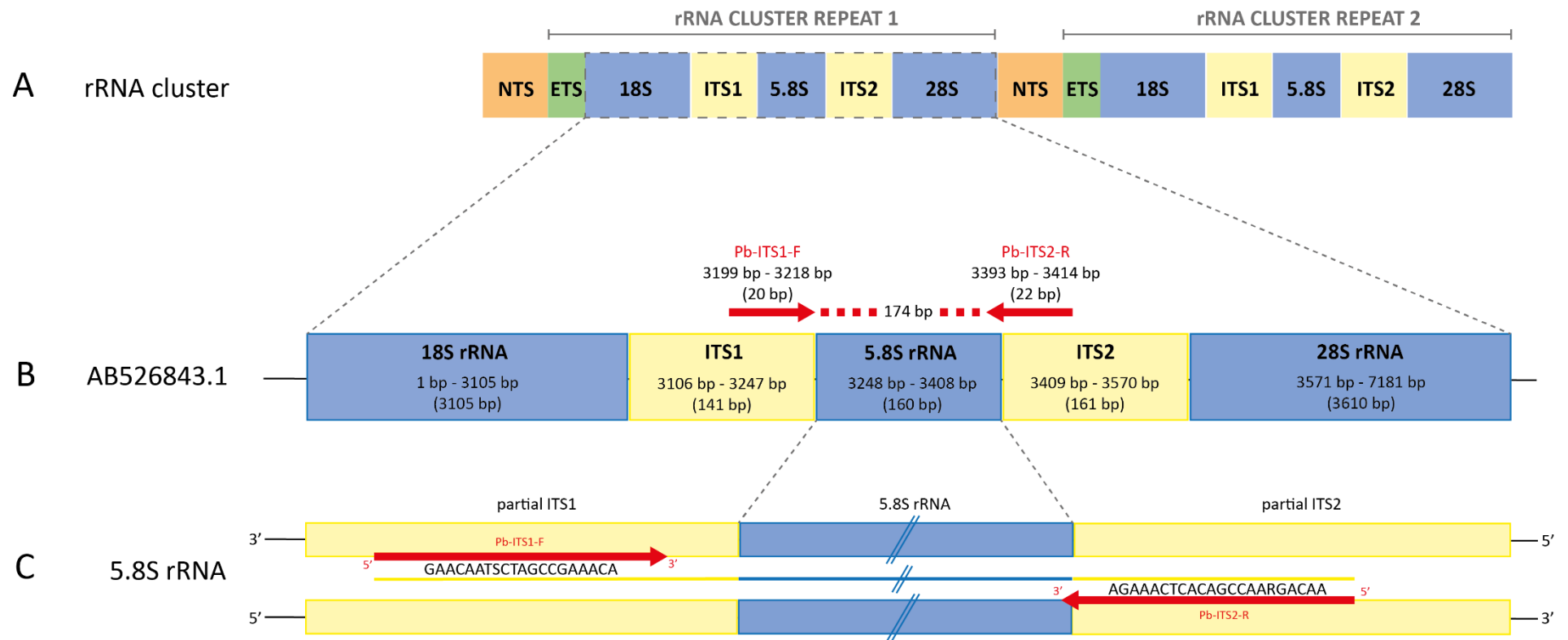
Figure 2.10: PB-primer pair alignment based on the gene sequence AB526843.1

|A| Ribosomal RNA gene cluster of eukaryotes. Sequences are organised in tandem-repeated units. One cluster unit contains external transcribed spacer (ETS, green), 18S rRNA (blue), internal transcribed spacer 1 (ITS1, yellow), 5.8S rRNA (blue), internal transcribed spacer 2 (ITS2, yellow), and 28S rRNA (blue). Units are connected via non-transcribed spacers (NTS, orange) |B| 80S cluster of the Japanese isolate NGY (AB526843.1) used as reference for Pb-primer design. |C| 5.8S rRNA gene (blue) with partial ITS 1 and 2 (yellow), amplified by Pb primer pair (red arrows).

Primer name	Characteristics
Pb-ITS1-F	5'-GAACCATSCTAGCCGAAACA-3' (20 bp) Tm: 60.1°C, GC: 50%, IUPAC nucleotide code S: G or C
Pb-ITS2-R	5'-AACAGRAACCGACACTCAAAGA-3' (22 bp) Tm: 58.9°C, GC: 40.9%, IUPAC nucleotide code R: A or G

A

2% Agarose gel in 1x TAE stained with EtBr
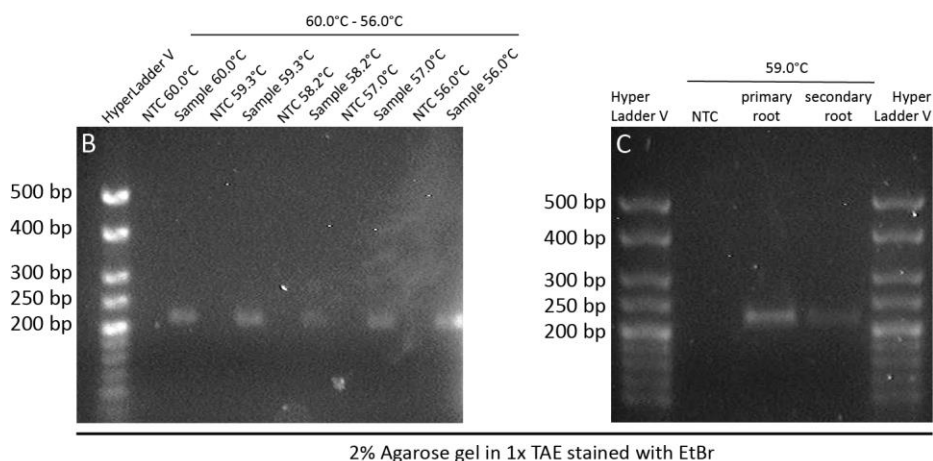
D

PCR step	Temperature	Time	Number of cycles
Initial denaturation	95 °C	5 min	1
Denaturation	95 °C	30 sec	
Annealing	59 °C	30 sec	30
Extension	72 °C	30 sec	
Final extension	72 °C	5 min	1

E

Component	Volume/tube	Reaction concentration
10 x PCR buffer (Bioline)	5 µl	1 x PCR buffer (Bioline)
50 mM MgCl₂ (Bioline)	2.5 µl	2.5 mM MgCl₂ (Bioline)
10 mM dNTPs	1 µl	0.2 mM dNTPs
10 µM Forward Primer	1 µl	0.2 µM Forward Primer
10 µM Reverse Primer	1 µl	0.2 µM Reverse Primer
Template DNA	3 µl	
5 U/ µl Taq polymerase (Bioline)	0.5 µl	2.5 U/ µl Taq polymerase (Bioline)
dH₂O (nuclease free, Ambion)	36 µl	

Figure 2.11: Pb-primer test with DNA from clubroot infected Chinese Cabbage Wong Bok

[Legend on next page]

[Legend to figure 2.11]

|A| Pb-primer characteristics |B| 2% agarose gel (80 V, 1.5 h) of control (no template) and amplified DNA (5 µl) from a gradient PCR with Pb primers (annealing temperature: 56-60°C) |C| 2% agarose gel (80 V, 1.5 h) of amplicons (5 µl) from a selected PCR (annealing temperature: 59°C) to test Pb-primer specificity. The amplicon is in a band at 216 bp |D| PCR condition |E| Mix of PCR components for a total volume of 50 µl using the PCR kit from Bioline.

2.5.5. PREPARATION OF DNA STANDARD FOR qRT-PCR

2.5.5.1. CLONING OF PB-GENE INTO pGEM-T-EASY VECTOR

Genomic DNA of primary root samples from clubroot infected Chinese Cabbage Wong Bok was amplified with Pb-primers (see section 2.5.3). Amplicons were then purified using QIAquick PCR purification kit (QIAGEN), following the manufacturer's instructions. Thereafter, 1 µl purified PCR product (approx. 30 ng DNA) was ligated into 1 µl pGEM-T-easy using 1 µl T4 DNA Ligase (Bioline) with 5 µl of the supplier Ligation buffer in a total reaction volume of 10 µl. The ligation was performed overnight at 4°C with positive and negative control, and terminated next day with enzyme inactivation at 65°C (heat-block) for 10 min. Subsequently, 2 µl of each ligation product was transformed into 50 µl competent *E.coli* DH5α cells via heat-shock (50 sec incubation at 42°C, water bath). Bacteria were then cultured on sterile LB[amp] medium[6] with X-gal solution[7], and incubated overnight at 37°C. White colonies were picked, and cultivated in 5 ml sterile liquid LB[amp] medium[8] overnight at 37°C for a mini-prep using QIAprep Spin Miniprep kit (QIAGEN), following the manufacturer's instructions. The whole cloning procedure is summarized in figure 2.12 and further explained in 2.5.5.2.

---

[6] 0.4 g Tryptone + 0.2 g yeast extract + 0.2 g NaCl + 0.6 g agar + add 40 ml dH$_2$0 + pH 7 (NaOH) + 40 µl Amp[100]

[7] X-gal stock: 100 mg X-gal + 2 ml DMF; working solution: 50 µl dH$_2$O + 20 µl X-gal stock

[8] 1 g Tryptone + 0.5 g yeast extract + 0.5 g NaCl + add 100 ml dH$_2$0 + pH 7.0 (NaOH) + 100 µl Amp[100]
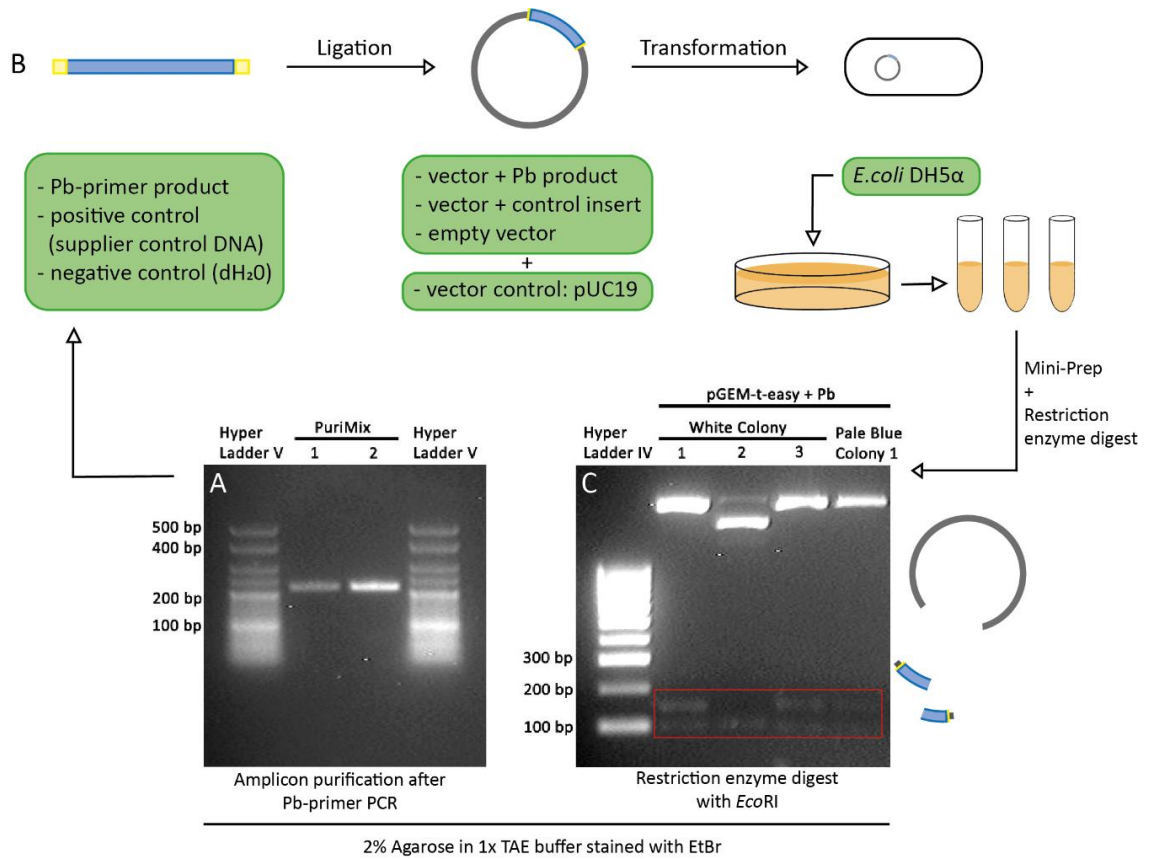
Figure 2.12: Cloning overview I

|A| 2% agarose gel (80 V, 1.5h) with 5 µl of purified Pb-amplicons after conventional PCR with Pb-primer |B| Illustration of cloning steps: Ligation of Pb-amplicon into pGEM-t-easy, Pb-construct transformation into *E.coli* DH5α, bacteria cultivation in solid and liquid LB^{Amp} medium, Pb-construct extraction (mini-prep), and restriction enzyme digest for insert removal |C| 2% agarose gel (80 V, 1.5 h) with 5 µl of *Eco*RI restriction enzyme digest showed 3 fragment, matching the virtual cloning result: 2997, 138, and 98 bp.

2.5.5.2. INSERT CONFIRMATION THROUGH RESTRICTION ENZYME DIGEST AND SEQUENCING

An *Eco*RI restriction enzyme digest was conducted for insert confirmation. The multiple cloning side (MCS) of pGEM-t-easy contains two *Eco*RI restriction sides (figure 2.13 A); the Pb-insert a third one (figure 2.13 B and C). Fragment sizes of 2997, 138, and 98 bp were expected using the virtual digest function of Serial Cloner V2.5 software (figure 2.13 D). For *Eco*RI digest, 2 µl of plasmid-DNA was mixed with 0.5 µl *Eco*RI (Bioline), 1.5 µl reaction buffer H, and 0.15 µl BSA buffer in a total reaction volume of 15 µl. The mix was then incubated for 1h at 37°C with subsequent enzyme inactivation at 65°C for 20 min. Thereafter, gel electrophoresis was performed to confirm the cloning success (figure 2.12 C).

Cloned sequences (*E.coli* DH5α colony 1-3) were then sent to the Core Genomic Facility Sheffield for sequencing with T7 and SP6 primer (figure 2.14 A). Sequence analysis was performed by aligning pGEM-t-easy sequence and the expected insert sequence with cloned sequences using BioEdit software and online NCBI blast. Cloned sequences for colony 3 aligned 99% in reversed orientation with the expected insert sequence and the MCS of pGEM-t-easy.
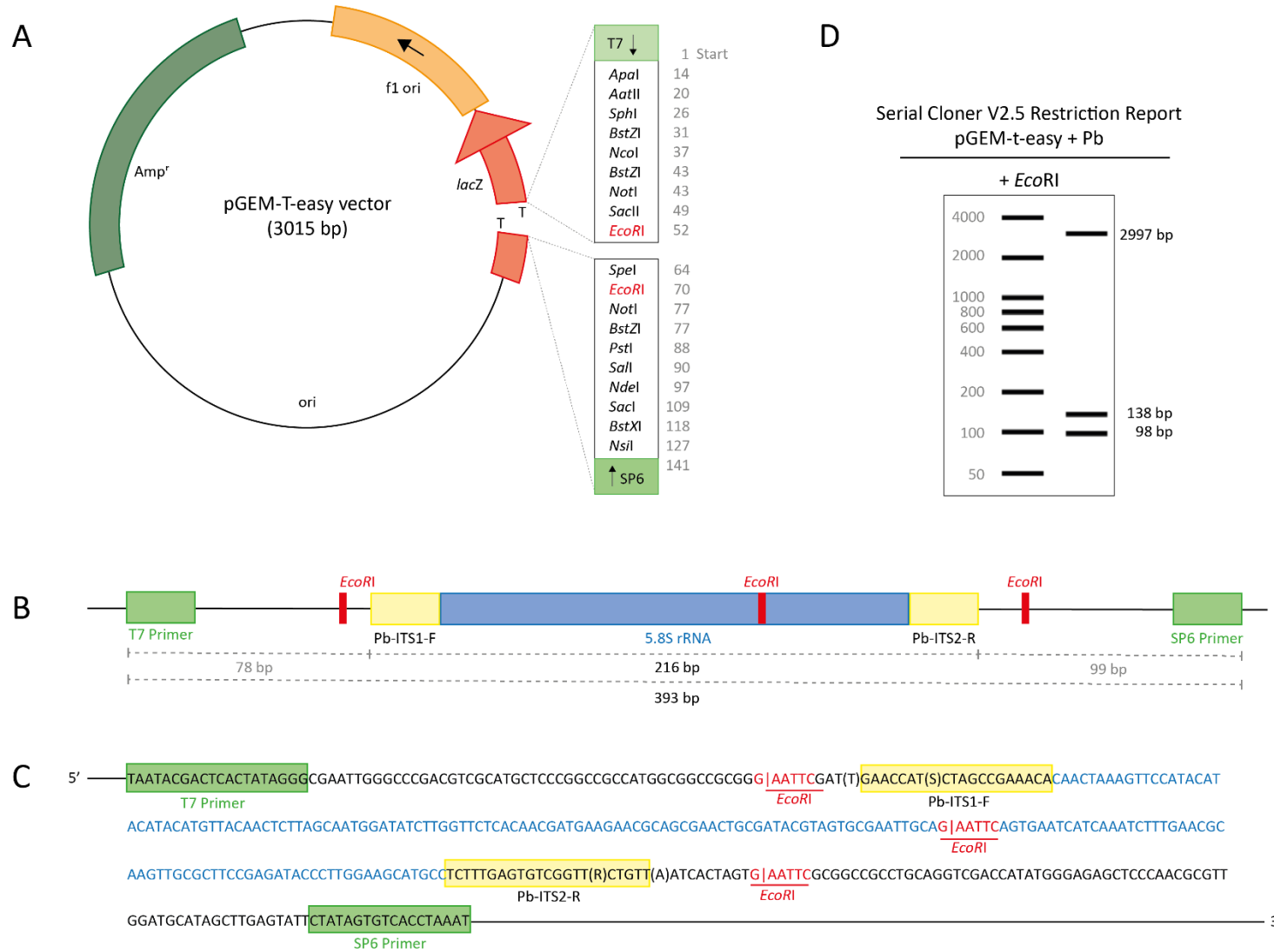
Figure 2.13: Cloning overview II

|A| Empty vector pGEM-t-easy with all restriction sides within the multiple cloning side (MCS). *Eco*RI is highlighted in red

|B|+|C| Overview and theoretical nucleotide sequences of the MCS of pGEM-t-easy+Pb. The Pb-insert is shown in blue, Pb-primer in yellow, SP6 and T7 primer in green, and all 3 *Eco*RI restriction sides in red

|D| Virtual restriction report for pGEM-t-easy+Pb using *Eco*RI

2.5.5.3. INSERT AMPLIFICATION USING T7 AND SP6 PRIMER

Circular (supercoiled plasmid) and linear DNA fragments had different take-off times during qRT-PCRs[9]. For linearisation, MCS + Pb of pGEM-t-easy were amplified with T7 and SP6 primer (figure 2.14 A). The PCR reaction contained 0.025 U/µl Taq-polymerase (NEB), supplier PCR buffer (1x final concentration), 0.2 mM dNTPs, and 0.2 µmol of each primer in a total volume of 50 µl (figure 2.14 D). PCRs were performed with an initial incubation at 95°C for 5 minutes, then 30 cycles of 95°C, 45°C, and 72°C each for 30 seconds with a final extension step of 5 minutes at 72°C (figure 2.14 C). Subsequently, gel-electrophoresis was performed (figure 2.14 B) and the amplicon extracted from the 2% agarose gel using QIAquick Gel Extraction Kit (Qiagen) following the manufacturer's instructions (figure 2.15 A). During gel extraction only the longer (upper) amplicon was removed from the gel whilst ignoring the smaller contamination. The extracted amplicon was then tested via conventional PCR with Pb-ITS1-F and Pb-ITS2-R primer (figure 2.15 B).

Sp6/T7-amplicon concentration was measured via NanoDrop (Thermo Scientific NanoDrop 8000 Spectrophotometer), and the molecular weight of one copy calculated according to the DNA sequence (figure 2.13 C, figure 2.15 C). The molecular weight was then converted into nano-grams per copy to calculate the number of Sp6/T7-amplicons in the stock solution. Finally, a dilution series was prepared as DNA standard in qRT-PCRs: 10, 100, 1000, 1×10^4, 1×10^5, and 1×10^6 copies/µl.

---

[9] Data not shown. qRT-PCR machine overheated and switched off, only leaving a frozen computer screen showing an image of a partial run

Primer name	Characteristics
T7 primer	5'- TAATACGACTCACTATAGGG -3' (20 bp) Tm: 48.0°C, GC: 40%
SP6 primer	5'- ATTTAGGTGACACTATAG -3' (18 bp) Tm: 41.0°C, GC: 33%

B

2% Agarose gel in 1x TAE stained with EtBr
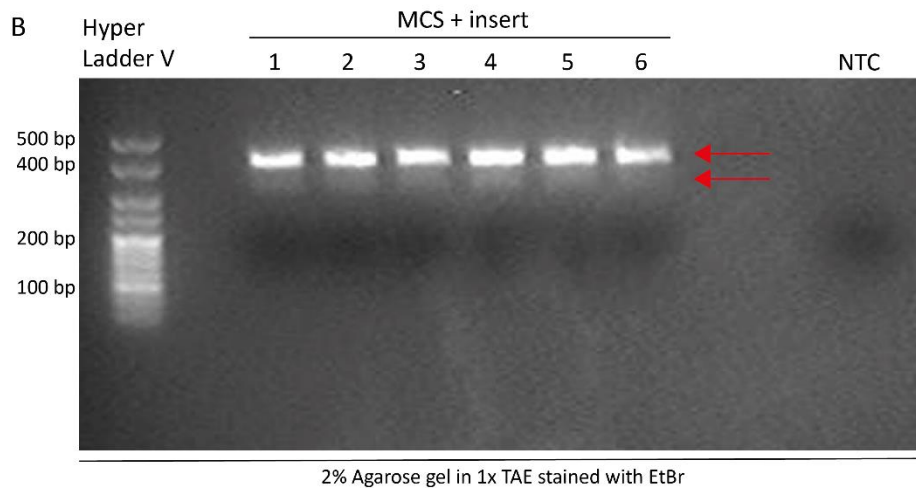
C

PCR step	Temperature	Time	Number of cycles
Initial denaturation	95 °C	5 min	1
Denaturation	95 °C	30 sec	
Annealing	45 °C	30 sec	30
Extension	72 °C	30 sec	
Final extension	72 °C	5 min	1

D

Component	Volume/tube	Reaction concentration
10 x PCR buffer (NEB)	5 µl	1 x PCR buffer (NEB)
10 mM dNTPs	1 µl	0.2 mM dNTPs
10 µM Forward Primer	1 µl	0.2 µM Forward Primer
10 µM Reverse Primer	1 µl	0.2 µM Reverse Primer
Template DNA (20 ng/µl)	1 µl	
5 U/ µl Taq polymerase (NEB)	0.25 µl	0.025 U/ µl Taq polymerase (NEB)
dH₂O (nuclease free, Ambion)	40.75 µl	

Figure 2.14: DNA standard preparation for the qRT-PCR – Part 1

|A| Characteristics of T7 and SP6 primer |B| 2% agarose gel (90 V, 70 min) of amplicons (50 µl) from a selected PCR with SP6 and T7 primer using pGEM-t-easy + Pb as template. Two amplicons are seen. The stronger band represents the expected amplicon with 393 bp, and was subsequently gel-extracted |C| PCR condition |D| Mix of PCR components for a total volume of 50 µl using the PCR kit from NEB.

Figure 2.15: DNA standard preparation for the qRT-PCR – Part 2

|A| 2% agarose gel (80 V, 1.5 h) of gel-extracted T7/SP6 amplicons (5 µl), showing a band at 393 bp |B| 2% agarose gel (80 V, 1.5 h) of PCR products (5 µl) amplified with the Pb-primer pair, showing an amplicon at 216 bp |C| Graphic of T7/SP6 amplicons alongside the molecular weight of the sequence.

2.5.6. qRT-PCR, DATA ACQUISITION AND ANALYSIS

All qRT-PCR reagents were pipetted using a robot (QIAgility with supplier software, QIAgen), and the reaction performed with a Rotor-Gene 6000 thermal cycler (Corbett Research) running with Rotor-Gene Q-Rex software (QIAgen). Each qRT-PCR reaction contained 0.8x Rotor-Gene SYBR® Green master mix (QIAgen, Cat No. 204074), and 0.5 µM primer mix (Pb-ITS1-F and Pb-ITS2-R) in a total volume of 10 µl (figure 2.16 A). As template 1 µl Brassica gDNA (5 ng/µl) or 1 µl clubroot ITS standard (10-100 million copies/µl) was used. qRT-PCRs were set-up as 3-step-PCRs with initial incubation at 95°C for 5 minutes, followed by 45 cycles of 95°C, 59°C, and 60°C each for 30 seconds (figure 2.16 B). Primer specificity was verified by assessing melting curves of PCR products. Total quantification of *P. brassicae* in clubroot/mock- inoculated Brassica cultivars was calculated by referring plant sample take-off values to a clubroot standard curve (take-off values versus LOG10 ITS copy numbers) (figure 2.16 C).

A

Component	Volume/tube	Reaction concentration
2x SYBRgreen master mix	4 µl	0.2x SYBRgreen master mix
2.5 µM Primer mix	2 µl	0.25 µM Primer mix
5 ng/µl gDNA	1 µl	0.5 ng gDNA
dH₂O	3 µl	

B

PCR step	Temperature	Time	Number of cycles
Initial denaturation	95 °C	5 min	1
Denaturation	95 °C	30 sec	
Annealing	59 °C	30 sec	45
Extension	60 °C	30 sec	

C
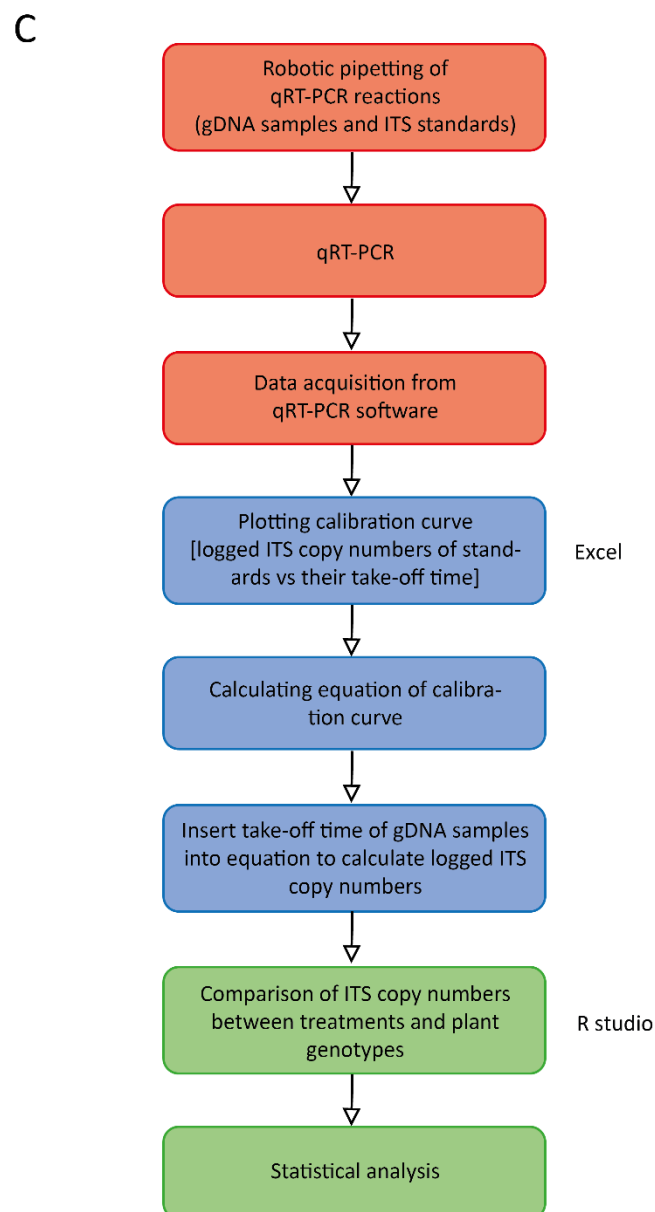
Figure 2.16: qRT-PCR reaction, program, and work-flow of data analysis

[Legend on next page]

[Legend to figure 2.16]

|A| Table of qRT-PCR components

|B| Table of qRT-PCR program

|C| Work-flow of qRT-PCR data analysis

2.6. METABOLOMICS

2.6.1. METABOLITE EXTRACTION FOR UNTARGETED PROFILING

Metabolite extraction followed the procedure of Pétriacq published in [112]. Freeze-dried leaf and root samples were weighed, put into 2.0 ml safe-lock reaction tubes containing 2 stainless-steel beads (3 mm diameter, Atlas ball + bearing CO. LTD.), and kept in liquid nitrogen before homogenisation. Samples were homogenised using a bead-beater (QIAGEN TissueLyser II) for 2 min at 30 Hz. Subsequently, 1 ml ice-cold extraction buffer[10] was added to the powder, and mixed (bead-beater, 2 min, 30 Hz) to obtain both polar and non-polar components. Samples were then centrifuged for 10 minutes at 17,000 x g and 4°C. The supernatant (supernatant 1, approx. 800 µl) was transferred into a new 2.0 ml safe-lock reaction tube, and the pellet (pellet 1) re-suspended in 500 µl extraction buffer (bead-beater, 2 min, 30 Hz) with subsequent centrifugation (10 min, 17,000 x g, 4°C). The resulting supernatant (supernatant 2, approx. 400 µl) was pooled with the first one (figure 2.17 A). Thereafter, the combined supernatant (approx. 1200 µl) was vortexed, centrifuged (15 min, 17,000 x g, 4°C), split into 2 x 500 µl aliquots, and placed under vacuum with medium heat in a centrifugal evaporator (Thermo Scientific SpeedVac Plus SC210A, Savant, UK) attached to a Refrigerated Vapor Trap (RVT100, Savant, UK) until completely dry (approx. 2h). Dried samples were then stored at -80°C until required.

Prior to Ultra-Performance Liquid Chromatography (ULPC) quadruple time-of-flight (qTOF) Mass Spectrometry (MS), samples were re-suspended in 200 µl re-suspension buffer[11], sonicated in a water bath at 4°C (Thermo Scientific) for 20 minutes, vortexed, and centrifuged (15 min, 17,000 x g, 4°C). Thereafter, 180 µl supernatant was transferred into a glass bottle with insert (LCMS Certified Vials, Waters, UK). Additionally, 5 µl supernatant was taken from each sample and mixed in a separate glass bottle with insert as quality control (QC) (figure 2.17 B). One QC for each tissue type was used (i.e. QC1 for root, QC2 for leaf, QC3 for root + leaf).

---

[10] Methanol:dH_2O: formic acid, 95:4.9:0.05 (v:v:v)
[11] Methanol:dH_2O: formic acid, 50:49.9:0.1 (v:v:v) for exp. 1, and 95:4.9:0.05 (v:v:v) for exp. 2
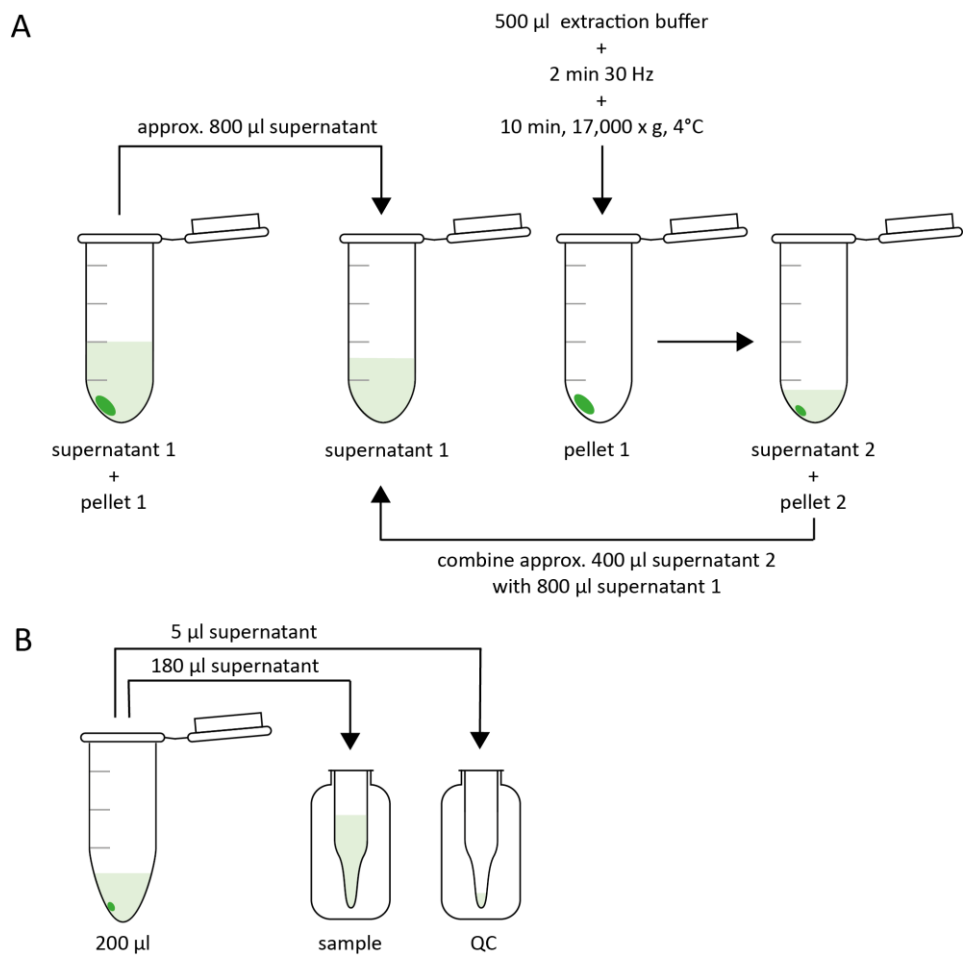
Figure 2.17: Metabolite extraction and preparation for UPLC-qTOF-MS

|A| Graphic of metabolite extraction |B| Graphic of sample preparation for UPLC-qTOF-MS.

2.6.2. UNTARGETED METABOLOMIC PROFILING BY UPLC-qTOF MS

Metabolic profiles of root and leaf methanol extracts were determined on an ACQUITY Ultra-Performance Liquid Chromatography (UPLC) connected to a SYNAPT G2 HDMS qTOF mass spectrometer with electrospray source for ionisation (ESI) (Waters, Manchester, UK). Chromatographic separation was performed using a UPLC BEH C18 column (2.1 × 50 mm, 1.7 µm, Waters) with a pre-column (VanGuard, 2.1 x 5 mm, 1.7 µm, Waters) that separated compounds at a flow rate of 400 µl min^{-1}. The mobile phase consisted of solvent A (reverse osmosis water: formic acid, 99.95%: 0.05%) and B (acetonitrile: formic acid, 99.95%: 0.05%) with the following gradient applied: 0-3 min 5-35% B, 3-6 min 35-100% B, holding at 100% B for 2 min, 8-10 min 100-5% B. Column and gradient matrix were kept at constant temperature (45°C) with an injection volume of 10 µl. All metabolites were detected in negative (ESI$^-$) ionisation mode (see table 2.5 for settings) over a mass range of 50-1200 Da, using a scan time of 0.2 seconds with the instrument operating in sensitivity mode (MS full scan). Buffer (50% Methanol) was injected between treatments. The system was controlled by MassLynx software version 4.1 (Waters, UK).

Table 2.5: UPLC-qTOF-MS settings

Setting	ESI-
Capillary Voltage [kV]	-3
Sampling Cone Voltage [kV]	-25
Extraction Cone Voltage [kV]	4.5
Source Temperature [°C]	120
Desolvation Temperature [°C]	350
Desolvation Gas Flow [l/h]	800
Cone Gas Flow [l/h]	60

2.6.3. DATA ACQUISITION AND STATISTICAL ANALYSIS FOR UNTARGETED PROFILING

RAW data was acquired from MassLynx software version 4.1 (Waters, UK), and converted into CDF format using the "Databridge" function in MassLynx. The resulting CDF files were subdivided according to tissue type (i.e. root and leaf), and analysed separately. Analysis was performed in R studio using the packages XCMS [113] and MetaboAnalystR [114][115]. The former was used for basic data processing, the latter for statistical analysis.

XCMS in R studio

Detection, alignment, assignment, and identification of peaks was performed using XCMS. Initial peak detection used the centWave option, selecting signals above 10 counts and an expected peak width between 5-12 seconds. The detected peaks were deployed to correct for differences in retention time using the the ObiWarp option with m/z bin size 0.1. Peaks were then re-aligned and grouped, requiring peaks to be present in a minimum of 3 samples. Missing peaks were filled in. At each stage the results of parameter choice and output were viewed and checked. Examples are shown in figure 2.18. Subsequently, underlying peak data was extracted, containing mean Rt, mean m/z, total ion counts (TICs), features, and count data of features in each sample.

MetaboAnalyst in R studio

The peak data was loaded into MetaboAnalystR, median-normalised, cube-root transformed and pareto-scaled. Principal component analysis (PCA) was used to visualise the variance in the data with the contribution of individual components displayed in a scree plot. PCs that explained the biggest fraction of total variance were visualised in PCA plots. PERMANOVAs ("Adonis", $p < 0.05$) were carried out to determine which factors contributed significantly to the differences in variance between the samples. One-way ANOVAs ($p < 0.05$) with Benjamini-Hochberg false discovery rate correction (FDR) were performed to identify features that differed significantly between treatment groups (e.g. significantly up or down, displayed in Venn diagram). Subsequently, post-hoc tests (Fisher's LCD, $p < 0.05$) were applied, fold-changes calculated, and t-tests ($p < 0.05$) performed. A work-flow chart of both basic data processes and statistical analysis is displayed in figure 2.19.
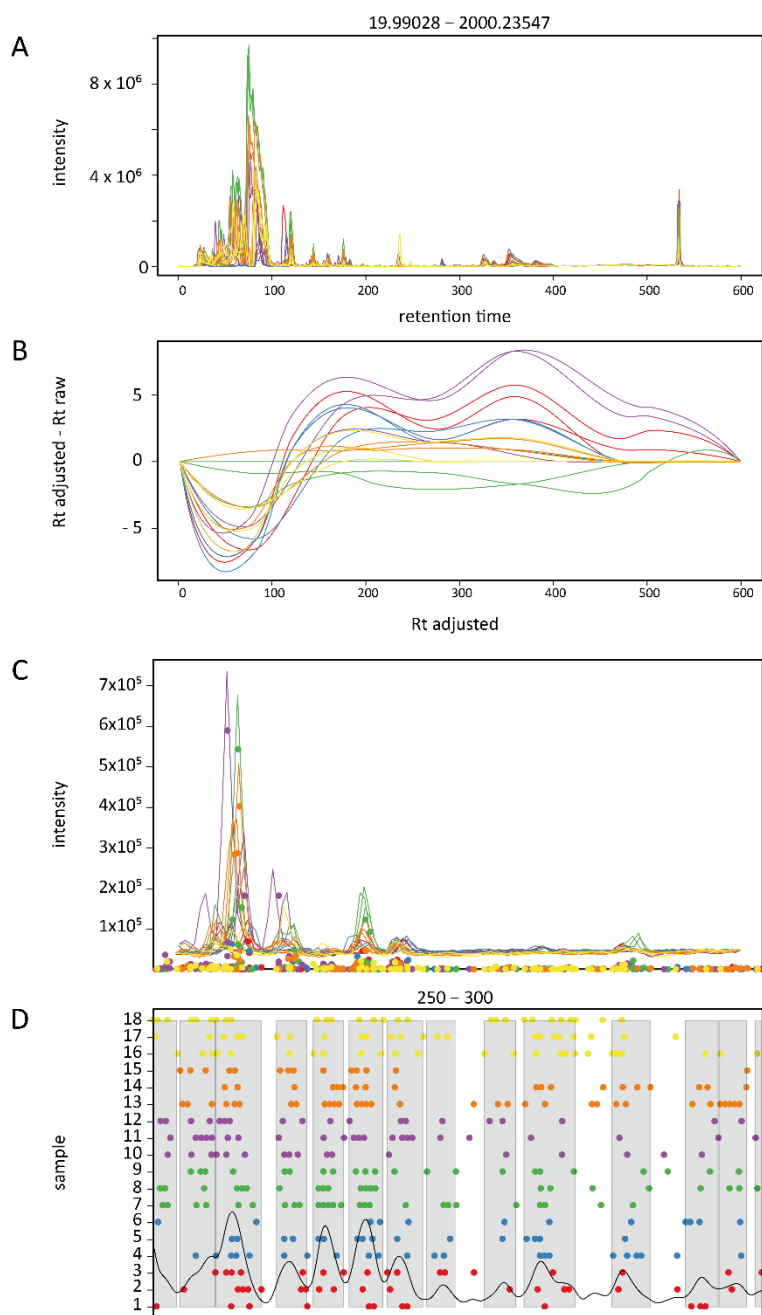
Figure 2.18: Examples of adjustments performed during basic data processing in XCMS. Displayed are root samples of exp.1 |A| Chromatogram after retention time correction |B| Diagram of adjusted retention time. Adjustments range between -10 sec. and +10 sec. |C| Chromatogram during peak identification steps. Coloured points highlight identified peaks |D| Chromatogram with selected peaks
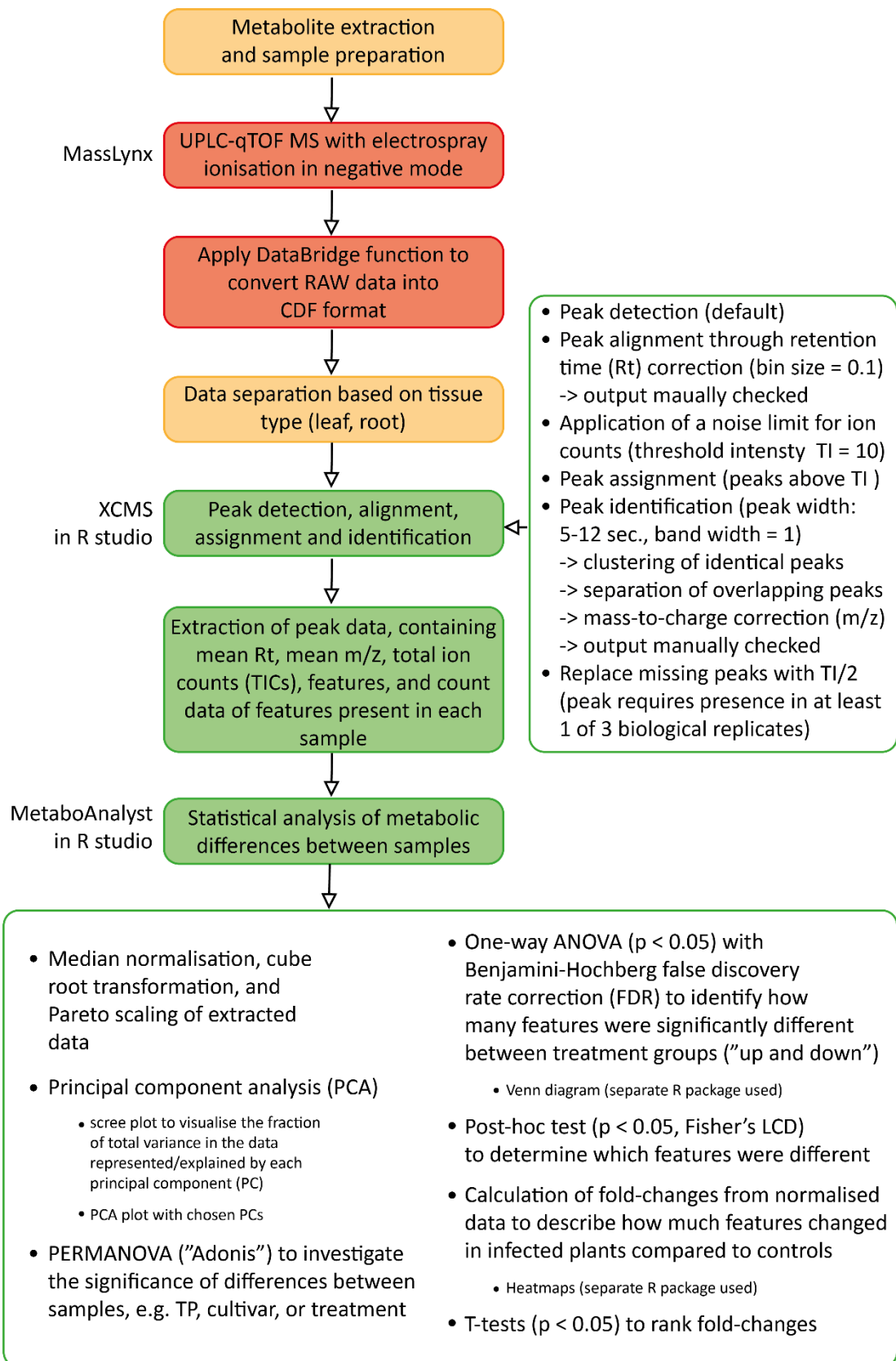
Figure 2.19: Work-flow of untargeted metabolite analysis

CHAPTER 3: PHENOMICS

3.1. INTRODUCTION

Within the same population of a species phenotypic variation (polymorphism) can be observed. A polymorphism appears due to different alleles of a gene. Different alleles are caused by point mutations in coding-regions on the genome. Point mutations in non-coding regions usually lead into functionally silent differences in DNA sequences, and are more frequently due to a lack of selection pressure. However, a DNA sequence variation within a population based on point mutations in coding and non-coding regions is called single nucleotide polymorphism (SNP). Based on SNPs it is possible to find quantitative trait loci (QTLs). QTLs contain genes that contribute to a quantitative trait (QT), and therefore refer to a specific phenotype [116].

The genome-wide association study (GWA) [117] describes the identification of SNPs and other variants in genomes which are associated with a specific phenotype. Therefore, it is used to examine genetic variants within different individuals to finally link a variant (one allele) to a visible trait. However, phenotypes can change over environmental conditions, and promising QTLs can turn out to be irrelevant (false positive QTLs). Therefore, phenotypic descriptions are needed simultaneously to genomic approaches to avoid false positive QTLs [118].

Phenomics is complementary to genomics, and is defined as large-scale and high-throughput phenotyping that links genotypes (i.e. genetic traits) to phenotypes (i.e. visible traits) and the environment. It can be distinguished between forward and reverse phenomics. The former describes the selection of crops with unknown genetic traits (QTLs) that show most promising phenotypic responses to different environmental conditions, including biotic (i.e. drought) and abiotic (i.e. disease) stresses. The latter studies pre-selected genotypes containing desired QTLs and their response to different environmental conditions to get a better understanding of underlying mechanisms. In both cases, best performing crops based on visible traits are used for best-genotype breeding or hybridisation programs. This can potentially avoid the introduction of false positive QTLs in new generations of crop plants [119][120].

Phenomics screens are based on automated imaging, weighing and watering techniques. The former is performed by scanners that underlie high-performance computing, and can be conducted on fields and in greenhouses. Scanning procedures in greenhouses mostly rely on conveyor systems ("phenomics platform"), where plants are transported from one measuring location to the next. Focus are changes in the aerial plant body, in particular leaves. Leaf characteristics change upon biotic and abiotic stresses, and usually include alterations in pigmentation, water content, transpiration, or photosynthesis. Those changes have an impact

on light reflectance, absorption, diffusion, and transmission. To inspect those light-leaf interactions in detail, non-invasive imaging techniques focus on different wavelengths within the electromagnetic spectrum [119][120]. Table 3.1 lists examples for the most common phenomics techniques.

Table 3.1: Examples for common phenomics techniques [119][120]

Phenomics technique	Information
RGB imaging (visible spectum)	- Plant growth, pigmentation, necrosis - Pathogen structures (foliar disease)
Near-infrared (NIR) imaging	- Water content of plant and soil
Thermal imaging (long-wavelength infrared, LWIR)	- Thermal radiation emitted by leaves is converted into visual images - Leaf tempeature, indirect quantification of transpiration - Ideal for pathogens that colonise the vascular system
Chlorophyll fluorescence:	- Physiological state of the photosynthetic machinery - Estimation of the maximum quantum yield of photosystem II (Fv/Fm) - Fv/Fm = 0.84 in healthy plants - Ideal for pathogens that target carbon metabolism
Weighing and watering	- Water usage (abiotic: drought, salinity; biotic: microbial disease)

Clubroot, caused by *P. brassicae*, is an abundant root disease amongst Brassica plants, with below-ground gall formation, and above-ground symptoms similar to drought phenotypes (i.e. stunted growth and wilted leaves with signs of chlorosis and necrosis). Due to the pathogen's biotrophic life style, clubroot disease symptoms in host plants occur rather late, and the only obvious indicator for disease severity is timing of club-shaped root deformation and gall size. Root excavations and visual root assessments [109] help to categorise susceptible and resistant plants, but it is destructive and laborious. Methods to identify clubroot infection before the occurrence of gall formation are desirable. An interesting incentive derived from a study on clubroot inoculated Chinese Cabbage Wong Bok (1 ml inoculum with 10^6 spores/ml, pathotype ECD 16/2/12 from Penyrheol in South Wales) that showed above-ground growth stimulation during early days of infection (9 dpi) [59].

In this chapter, several disease phenomics screens were conducted to test the applicability of phenomics screens for detection of clubroot disease, to find potential above-ground disease indicators before the onset of visible disease symptoms, and to identify host plants tolerant or resistant to clubroot. For the latter, plants were inoculated with two different concentrations of one pathotype. The objectives of the chapter's study were the observation of above-ground changes over time using non-invasive imaging techniques, and the comparison of differences in plant performance depending on inoculum densities. Table 3.2 shows the phenomics techniques applied in this chapter.

Table 3.2: Applied phenomics techniques in this chapter

Disease symptom	Phenomics technique
Reduction in xylogenesis: altered water uptake	water usage through weighing and watering
drough stress: altered stomata conductance	leaf temperature through thermal imaging
disequilibrium of sink-source balance: growth distortion	RGB imaging and weighing (biomass)

3.2. RESULTS

3.2.1. PRELIMINARY EXPERIMENTS AT AWEC

Two preliminary screens were conducted at AWEC[12] to test if pre-selected environmental and growth conditions were appropriate (see table 2.2 in section 2.3 for details). The aims were to ensure consistent clubroot infection, and to gain experience with clubroot disease development whilst focussing on end-point disease severity.

Three Brassica varieties were selected for the initial experiment: Chinese Cabbage Wong Bok (very susceptible), Ragged Jack Kale and Winter Oilseed Rape Temple. All three cultivars were inoculated with 5 different concentrations of clubroot spores (6.25×10^1 -6.25×10^5 spores/ml), and scored at 51 dpi. Large galls were evident in roots of infected Chinese Cabbage Wong Bok for all spore concentrations. Infected plants were smaller than mock-treated (dH_2O) control plants (figure 3.1 A). In contrast, no galls were seen in inoculated Ragged Jack Kale at any clubroot spore concentration. At high spore densities (6.25×10^5 spores/ml), inoculated Raged Jack Kale was smaller than mock-treated controls but at low spore densities (6.25×10^2 spores/ml) some above-ground growth stimulation was apparent (figure 3.1 B). Winter Oilseed Rape Temple showed an intermediate phenotype (figure 3.1 C). Galls were present only at 6.25×10^3 spores/ml and higher. Above-ground biomass appeared to be greater at lower spore concentrations (i.e. 6.25×10^1 spores/ml) and markedly reduced at higher spore concentrations (6.25×10^5 spores/ml). Scoring results according to the standard clubroot classification system are shown in figure 3.1.

The differences in disease development and severity in all three plant lines, particularly the growth stimulation at lower spore concentrations, qualified them as ideal Brassica candidates for subsequent preliminary phenomics studies at IBERS[13] in Aberystwyth (Wales).

---

[12] Arthur-Willis Environmental Centre at the University of Sheffield. It is a medium-sized greenhouse separated into several independent compartments (growth chambers), each allowing experiments under semi-controlled environmental conditions with good consistency and reproducibility.
[13] Institute of Biological, Environmental and Rural Sciences of the University of Aberystwyth in Wales. It is a large greenhouse facility containing a Lemnatech conveyor system to perform phenomics screens based on automated imaging and weighing techniques. The greenhouse is separated in semi-open compartments, which cannot be environmentally controlled.
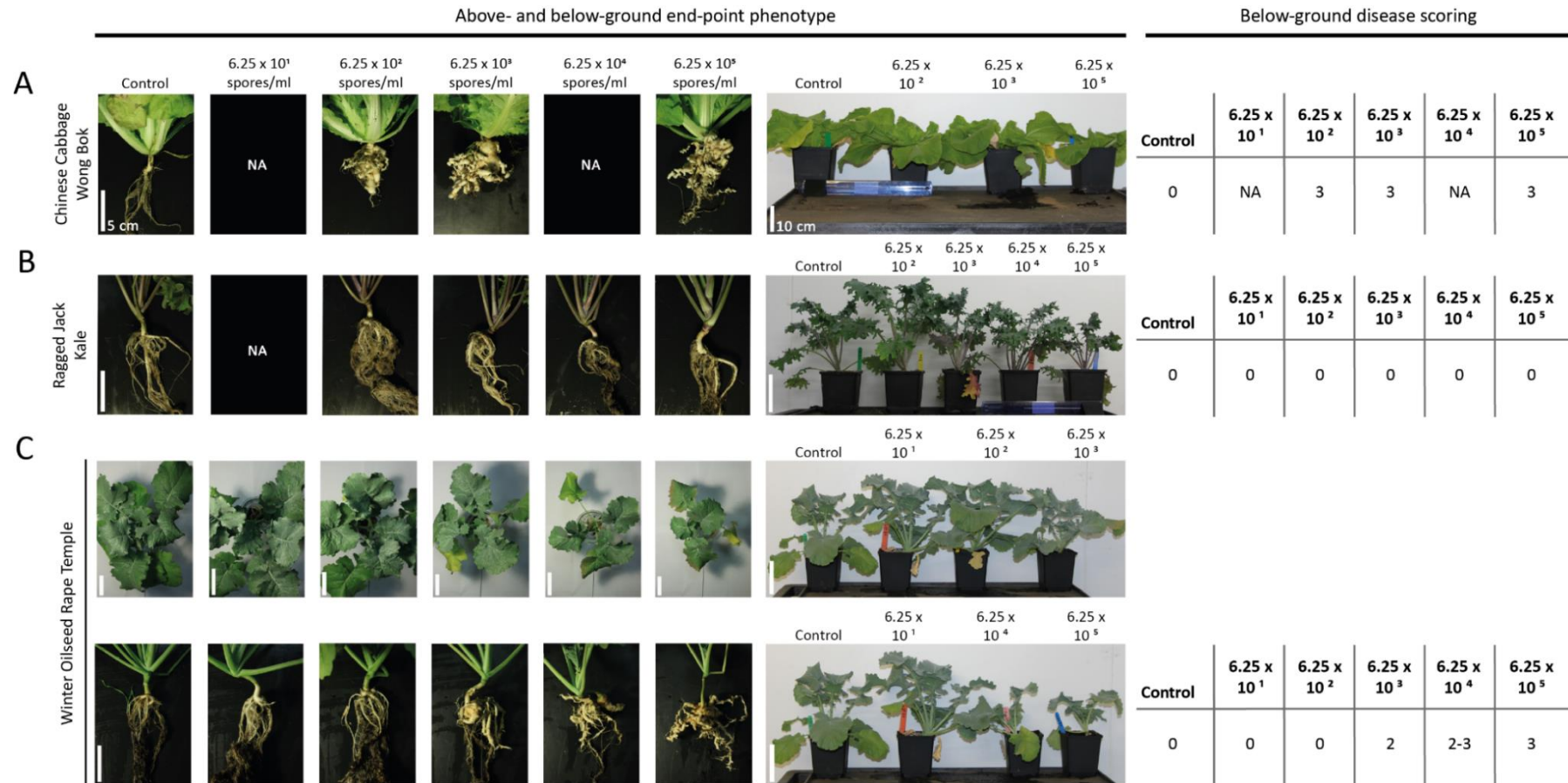
Figure 3.1: End-point phenotype and disease scoring – Preliminary experiment at AWEC

[Legend on next page]

Legend to figure 3.1:

|A|-|C| Below- and above-ground phenotype and clubroot infection scores of Brassica cultivars at 51 dpi. Scale bars for left (below-ground) and right panel (above-ground) are 5 and 10 cm, respectively. The scoring system used in this study is described in section 2.2.2 |A| Chinese Cabbage Wong Bok |B| Ragged Jack Kale |C| Winter Oilseed Rape Temple.

3.2.2 PHENOMICS SCREEN *TRIAL 1* AT IBERS

A small-scale disease phenomics screen (*Trial 1*) was performed at IBERS (University of Aberystwyth, Wales) using a Lemnatech phenomics platform and automated conveyor system. The aim was to identify suitable parameters for clubroot disease quantification, and to test the equipment's capability for future large-scale phenomics screens. As *P. brassicae* causes distortions in source-sink balance, alterations in cambial stem cell maintenance and differentiation, and perturbations of vascular development with reduction in xylogenesis [73], water- and growth-related measurements (including above-ground growth stimulation) were the focus of the trial. The universally susceptible Chinese Cabbage (Wong Bok), two kale (Ragged Jack, Siberian) and two oilseed rape varieties (Temple, Cracker) were used in the screen with 4 replicates and 3 treatments (mock-treated with dH_2O, and inoculated with low and high clubroot spore densities). Cultivars were placed on the conveyor system at 14 dpi (= 18 days after germination), and measurements were made for 37 days until destructive harvest at 51 dpi (see table 2.2 in section 2.4 for further details).

During the screen, measurements of plant growth (area and height) were conducted daily based on RGB pictures from 2 different angles (figure 3.2, and supplementary figure 1 and 2). Typically, plant growth showed a sigmoidal pattern, with rapid growth from 20 dpi onwards, before reaching a plateau at approx. 30 dpi. Occasional defoliation during the experiment was seen as a decline in area/ height. Not all varieties had ceased growing at the end of the experiment, which caused a reduced or absent plateau. Maximum values for area and height were calculated for each plant as described in section 2.4.3. These calculated end-point values are shown in figure 3.3, and the corresponding end-point biomass (above-and below ground) in figure 3.4.

The maximum growth values (area and height) and biomass data indicated variation between cabbage, kale, and oilseed rape cultivars as a consequence of morphological differences. Further variation was observed within each treatment group (control, low spore, high spore) with the largest variation seen in Chinese Cabbage Wong Bok for both growth (area and height), and biomass. However, a trend for treatment-dependent differences was noticeable in this cultivar and Winter Oilseed Rape Temple: Clubroot caused growth and above-ground biomass reduction, and an increase in below-ground biomass (fresh and dry weight). The reduction was seen for high inoculum concentrations in both cultivars ($p > 0.05$, One-way ANOVA), and increase for low spore densities in Wong Bok ($p > 0.05$, One-way ANOVA) and high spore densities in Temple ($p < 0.05$, One-way ANOVA with TukeyHSD test).
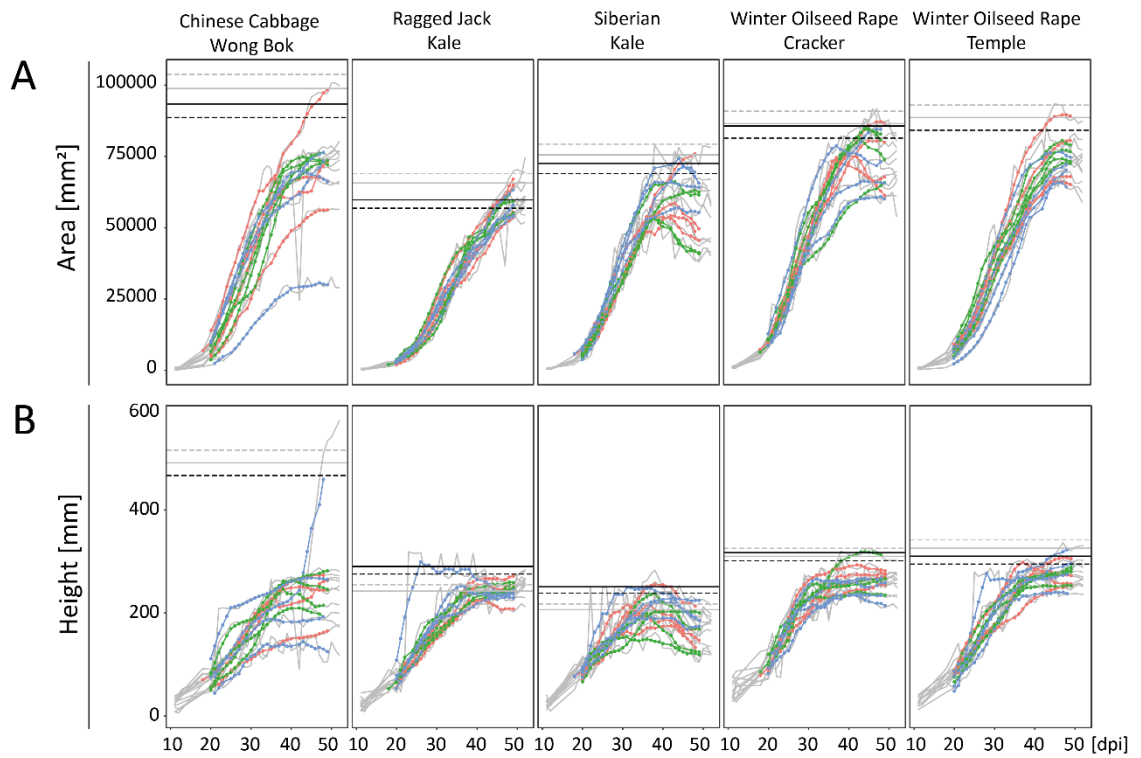
Figure 3.2: Area and height RAW data – IBERS *Trial 1*

|A|-|B| Area and height data of 5 Brassica cultivars (three treatments, 4 biological replicates per treatment) measured using RGB images. Area data is the calculated stem and leaf area of the whole plant based on RGB images taken from 2 different angles. Height data describes the height of the main stem including the highest leaf attached.

RAW data is shown as grey line, a rolling average (central 7 day window) as connected coloured dots. Mock treated cultivars (dH$_2$O) are red, clubroot spore treated cultivars green (low concentration) and blue (high concentration). Final and maximum values of the biggest plants are indicated as solid horizontal lines of grey and black colour, respectively. Dashed horizontal lines in black represent the area/ height when values approached 95% of the maximum value. Dashed horizontal lines in grey highlight when plants were still growing at the end of the experiment (= final value + 5%).

|A| Area in mm^2 |B| Height in mm
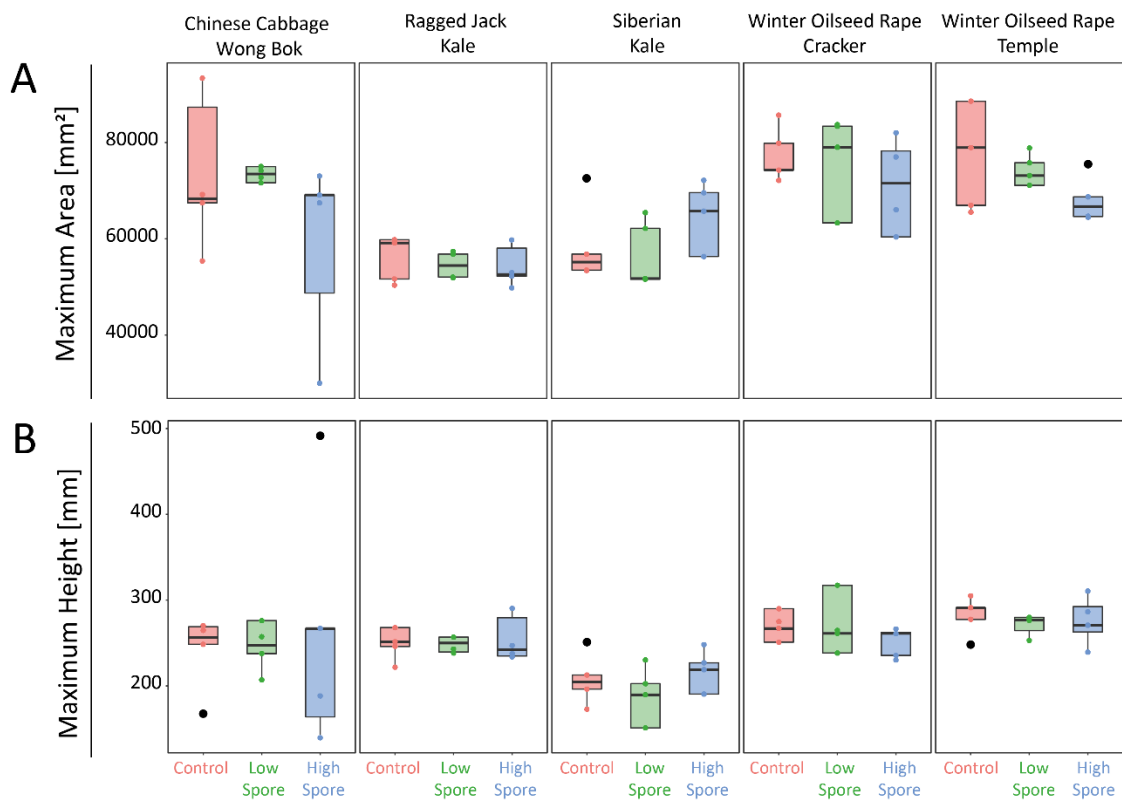
Figure 3.3: Maximum values of area and height data – IBERS *Trial 1*

|A|-|B| Boxplots of end-point values for area and height data of 5 Brassica cultivars (three treatments, 4 biological replicates per treatment). The median is shown as horizontal black line across the box (= middle of the data), and the lower and higher quartile as horizontal black lines at both ends of the box (= 25% of the data which is lower or greater than the median). Variability outside the quartiles is indicated as lines extending vertically from the box (whiskers) to the most extreme data points (= minimum and maximum). Points outside the whiskers (outliers) are plotted in black. Red boxes represent data distribution of mock treated cultivars (dH$_2$O), green and blue boxes of low and high spore inoculated plants. Underlying individual data points are displayed as coloured points in red (control), green (low spore), and blue (high spore) |A| Maximum area in mm^2 |B| Maximum height in mm
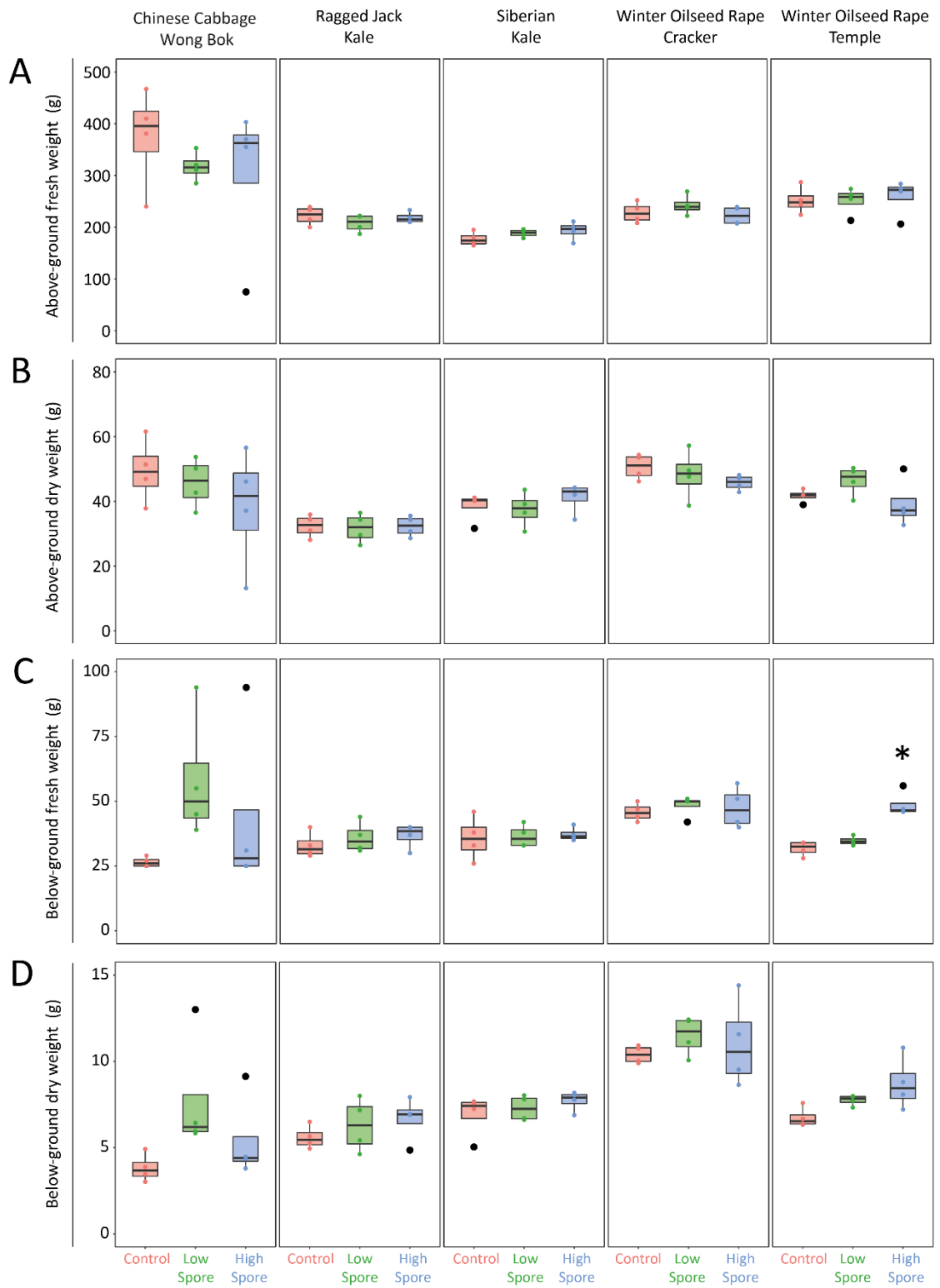
Figure 3.4: Biomass data – IBERS Trial 1 [Legend on next page]

[Legend to figure 3.4]

|A|-|D| Boxplots of fresh and dry weight measurements of above- and below-ground plant material obtained from 5 different Brassica cultivars (three treatments, 4 biological replicates per treatment). The median is shown as horizontal black line within the box, and the lower and higher quartile as horizontal black lines at both ends of the box. Variability outside the quartiles is indicated as lines extending vertically from the box (whiskers) to the most extreme data points. Data points outside the whiskers (outliers) are plotted in black. Data distribution of mock treated cultivars (dH_2O) and clubroot inoculated plants is shown as red (control), green (low spore), and blue (high spore) boxes. Underlying individual data points follow the same colour code |A| Fresh weight of above-ground plant material in g |B| Dry weight of above-ground plant material in g |C| Fresh weight of below-ground plant material in g. High spore inoculated Temple shows significance with $p < 0.05$ (One-Way-ANOVA with TukeyHSD test) |D| Dry weight of below-ground plant material in g

Selected photographs representative of each cultivar and treatment are shown in figure 3.5 together with visual scoring results. All photographs were taken immediately after destructive harvest at 51 dpi, and show above- and below-ground plant material. Root material was then scored visually according to the clubroot classification system as described in section 2.2.2.

Phenotypically, both kale varieties (figure 3.5 A, B, and G), and Winter Oilseed Rape Cracker (figure 3.5 C and G) showed no above- and below-ground indication for clubroot infection, while Winter Oilseed Rape Temple (figure 3.5 B and G) was susceptible at high spore concentrations. However, gall formation occurred non-uniformly only on secondary roots. The above-ground phenotype was healthy with no growth reduction. Chinese Cabbage Wong Bok showed very variable infection at high spore treatments (figure 3.5 F). Above-ground symptoms included early flowering. Below-ground clubroot infection varied from no apparent infection to formation of large galls (figure 3.5 E and G).

Cultivar	Control	Low Spore	High Spore
Ragged Jack Kale	0	0	0
Siberian Kale	0	0	0
Winter Oilseed Rape Cracker	0	0	0
Winter Oilseed Rape Temple	0	0	1-2
Chinese Cabbage Wong Bok	0	Heterogeneous infection between 0 and 3	Heterogeneous infection between 0 and 3
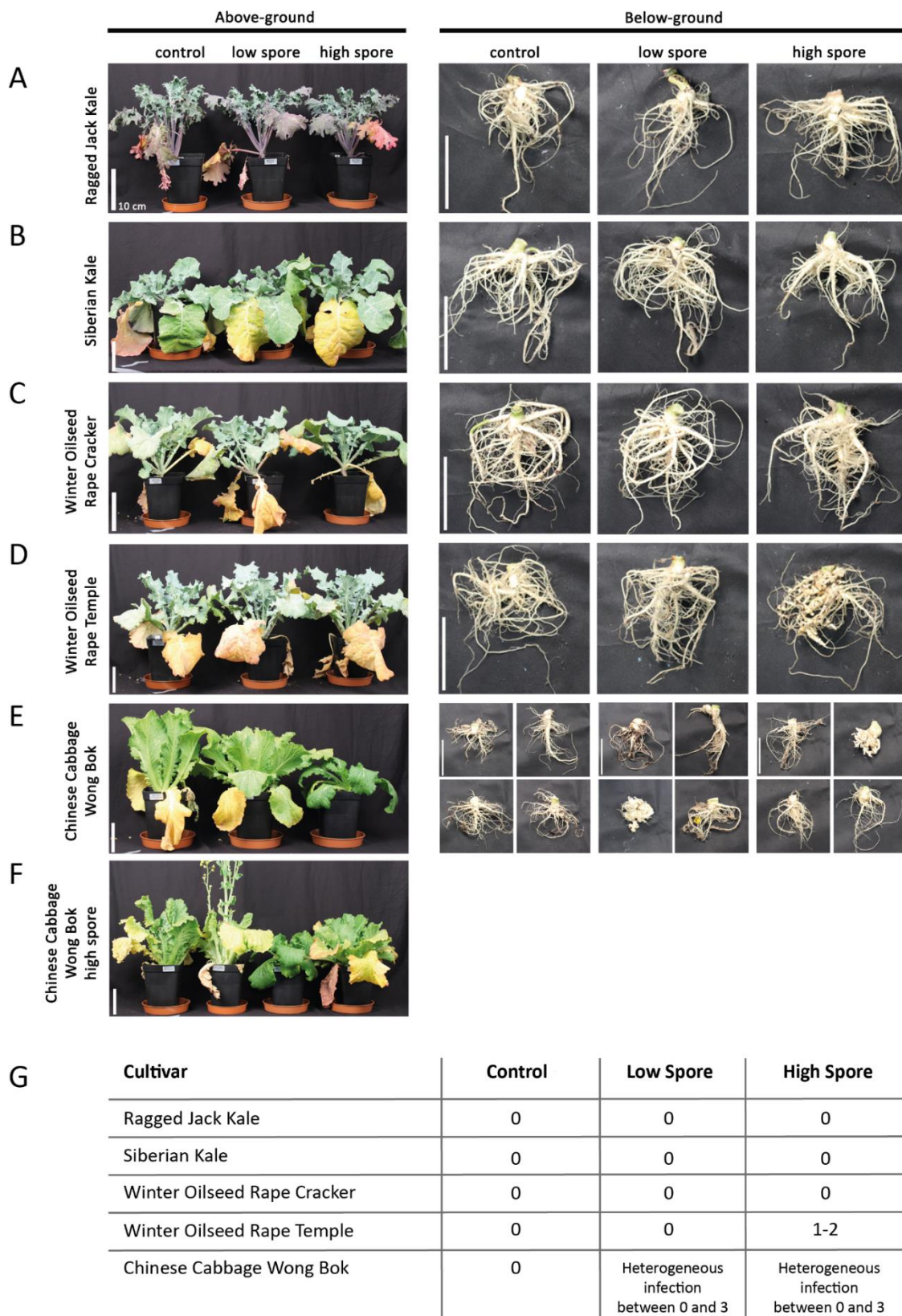
Figure 3.5: End-point phenotype and disease scoring – IBERS Trial 1

[Legend on next page]

[Legend to figure 3.5]

|A|-|F| End-point phenotype of 5 Brassica cultivars. Unless stated, individual plants of each cultivar were selected for each treatment group with 4 biological replicates. Scale bars are 10 cm |A| Ragged Jack Kale |B| Siberian Kale |C| Winter Oilseed Rape Cracker |D| Winter Oilseed Rape Temple |E| Chinese Cabbage Wong Bok. Below ground pictures (right panel) displays all biological replicates for each treatment group |F| Above-ground phenotype of all Chinese Cabbage Wong Bok inoculated with high spore concentrations |G| Table with visual scoring results of all 5 Brassica cultivars. The scoring system used in this study is described in section 2.2.2.

Variable clubroot infection and the observation of dry soil patches in plant pots during destructive harvest, led to concerns that the automated watering system was not keeping plants adequately watered. This was important as clubroot disease development is known to be impeded by drought [8]. Plant watering was performed daily using an automated watering system (with occasional hand-watering if the system malfunctioned) that kept the plant pots at constant weight by adding water until a fixed reference value was obtained. Daily weighing before and after watering allowed calculations of water use by taking the difference between two values on consecutive days (see section 2.4.2 for details). Figure 3.6 shows results of water use measurements together with cumulative sums.

Water use rose between 20 dpi and 40 dpi, and then declined until the end of the experiment (51 dpi). Total, average and maximum water use was calculated, and the duration between clubroot inoculation and maximum water use examined as described in section 2.4.2. All values are displayed in figure 3.7 and supplementary figure 3.

Total, average and maximum water use was similar between and within cultivars. No apparent treatment-dependent difference within kale (Ragged Jack, Siberian) and oilseed rape varieties (Cracker, Temple) were observed for water consumption and days until maximum water use ($p > 0.05$, Two-way-ANOVA). An impact of clubroot might have occurred in Chinese Cabbage Wong Bok. In this cultivar, water consumption and days until maximum water use was slightly reduced. However, the variability of infection within both spore treatments made comparisons difficult ($p > 0.05$, Two-way-ANOVA).
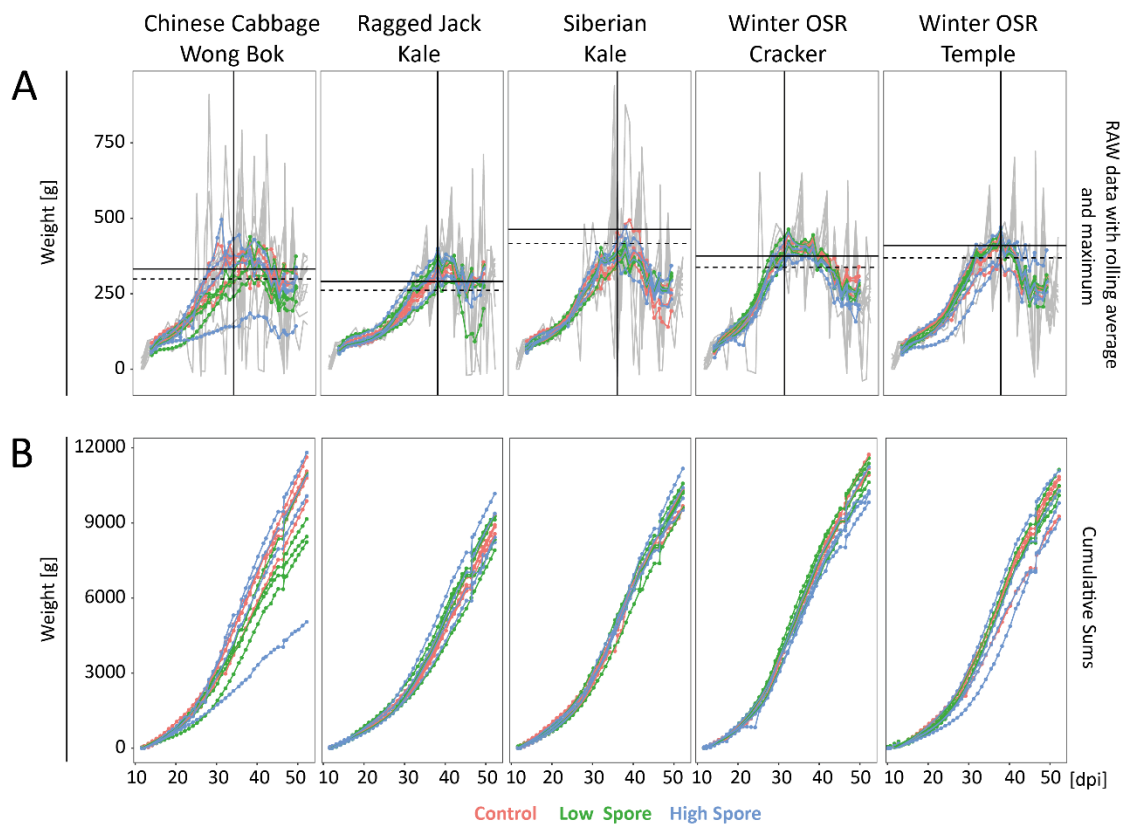
Figure 3.6: RAW data for water use and cumulative sums – IBERS Trial 1

|A| Water use data for 5 Brassica cultivars (3 treatments, 4 biological replicates per treatment). RAW daily water use is displayed as solid grey line. A rolling average (central 7 day window) is shown as connected dots in red (mock treated cultivars with dH_2O), green (low spore), and blue (high spore). Solid and dashed horizontal lines in black indicate maximum values and the position when values approached 90% of the maximum value, respectively. Vertical solid lines show the day when the maximum is reached |B| Cumulative sums of 5 Brassica cultivars (3 treatments, 4 biological replicates per treatment). Same colour code applies for mock-treated and clubroot inoculated cultivars.
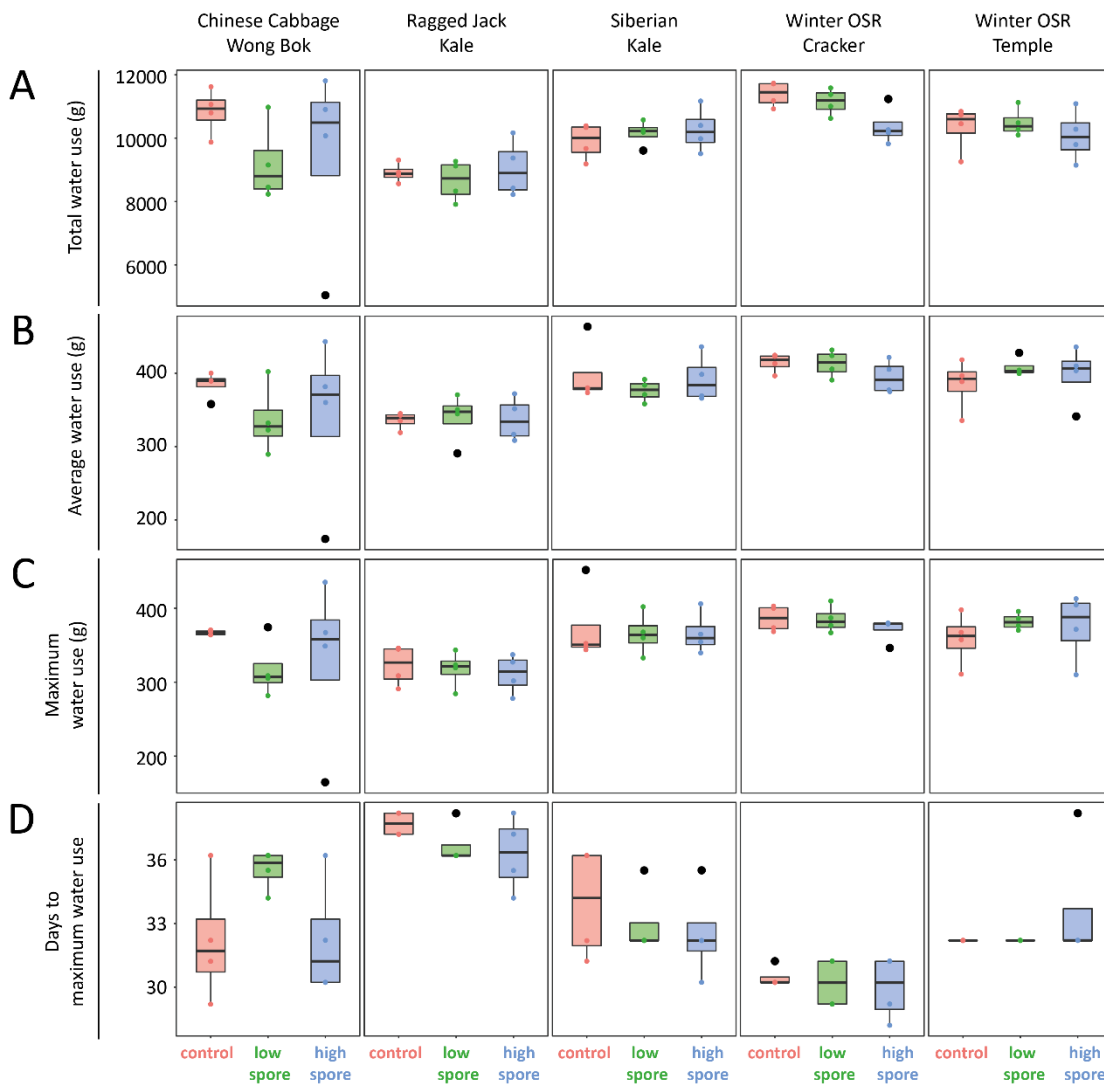
Figure 3.7: Water use results – IBERS Trial 1

|A|-|D| Boxplots of water use results from 5 Brassica cultivars (3 treatments, 4 biological replicates per treatment). The median is shown as horizontal black line within the box, and the lower and higher quartile as horizontal black lines at both ends of the box. Variability outside the quartiles is indicated as lines extending vertically from the box (whiskers) to the most extreme data points. Data points outside the whiskers (outliers) are plotted in black. Data distribution of mock treated cultivars (dH$_2$O) and clubroot inoculated plants is shown as red (control), green (low spore), and blue (high spore) boxes. Underlying individual data points follow the same colour code. P > 0.05 (Two-way-ANOVA) |A| Total water use at 51 dpi in g |B| Average water use in g |C| maximum water use in g |D| Days to maximum water use

During the screen, thermal images were taken at 29, 43, and 51 dpi. Leaf temperature data was then extracted from the images in both an automated and manual approach as described in section 2.4. Results are displayed in figure 3.8, and compared in figure 3.9.

Results of thermal image data analysis using the manual method (figure 3.8 A) showed treatment-dependent temperature changes during disease development. Large variation was seen in Chinese Cabbage Wong Bok with a gradual leaf temperature increase at later time points for both spore treatments. Both kale varieties (Ragged Jack, Siberian) did not show strong responses to clubroot treatment: Leaves of low and high spore inoculated Ragged Jack Kale were colder than control plants at 51 dpi, and clubroot-inoculated Siberian Kale was cooler at the low spore treatment and warmer for high spore treatment, both at 43 and 51 dpi. In winter OSR Cracker elevated temperatures were evident at low spore densities, and only a small temperature increase was seen in high spore inoculated plants. However, elevated temperatures were greater in winter OSR Temple at both spore densities compared to control plants. Gradual temperature increase occurred at late time points, while inoculated plants at 29 dpi appeared colder than their controls.

The automated method for data extraction (figure 3.8 B) provided similar results as the manual method for all cultivars, but with more outliers. Comparisons of both methods (figure 3.9) showed good correlations (> 90%) for all 3 time points.
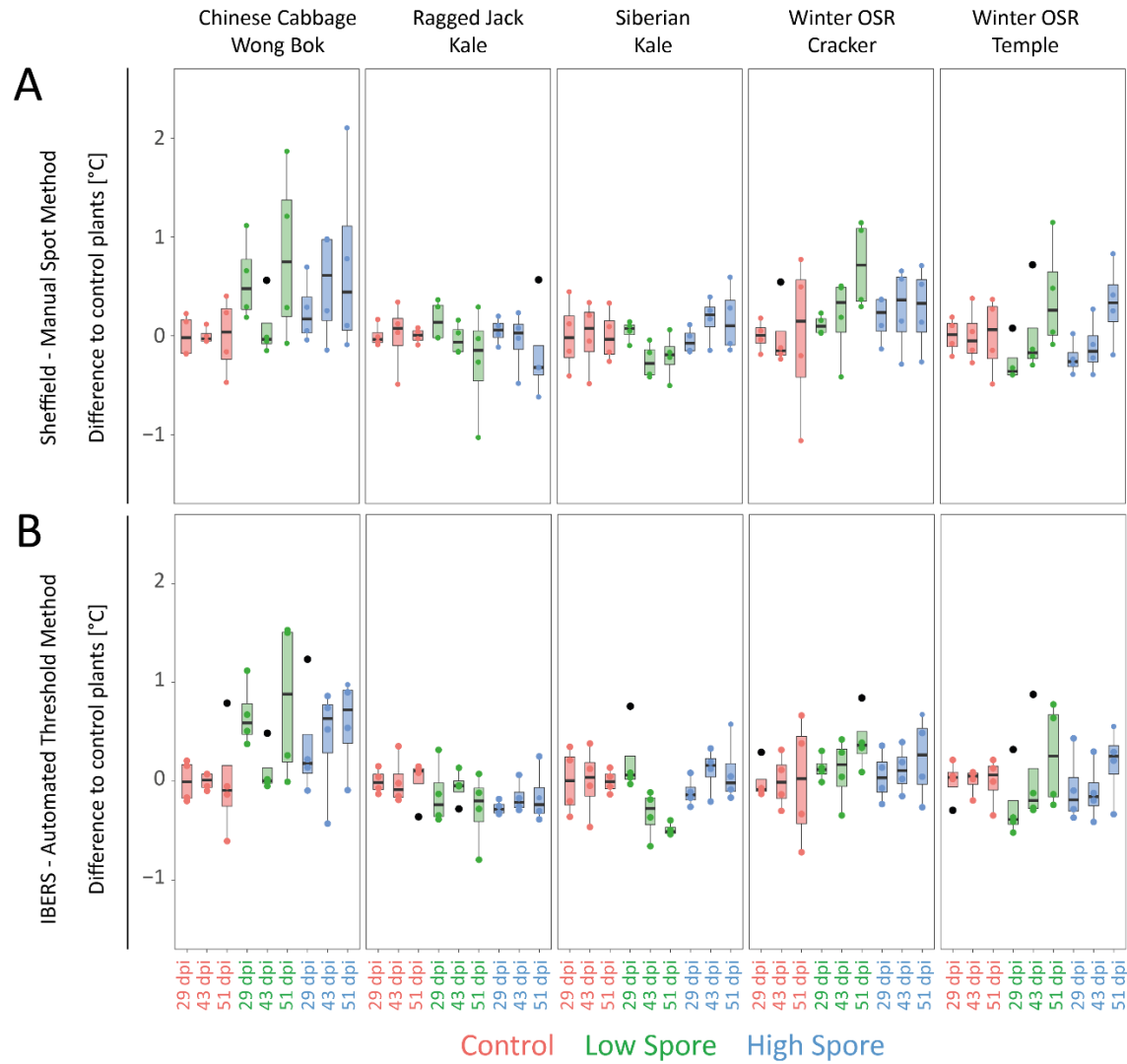
Figure 3.8: Thermal image results – IBERS Trial 1

|A|-|B| Boxplots of plant leaf temperatures of 5 Brassica cultivars (3 treatments, 4 biological replicates per treatment). Temperatures of clubroot inoculated cultivars were compared to mock treated plants (dH$_2$O) during 3 time points (29, 43, and 51 dpi). The median is shown as horizontal black line within the box, and the lower and higher quartile as horizontal black lines at both ends of the box. Variability outside the quartiles is indicated as lines extending vertically from the box (whiskers) to the most extreme data points. Data points outside the whiskers (outliers) are plotted in black. Data distribution of mock treated cultivars (dH$_2$O) and clubroot inoculated plants is shown as red (control), green (low spore), and blue (high spore) boxes. Underlying individual data points follow the same colour code

|A| Thermal image results obtained by the manual spot method |B| Thermal image results obtained by the automated threshold method
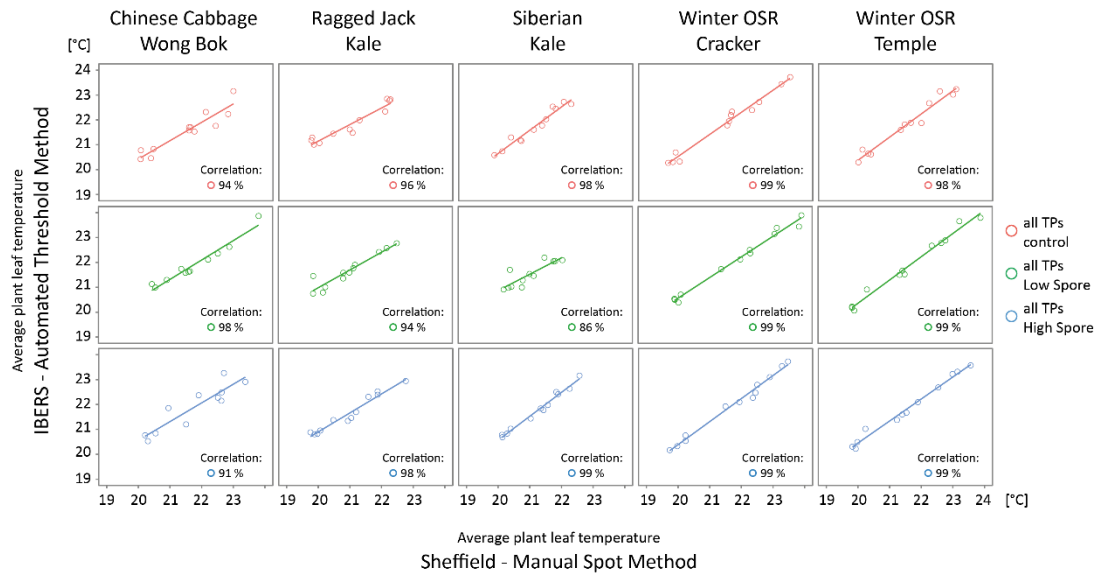
Figure 3.9: Correlation of manual spot and automated threshold method for extraction of leaf temperature from thermal images – IBERS Trial 1 | Graphical view showing comparisons of average plant temperatures of 5 Brassica cultivars (3 treatments, 4 biological replicates per treatment) over the course of 3 time points with focus on treatment groups. Temperatures were obtained by spot and threshold method, with spot method results on x-axis and threshold method results on y-axis. Mock treated cultivars (dH$_2$O) and clubroot inoculated plants are shown in red (control), green (low spore), and blue (high spore)

3.2.3. PHENOMICS SCREEN *TRIAL 2* AT IBERS

Phenomics screen *Trial 1* at IBERS revealed problems with the automated watering regime since the fixed reference point did not account for increased plant biomass. This caused drought in growing cultivars, and inhibited clubroot infection. As a consequence, the watering algorithm was adjusted to compensate for biomass increase over time. At IBERS, changes in biomass were estimated based on growth data (area and height), and the watering reference point adapted to plant growth. Additionally, water was added from both top and bottom. A second phenomics screen (*Trial 2*) was performed.

For *Trial 2*, a selection of Brassica cultivars was subdivided into 2 sets of 14 and 15 oilseed rape varieties, and placed on the conveyor system at 20 dpi (= 24 days after germination) with planting staggered to maximise the use of the conveyor capacity. Oilseed rape varieties were tested as their upright growth habit facilitated automated watering.

On the conveyor system, measurements were made for 31 days until destructive harvest at 51 dpi (see table 2.2 in section 2.3 for details). Watering was performed twice daily (morning and evening). First, plants were watered from the bottom (set 1). However, insufficiencies were noticed by staff, and the watering was subsequently changed to avoid drought. This resulted in alternated top and bottom watering for set 2. Images of plant growth were taken from 3 different angles, and thermal imaging took place on 5 days. Water use, plant growth (area and height), and average leaf temperatures (thermal images) were calculated as in *trial 1* (see section 2.4 for details). At the end of the experiment, plant roots were assessed visually, and above- and below ground material collected for biomass measurements.

Despite the improvements to the watering regime, drought was still evident. During the final destructive harvest a severe drought problem was indicated: (I) Plants were small with purple leaves, (II) there was either no infection or heterogeneous and limited gall formation, and (III) dry soil patches were found within plant pots. Gall formation mostly occurred within those wet patches, giving the plant a mosaic-like root phenotype.

Root material was scored according to the clubroot classification system. Scoring results for set 1 and an illustration of water distribution in plant pots are displayed in figure 3.10. No pictures were taken during the harvest.

A

Oilseed Rape Cultivars	Control		Low Spore		High Spore	
	number of infection	visual score	number of infection	visual score	number of infection	visual score
Cracker	0/3	0	0/3	0	0/3	0
Temple	0/3	0	0/3	0	2/3	1-3
Apex	0/3	0	0/3	0	1/3	2
Bravour	0/3	0	0/3	0	1/3	2
Verona	0/3	0	0/3	0	1/3	1
Tapidor	0/3	0	0/3	0	0/3	0
Eurol	0/3	0	NA	NA	3/3	3
Lembkes Malchower	0/3	0	1/3	1	3/3	1-3
Jet Neuf	0/2	0	0/3	0	2/3	1+3
Baltia	0/3	0	0/3	0	3/3	2-3
Coriander	0/3	0	1/3	1	3/3	1-3
Dippes	0/3	0	0/2	0	0/3	0
Ramses	0/3	0	0/3	0	3/3	1-2
Moana	0/3	0	1/3	2	3/3	3

B

Trial 1
dH₂O from top
drought at bottom

Trial 2 Set 1
dH₂O from bottom
drought at top

Trial 2 Set 2
dH₂O from top and bottom
drought in the middle

C

patchy clubroot
infection
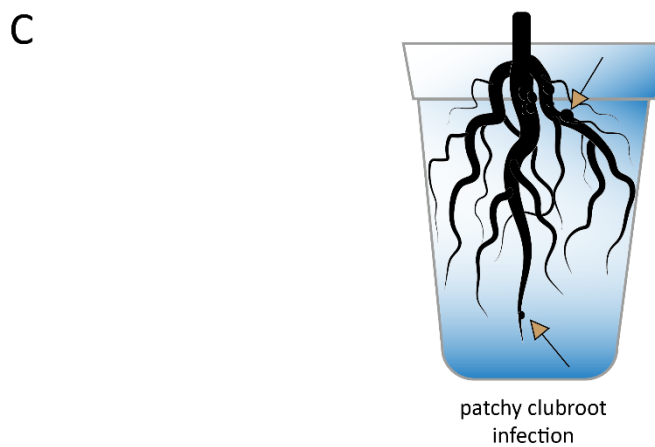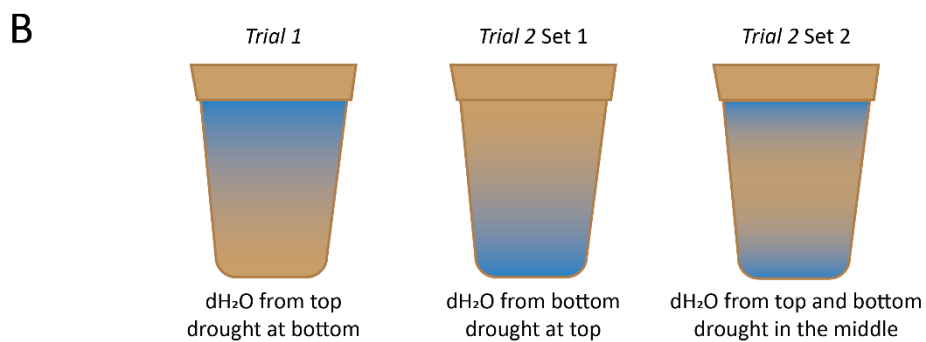
Figure 3.10: Visual scoring results of set 1 with water distribution in plant pots

[Legend on next page]

[Legend to figure 3.10]

|A| Table of visual scoring results of 14 oilseed rape varieties with 3 treatments (control, high spore, low spore) and 3 biological replicates per treatment. Cultivars with gall formation are highlighted in green (low spore) and blue (high spore). The scoring system used in this study is described in section 2.2.2 |B| Graphical view showing water distribution and drought spots in plant pots during destructive harvest |C| Example of mosaic-like clubroot infection due to wet and dry spots in a plant pot. Gall formation occurs around wet soil.

Based on the outcome of the visual scoring, 6 oilseed rape cultivars were chosen with the most uniform clubroot infection to analyse watering, growth, thermal, and end-point biomass data collected during the phenomics screen (20 – 51 dpi).

Watering data is displayed in figure 3.11 A. The water use curve did not show the rising pattern as was seen in *Trial 1*. Instead, the amount of water used by the plants decreased over time. The same pattern can be seen for water added to the plants. This indicates a feedback mechanism between plant and watering regime. In this interplay, the plant reduces water consumption in an environment of reduced water availability. This is recognised by the algorithm, and as a consequence the plant receives less water. Cumulative sums of both added and used water exhibit shallow curves in figure 3.11 B, and confirm water shortage. This again correlates with growth stagnation seen in figure 3.12. No sigmoidal pattern is seen in comparison to *Trial 1*. Initially, plants of *Trial 2* were growing, but then reached a plateau at approximately 30 dpi until destructive harvest at 51 dpi. No treatment-dependent differences were visible, even though oilseed rape Eurol showed poor growth (dead at the experimental end) for low spore treated plants. On the contrary, end-point biomass data (figure 3.13) revealed a treatment-dependent trend for above- and below-ground plant material despite large variation within high spore inoculated cultivars. There is an above-ground biomass decrease with simultaneous below-ground biomass increase for some cultivars (i.e. Baltia, Coriander, and Eurol) if inoculated with high density spores. However, the analysed 6 oilseed rape cultivars were pre-selected according to their more uniform class 3 clubroot phenotype, and root biomass increase was therefore expected. Surprisingly, and despite all trade-offs (i.e. drought with stagnated plant growth and heterogeneous infection), thermal measurements detected a clubroot-related signal evident as elevated temperatures for low and high spore inoculated cultivars if compared to their control counterparts (figure 3.14). However, temperature fluctuations in the greenhouse due to changing weather or daytime, caused rise and fall of leaf temperatures (all treatments) throughout the experiment, and made it difficult to assess the impact of clubroot on inoculated plants.
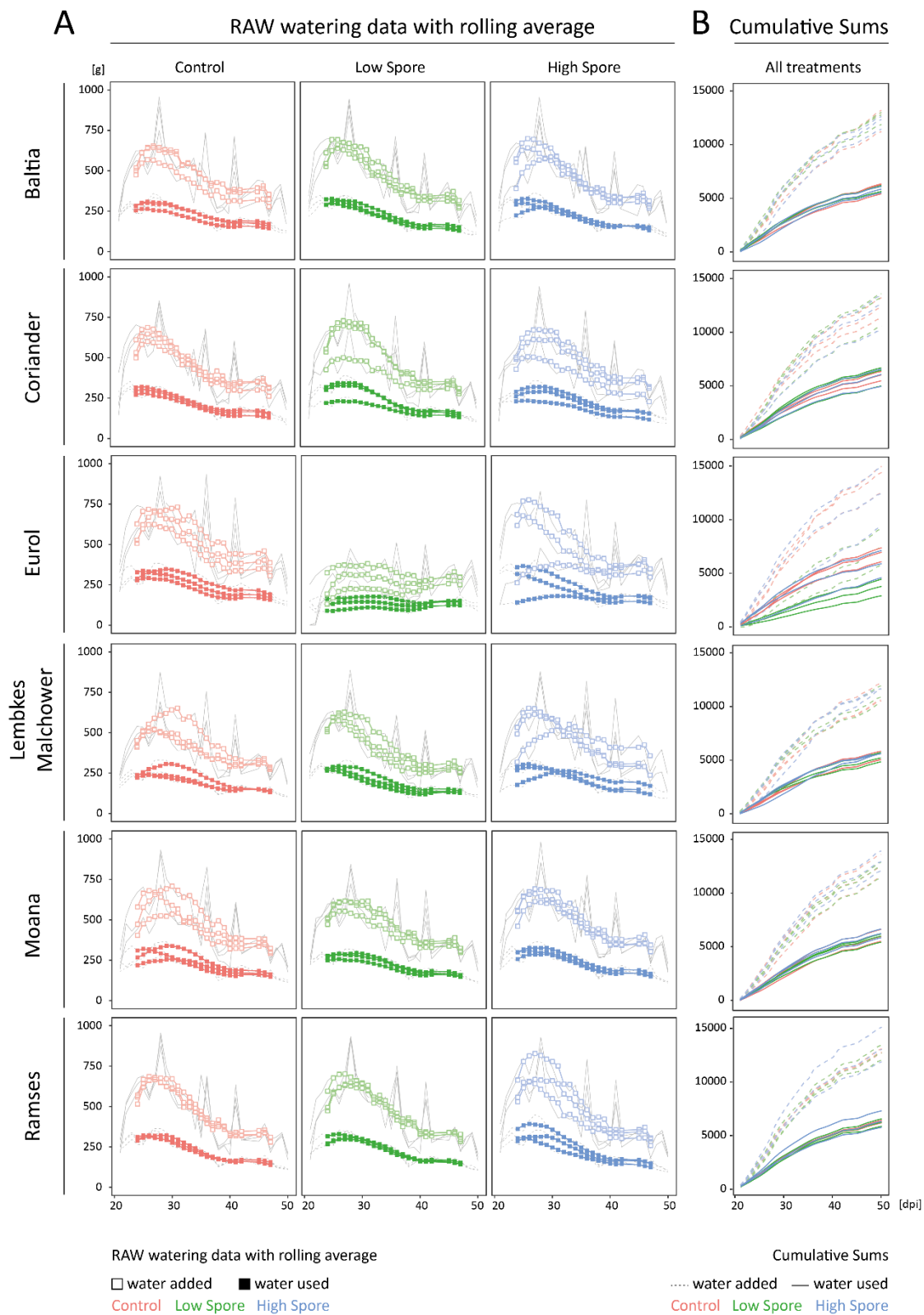
Figure 3.11: Watering results of 6 selected oilseed rape cultivars – IBERS Trial 2

[Legend on next page]

[Legend to figure 3.11]

|A| Watering data of 6 selected oilseed rape cultivars (3 treatments, 3 biological replicates per treatment). Added and used water is displayed as solid and dashed grey line, respectively. A rolling average (central 7 day window) is shown as connected squares, with colour-outlined squares representing added water, and colour-filled ones stand for used water. Mock treated (dH$_2$O) cultivars are shown in red, and clubroot inoculated cultivars with low and high spore densities in green and blue, respectively |B| Cumulative sums of 6 selected oilseed rape cultivars (3 treatments, 3 biological replicates per treatment). Total added water is displayed as dashed coloured lines, and total used water as solid coloured lines. Same colour code applies for treatments.
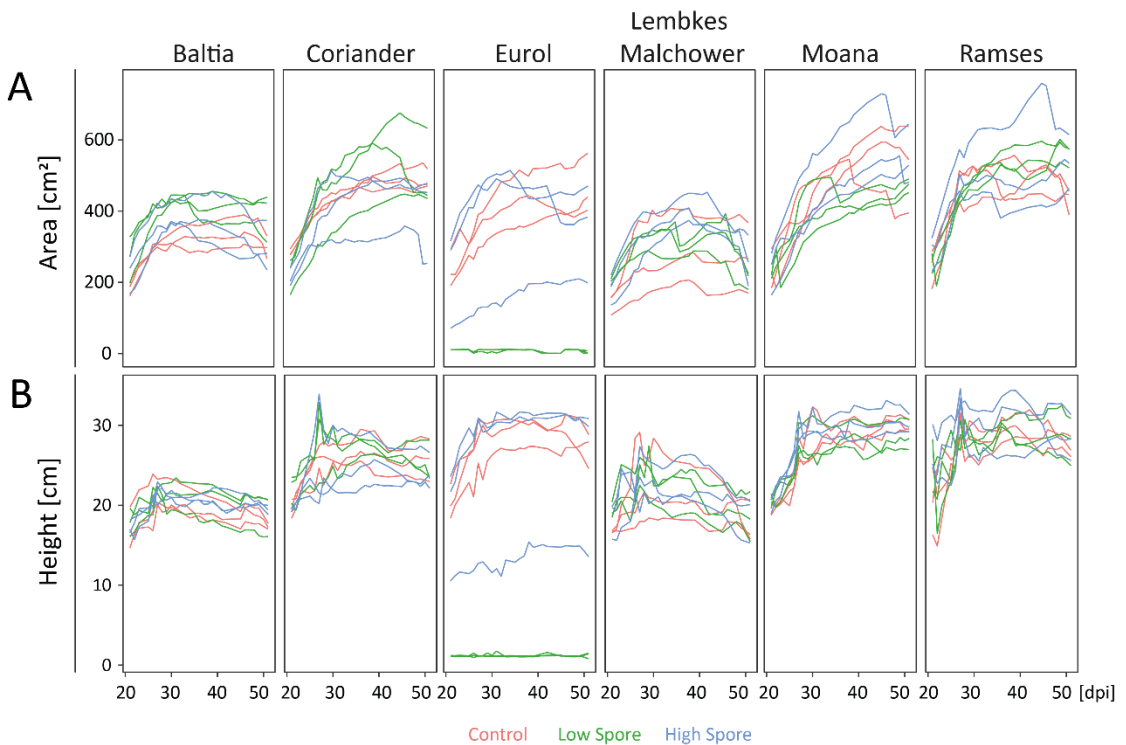
Figure 3.12: Growth results of 6 selected oilseed rape cultivars – IBERS Trial 2

|A|-|B| Area and height RAW data of 6 selected oilseed rape cultivars (3 treatments, 3 biological replicates per treatment) measured using RGB images. Data is shown as coloured lines. Mock treated cultivars (dH$_2$O) are red, clubroot spore treated cultivars green (low concentration) and blue (high concentration) |A| Area in cm^2 |B| Height in cm
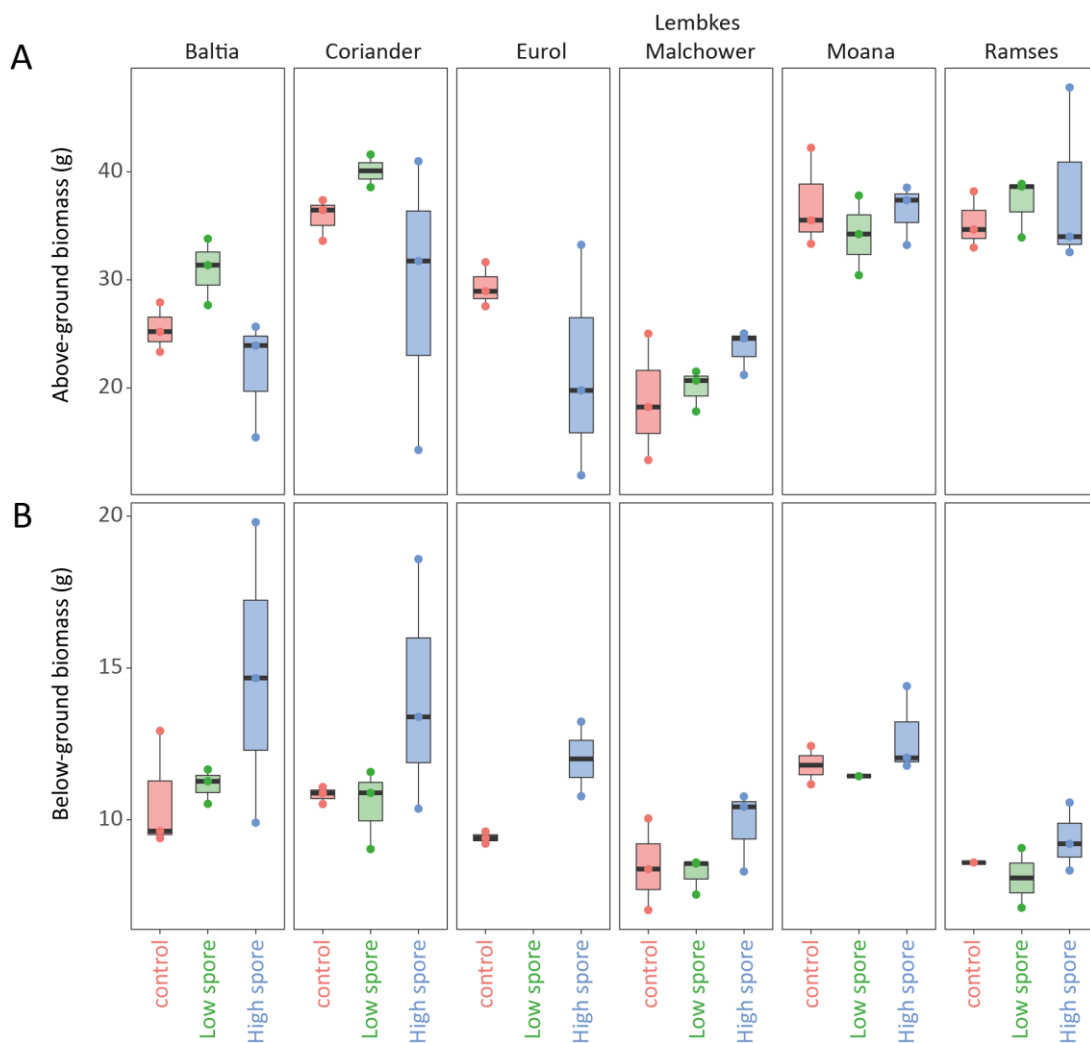
Figure 3.13: Biomass results of 6 selected oilseed rape cultivars – IBERS Trial 2

|A|-|B| Boxplots of dry weight measurements of above- and below-ground plant material obtained from 6 selected oilseed rape cultivars (3 treatments, 3 biological replicates per treatment). The data's median is shown as horizontal black line within the box, and the lower and higher quartile as horizontal black lines at both ends of the box. Variability outside the quartiles is indicated as lines extending vertically from the box (whiskers) to the most extreme data points. Data distribution of mock treated cultivars (dH$_2$O) and clubroot inoculated plants is shown as red (control), green (low spore), and blue (high spore) boxes. Underlying individual data points follow the same colour code |A| Dry weight of above-ground plant material in g |B| Dry weight of below-ground plant material in g
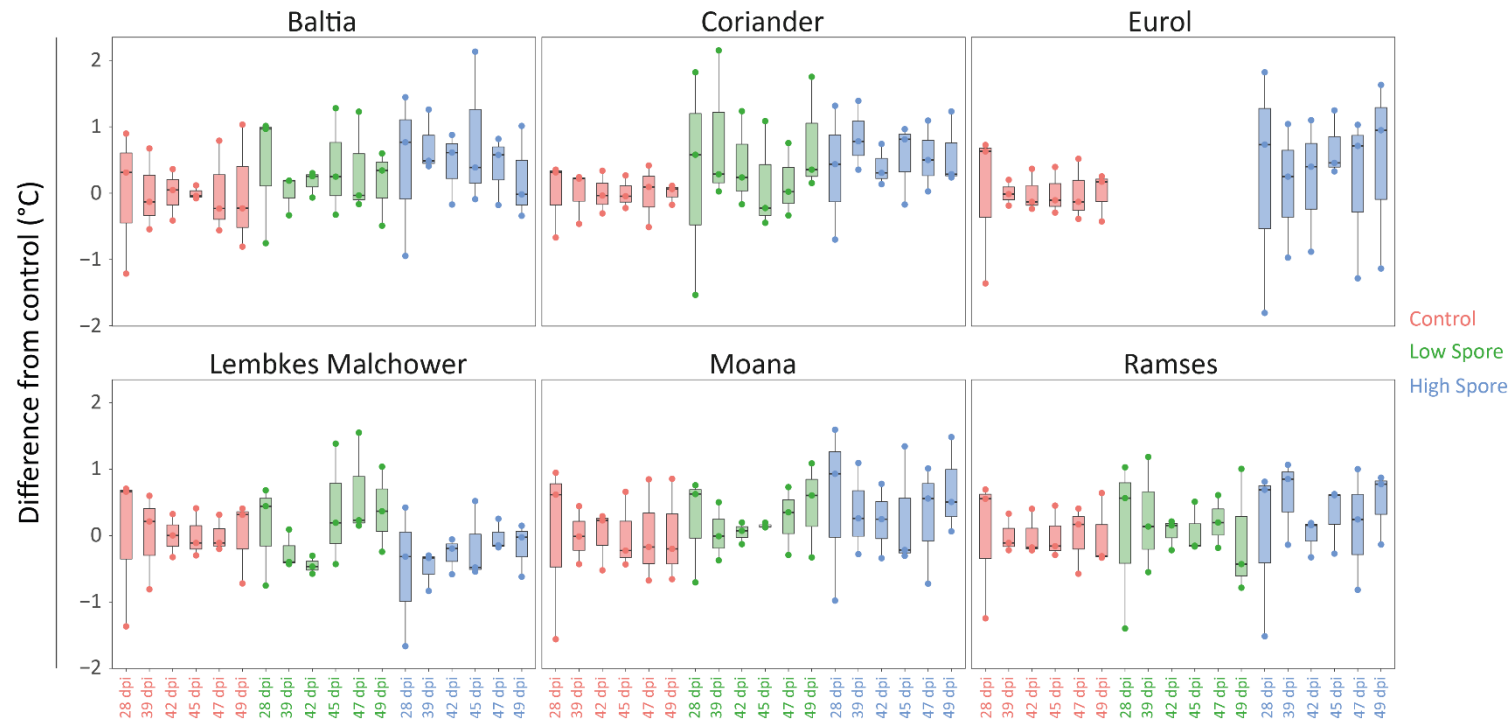
Figure 3.14: Thermal imaging results of 6 selected oilseed rape cultivars – IBERS Trial 2

Boxplots of plant leaf temperatures of 6 selected oilseed rape cultivars (3 treatments, 3 biological replicates per treatment) obtained by the manual spot method.

Temperatures of clubroot inoculated cultivars were compared to mock treated plants (dH$_2$O) during 5 time points (28, 39, 42, 45, 47, and 49 dpi). The data's

median is shown as horizontal black line within the box, and the lower and higher quartile as horizontal black lines at both ends of the box. Variability outside the

quartiles is indicated as lines extending vertically from the box (whiskers) to the most extreme data points. Data distribution of mock treated cultivars (dH$_2$O) and

clubroot inoculated plants is shown as red (control), green (low spore), and blue (high spore) boxes. Underlying individual data points follow the same colour

code.

3.2.4. PHENOMICS SCREEN *TRIAL 3* AT AWEC

As automated watering systems were problematical, a small scale screen was performed at AWEC using hand-watering. Due to limited growth room availability, the screen was conducted in a greenhouse growth chamber with fixed environmental conditions whose day length and temperature was below the optimal clubroot environment. For the screen, six different Brassica cultivars (Cauliflower, Cabbage, Kale, Kohlrabi, and two oilseed rapes) were used with 6 replicates and 3 treatments (mock-treated with dH_2O, and inoculated with low and high clubroot spore densities). All cultivars were positioned in trays according to treatment groups, and manually watered when required: initially every 3 days, later daily. Plant water use was measured weekly as described in section 2.4.2.2. At the end of the experiment, plants were destructively harvested, scored according to disease severity, and prepared for biomass measurements. Results for water use, disease scoring results/ end-point phenotype and biomass (fresh and dry weight) are seen in figure 3.15, 3.16, and 3.17.

Water use increased over time in all treatments for all cultivars. Thereby, differences between control and clubroot inoculated plants became apparent at later time points (i.e. week 5 onwards). In both Chinese Cabbage Wong Bok and Winter Oilseed Rape Temple, inoculated plants showed reduced water use (approx. 30-40% less). The opposite was seen in Ragged Jack Kale. However, scoring/end-point phenotypes and biomass data revealed heterogeneous clubroot infection with hardly any gall formation for the most susceptible cultivar Chinese Cabbage Wong Bok (figure 3.16 B). Extremely small roots were noticeable for all cultivars. Surprisingly, the clubroot resistant oilseed rape variety Cracker showed gall formation in one out of six high-spore inoculated plants. However, the infected individual plant could be classified as breeding-by-product since 30% of all clubroot resistant lines do not contain the desired resistance gene (Elke Diederichsen, personal communication).
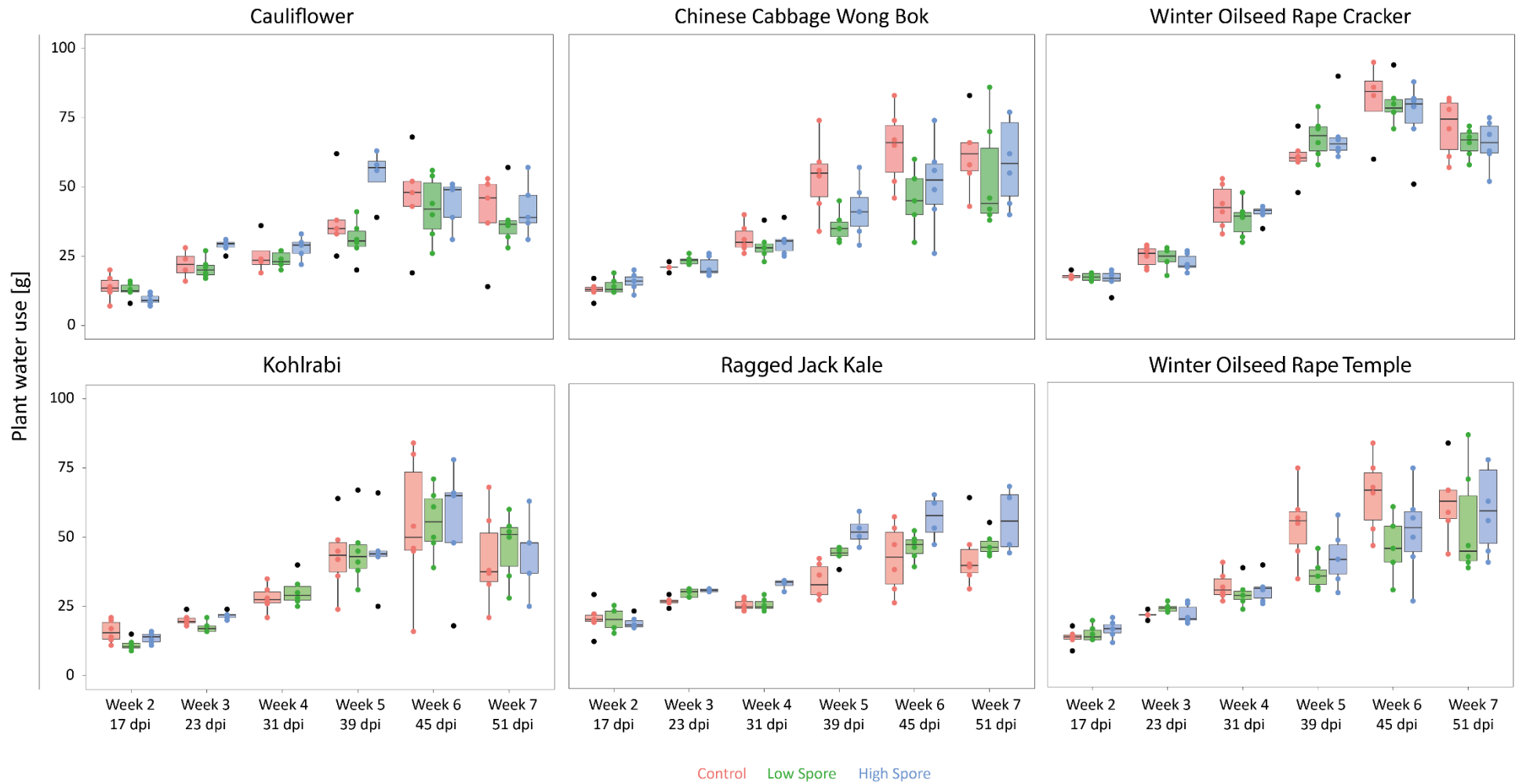
Figure 3.15: Watering results of 6 Brassica cultivars – AWEC *Trial 3* [legend on next page]

[Legend to figure 3.15]

Boxplots of water use from 6 Brassica cultivars (3 treatments, 6 biological replicates per treatment) obtained by a weekly performed hand-watering protocol at 17, 23, 31, 39, 45, and 51 dpi. The data's median is shown as horizontal black line within the box, and the lower and higher quartile as horizontal black lines at both ends of the box. Variability outside the quartiles is indicated as lines extending vertically from the box (whiskers) to the most extreme data points. Data points outside the whiskers (outliers) are plotted in black. Data distribution of mock treated cultivars (dH$_2$O) and clubroot inoculated plants is shown as red (control), green (low spore), and blue (high spore) boxes. Underlying individual data points follow the same colour code.

A

Brassica Cultivars	Control number of infection	Control visual score	Low Spore number of infection	Low Spore visual score	High Spore number of infection	High Spore visual score
Cauliflower	0/5	0	0/6	0	3/5	1-2
Chinese Cabbage Wong Bok	0/6	0	2/6	1	1/5	2
Winter OSR Cracker	0/6	0	0/6	0	1/6	1
Kohlrabi	0/6	0	0/6	0	2/5	1
Ragged Jack Kale	0/6	0	0/6	0	0/4	0
Winter OSR Temple	0/6	0	0/6	0	3/6	1-3

B
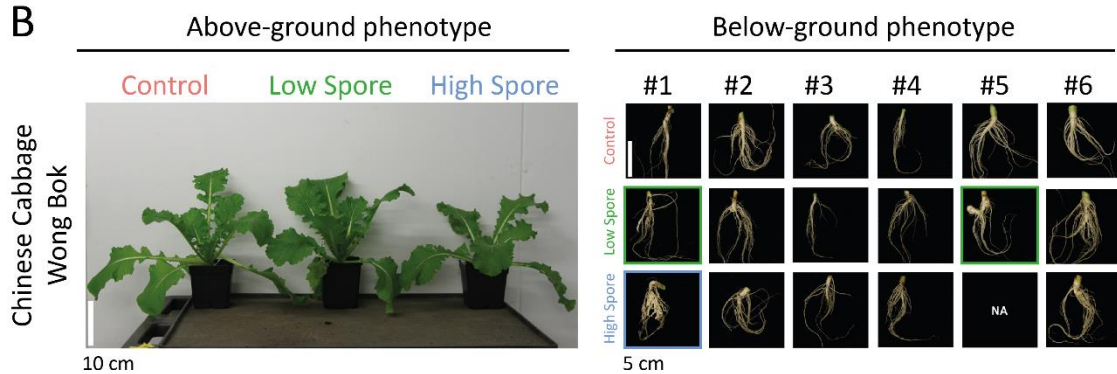
Figure 3.16: Disease scoring and end-point phenotype of Cabbage – AWEC *Trial 1*

|A| Table of visual scoring results of 6 Brassica cultivars (3 treatments, unless stated 6 biological replicates per treatment |B| Above- and below-ground phenotype of Chinese Cabbage Wong Bok (3 treatments, unless stated 6 biological replicates per treatment) at 51 dpi. Left panel shows selected plants representing the above-ground phenotype of each treatment group (mock-treated with dH$_2$O, and inoculated with low and high spore densities). Scale bars are 10 cm. Right panel displays all roots after excavation with gall formation highlighted in green (low spore) or blue (high spore). Scale bars are 5 cm.
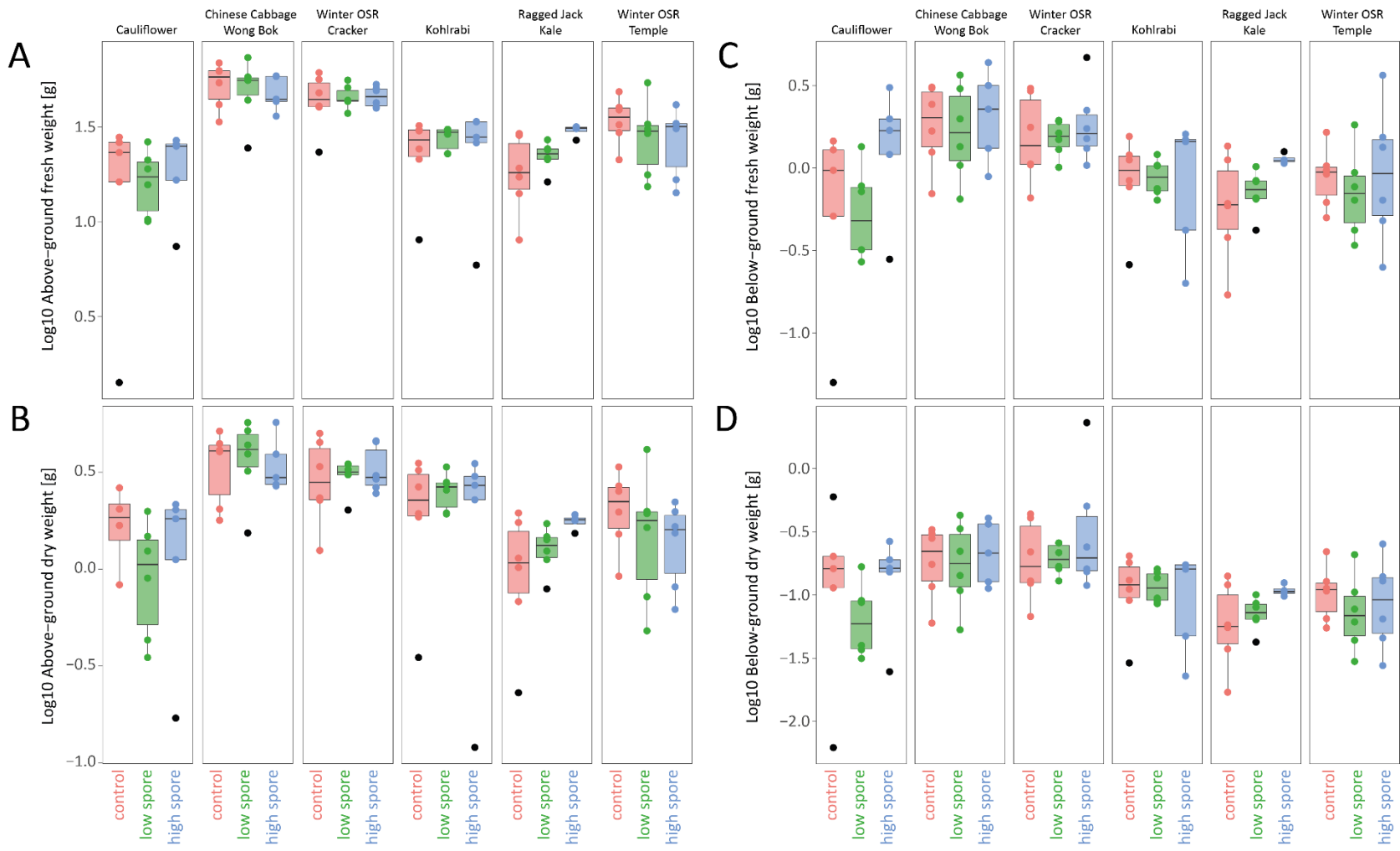
Figure 3.17: Biomass results of 6 Brassica cultivars – AWEC *Trial 1* [Legend on next page]

[Legend to figure 3.17]

|A|-|D| Boxplots of fresh and dry weight measurements of above- and below-ground plant material obtained from 6 Brassica cultivars (3 treatments, 6 biological replicates per treatment). The data's median is shown as horizontal black line within the box, and the lower and higher quartile as horizontal black lines at both ends of the box. Variability outside the quartiles is indicated as lines extending vertically from the box (whiskers) to the most extreme data points. Data points outside the whiskers (outliers) are plotted in black. Data distribution of mock treated cultivars (dH$_2$O) and clubroot inoculated plants is shown as red (control), green (low spore), and blue (high spore) boxes. Underlying individual data points follow the same colour code. P > 0.05 (2-Way-ANOVA)

|A| Log10 fresh weight of above-ground plant material in g

|B| Log10 dry weight of above-ground plant material in g

|C| Log10 fresh weight of below-ground plant material in g

|D| Log10 dry weight of below-ground plant material in g

3.3. DISCUSSION

Clubroot-mediated growth promotion and inhibition

Severe clubroot disease in Brassica host plants cause gall formation and stunted growth of the aerial plant body, resulting in dwarfed phenotypes. However, in 2005, Devos *et al*. reported above-ground growth stimulation in Chinese Cabbage Wong Bok after inoculation with 1 ml spore suspension containing 1 x 10^6 spores/ml of the pathotype ECD 16/2/12 from Penyrheol, South Wales [59]. In this chapter, during preliminary screens at AWEC, above-ground growth stimulation was not only seen in Chinese Cabbage Wong Bok, but also in Winter Oilseed Rape Temple and Ragged Jack Kale when inoculated with 50 ml spore suspension containing 6.25 x 10^1 and 6.25 x 10^2 spores/ml of the same pathotype. In contrast, all three cultivars showed growth inhibition when inoculated with higher spore densities (i.e. 6.25 x 10^4 and 6.25 x 10^5 spores/ml). Spore density-dependent growth differences was the trigger for larger phenomics screens at the phenomics platform IBERS in Wales. However, results seen at AWEC could not be repeated at IBERS. One of the reasons for the absence of growth stimulation at low spore densities could have been altered environmental conditions (e.g. soil type, soil moisture, temperature, and irradiance; see table 2.2 in section 2.3). Clubroot disease establishment not only depends on host susceptibility, but also on environmental factors (e.g. temperature, light, soil composition, and humidity).

Genotype + Environment = Phenotype

The majority of performed screens were not reproducible or reliable. The underlying reason is that phenotypes are not only closely linked with genotypes, but also with the environment. Changes in the environment can cause changes in phenotypes. Infected plants interact with both their microbial intruders (i.e. biotic factors) and the physical environment (i.e. abiotic factors). The same applies to pathogens. These complex and dynamic interactions between host plant, pathogen and the physical environment must be considered when performing disease phenomics screens [119][120]. Locations and time frames are important. Field studies are more applicable for farmers since they reflect real-life scenarios. Seasonal changes (e.g. temperature, photoperiod, irradiance, or humidity) reduce repeatability and cause inconsistent data sets. The same applies for screens in greenhouses, where environmental conditions are either difficult to control (e.g. IBERS *Trial 1* and *2*) or pre-set and therefore not changeable (e.g. AWEC *Trial 3*). This can be particularly problematic, when disease screens (e.g. clubroot) rely on optimal environmental conditions to guarantee uniform infection. Two strategies might be advisable to minimise problems of repeatability and inconsistencies: (I) replicated field trials across seasons

over several years, or (II) replicated trials in closed systems (e.g. laboratory growth chambers) with consistent environments that are changeable if required.

Another layer of complexity to clubroot phenomics screens adds genotypic heterogeneity of host and pathogen. Individuals of the same Brassica genotype vary slightly in phenotypes, and the *P. brassicae* strain ECD 16/2/12 from Penyrheol contains several pathotypes of unknown proportions. In this chapter, for each screen at AWEC and IBERS, a new clubroot inoculum was freshly extracted from galls of Chinese Cabbage Wong Bok. It was therefore likely that each inoculum contained the same pathotypes, but different proportions thereof. For future screens, the problem of inoculum heterogeneity could be tackled in two ways: Usage of single spore isolates, or aliquots from one clubroot inoculum[14]. Problems of plant variation on the other hand cannot be solved for phenomics screens since successful (better-yielding) QTL investigations rely on high numbers of genotypes than on biological replicates [121][122].

Automated watering: Drought-triggered reduction of clubroot infection

The biggest factor for experimental problems at IBERS was the failure of the automated watering system. The watering algorithm for *trial 1* did not include plant biomass increase over time, and the biomass-corrected algorithm for *trail 2* struggled to meet the plant's actual requirements for water. In both cases, water was withheld by the system, and plants were systematically droughted. Plants recognise a water deficit in roots through turgor loss and reduced water potential. This activates biosynthesis of ABA. ABA is then transported from roots to leaves where it triggers stomata closure and reduced stomatal conductance (i.e. rate of CO_2 entering and water vapour exiting stomata). This has two effects: elevated leaf temperatures due to restricted water evaporation (i.e. minimized cooling effect), and decrease of internal CO_2 concentrations. The latter perturbs photosynthesis and downregulates the rate of carbon fixation. This results in limited availability of carbohydrates, and therefore reduces plant growth and biomass production [123]. Drought symptoms are therefore similar to those occurring during clubroot disease. However, "actual" drought is caused by soil water scarcity, while clubroot-mediated drought is based on difficulties to transport water to the aerial plant body. The underlying reason is the reduction of xylogenesis at the onset of gall formation [73]. Hence, drought-stress signals in infected plants (e.g. elevated leaf temperatures) usually occur despite high water content in soil – this was seen during IBERS *trial 1*. However, clubroot infection is impeded by drought since soil water scarcity inhibits the movement of primary and secondary zoospores to root hairs (i.e. reduced primary and secondary infection). Reduced clubroot infection was particularly

---

[14] Aliquots of a *P. brassicae* inoculum can be stored at -20°C until required. Freezing clubroot aliquots harbours a minimal risk of losing spore viability. However, the number of losses is neglectable (Elke Diederichsen, personal communication).

noticeable during *trial 2*, when the location of gall formation was compared with the water distribution in plant pots. If gall formation was apparent, it mostly occurred within wet soil patches. Roots within dry soil patches did not exhibit disease symptoms. Hence, uneven water distribution caused mosaic-like root phenotypes. Cultivars of *trial 2* exhibited growth stagnation (i.e. area and height), and thermal imaging results showed no discernible pattern associated with disease (data shown for 6 pre-selected cultivars with the most uniform disease symptoms). Instead, great variation in temperature over time was observed for all treatments. It is therefore very likely that drought signals were interfering with clubroot signals. This needs to be addressed during future screens using well-watered and clubroot inoculated cultivars.

Equipment and data management

Functioning equipment for experimental needs alongside the management of huge and complex data sets are challenging aspects of phenomics screens. It underlines the importance of collaborations between biologists, mechanical engineers, computer scientists, and statisticians (ideally acquainted to biological systems) to bundle multi-disciplinary knowledge. This includes maintenance of equipment, exploration of possibilities and limitations of existing software, development of new software, and appropriate data handling. Sometimes, the absence of regular access to these skill sets can limit the use of equipment (e.g. usage of NIR imaging or chlorophyll fluorescence techniques) or data interpretation.

Conclusion

Non-invasive and non-destructive imaging and weighing techniques as part of the conducted disease phenomics screen could not quantify early and for the human eye invisible above-ground plant responses to below-ground clubroot disease. The main reason can be appointed to a lack of homogenous clubroot infection due to unfavourable environmental conditions (e.g. low temperature) and absence of adequate watering (e.g. systemic drought). Phenomics screens might be a promising tool in the future to detect abnormalities in plant development caused by both soil-borne pathogens (i.e. promising thermal imaging results), but in this study problems predominated the utility value.

CHAPTER 4: END-POINT DISEASE ASSESSMENT

4.1. INTRODUCTION

Plants are the primary producers on the planet, and fundamental for our existence. But like all living organisms they get infectious diseases caused by microbial pathogens. Pathogens have a profound impact on yield and product quality of agriculturally important crop systems. Since the vascular system serves as conduit for carbohydrate allocation and partitioning between source and sink organs [63], it is an attractive target for pathogens to ensure a reliable supply of host resources. The root vasculature of Brassica crops is the target of *P. brassica,* the causal agent of clubroot disease, after entering host plants via root hairs [28][17]. It provides the eukaryotic single cell organism with assimilates (i.e. carbohydrates, amino acids, and lipids), and plays a central role for the completion of its lifecycle at the expense of the plant's overall performance. During infection stages, manipulation of the host's cambial stem cells (i.e. excessive cell elongation and expansion through altered auxin-cytokinin signalling), and rearrangement of the host's root vascular system (i.e. reduction of xylogenesis) [12] transform the root into a large club-like gall which serves as strong sink for carbohydrates. Excessive root growth and deformation thereof stands in contrast to stunted above-ground growth. It reflects unbalanced root and shoot growth with changes in shoot-root ratios and total biomass. Therefore, biomass measurements can potentially be used as physiological measurements to quantify clubroot disease severity and host susceptibly/resistance. To date, the most obvious indicator for clubroot disease severity and host susceptibility/resistance is gall size and timing of gall formation. The existing standard clubroot classification system, which focusses on gall size, is the simplest and quickest way of classifying disease severity [109]. However, visual scoring is subjective and crude only classifying mild, intermediate, and severe gall formation. The limitations are unimportant when screening for qualitative resistance, but a limiting factor when performing screens for quantitative resistance, where small differences in root phenotypes can be crucial. Therefore, it is desirable to establish more precise methods with potential of low-cost large-scale application to quantify disease and host susceptibility/resistance.

A number of diagnostic molecular assays have been developed in the past to detect resting spores of *P. brassicae* in soil samples and water. These assays are based on conventional PCR techniques, or modifications thereof (i.e. nested PCR) [124][125][126] using primer pairs based on the sequence of *ipt*[15] genes or rRNA sequences (i.e. mostly 18S or ITS). But despite their reliability, sensitivity issues are encountered, and procedures experienced as time-consuming

---

[15] Encode isopentenyltransferases; key enzymes during biosynthesis of cytokinins

and laborious (i.e. double-PCRs, in which the amplicon of the first PCR was used as template for the second PCR). Subsequently, PCR-based assays were improved for quick and easy application (i.e. single PCR) [127]. In 2017, conventional PCR was performed to detect and identify geographical isolates of *P. brassicae* using 18S rRNA sequences [128][111]. However, the wish to quantify the concentration of *P. brassicae* in both soil and plant triggered the development of diagnostic assays based on qRT-PCR. In Canada, several qRT-PCR based assays have been used, for example to compare concentrations of *P. brassicae* in soil after one cropping cycle with Canola [129], or to test pathogenicity of new strains on susceptible/resistant Canola [130].

In this chapter, a conventional greenhouse resistance screen was conducted, focussed on end-point disease phenotypes of a *B. napus* population (= subset of the Brassica ASSYST panel [108]). The aim was to test the applicability and utility of biomass and molecular measurements for disease quantification compared to the clubroot classification system (i.e. visual scoring of gall sizes). The objectives of the chapter are (1) the development of a qRT-PCR based DNA assay for total quantification of *P. brassicae* in inoculated roots, (2) measurements of above- and below-ground biomass, (3) scoring of gall sizes according to the clubroot classification system, and (4) comparisons of results obtained from all methods applied.

For the latter, the following questions are asked:

- Do biomass and molecular assessments allow uninfected and infected cultivars to be distinguished?
- What correlations exist between clubroot gene copy numbers and biomass?
- Does the molecular assay allow a more precise quantification of disease than the common scoring system or biomass measurements?

4.2. RESULTS

A subset of the ASSYST panel of Brassica cultivars [108] was grown at AWEC (University of Sheffield) for an end-point disease screen. The group consisted of 33 genotypes, which included 2 swedes (Tina, Vige), 2 kales (Siberian Kale, Ragged Jack Kale), and 29 oilseed rape varieties (both Winter and Spring) (see supplementary table 1). The experiment was set up with 3 replicates and 2 treatments (mock-treated with dH_2O, and inoculated with 50 ml of $6.25x10^5$ clubroot spores/ml). Plants were grown, and destructively harvested at 51 dpi as described in table 2.4 of section 2.3.

At harvest, each plant was photographed and visually assessed according to the clubroot classification system (see table 2.1 in section 2.2). Primary root material was then collected for gDNA extraction, and the remaining root and shoot tissue dried for biomass measurements. DNA extraction was performed following a CTAB-based protocol with upstream bead-beater tissue homogenisation. Subsequently, the DNA concentration was measured (Quant-iT Pico Green with Herring sperm DNA as standard), and samples diluted to 5 ng/µl. For quantification of the clubroot pathogen in inoculated Brassica cultivars, the eukaryotic ribosomal cluster of *P. brassicae* was utilised. First, a primer pair aligning within the ITS + 5.8S rRNA region of the ribosomal cluster was used to prepare a standard (= ITS standard). Hence, the *P. brassicae* ITS + 5.8S rRNA fragment was amplified, cloned into pGEM-t-easy, sequenced, and prepared as 10-10^6 copies/µl (see section 2.5). Total gDNA (plant + pathogen) from samples was amplified using qRT-PCR and the ITS primer pair, and then compared to the ITS standard.

Figure 4.1 displays the visual scoring results of mock and clubroot inoculated genotypes after root excavation at 51 dpi.

Clubroot infection was absent in all mock-treated cultivars as well as in six clubroot inoculated genotypes. No gall formation was noticed (score "0"). Six clubroot inoculated genotypes showed root phenotypes of intermediate infection with four of them classified as "1" and two as "2". Sixteen genotypes were scored as "3" due to formation of large galls. However, Winter Oilseed Rape Cracker showed variable root phenotypes. The roots of two replicates were without visible disease symptoms (score 0), but one replicate showed gall formation (score 2).
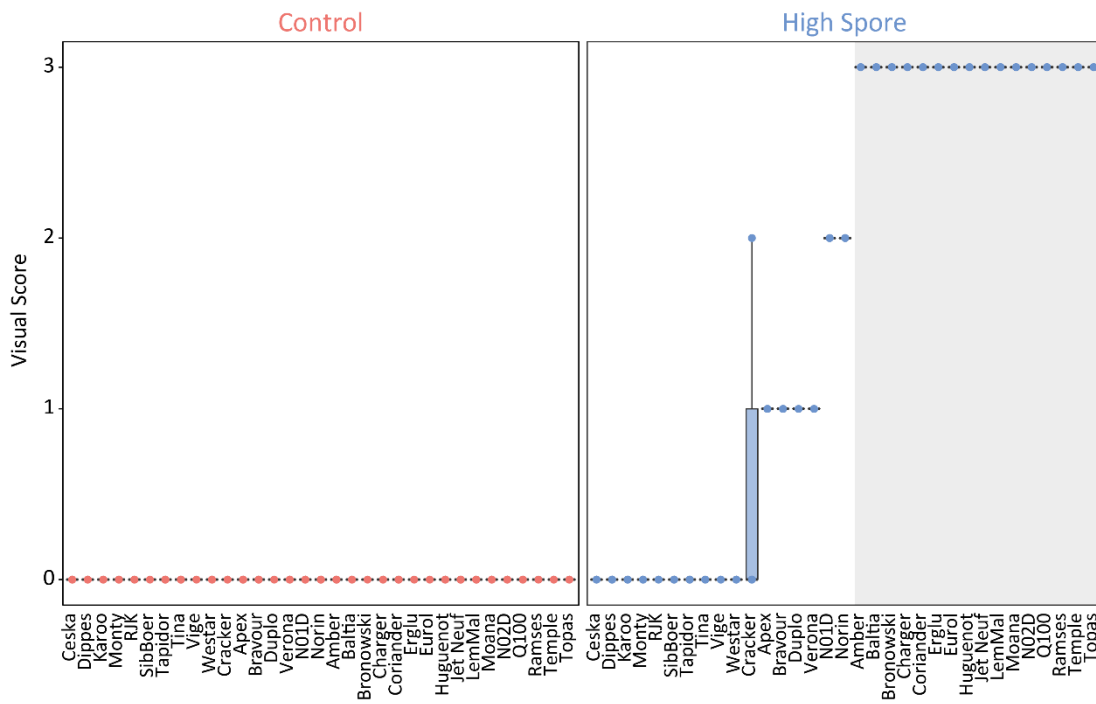
Figure 4.1: Boxplots displaying results of visual root assessments of 33 genotypes at 51 dpi (2 treatments, 3 biological replicates per treatment). The scoring system used in this study is described in section 2.2.2. The data's median is shown as horizontal black line across the box, and the lower and higher quartile as horizontal black lines at both ends of the box. Variability outside the quartiles is indicated as lines extending vertically from the box (whiskers) to the most extreme data points (= minimum and maximum). Underlying data points of mock- and clubroot inoculated cultivars are displayed in red and blue, respectively. Grey areas represent cultivars with most severe gall formation.

Biomass measurements of above- and below-ground plant material as seen in figure 4.2 (log10 data) indicated differences between genotypes but also above- and below ground biomass changes as a consequence of clubroot disease. However, these variations in the RAW data caused difficulties to extract more information of plant performance (i.e. changes in total biomass and the driver for these changes). Therefore, biomass data of above- and below ground plant material of clubroot-inoculated cultivars was first mean-normalised to mock-inoculated genotypes, and then ranked for biomass increase/decrease. Subsequently, total biomass (root + shoot), and the impact of root biomass on total biomass (root/ root + shoot) could be analysed. The results are seen in figure 4.3.
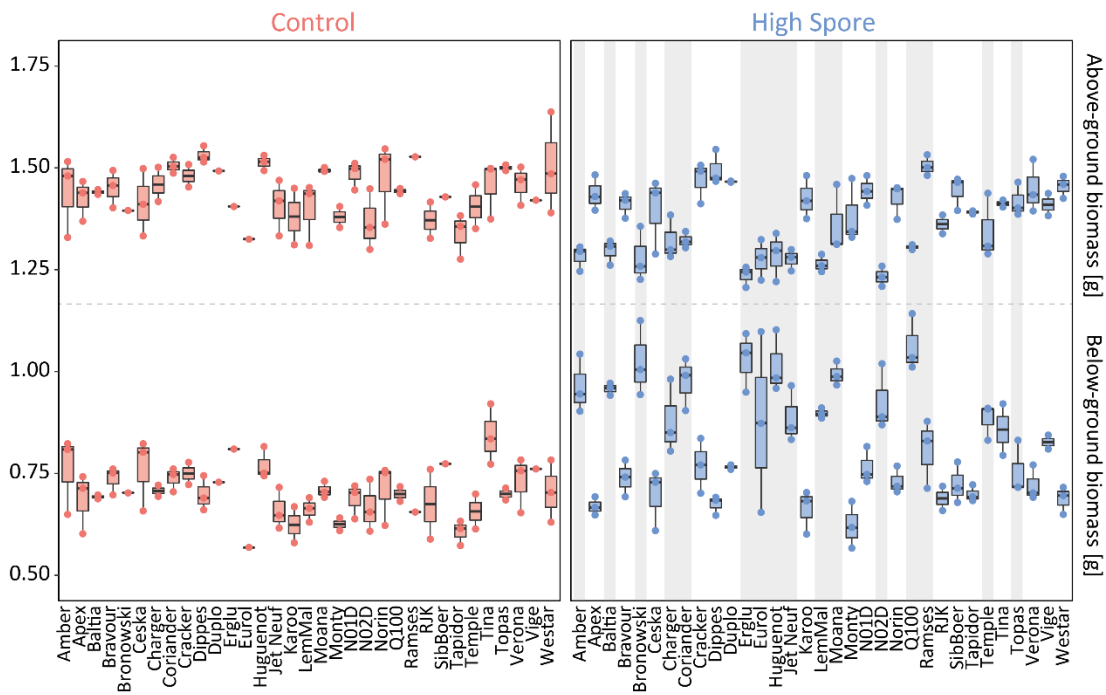
Figure 4.2: Boxplots of RAW biomass data (log10) obtained from above- and below-ground plant material of 33 genotypes with 2 treatments (mock-treated with dH$_2$O, and clubroot inoculated with 6.25x10^5 spores/ml) and 3 biological replicates per treatment. The data's median is shown as horizontal black line across the box, and the lower and higher quartile as horizontal black lines at both ends of the box. Variability outside the quartiles is indicated as lines extending vertically from the box (whiskers) to the most extreme data points (= minimum and maximum). Red boxes represent data distribution of mock-treated cultivars, and blue boxes of high spore inoculated plants. Underlying individual data points corresponding to biological replicates are displayed in red (control), and blue (high spore). Grey areas in the right panel indicate genotypes with severe clubroot infection (class 3 of the scoring system as described in section 2.2.2). The horizontal dashed grey line separates out data of above- and below-ground biomass.

Total biomass (figure 4.3 A) of all 33 genotypes shows variation within each mock- and clubroot treated genotype. Clubroot-inoculated genotypes fell into 3 groups: those with bigger, equal, or smaller total biomass in comparison to control counterparts. Reduced total biomass was more apparent in severely infected genotypes (class "3"), but could also appear in genotypes classified as "0-2" (i.e. Bravour, Norin and Westar). Interestingly, not all genotypes with large galls showed reduced total biomass (highlighted in grey). Some maintained equal biomass to their controls (i.e. Temple and Bronowski), others were slightly bigger (i.e. Eurol). However, in all severe cases of clubroot infection, root biomass had a major impact on total biomass (figure 4.3 B).

Figure 4.4 highlights both below- and above-ground biomass separately for all 33 genotypes (log10 data, mean normalised) alongside the correlation of below- and above-ground biomass (log10 data, not mean normalised). The data indicates that all severely infected genotypes show higher below- (figure 4.4 A) and generally lower above-ground biomass (figure 4.4 B) compared to their controls. However, some of the severely infected genotypes must have maintained above-ground growth to some extent (data points are close to the baseline), while the majority sent most available resources towards the roots to *P. brassicae*, leading to above-ground growth stagnation. Figure 4.4 C reveals an allometric relationship between above- and below-ground biomass of mock-inoculated genotypes (left panel). Clubroot inoculated plants (right panel) fell into 2 groups: those that show the same allometry between above- and below-ground as seen in control plants, and those with greater proportion of root/gall biomass. In these cultivars an increase in root biomass correlated with a decrease in shoot biomass, as previously stated. Following up on that, above-ground biomass measurements have the potential to be good indicator of clubroot susceptibility, tolerance, or resistance next to the assessment of below-ground biomass.
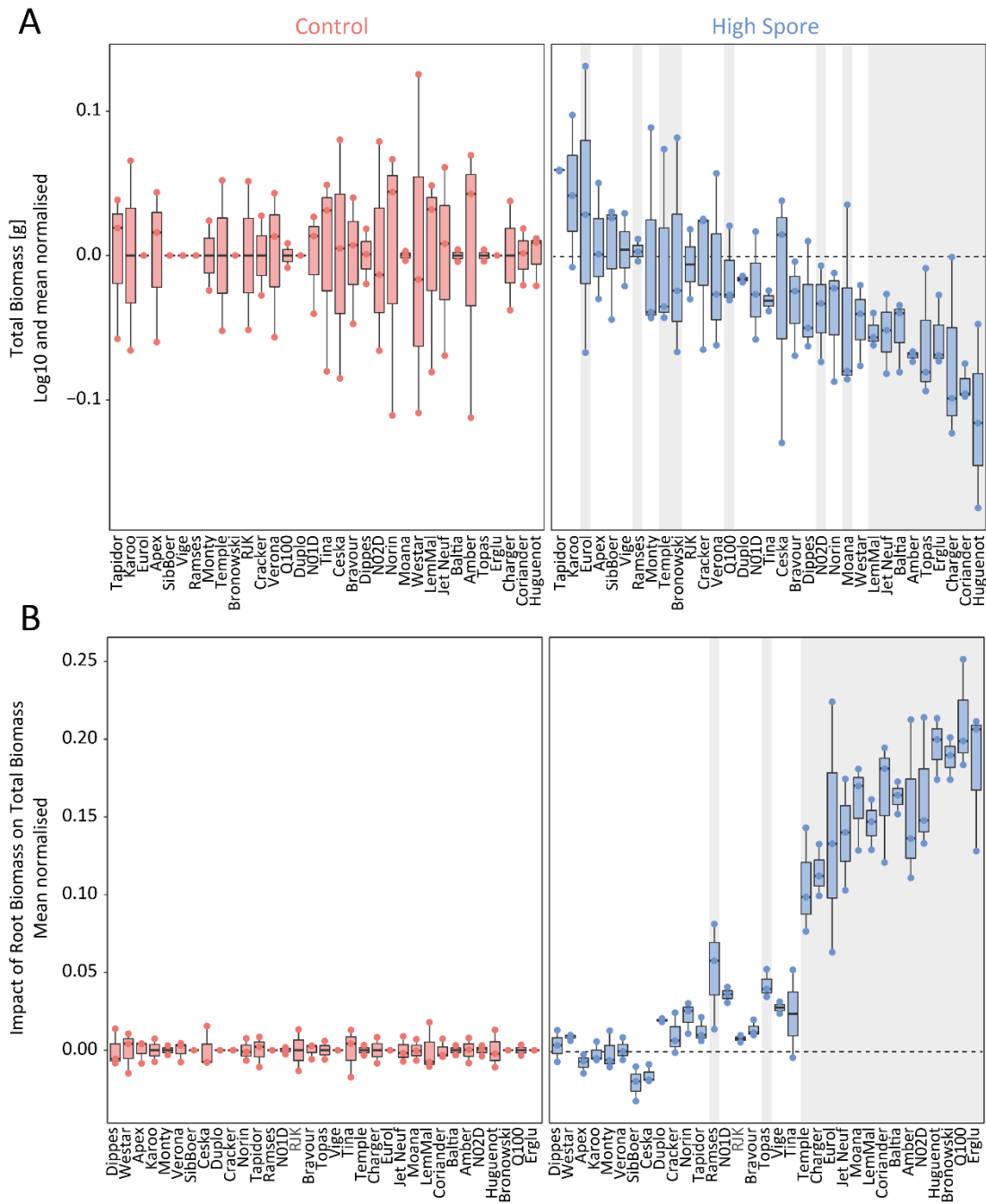
Figure 4.3: Biomass data of 33 genotypes at 51 dpi – Part 1

[Legend on next page]

[Legend to figure 4.3]

|A| + |B| Boxplot showing the biomass of 33 genotypes with 2 treatments (mock-treated with dH$_2$O, and clubroot inoculated with 6.25x10^5 spores/ml) and 3 biological replicates per treatment. The data's median is shown as horizontal black line across the box, and the lower and higher quartile as horizontal black lines at both ends of the box. Variability outside the quartiles is indicated as lines extending vertically from the box (whiskers) to the most extreme data points (= minimum and maximum). Red boxes represent data distribution of mock-treated cultivars, and blue boxes of high spore inoculated plants. Underlying individual data points corresponding to biological replicates, are displayed as coloured points in red (control), and blue (high spore). Data is logged (base 10) and mean-normalised. Grey areas indicate genotypes with severe clubroot infection (class 3 of the scoring system as described in section 2.2.2), and the horizontal dashed black line highlights the baseline after normalisation.

|A| Total biomass (log10 and mean normalised, displayed in descending order) |B| Impact of root biomass on total biomass (log10 and mean normalised, displayed in ascending order)
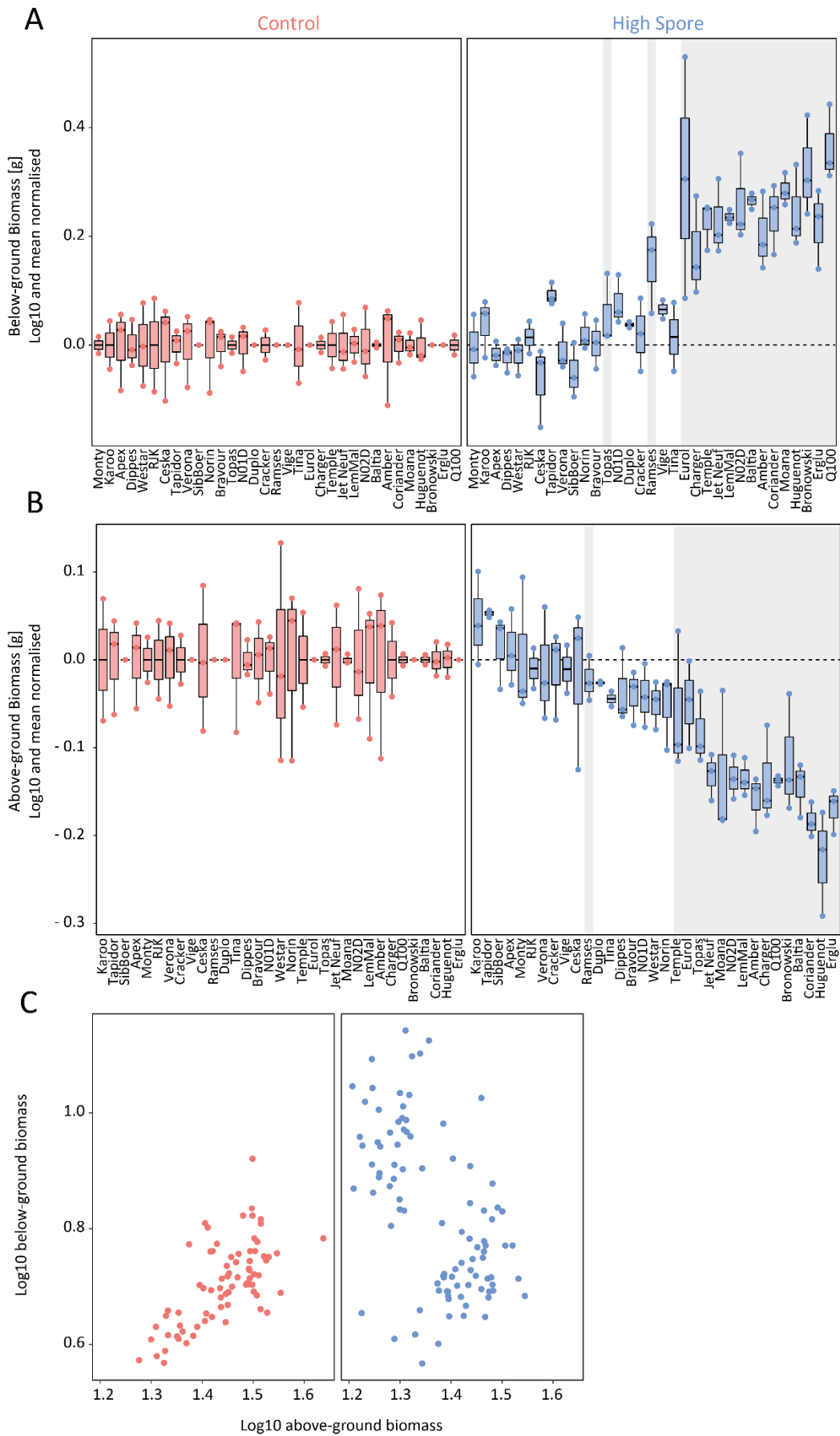
Figure 4.4: Below- and above-ground biomass data of 33 genotypes at 51 dpi – Part 2

[Legend on next page]

[Legend to figure 4.4]

|A| + |B| Boxplot showing the biomass of 33 genotypes with 2 treatments (mock-treated with dH$_2$O, and clubroot inoculated with 6.25x10^5 spores/ml) and 3 biological replicates per treatment. The data's median is shown as horizontal black line across the box, and the lower and higher quartile as horizontal black lines at both ends of the box. Variability outside the quartiles is indicated as lines extending vertically from the box (whiskers) to the most extreme data points (= minimum and maximum). Red boxes represent data distribution of mock-treated cultivars, and blue boxes of high spore inoculated plants. Underlying individual data points corresponding to biological replicates, are displayed as coloured points in red (control), and blue (high spore). Data is logged (base 10) and mean-normalised. Grey areas indicate genotypes with severe clubroot infection (class 3 of the scoring system as described in section 2.2.2), and the horizontal dashed black line highlights the baseline after normalisation.

|A| Below-ground biomass (log10 and mean normalised, displayed in ascending order)

|B| Above-ground biomass (log10 and mean normalised, displayed in descending order)

|C| Scatter plot of biomass data (log10) showing the relationship of above- and below-ground biomass of 33 genotypes. Data is separated by treatment (2 treatments, 3 biological replicates per treatment). Mock- and clubroot inoculated cultivars are displayed in red and blue, respectively.

Figure 4.5 summarises the molecular results from all 33 genotypes. The qRT-PCR assay could detect differences in ITS copy numbers between mock- and clubroot inoculated cultivars. Although the ITS primers were specific for *P. brassicae*, a low level of amplification was seen in control groups – the equivalent of between 10^2 and 10^4 ITS copies. Primer unspecificity was ruled out since a standard PCR using DNA samples of control and infected test plants showed no signal for the control, but a clear band for the clubroot-containing sample (data not shown). However, contamination caused by automated sample homogenisation (occasional breakage of reaction tubes) or by robotic pipetting of the qRT-PCR reactions could be a potential reason.

According to the molecular results, clubroot-inoculated genotypes fell into 2 groups: those with low ITS copy numbers as seen in mock-treated controls (10 out of 33 genotypes, 30.3%), and those with high ITS values (21 out of 33 genotypes, 63.6%). The "high-ITS"- group contained the majority of clubroot inoculated genotypes, and showed low variation in ITS values between biological replicates of each genotype. On the contrary, variation between biological replicates of genotypes within the "low-ITS"- group is higher. Particularly high variation in ITS values was noticeable in the oilseed rape varieties Cracker and Verona (2 out of 33 genotypes, 6.1%), ranging from low (control-like) to high numbers of ITS copies. However, the variation in ITS copy numbers was consistent with their variable root phenotypes (figure 4.5 B). Clubroot inoculated Cracker showed heterogeneous phenotypes with 2 replicates revealing no visible symptoms and 1 showing gall formation. Secondary roots of Verona contained bubble-like clubs which differed in number and size amongst biological replicates. It is therefore most likely, that collected root samples contained variable amounts of gall material. Interestingly, Cracker's intermediate sized gall (score "2") and Verona's small clubs on secondary roots (score "1") did not have an impact on root biomass data (figure 4.5 C). While root biomass between mock-treated and clubroot inoculated Cracker and Verona was identical with $p > 0.05$ (two-sample t-test), ITS values differed between treatment-groups.

For statistical analysis of the molecular results, the approach of an interval estimate was applied to separate out healthy from infected plants within the population. First, log10 ITS values of samples derived from all 33 genotypes were plotted as histogram (figure 4.5 D). Then, the population's mean (control + inoculated genotypes) was calculated, and a confidence interval applied (mean + 3x standard deviation = 99%). The confidence interval aimed to find out the true value of the population mean, and to highlight genotypes that contain or lack the true value of the mean. It therefore, created a boundary within which the true value of the population's mean will fall (= healthy genotypes). Hence, genotypes containing the true value of the mean (= low ITS copy numbers) could be classified as "healthy" (left panel), and genotypes lacking it (high ITS copy numbers) categorised as "infected" (right panel).
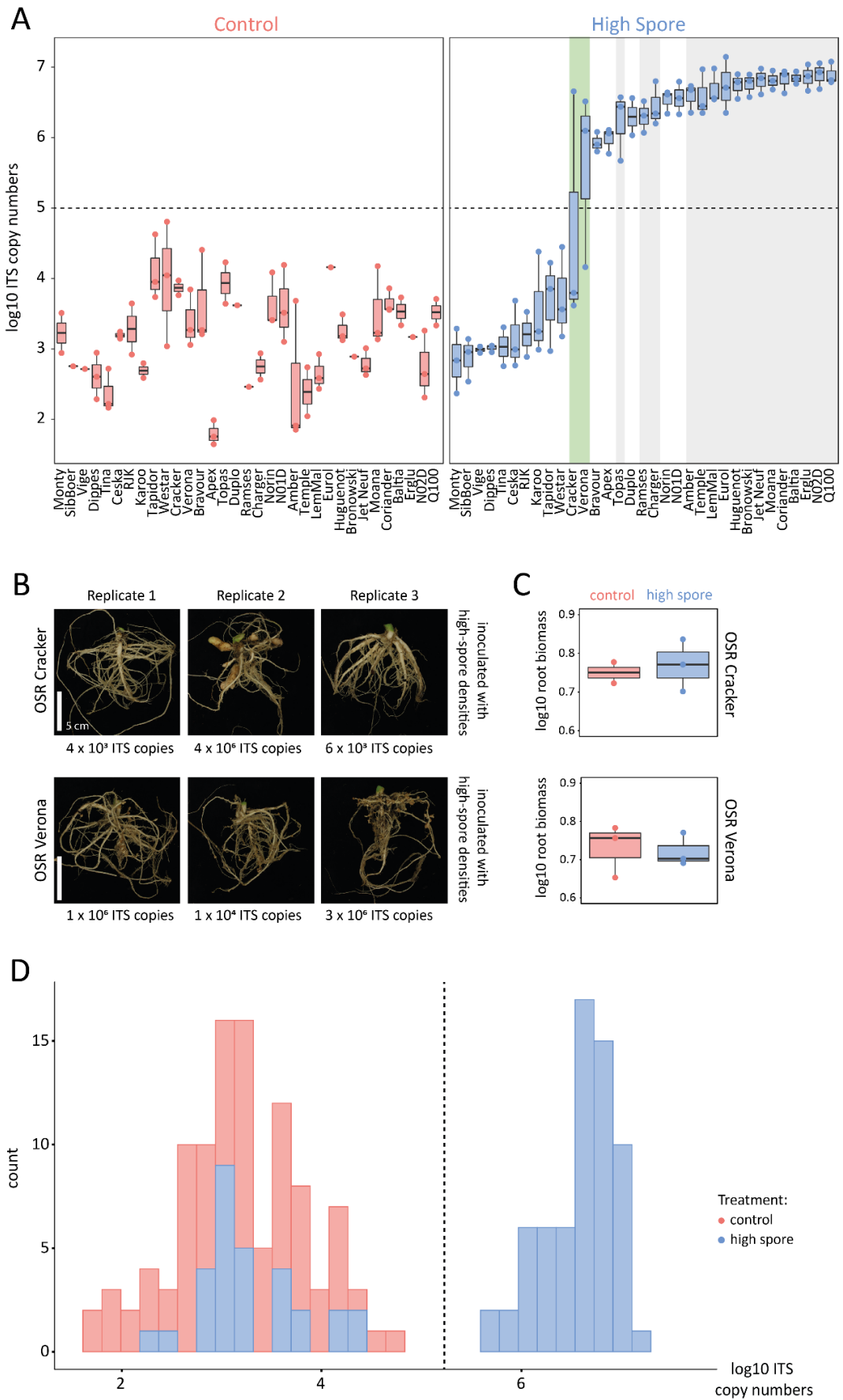
Figure 4.5: ITS copy numbers of 33 genotypes at 51 dpi [Legend on next page]

[Legend to figure 4.5]

|A| Boxplot showing logged ITS copy numbers (base 10) of 33 genotypes in ascending order (2 treatments, 3 biological replicates per treatment). The data's median is shown as horizontal black line across the box, and the lower and higher quartile as horizontal black lines at both ends of the box. Variability outside the quartiles is indicated as lines extending vertically from the box (whiskers) to the most extreme data points (= minimum and maximum). Red boxes represent data distribution of mock-treated cultivars (dH$_2$O), and blue boxes of high spore inoculated plants (6.25x10^5 spores/ml). Underlying individual data points corresponding to biological replicates, are displayed as coloured points in red (control), and blue (high spore). Grey areas indicate genotypes with severe clubroot infection (class 3), and green areas highlight genotypes with heterogeneous phenotypes. The horizontal dashed black line is artificially set and shows the point when samples separate into low and high ITS copy numbers |B| Root phenotype of inoculated (6.25x10^5 spores/ml) and most variable genotypes (oilseed rape Cracker and Verona) with corresponding log10 ITS copy numbers below photographs |C| Boxplot showing log10 root biomass of Cracker and Verona at 51 dpi. Same colour code applies. Scale bars are 5 cm. $P > 0.05$ (Two-sample t-test) |D| Histogram displaying data distribution of log10 ITS copy numbers. Counts of log10 ITS copy numbers derived from mock- and clubroot inoculated genotypes are represented on red and blue, respectively. The vertical dashed black line highlights the confidence interval (population's mean + 3x SD) which separates out healthy (left panel) and infected (right panel) genotypes.

In figure 4.6 A results obtained from molecular assessments (ITS copy numbers), visual scores, and biomass measurements (root-shoot ratios) were compared. Uninfected cultivars showed low root-shoot ratios ($> 10^2$) and low ITS copy numbers ($> 10^5$ copies). For mildly and intermediately infected cultivars root-shoot ratios remained unchanged ($> 10^2$), while ITS values increased gradually (5×10^5-5×10^6 copy numbers). Severely infected cultivars were the most diverse of all inoculated genotypes. Root-shoot ratios varied considerably (5×10^1 and 5×10^6), and ITS values were ranging between 10^6 and 10^7 copy numbers. They therefore covered the whole spectrum of ITS values expected for any clubroot infected cultivar. The observed pattern can also be seen in figure 4.6 B. Superficially, ITS copy numbers, total biomass, and root-shoot ratios correlated with the scoring system. Hence, severely infected genotypes showed higher ITS values and bigger root-shoot ratios, while the opposite was seen in uninfected or mildly infected genotypes. However, it was possible to highlight subtle differences between severely infected genotypes, and to go beyond the capabilities of the crude scoring system. Three sub-classes can be observed: genotypes with a correlation between root-shoot ratios and ITS copy numbers (= either low or high, i.e. Q100, Erglu, and N02D), genotypes with bigger root-shoot ratios and low numbers of ITS copies (i.e. Bronowski, Huguenot, and Amber), and genotypes with smaller root-shoot ratios and high numbers of ITS copies (i.e. Baltia, Coriander, and Moana). Figure 4.6 C gives an overview of various gall phenotypes, and underlines the diversity within severely infected genotypes. Photographs of all genotypes are displayed in supplementary figure 4.
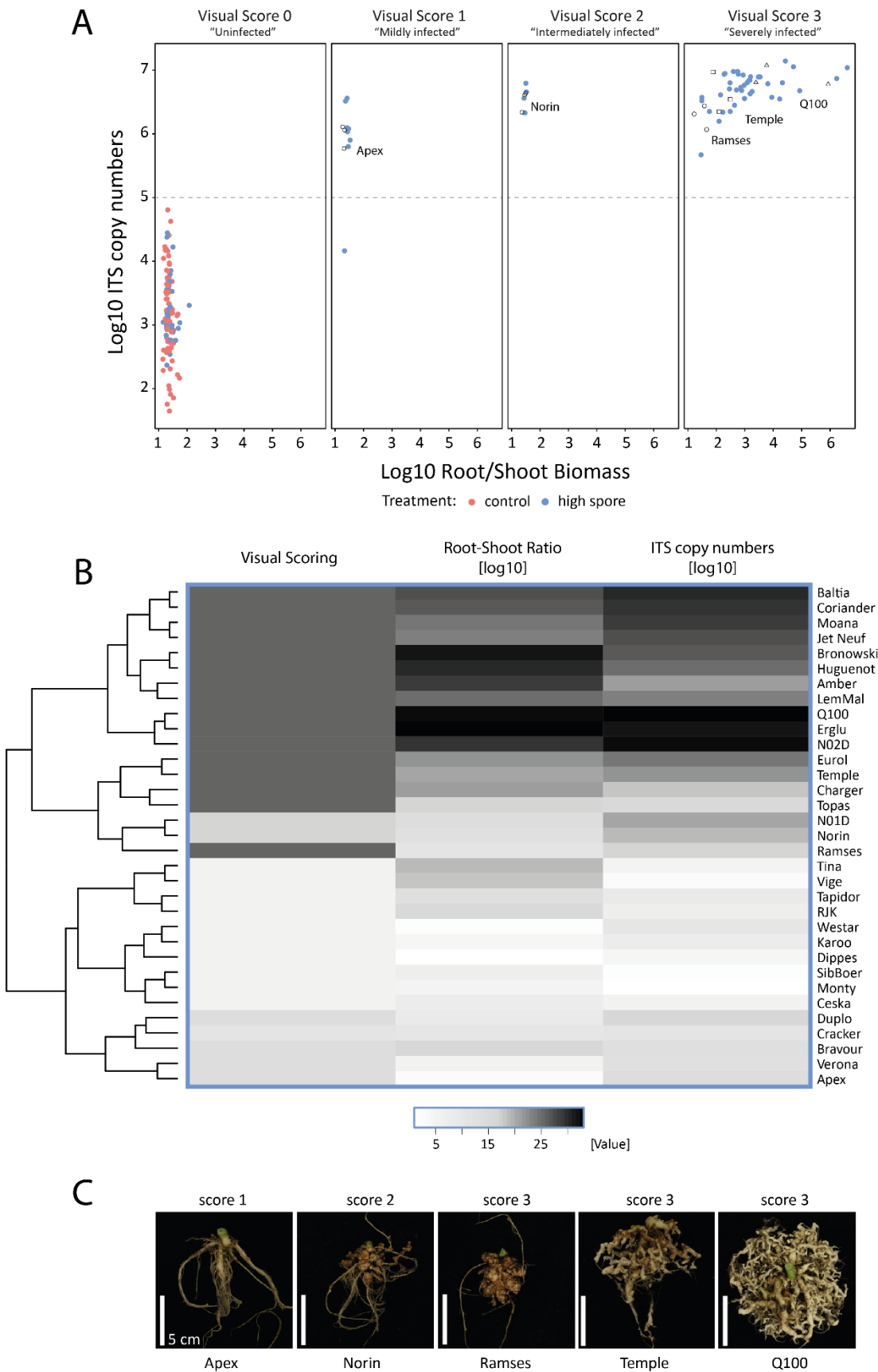
Figure 4.6: Comparison of molecular results to visual assessment and biomass

[Legend on next page]

[Legend to figure 4.6]

|A| Scatterplot showing the impact of root biomass on total biomass in relation to molecular and visual assessments (log10 ITS copy numbers and visual scores from 0-3 as described in section 2.2.2). Mock-treated and clubroot inoculated cultivars are displayed in red and blue, respectively. Black outlined symbols (circles, squares, and triangles) highlight biological replicates of 5 selected cultivars. Each cultivar is represented by one biological replicate in photographs below

|B| Heatmap showing results of visual scoring (class 0-3), ITS copy numbers, total biomass, and shoot-root ratios. Data was obtained from 33 clubroot-inoculated genotypes (3 biological replicates) with an inoculum density of 6.25×10^{5} spores/ml in a total volume of 50 ml. It is logged (base 10), mean calculated, and ranked by the average. A grey-scale spectrum highlights the lowest values in white, and the highest values in black

|C| Selection of root phenotypes representing each scoring group, including variation of phenotypes in group "3". Scale bars are 5 cm

4.3. DISCUSSION

In this study, the establishment of a new strong sink during clubroot infection had a profound effect on the source-sink balance of host plants. Therefore, biomass data was consistent with published literature of experiments using *A. thaliana* and selected *B. rapa* [69]. However, the use of a whole population of *B. napus* genotypes offered insights into how variable growth distortion can be between cultivars of the same species. All genotypes were inoculated with high spore densities (50 ml of 6.25 x 10^5 spores/ml) of the *P. brassicae* pathotype ECD 16/2/12, but not all genotypes showed gall formation, and not all genotypes with gall formation exhibited increased shoot-root ratios. Little galls of mildly/intermediately infected genotypes (i.e. class 1 and 2 according to the clubroot classification system) did not have an impact on biomass results. However, an impact on biomass results was observed for large galls of severely infected genotypes (i.e. class 3 according to the clubroot classification system). Above-ground biomass, shoot-root ratios and total biomass varied considerably between those genotypes. Based on their total biomass results, three subclasses could be identified. The first subclass contains genotypes with bigger total biomass than controls, the second subclass holds genotypes whose total biomass is equal to control plants, and the third subclass includes genotypes with smaller total biomass than controls. A model to all three subclasses with corresponding explanations is displayed in figure 4.7. However, the model is only based on morphological observations. Therefore, it would be useful to conduct physiological measurements using a small selection of *B. napus* cultivars, each representing one subclass. Physiological measurements could include imaging techniques (e.g. chlorophyll-fluorescence, thermal imaging), or starch/sucrose concentration assays with leaf and root material. The former could give information about photosynthetic activity or stomatal conductance as response to clubroot-mediated drought stress. The latter would be informative to define distortions of source-sink balance during clubroot infection in more detail.

Subclass 1

Control   <   Infected
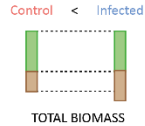
TOTAL BIOMASS

Total biomass of severely infected genotypes is bigger than total biomass of their controls

Severely infected plant maintains above-ground growth. It provides continuous supply of photosynthates to aerial plant parts (e.g. sink leaves) despite increased allocation of photosynthates to club-shaped roots. This is most likely to happen due to maximised photosynthetic activity, mediated by distorted feedback control from the root/gall (strong sink). It is assumed that water and nutrient uptake from root/gall to source leafs is still sufficient enough to increase the rate of photosynthesis.

Subclass 2

Control   =   Infected
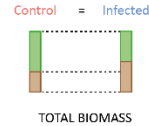
TOTAL BIOMASS

Total biomass of severely infected genotypes is identical with total biomass of their controls

Severely infected plant has difficulties to maintain above-ground growth. Increased allocation of photosynthates to the root/gall is like to happen at the expense of sink leaf supply. Reduced supply could cause developmental stagnation, and this could inhibit transformation from sink leafs to source leafs. It is assumed that photosynthetic activity is not increased to compensate the lack of photosynthates for sink leafs. Thereby, it is likely that impeded water and nutrient supply inhibits maximisation of photosynthesis, but still allows the standard rate. Simultaneously, distorted feedback control from below-ground guarantees continuous supply to the root/gall.

Subclass 3

Control   >   Infected
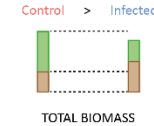
TOTAL BIOMASS

Total biomass of severely infected genotypes is smaller than total biomass of their controls

Severely infected plant is not able anymore to maintain above-ground growth. Lack of water and nutrient uptake causes starvation, and slows down metabolic processes due to deficiencies. This drastically reduces photosynthetic activity. The majority of photosynthates is likely to be allocated below-ground due to distorted communication between source leafs and root/gall

Figure 4.7:

Model of three subclasses within severely infected *B. napus* cultivars and their disrupted source-sink balance (see section 1.4.5. in chapter 1 for details about source-sink balance in healthy plants)
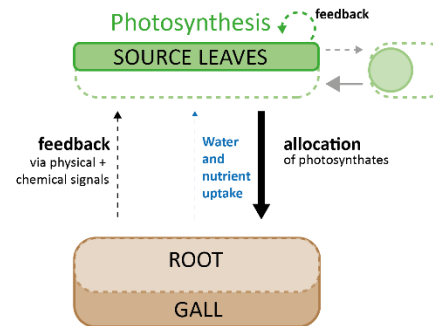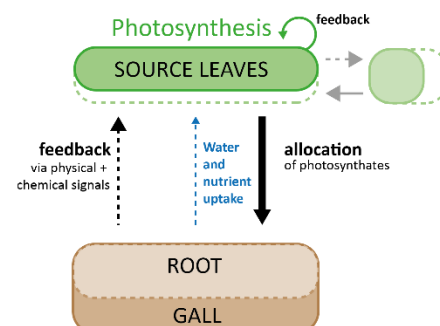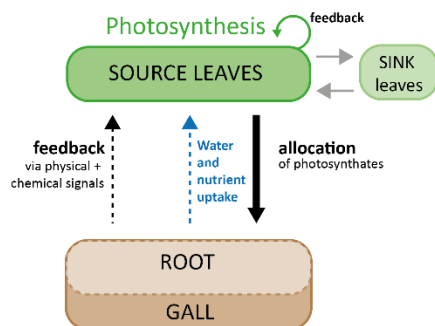
Increasing perturbations in water + nutrient uptake, and decreasing root-mediated feedback control of photosynthesis cause metabolic deficiencies in source leaves with gradual decrease of photosythetic activity

ITS values allowed to distinguish between clubroot infected plants and their controls. Two major classes were observed: low (10^2 and 10^4) and high (10^5 and 10^7) ITS values. The former was noise (probably contamination) and included mock-inoculated genotypes and genotypes with visually healthy root systems. The latter contained clubroot-inoculated genotypes with visible gall formation. It could be shown, that ITS values of mildly and intermediately infected cultivars increased from $5x10^5$ to $5x10^6$ ITS copy numbers, whereas ITS values of severely infected cultivars ranged between 10^6 and 10^7 ITS copy numbers. The latter is of particular interest, since it demonstrated the potential of the molecular method to detect subtle differences between severely infected genotypes, which were unable to be picked up by the crude scoring system. Interestingly, there is no discernible pattern between ITS copy numbers and biomass results. Hence, severely infected genotypes (i.e. class 3, big gall) with high shoot-root ratios (i.e. subclass 3, smaller total biomass), and severely infected genotypes with low shoot-root ratios (i.e. subclass 1, bigger total biomass) can contain ITS copy numbers between 10^6 and 10^7. The same observation was made for severely infected genotypes whose total biomass is identical to control plants (i.e. subclass 2). ITS and biomass results of the genotypes Q100 and Charger serve as good examples, and are shown in Table 4.1.

Table 4.1: Examples for the absence of discernible patterns between ITS and biomass results

B. napus Q100	*B. napus* Charger
class 3 infection (2nd biggest gall according to root biomass)	class 3 infection (13th biggest gall according to root biomass)
subclass 2 (total biomass = control)	subclass 3 (total biomass < control)
10^7 ITS copies (Highest value on the ITS spectrum for severe infection)	10^6 ITS copies (Lowest value on the ITS spectrum for severe infection)

n = 33 genoytpes

Visual scoring, biomass (i.e. root, shoot, total, root-shoot-ratios), and molecular assessments are useful approaches to quantify clubroot disease in Brassica cultivars. They all have advantages and disadvantages when applied during large scale screens. The biggest disadvantage is the destructive nature of all methods. They require laborious root excavation prior to actual measurements. As a consequence, screens are limited by the number of plants which can be processed during the day. The visual scoring system is the quickest and easiest way of classifying disease severity after uprooting. However, it only allows to distinguish between no, little, intermediate and severe infection, which can be very subjective and crude. The crudity is particularly apparent when root phenotypes of severely infected cultivars are compared. In contrast, the molecular assessment is more sensitive to clubroot. It allows better differentiation of disease severities (e.g. class 0-3), and unravels differences amongst plants with similar disease phenotypes (e.g. class 3). However, it needs further improvements due to higher numbers of ITS copies in control samples. Improvements include (I) reduction of contamination, which might have been caused by automated homogenisation or robotic pipetting of qRT-PCR reactions, and (II) primer optimisation by designing additional primer pairs based on current sequence information of *P. brassicae*. An improved molecular assay for clubroot offers many advantages: It has the potential to be non-destructive (i.e. only invasive) since only small amounts of root tissue is required for the assessment. As a result, it would make it applicable for both greenhouse and field screens. However, the former would require bigger plant pots to allow less limited plant growth and better root expansion. The latter would need validation through a primer specificity test with DNA of soil-borne microorganisms found around Brassica crops (both beneficial and pathogenic). This improved method has some clear advantages. Despite the improvements, this method remains slow, requires uniform sampling for comparisons (e.g. sampling of primary and/or secondary root material, or adjusted to gall position), and is relatively expensive. Less expensive, but also informative are biomass measurements. They might lack accuracy for mild or intermediate clubroot infection, but enable to detect fine differences in growth distortions within severely infected cultivars. During the study, those differences demonstrated that disease severity does not always lead to dwarfed above-ground phenotypes as mostly published in the literature [30]. Therefore, biomass measurements could be a complementary method to the molecular assessment for the quantification of clubroot disease and host responses.

Conclusion

The end-point disease screens highlighted the low resolution of the scoring system, and the need for more sensitive approaches to classify clubroot disease severity to eventually detect quantitative resistance. The developed molecular assessment could distinguish between control and infected Brassica cultivars, but needs further improvements. This includes primer optimisation and minimization of contaminations in control samples potentially caused by automated homogenisation (i.e. bead-beater) and robotic pipetting of qRT-PCR reactions. Biomass measurements (total, above- and below-ground biomass) were proven to be a good complementary tool to unravel clubroot disease severity in more detail.

CHAPTER 5: METABOLOMICS

5.1. INTRODUCTION

Metabolomics is the study of large numbers of small metabolites derived from biochemical processes in cells, tissues, organs, and organisms. It enables metabolic profiling through identification of intermediates and end-products from metabolic pathways. Therefore, the result is a snap-shot of an organisms' physiological state. A set of all metabolites in an organism is termed metabolome. Metabolomics studies follow a typical workflow, which consists of sample collection (mostly after treatment), sample preparation via metabolite extraction, sample analysis through mass spectrometry (MS), data acquisition, and data analysis with subsequent data interpretation. Mass spectrometry is performed by a mass spectrometer, and describes an analytical technique that fragments metabolites through ionisation, and sorts the generated ions based on their mass-to-charge (m/z) ratio. A typical mass spectrometer contains an ion source, a mass analyser and a detector (figure 5.1). In many cases, due to high complexity of metabolomic analytes or volatile components (e.g. Ethylene in plants), samples are separated through chromatography (gas or liquid, GC or LC) prior to MS application. During LC (e.g. ultra-performance liquid chromatography, UPLC), a liquid solvent containing the sample is passed through a column that contains a solid absorbent granular material for separation of samples [131]. The time it takes for a sample to pass through the column is termed retention time (Rt). After chromatography, separated samples are ionised. Depending on the sample state (e.g. gas, liquid, solid), several techniques for ionisation can be performed. For liquid samples, electrospray ionisation (ESI, positive and negative mode) and matrix-assisted laser desorption/ionisation (MALDI) are common. After ionisation, ions are accelerated by an electric field into a mass analyser. Several mass analysers are available, for example a time-of-flight (TOF) analyser. A TOF analyser is a vacuum chamber without an electric field, through which ions drift based on the kinetic energy they obtained from the potential energy of the electric field. Under the assumption that all ions acquire the same kinetic energy, the velocity of ions depends on the m/z ratio. A detector positioned at the end of the analyser, measures the arrival time of ions [131][132].
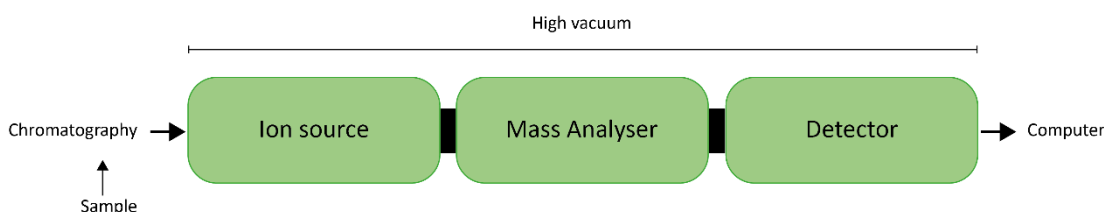
Figure 5.1: Simplified scheme of a mass spectrometer (see main text for details)

Common data representations are chromatograms, whose underlying information can be acquired and manipulated through specific software (e.g. XCMS in R studio). The subsequent analysis of metabolomes can be conducted as a targeted and/or untargeted approach. The former is used to investigate specific groups of components, the latter to analyse all measurable compounds in a sample. Untargeted analysis of metabolites relies heavily on peak resolution. A crucial parameter for peak resolution at the end of MS application is the flow-rate of metabolomic analytes during its separation through chromatography. Low flow-rates obtain the best peak resolution, which enables the identification of metabolites according to their m/z-values with more confidence. However, low flow-rates stretch the duration of MS application and are therefore cost-intensive. As a consequence, many MS approaches find a compromise between monetary input and peak resolution. Most facilities operate with a medium flow-rate, causing peaks to overlap when m/z-values are very similar. Metabolomic databases (e.g. METLIN) are designed to aid metabolite identification based on m/z-values with simultaneous consideration of adducts. The bigger the similarities in m/z-values, the more difficult the metabolite identification. In those cases, it is advisable to proceed with a targeted approach.

Targeted and untargeted approaches can be applied to understand plant immunity [133]. In several studies, metabolomics approaches have been applied to elucidate host-pathogen interactions and to identify resistance related metabolites (RRMs). One of those studies used liquid chromatography high resolution MS (LC-HRMS) to decipher resistance to late blight (*Phytophthora infestans*) in susceptible and resistant potato genotypes (*Solanum tuberosum* L. Group *Phureja*). During an untargeted analysis, resistant plants showed altered metabolic profiles for phenylpropanoids (in particular hydroxycinnamic acid amides, HCAAs), flavonoids and alkaloids. The deposition of phenylpropanoids was responsible for cell wall thickening, which was then associated to late blight resistance [134]. In a different study, responses of rice (*Oryza sativa*), and barley (*Hordeum vulgare*) to rice blast infection (*Magnaporthe grisea*) were investigated through injection electrospray ionization MS (FIE-MS) and gas chromatography MS (GC-MS). During untargeted and targeted metabolite profiling, alterations in energy and nutrient metabolism, changes in phenylpropanoid pathways and modulations of defence-related ROS

production (e.g. delayed ROS production and enhanced synthesis of compounds for ROS protection) were found [135]. Another study used LC-hybrid-MS to unravel RRMs against head blight (FHB, *Fusarium graminearum*) in barley. They found fatty acids (e.g. linolenic acid), flavonoids (e.g. catechol glucoside), and phenylpropanoids (e.g. p-coumaric) to accumulate in resistant plants [136]. The reason for the accumulation of fatty acids was unknown.

Many studies of clubroot have sought to understand below-ground changes during gall development, using methods such as *A. thaliana* mutant-line analysis, transcriptomics (e.g. micro-array or RNAseq), or proteomics approaches [82][61][60][12]. In contrast, metabolomics tools have not been widely exploited. Wagner and colleagues (2012) applied targeted metabolomics using root samples of 18 clubroot inoculated *B. napus* genotypes to focus on alterations in primary metabolism (41dpi). Through UPLC-tandem MS (UPLC-MS/MS) and GC-MS the accumulation of the antioxidant glutathione (GSH), the sugar trehalose, and several amino acids, in particular those rich in sulphur or nitrogen, were found. Observations correlated with host susceptibility [137]. The study's observation were supported when the *P. brassicae* genome was sequenced [49][62]. The clubroot genome project elucidated the presence of genes for the synthesis of trehalose and the enzyme trehalase, but also a lack of genes crucial for the uptake of sulphur and nitrogen as well as for the synthesis of several amino and fatty acids. For the latter, data suggested a microsomal elongase pathway, in which *P. brassicae* elongates and modifies host fatty acids through lipase activity [62]. During GC-MC analysis of lipid droplets, arachidonic acid (ARA, 20:4) was found to be the most abundant fatty acid in resting spores – *P. brassicae's* energy source during spore germination [138]. But it was also present in root tissue of clubroot infected *B. napus* when ARA was tested as potential fatty acid biomarker for quantification of *P. brassicae* (whole-cell fatty acid analysis, WCFA)[139].

In this chapter, an untargeted metabolomics approach was performed through application of UPLC-qTOF-MS using both root and leaf material. The study aimed to investigate patterns of resistance and susceptibility in both tissue types of *B. napus* cultivars (Temple and Cracker) during clubroot infection. The objectives were the detection of metabolic changes in leaves over the course of below-ground clubroot infection, and comparisons of leaf and root patterns in clubroot susceptible and resistant cultivars. This is the first time that leaf metabolites were investigated for signs of a below-ground developing disease.

5.2. RESULTS

Two metabolomics screens were conducted using UPLC-qTOF-MS to investigate patterns of resistance and susceptibility in host plants during clubroot infection. Three time points (TP) were chosen as representatives of primary infection, early secondary infection, and late secondary infection: 11 dpi (TP1), 35 dpi (TP2), and 50 dpi (TP3). *B. napus* genotypes were inoculated with 50 ml of dH$_2$O (mock-treatment) or 50 ml of 6.25 x 10^5 spores/ml (clubroot treatment), and subjected to the same environmental conditions (see table 2.3 in section 2.3).

5.2.1. METABOLOMICS EXPERIMENT 1

Metabolomics experiment 1 was performed with destructive harvests at each TP to collect leaf and root material of host genotype *B. napus* Temple. Metabolites were extracted as described in section 2.6., and m/z ratios measured using UPLC-qTOF-MS with electrospray ionisation in negative mode. Chromatograms were processed (package XCMS in R studio) and data statistically analysed (package MetaboAnalystR in R studio). Principal component analysis (PCA) was used to visualise variances in the data. Scree plots (showing the variance associated with each component) and PCA plots (showing variance between samples) are displayed in figure 5.2.
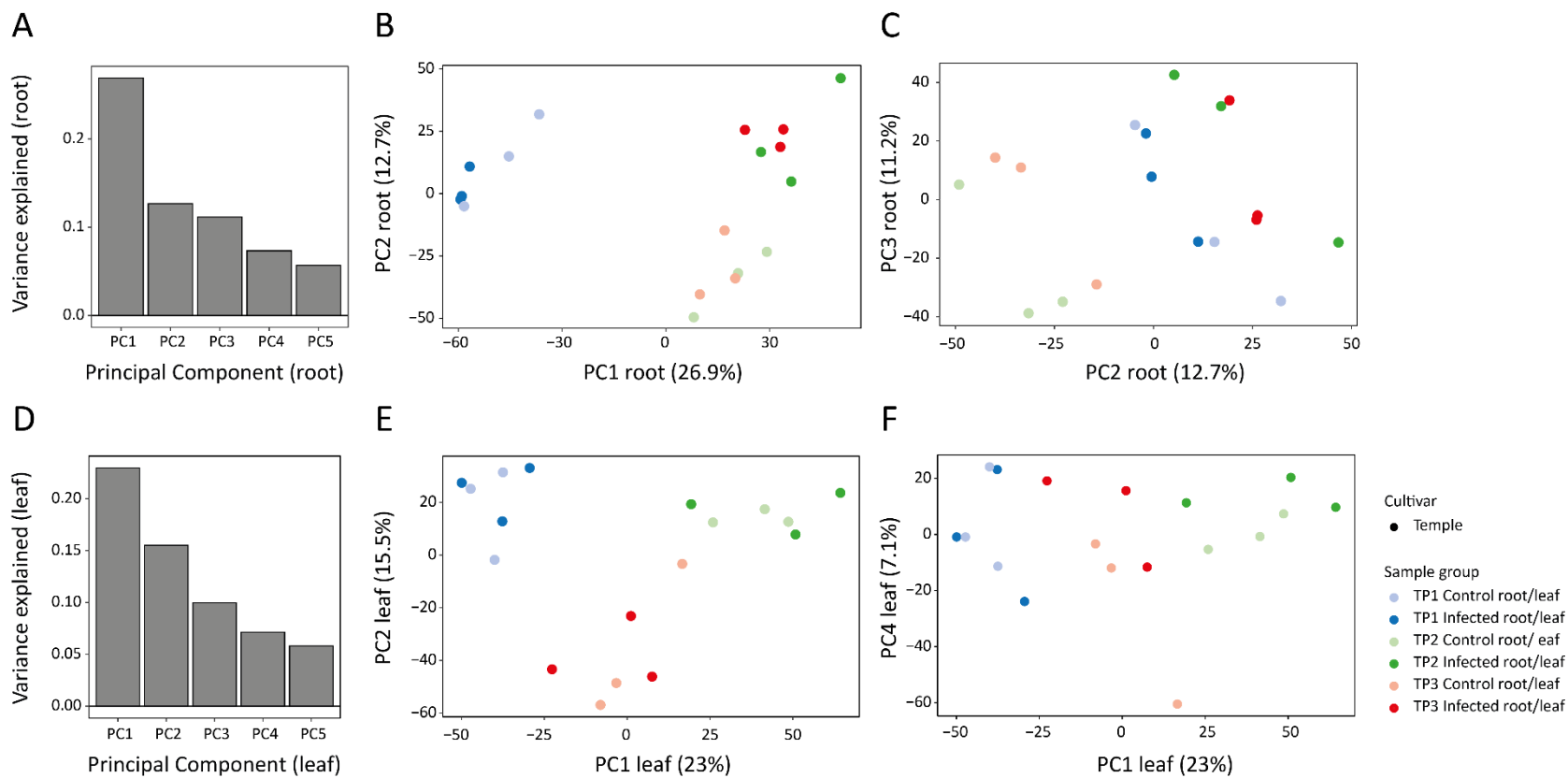
Figure 5.2: Principal component analysis of metabolites from *B. napus* Temple

|A| Scree plot for root data |B| PCA plot of PC1 and PC2 obtained from root metabolies |C| PCA plot of PC2 and PC3 obtained from root metabolites | Equivalent results for leaf metabolites are shown in |D|,|E|, and |F|. Infected samples for TP1, TP2, and TP3 are displayed in blue, green, and red, respectively. A tinted version of each colour represents control samples

The biggest fraction of the total variance in the root data was explained by PC1 (26.9%), followed by PC2 (12.7%), PC3 (1.2%), PC4 (7.3%), and PC5 (5.7%) (figure 5.1 A). Plots of PC1 vs PC2 and PC2 vs PC3 are shown in figure 5.2 B and C. Inspection of PC1 vs PC2 highlighted a time point and treatment effect. TP2 and TP3 clustered together but were distinct from TP1. There was no obvious difference between treatments for TP1, but within TP2 and TP3 control roots differed from infected roots. Comparisons of PC2 vs PC3 further underlined the separation of treatments for TP2 and TP3, but also indicated that controls of TP2 differed slightly from controls of TP3. The same applied for infected roots. This effect was not seen for TP1.

The biggest fraction of total variance in the leaf data was explained by PC1 (23%), followed by PC2 (15.5%), PC3 (10%), PC4 (7.1%), and PC5 (5.8%) (figure 5.1 D). Comparisons of PC1 vs PC2 and PC1 vs PC4 are displayed in figure 5.2 E and F. Both PC1 vs PC2 and PC1 vs PC4 revealed an effect of time point, but PC1 vs PC4 also showed some separation due to treatment. Therefore, in contrast to root data, the biggest effect was leaf age, and only PC4 started to separate out differences due to infection.

PERMANOVAs (package "Adonis" in R studio) were then used to determine which factors explained the variance between treatments. The PERMANOVAs required that the variance between treatments was not significantly different, which was confirmed using permutation tests for homogeneity of multivariate variance (PTHMV) ("betadisp" function) ($p = 0.71$ for root, and $p = 0.951$ for leaf). The output of the PERMANOVA is a significance value (p) for a factor and the contribution of this factor to the variance between all samples (R^2). For root samples, PERMANOVAs highlighted a significant effect of treatment (control vs infected, $p = 0.014$, $R^2 = 0.10218$), and time point ($p = 0.001$, $R^2 = 0.30084$), but no significant effect for the interaction between the two ($p = 0.124$, $R^2 = 0.10946$). For leaf samples effects of time point were significant ($p = 0.001$, $R^2 = 0.34616$), but no significance was found for treatment ($p = 0.426$, $R^2 = 0.04362$) and the interaction between time point and treatment ($p = 0.672$, $R^2 = 0.07780$).

One-way ANOVAs ($p < 0.05$) with Benjamini-Hochberg false discovery rate (FDR) correction, host-hoc tests ($p < 0.05$, Fisher's LCD) and fold-change calculation were performed to identity metabolites that differed significantly between treatment groups. The results for roots are shown in figure 5.3, and for leaves in figure 5.4.

Figure 5.3: Significantly up- and down-regulated root metabolites in inoculated *B. napus* Temple relative to controls |A| Table of root metabolites significantly different between infected and control roots for each time point |B| Venn-diagram for root metabolites significantly up-regulated between infected and control roots for each time point. TP1, TP2, and TP3 are displayed in blue, green, and red, respectively |C| Venn-diagram for root metabolites significantly down-regulated between infected and control roots for each time point. TP1 is shown in blue, TP2 in green, and TP3 in red |D| Heatmap visualising log2 fold-changes of significantly different root metabolites for all 3 time points. Significantly up- and down-regulated metabolites are displayed in tinted versions of blue and red, respectively.

Time point	Comparison	Number of leaf metabolites different
TP1	Up in inoculated Temple relative to control	54
	Down in inoculated Temple relative to control	33
TP2	Up in inoculated Temple relative to control	96
	Down in inoculated Temple relative to control	43
TP3	Up in inoculated Temple relative to control	45
	Down in inoculated Temple relative to control	43
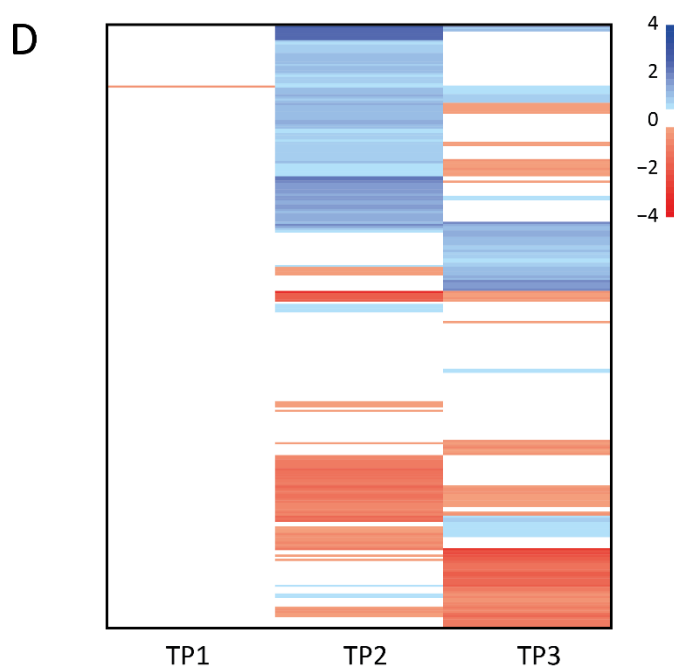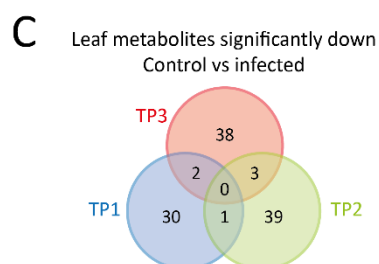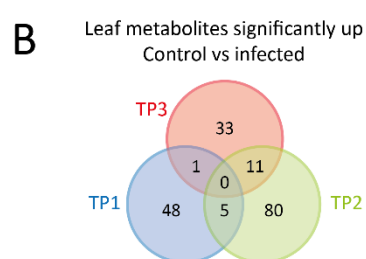
Figure 5.4: Significantly up- and down-regulated leaf metabolites in inoculated *B. napus* Temple relative to controls |A| Table of leaf metabolites significantly different between infected and control roots for each time point |B| Venn-diagram for leaf metabolites significantly up-regulated between infected and control roots for each time point. TP1, TP2, and TP3 are displayed in blue, green, and red, respectively |C| Venn-diagram for leaf metabolites significantly down-regulated between infected and control roots for each time point. TP1 is shown in blue, TP2 in green, and TP3 in red |D| Heatmap visualising log2 fold-changes of significantly different leaf metabolites for all 3 time points. Significantly up- and down-regulated metabolites are displayed in tinted versions of blue and red, respectively.

136

In all root samples, 20 605 features were detected (m/z features at a specific Rt). Significantly up- and down-regulated root metabolites are shown in figure 5.3. 174 metabolites differed at TP1, 611 at TP2, and 492 at TP3 (figure 5.3 A). Venn-diagrams revealed little overlap between TP1 and TP2/3, but 162 metabolites were in common for TP2 and TP3 (figure 5.3 B and C). A heatmap (figure 5.3 D) confirmed a similar pattern between TP2 and TP3 that differed from TP1.

In leaf samples, numbers of significantly different metabolites between treatments were lower than in roots (figure 5.4 A). Again, there was little overlap between TP1 and TP2/3 and limited overlap between TP2 and TP3 (figure 5.4 B and C). A heatmap (figure 5.4 D) confirmed the results. It revealed differences between all TPs, while TP2 and TP3 were more similar in comparison to TP1. All data visualisations for root and leaf material were consistent with PERMANOVA results.

Student's t-tests (p < 0.05) were applied to list the most significant root and leaf metabolites for each time point, and for TP2+TP3 overlaps. However, identification of specific metabolites is difficult from the relatively short chromatographic separation times typical for metabolomics experiments and significant uncertainty in putative IDs is common. Therefore, no attempts to identify specific metabolites were made.

5.2.2. METABOLOMICS EXPERIMENT 2

Metabolomics experiment 2 was conducted as a time-course screen with 3 time points using the host genotypes *B. napus* Temple and Cracker. Leaf material was collected at 11 dpi (TP1), 35 dpi (TP2), and 51 dpi (TP3), but root material only at TP3 after destructive harvest. The sampling procedure allowed the observation of metabolic changes in leaves over time in the same plant, but also ensured that *B. napus* Cracker showed healthy root phenotypes at 51 dpi as evidence of "Mendel" clubroot resistance. Metabolite extraction, UPLC-qTOF-MS, and basic data processing (package XCMS in R studio) were performed as described in section 2.6. Scree plots and PCA plots of chosen PCs for root and leaf peak data are displayed in figure 5.6.

The biggest fraction of total variance in the root data was explained by PC1 with 33.7%, followed by PC2 with 10.3%, PC3 with 9.5%, PC4 with 7.8%, and PC5 with 6.9% (figure 5.6 A).Comparisons of PC1+PC2 and PC1+PC3 are displayed in figure 5.6 B and C. Both PC1+PC2 and PC1+PC3 showed a cultivar difference (Temple vs. Cracker), and a treatment effect for Temple (control vs. infected). A small difference between infected Temple and Cracker samples of both treatment groups was visible for PC1+PC3 comparisons.

In the leaf data, the biggest fraction of total variation was explained by PC1 (27.4%), followed by PC2 (10.4%), PC3 (6.2%), PC4 (5%), and PC5 (3.9%) (figure 5.6 D). Comparisons of PC1 vs PC2 and PC4 vs PC5 are shown in figure 5.6 E and F. They exhibited a time point effect for both cultivars, in which TP2+TP3 were clustered and separated from TP1. In PC4 vs PC5 comparisons, a cultivar effect was visible for TP2 and TP3, but not for TP1. Cracker (both treatments) and Temple (both treatments) were clearly split into two groups for TP2+3 (Temple group vs Cracker group), while samples of TP1 were present in both groups.

To determine which factors explained the variance between root/ leaf samples, PERMANOVAs were conducted (PTHMV: p = 0.445 for root, and p = 0.957 for leaf). PERMANOVAs for root samples showed a significant effect for cultivar (p = 0.001, R^2 = 0.17913), treatment (p = 0.001, R^2 = 0.14691), and for the interaction between the two (p = 0.001, R^2 = 0.16177). For leaf samples, effects of time point (p = 0.001, R^2 = 0.13746) and treatment (p = 0.042, R^2 = 0.03359) were significant alongside cultivar-TP interaction (p = 0.001, R^2 = 0.26265) and treatment-TP interaction (p = 0.032, R^2 = 0.06005). No significances were found for cultivar (p = 0.149, R^2 = 0.02475) or interactions between cultivar and treatment (p = 0.578, R^2 = 0.01523).
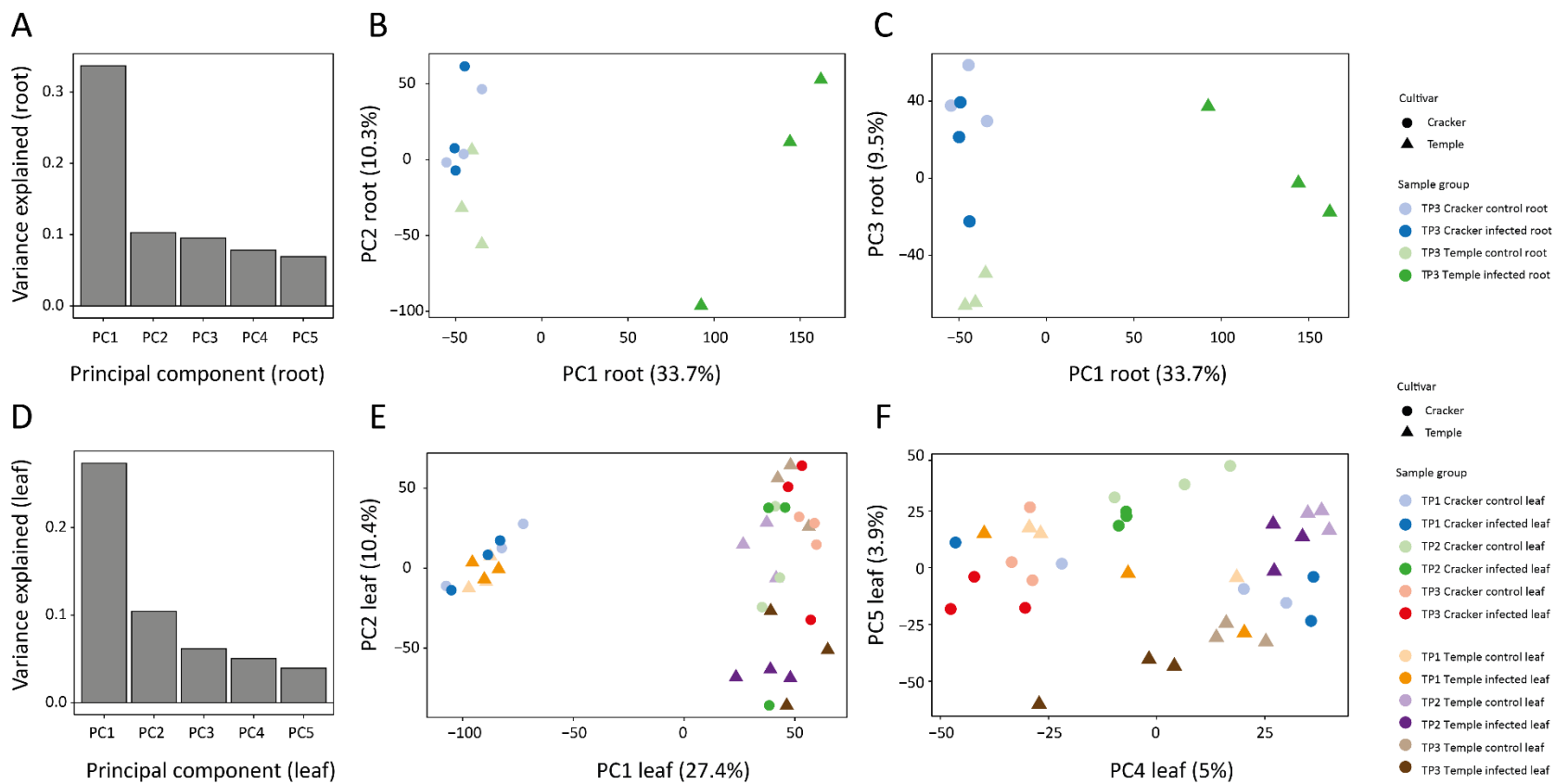
Figure 5.6: Principal component analysis of root and leaf data from *B. napus* Cracker and Temple

[Legend on next page]

Legend to figure 5.6:

|A| Scree plot for root data (TP3) |B| PCA plot with PC1 and PC2 obtained from root data (TP3) |C| PCA plot with PC1 and PC3 obtained from root data (TP3) |B+C| Infected Cracker and Temple are displayed as blue dots and green triangles, respectively. A tinted version of each colour represents control samples |D| Scree plot for leaf data |E| PCA plot with PC1 and PC2 obtained from leaf data |F| PCA plot with PC4 and PC5 obtained from leaf data |E+F| Infected Cracker for TP1, TP2, and TP3 is displayed as dots in blue, green, and red, respectively. Infected Temple for TP1, TP2, and TP3 are shown as triangles in orange, purple, and brown, respectively. A tinted version of each colour represents control samples for both Cracker (dots) and Temple (triangles).

The metabolites that differed significantly between treatment groups were identified through one-way ANOVAs ($p < 0.05$) with Benjamini-Hochberg FDR correction. Post-hoc tests ($p < 0.05$, Fisher's LCD) were performed and fold-changes calculated to determine metabolites and to describe how much they were changed in infected plants. The results for roots are shown in figure 5.7, and leaves in figure 5.8 and figure 5.9.

A		
Time point	Comparison	Number of root metabolites different
TP3	Up in inoculated Temple relative to control	2290
	Down in inoculated Temple relative to control	1623
	Up in inoculated Cracker relative to control	319
	Down in inoculated Cracker relative to control	195
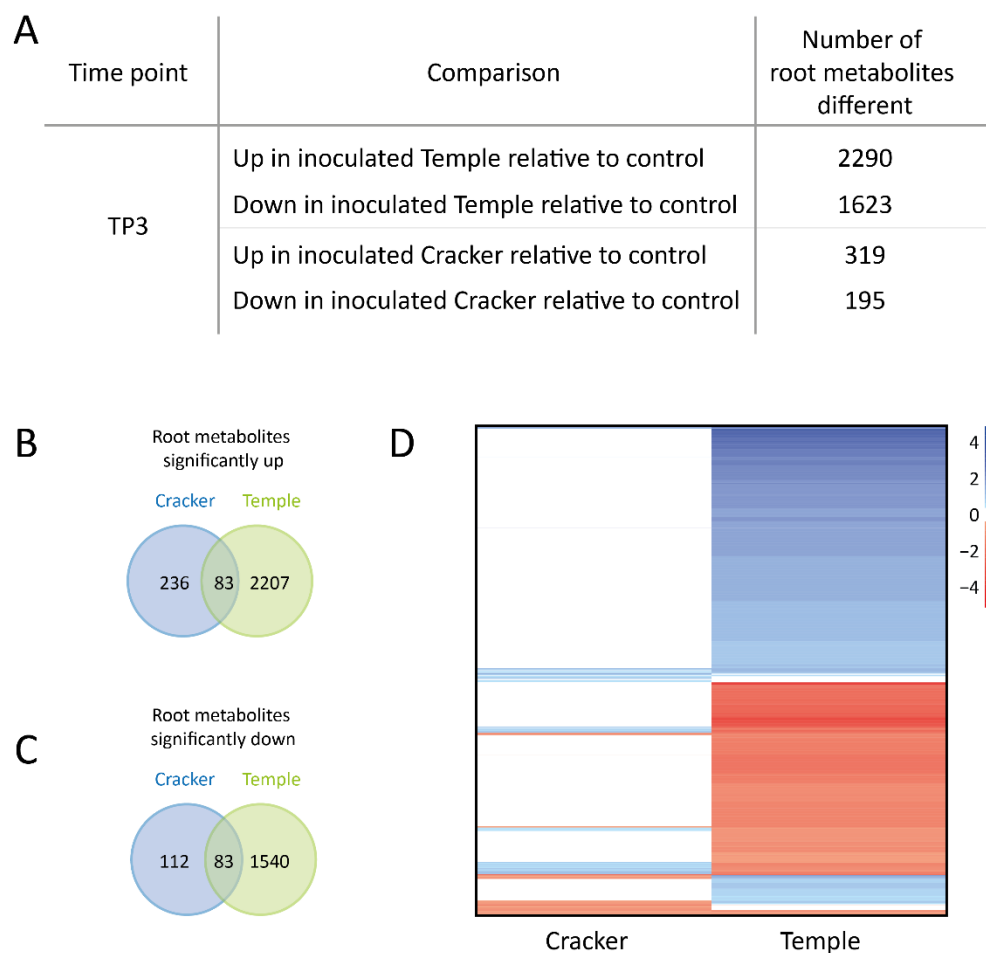
Figure 5.7: Significantly different root metabolites in *B. napus* Temple and Cracker |A| Table of root metabolites significantly different between infected and control roots of Temple and Cracker at TP3 |B| Venn-diagram for root metabolites significantly up-regulated between infected and control roots of Temple and Cracker for TP3. Cracker is shown in blue and Temple in green |C| Venn-diagram for root metabolites significantly down-regulated between infected and control roots of Temple and Cracker for TP3. Cracker is displayed in blue and Temple in green |D| Heatmap visualising fold-changes of significantly different root metabolites of Temple and Cracker. Significantly up- and down-regulated metabolites are coloured in tinted versions of blue and red, respectively.

Time point	Comparison	Number of leaf metabolites different
TP1	Up in inoculated Temple relative to control	393
	Down in inoculated Temple relative to control	572
	Up in inoculated Cracker relative to control	599
	Down in inoculated Cracker relative to control	382
TP2	Up in inoculated Temple relative to control	1686
	Down in inoculated Temple relative to control	1580
	Up in inoculated Cracker relative to control	568
	Down in inoculated Cracker relative to control	450
TP3	Up in inoculated Temple relative to control	2364
	Down in inoculated Temple relative to control	2221
	Up in inoculated Cracker relative to control	507
	Down in inoculated Cracker relative to control	385

B
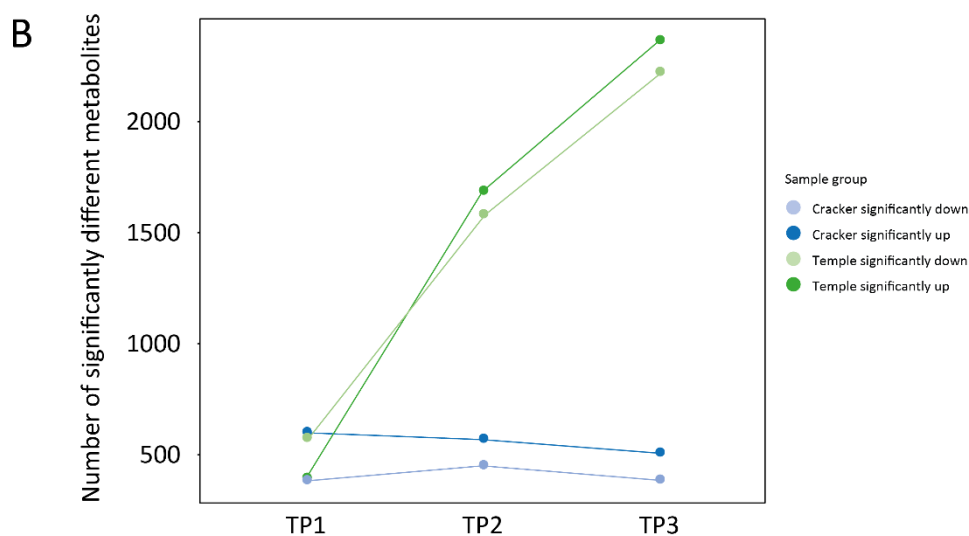
Figure 5.8: Leaf metabolites significantly up and down in *B. napus* Temple and Cracker

|A| Table of leaf metabolites significantly up and down

|B| Scatter plot. Upregulated metabolites in Cracker and Temple are shown in blue and green, respectively. A tinted version of both colours represents downregulated metabolites.
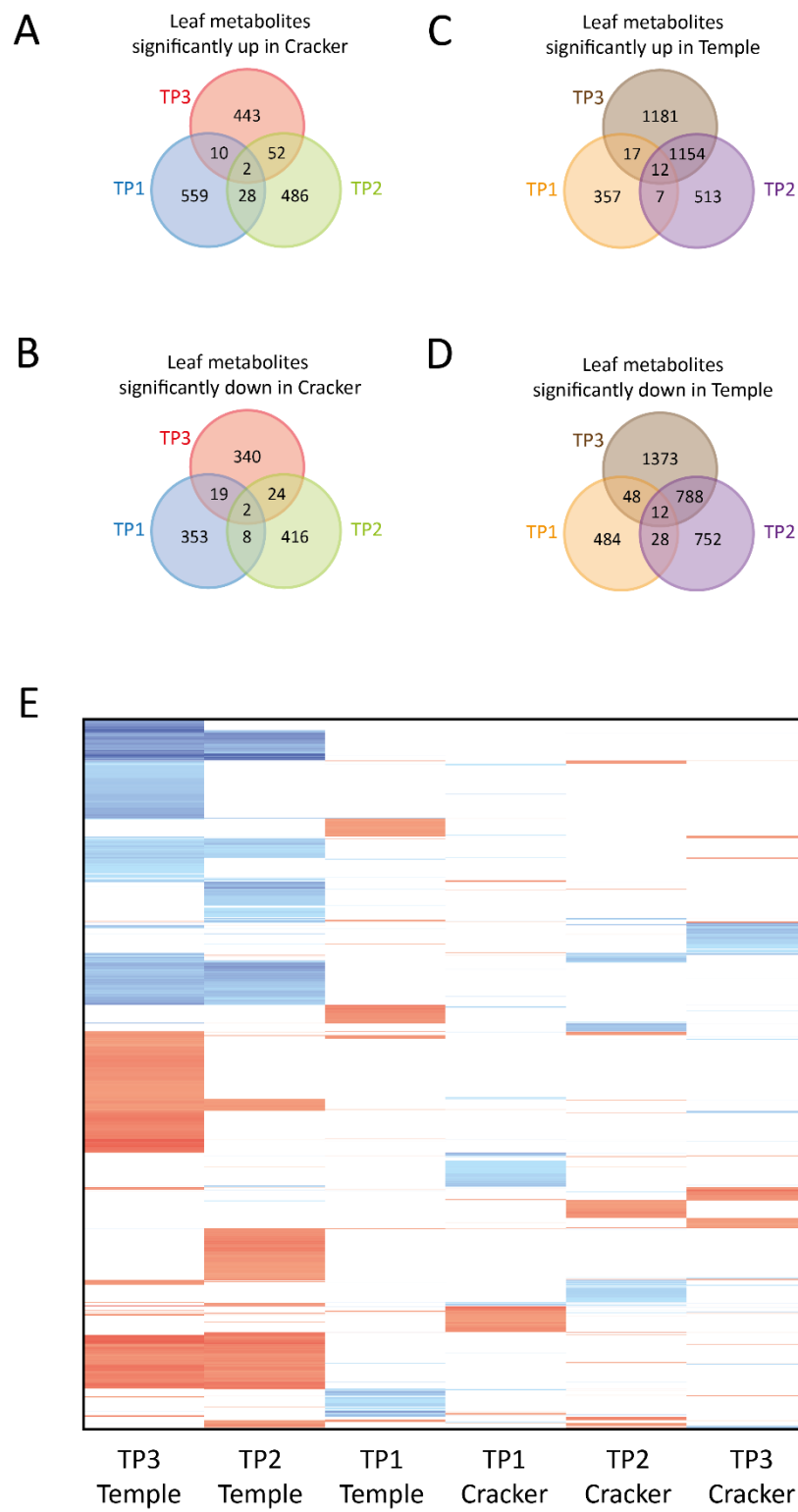
Figure 5.9: Significantly different leaf metabolites in *B. napus* Temple and Cracker

[Legend on next page]

[Legend to figure 5.9]

|A|+|B| Venn-diagram of leaf metabolites significantly different in Cracker. TP1, TP2, and TP3 are shown in blue, green, and red, respectively |A| Significantly up-regulated |B| Significantly down-regulated |C|+|D| Venn-diagram of leaf metabolites significantly different in Temple. TP1, TP2, and TP3 are displayed in orange, purple, and brown, respectively |C| Significantly up-regulated |D| Significantly down-regulated |E| Heatmap visualising fold-changes of significantly different leaf metabolites in Temple and Cracker. Significantly up- and down-regulated metabolites are coloured in tinted versions of blue and red, respectively.

Numbers of significantly up- and down-regulated root metabolites were 7-8x higher in Temple compared to Cracker (figure 5.7 A). Venn-diagrams showed some overlap between metabolites of both cultivars. 3.6% of Temple's significantly upregulated metabolites (figure 5.7 B), and 5.1% of Temple's significantly downregulated metabolites are shared with Cracker (figure 5.7 C).

Numbers of significantly different leaf metabolites were cultivar- and TP- dependent (Figure 5.8). At TP1 Temple showed more metabolites down- than upregulated. This was the opposite in Cracker. While Cracker kept the same level of differentially expressed metabolites at TP2 and TP3 compared to TP1, the number of significant metabolites up and down in Temple increased with TPs. Metabolites of TP2 are 3-4x higher compared to TP1, and metabolites of TP3 are 1.5x higher compared to TP2. Comparisons between cultivars for TP3 showed that leaf metabolites significantly up and down were 5x higher in Temple. Venn-diagrams exhibited little overlap of up- and down regulated metabolites for all TPs in Cracker (figure 5.9 A and B). This was different in Temple (figure 5.9 C and D). While TP1 and TP2 or TP1 and TP3 showed little overlap, many metabolites were shared between TP2 and TP3. Thereby, 69% of upregulated metabolites and 51% of downregulated metabolites present in TP2 were also detected in TP3. The described patterns for both root and leaf samples were confirmed in heatmaps (figure 5.7 D and figure 5.9 D) and are consistent with PERMANOVA results.

5.3. DISCUSSION

Like all biotrophic pathogens, *P. brassicae* relies on host nutrients (e.g. carbohydrates, amino acids, and lipids) to complete its life cycle. For successful colonisation and guaranteed host nutrient supply, the clubroot pathogen needs to subdue plant defence and simultaneously re-program host metabolism. Thus, the development of the pathogen is strongly influenced by the host plant, and depends on compatible metabolic interactions.

Changes in leaf and root metabolites in a susceptible genotype

The first experiment conducted in this study observed metabolic patterns of leaves and roots during clubroot infection in the susceptible *B. napus* genotype Temple. Most metabolic changes were seen below-ground. The total number of significantly different root metabolites was 4x higher compared to metabolites in leaves. This result was not surprising since roots are the site of infection and contain metabolites of both plant and pathogen. Interestingly, it is unknown whether *P. brassicae* metabolites are mobile. Recent RNAseq analysis as part of a departmental "MRes" project (Fatemeh Ghorbani Sini) could not detect transcript traces of *P. brassicae* in host leaves. So it is very likely, that leaves do not contain the pathogen but pathogen-derived metabolites may be present.

Metabolites of both leaves and roots shared a few common pattern. There were more upregulated than downregulated metabolites. The number of root metabolites (up- and downregulated) and upregulated leaf metabolites increased markedly between TP1 and TP2, b a minimal decrease between TP2 and TP3, while downregulated leaf metabolites were almost constant over time. Comparisons of commonalities between TPs within each tissue type, revealed little overlap of metabolites between TP1 and TP2 for both leaf and root. Differences between tissue types were seen in TP2-TP3 overlaps. While 48% of upregulated and 39% of downregulated root metabolites of TP2 were shared with TP3, only 12% and 7% of leaf metabolites of TP2 was also detected for TP3. The observed leaf and root pattern are consistent with scientific reports. Previous studies on roots of the susceptible *A. thaliana* ecotype Col-0 observed the absence of SA during early infection stages [78], and found downregulated genes for SA-mediated defence as well as upregulated genes for sugar metabolism at the onset of gall formation [61]. Ludwig-Müller and colleagues (2015) detected higher concentrations of root-derived MeSA in leaves, and suggested that *P. brassicae* utilises its SA-methyltransferase to inactivate SA-mediated defence signalling in roots [77]. Proteomics results using MALDI-TOF-MS detected downregulated tubulins involved in cell differentiation, and upregulated proteins for cell detoxification (e.g. catalase, glutathione S-transferase (GST) or ferredoxin-nitrite reductase) during gall formation [60]. Other studies on clubroot disease in *A. thaliana* revealed increased

amounts of IAA [37], indole-glucosinolates (GSLs) [37][140] and the phytoalexin Camalexin at the onset of gall formation [55][140]. It could be shown that indole-GDLs do not influence clubroot disease development [140], while Camalexin might contribute to partial resistance against *P. brassicae* [141]. All three components alongside other phytohormones (e.g. Cytokinin) or phytoalexins (e.g. Brassinin) could potentially be detected in *B. napus* Temple. The next stage of this investigation would be to identify metabolites for each TP by a more extensive analysis of selected tissues with appropriate standards; hence, a targeted analysis.

Comparisons of leaf and root metabolites in clubroot susceptible Temple and resistant Cracker

The second experiment in this study focussed on leaf and root patterns during clubroot infection between the susceptible *B. napus* genotype Temple and the resistant *B. napus* genotype Cracker. The latter is a descendant of the *B. napus* genotype Mendel, and therefore contains the "Mendel" resistance gene, whose mechanism was proven to be incompatible with the clubroot pathotype ECD 16/2/12 used in this study. However, since 10-30% of each "Cracker-batch" does not contain the resistance gene as a natural consequence of breeding procedures (Elke Diederichsen, personal communication), the study was carried out as time-course experiment. This ensured that extracted metabolites of *B. napus* Cracker derived from visually healthy root phenotypes. On the downside, root metabolic profiling was only available for TP3. Comparisons of metabolic profiles of both genotypes did not only show a clear pattern of susceptibility and resistance in roots, but also in leaves. There were 7-8x more significantly different root metabolites in Temple, approx. 50% more upregulated than downregulated root metabolites in both cultivars, and less than 5% of root metabolites were shared between Temple and Cracker. These results underline the massive impact of *P. brassicae* on root metabolism of susceptible Brassica cultivars. It can be assumed that Cracker maintains SA-mediated plant defence in roots, and therefore contains only low amounts of primary zoospores in root hairs with low metabolic content. A study on roots of the partially resistant *A. thaliana* ecotype Bur-0 showed the accumulation of considerably high amounts of SA, and expression of SA-responsive genes during secondary infection stages [78]. Consequently, pathogen recognition with subsequent induction of defence must have happened during earlier stages of infection compared to deactivation of defence in susceptible plants [77]. Since leaf metabolites over time exhibited a distinct pattern between both cultivars, and seemed to "mirror" below-ground clubroot-mediated changes, activation or repression of plant defence might have been apparent at TP1. During TP1 Temple and Cracker showed reversed numbers of significantly up- and downregulated metabolites. In Temple, more metabolites were down- than upregulated. This was the opposite in Cracker. However, both cultivars exhibited similar numbers of significantly different leaf metabolites at TP1. They started to differ considerably at TP2 and TP3. While Cracker kept a constant level of

significantly different metabolites throughout the experiment without much overlap between TPs, Temple showed a massive increase during the onset of gall formation. 50-70% of metabolites at TP2 were also present at TP3. Since clubroot alters carbohydrate metabolism, translocation and partitioning [68][61][69], it is most likely to see the impact of those changes in the leaf metabolome of susceptible plants, while Cracker might maintain plant defence.

Conclusion

The metabolomics approach using mass-spectrometrical analysis of leaf and root material of clubroot inoculated Brassica crops proved its utility to distinguish between metabolic profiles of susceptible and resistant host plants. Consistent with current literature, it could be shown that most metabolic changes happened at the onset of gall formation; hence, at the key stages of early and late secondary infection. This applied to both the root and leaf metabolome, with the latter "mirroring" the former. To further investigate the underlying metabolites responsible for the changes, a targeted analysis is crucial.

CHAPTER 6: GENERAL DISCUSSION

Clubroot infected plants develop large galls in the root system while the aerial plant body is dwarfed with signs of drought (e.g. wilting, stunting, chlorosis, and premature senescence). The underlying reasons are pathogen-mediated changes of primary and secondary host metabolism, alterations in host stem cell maintenance and differentiation, and perturbations of vascular development with reduction in xylogenesis [73]. Clubroot disease symptoms depend on host resistance and pathogenicity of clubroot strains. Between different Brassica genotypes, disease symptoms are usually time-shifted or they differ in intensities. Those variations can be a sign of incomplete resistance (i.e. quantitative resistance). This PhD thesis explored different ways to measure quantitative resistance in numerous Brassica genotypes after inoculation with the clubroot pathotype ECD 16/2/12. Physiological changes (e.g. water balance and growth), correlations between pathogen numbers in host plants and severity of disease symptoms, and metabolic pattern in roots and leaves of susceptible and resistant genotypes were investigated in chapter 3, 4 and 5, respectively. An overview of all methods is displayed in figure 6.1.

Water- and growth related measurements to monitor clubroot-mediated physiological changes

Reduction in xylogenesis causes difficulties in water uptake during clubroot infection. Reduced water uptake is sensed as water deficit, and initiates drought stress signalling through the phytohormone abscisic acid (ABA). ABA triggers stomata closure and reduction in stomatal conductance. As a consequence, water evaporation is restricted and internal CO_2 concentrations decrease [123][68]. The former results in elevated leaf temperatures, the latter in perturbations of photosynthesis. Usually, these physiological changes as well as water use and water content can be measured using thermal imaging, chlorophyll fluorescence, pot weighing techniques and NIR imaging. However, chlorophyll fluorescence and NIR imaging were not available, and thermal imaging and pot weighing did not obtain meaningful results due to absence of uniform clubroot infection in chapter 3.

Changes in host metabolism and alterations in stem cell maintenance/differentiation turns the plant root into a large gall, which serves as new strong metabolic sink. This causes changes in carbohydrate partitioning with serious impact on the host plant's sink-source balance [68]. The disequilibrium can be assessed by weighing above- and below-ground biomass with subsequent calculations of shoot-root ratios. The utility of biomass measurements was shown in chapter 4. Fine differences in growth distortions between severely infected cultivars were detected, and revealed that some cultivars still maintained above-ground growth whilst other plants exhibited typical dwarfed phenotypes.

Outside the PhD project, the use of electrical impedance tomography (EIT) was explored as a low-cost, non-destructive and non-invasive phenotypic method for continuous monitoring of root development during clubroot infection. EIT experiments were performed in collaboration with the engineering department at the University of Manchester (Bruce Grieve and Diego Corona López). *B. napus* plants were grown in a plant pot surrounded by two rings of electrodes (e.g. upper and lower ring). EIT then measured the electrical responses (impedance, EI) to an applied electrical excitation (e.g. an electrical current was applied to the compost growth medium). Thereby, the obtained EI was influenced by different electrical root properties, compost constituents, moisture content, and ionic strength. Alterations in EI were observed due to the interaction of roots with the growth medium (e.g. root exudate production, water and solute uptake). EIT was able to distinguish between roots and soil, and between healthy and clubroot infected roots. However, it needs improvements and more fine-tuning.
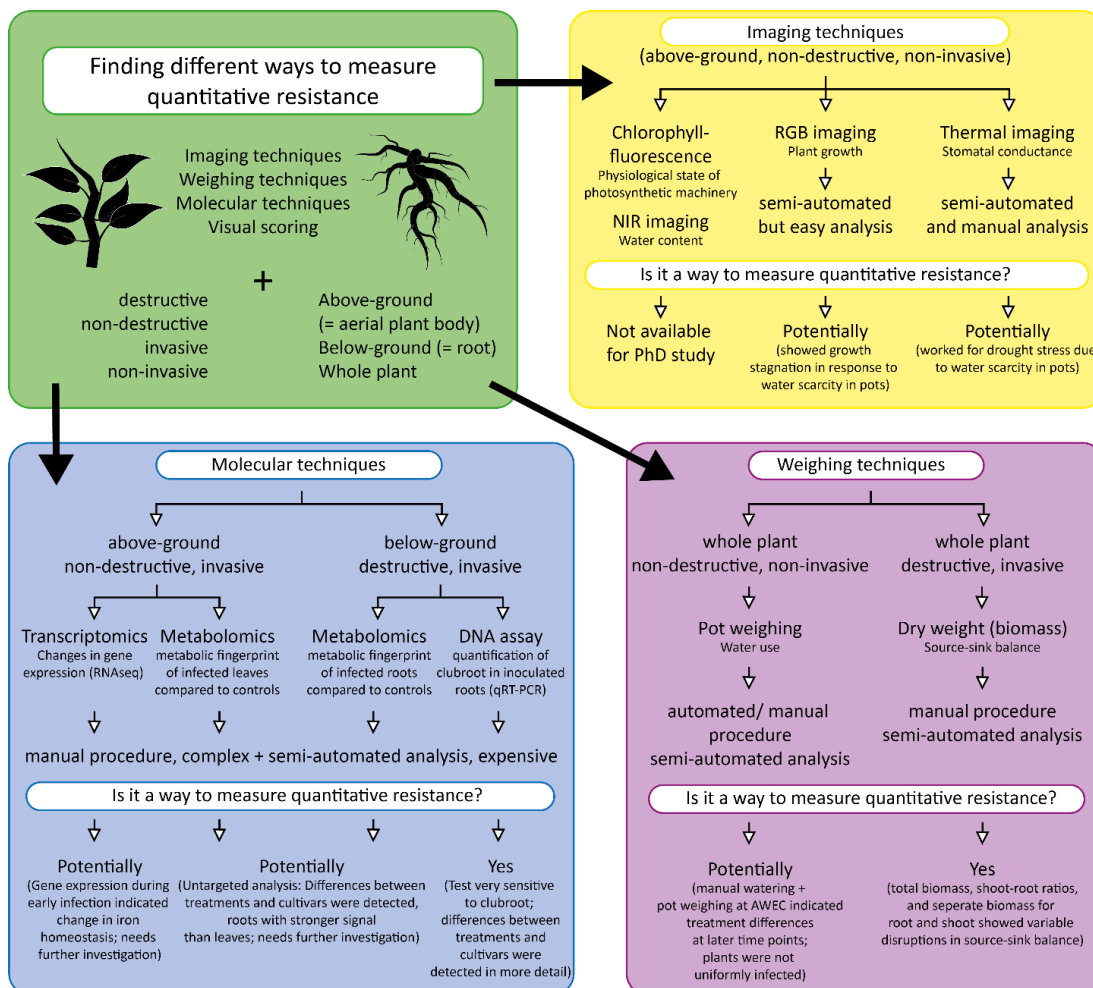
Figure 6.1: Overview of the work carried out during the PhD project – Part 1

Total quantification of P. brassicae in host plants and correlations to disease symptom severity

The most obvious indicator of clubroot disease severity is the size of root galls at the end of the pathogen's life cycle completion. An existing standard classification system for clubroot disease severity focuses on gall size after destructive harvest, and ranges from 0-3 [109]. It is the quickest and easiest way of disease classification after uprooting. However, it is also very subjective and of limited resolution. Therefore, a clubroot-sensitive DNA assay based on qRT-PCR was established for total quantification of *P. brassicae* in infected root tissue. In chapter 5, the assay proved its potential for future use. Subtle differences in source-sink disruptions and pathogen ITS copy numbers could be detected amongst plants with the same root phenotype. Thereby, no correlation between ITS copy numbers and growth distortions occurred. However, due to high control values for the clubroot specific ITS primer pair, molecular and technical optimisation of the DNA assay is necessary before field application can be performed. Molecular optimisation includes primer optimisation (e.g. multiple primer pairs based on complete *P. brassicae* sequences which were not available during the initial primer design), and primer validation through specificity tests (e.g. PCRs using microbial soil communities). Technical optimisation includes sampling, homogenisation and pipetting procedures (e.g. minimalising breakage of sample tubes during bead-beating and testing precision of pipetting robot to avoid contamination).

Metabolic profiling of leaves and roots to assess susceptibility and resistance

For life cycle completion, *P. brassicae* relies on host nutrients, such as carbohydrates, amino acids, and lipids. To accomplish reliable host nutrient supply, the pathogen needs to avoid or subdue plant defence and simultaneously re-program host metabolism. This involves a plethora of molecular changes, for example alterations in hormone homeostasis. This includes growth related hormones (i.e. IAA, CK and BRs), defence-related hormones (i.e. JA and SA), but also the drought-stress hormone ABA [68]. In chapter 6 it could be shown that the leaf metabolome "mirrored" the root metabolome during infection, and that the pattern of metabolites derived from a susceptible and a resistant Brassica cultivar differed considerably. For future research it would be interesting to identify those metabolites.

RNA sequencing (RNAseq) and analysis was conducted as part of a departmental "MRes" project (Fatemeh Ghorbani Sini) to investigate differential gene expression in leaves of *B. napus* Temple during primary clubroot infection (11dpi). The results indicated disruptions in iron homeostasis, for example upregulated ferritin, and downregulated genes associated with aconitase (see box 1 for underlying mechanisms). For a long time it is known that many human diseases are caused due to prokaryotic microorganisms scavenging iron from its host bodies to guarantee microbial

cell growth and survival [142]. Many medical, and lately also plant studies, suggested a correlation between bacterial iron requirement and virulence [142][143] with iron competition as key factor for infection [144]. Tests on *Arabidopsis thaliana* with the necrotrophic enterobacteria *Dickeya dadantii* (soft rot disease) showed production of bacterial iron chelator simultaneously to host disease symptom development. A lack of virulence was confirmed through bacterial mutant line analysis [143][144]. Further medical and plant studies highlighted the upregulation of human/ plant transferrin and ferritin synthesis as response to pathogenic iron-seeking intruders. As a consequence, withholding iron was seen as part of the (plant's innate) immune system alongside PAMP recognition to prevent microbial infection and iron piracy [144][142]. For clubroot research it would be interesting to elucidate whether iron is connected to *P. brassicae's* virulence and clubroot disease symptoms in host plants. Moreover, it might be good to investigate whether disrupted iron homeostasis is actively caused by *P. brassicae* to scavenge chelated iron within host plants, actively caused by the host plant to prevent iron piracy, or passively caused as a consequence of perturbations in plant hormone homeostasis (e.g. IAA) and ROS production. Therefore, comparisons of RNAseq and metabolomics results of leaf data might be advantageous, alongside the exploitation of already existing microarray data of clubroot infected *A. thaliana* roots. These root data could potentially unravel differentially expressed genes related to iron acquisition.

Basic requirements of uniform infection: sufficient water & optimal clubroot environment

During the PhD project, the importance of uniform infection for disease quantification was evident. Uniform infection was best achieved through a combination of both sufficient water supply and favourable environmental conditions. An overview is shown in figure 6.2. Sufficient water supply was successfully accomplished by following simple manual watering procedures seen in chapter 4 and 5, while automated watering used in chapter 3 failed. The watering algorithm was not adjusted to plant biomass increase or water demand, and therefore caused systematic drought as plants grew. Water scarcity in soil inhibited movements of zoospores to root hairs which subsequently impeded clubroot infection. Favourable environmental conditions are those that promote severe clubroot infection. Fully controlled growth chambers (laboratory) alongside small (AWEC) and large (IBERS) greenhouses were available during the PhD project. All facilities offered good control over clubroot disease due to the usage of pots. However, artificial conditions in growth chambers (chapter 5) and largely controlled environmental conditions in small greenhouses (chapter 4) obtained the best results. Infections were uniform, consistent, and reproducible.

Outlook

In this study, the most promising results were obtained from the qRT-PCR based DNA assay in combination with above- and below-ground biomass measurements. Future research could aim to improve the initial steps of the assay (e.g. sampling, homogenisation, and DNA extraction methods) and to optimise the primer pair to be able to screen the whole ASSYST panel. Molecular and biomass results obtained could then be used to identify genes or regions on the Brassica plant genome associated with quantitative resistance to clubroot infection. Due to the complex polyploid genome of Brassica plants one of the most suitable approaches for trait detection would be Associative Transcriptomics [108]. Unlike classic genetic methods, Associative Transcriptomics is based on transcriptome sequencing to identify molecular markers that represent variation in both gene sequences (QTLs) and gene expression (eQTLs). The latter describes single nucleotide polymorphisms (SNPs) in regulatory sequences that alter gene expression (i.e. transcript abundance) linked to a trait (see box 2 for further information about QTLs and eQTLs).
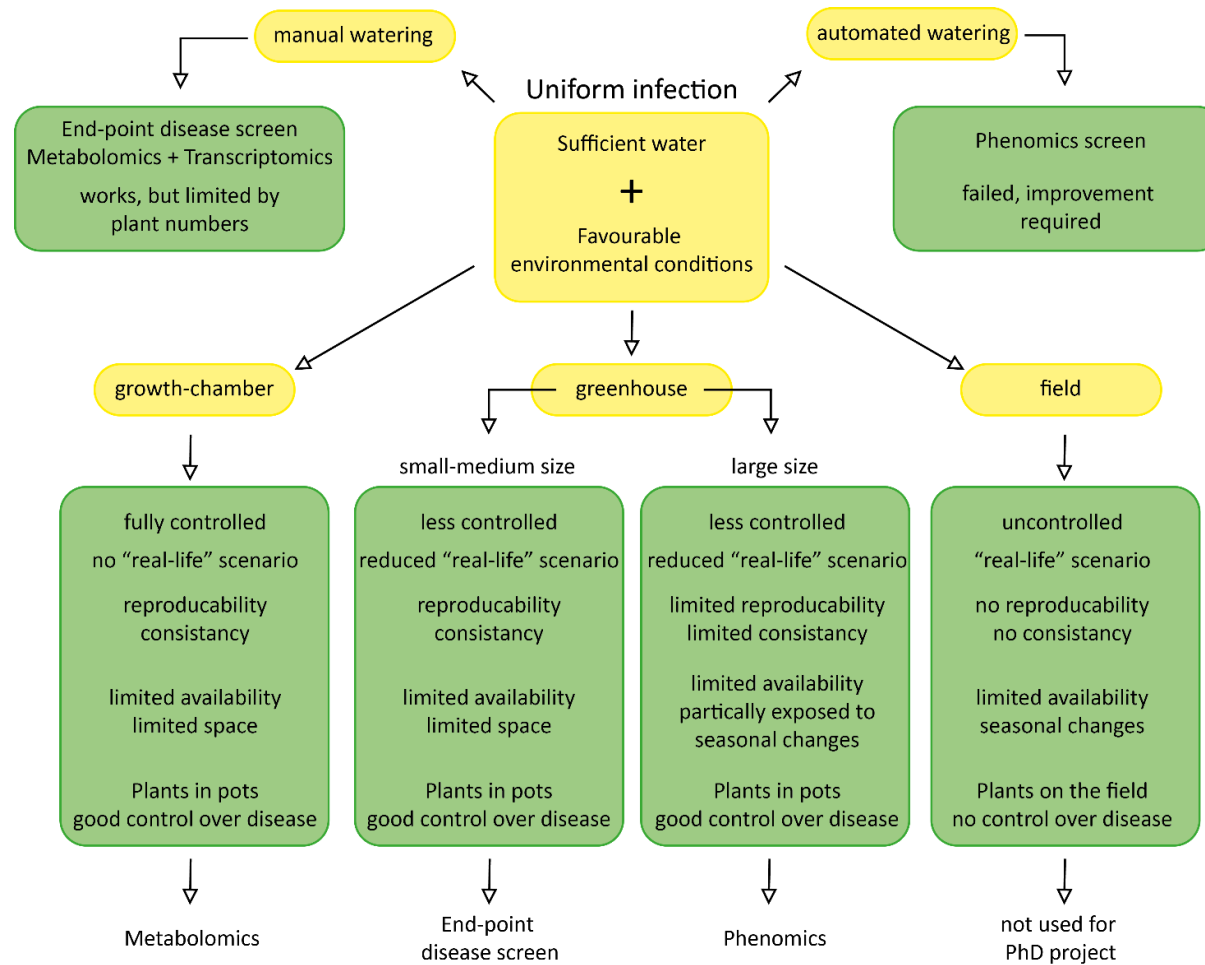
Figure 6.2: Overview of the work carried out during the PhD project – Part 2: The importance of how and where to grow plants to achieve uniform clubroot infection as basic requirement for disease quantification

BOX1: IRON

Iron is an important plant nutrient and a major cofactor of proteins involved in many essential biochemical processes due to its high redox potential. Therefore it enables crucial redox reactions and electron transfer chains during photosynthesis, respiration, or nitrogen fixation. Since most iron is bound as Fe (III) oxides, and almost insoluble at biological soil pH in aerobic environments, the bioavailable ferric iron concentration is below the requirement for optimal plant and microbial growth [144][145]. This causes competition amongst soil-based organisms [146][142].

Iron-deficiency signalling pathway: Iron solubility and acquisition

Plants evolved 2 different strategies to enhance Fe (III) oxide solubilisation and acquisition which generally involve 3 chemical reactions: protonation, chelation, and reduction [146][145][147]. Strategy 1 (dicots and non-graminaceous monocots) is characterised by morphological and physiological modifications. The former involve surface area increase through enhanced lateral root development alongside differentiation of specialised transfer cells. The latter include 4 activities: rhizosphere acidification via proton-pumping ATPases (*AtAHA* genes), iron chelation via secretion of phenolic/acidic compounds or flavins, enzymatic Fe (III) reduction through cell membrane-bound ferric reductase oxidase (At*FRO2* gene), and Fe (II) transport into root cells through high-affinity ferrous iron transporter (At*IRT1* gene) [146][145][147].
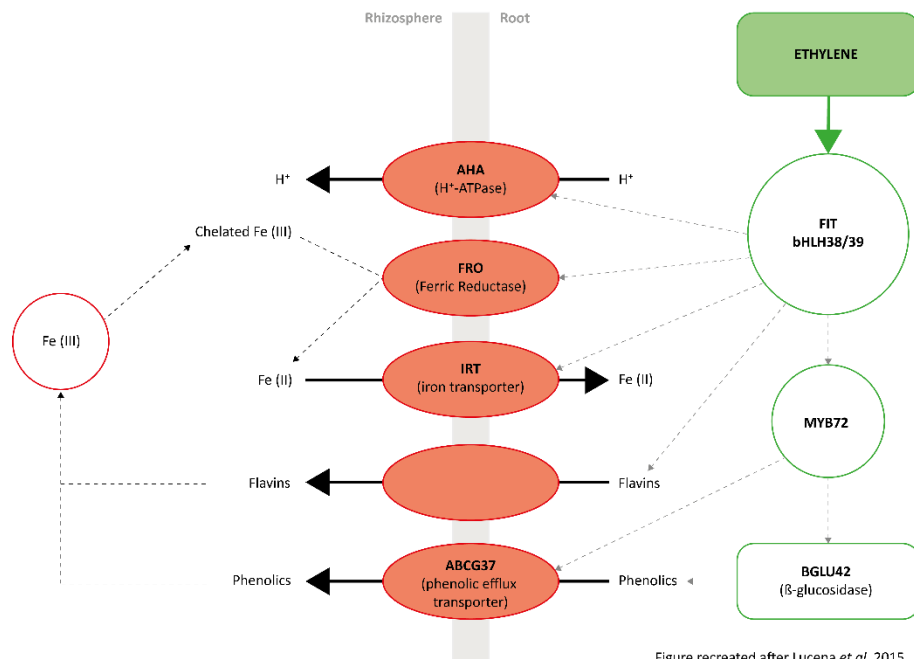
Figure recreated after Lucena *et al.* 2015

155

Iron Homeostasis – Transferrin and Ferritin

The regulation of the iron-deficiency signalling pathway is not well studied. However, several hormones and diverse signalling molecules are involved to regulate activation (e.g. IAA, ET, and nitric oxide) and suppression (e.g. CK, JA, and BRs) [145][147]. Maintenance of iron homoeostasis is crucial since unbound/free iron is toxic and catalytically generate hydroxyl radical ($\bullet OH$) production with damaging impact on molecules (i.e. DNA, proteins) and cell membranes (i.e. Phospholipids). Additionally, superoxide anions (O_2^-) can trigger iron release from iron-containing molecules causing a toxic cell environment. Regulation of homoeostasis between cell starvation and cell death acts on both transport and storage levels via Transferrin and Ferritin. The former is a glycol-protein for iron-uptake from root to leafs, the latter a spherical iron storage protein with central cavity capable of accommodating between 2000 and 4000 iron atoms in a non-toxic and soluble form for easy bioavailability [144]. Both have eukaryotic origin [142][144].

Plant ferritin biosynthesis is initiated in response to cellular iron. Under low-iron concentration, a repressor (mammals: Aconitase) interacts with a transcription factor on the iron-dependent regulatory sequence (IDRS) within the proximal promotor part, and inhibits transcription of the ferritin gene. High iron level triggers nitric oxide (NO) production in the chloroplast through nitric oxide synthase (NOS) activity leading to repressor ubiquitination and proteasome-dependent degradation in the nucleus with subsequent activation of ferritin gene expression. The upregulation is accompanied by Protein Phosphatase 2A (PP2A) activity. Soon after, the ferritin transcript is translated to a precursor polypeptide in the cytosol, transported to the chloroplast, and assembled to the mature ferritin protein [144].
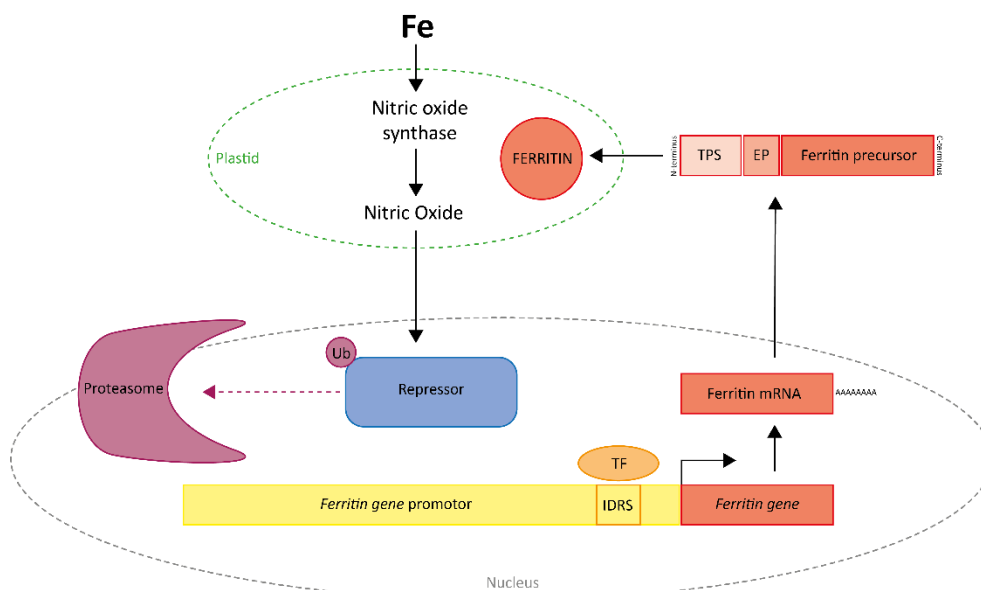
Figure recreated after Briat *et al.* 2010

BOX2: QTLs and eQTLs
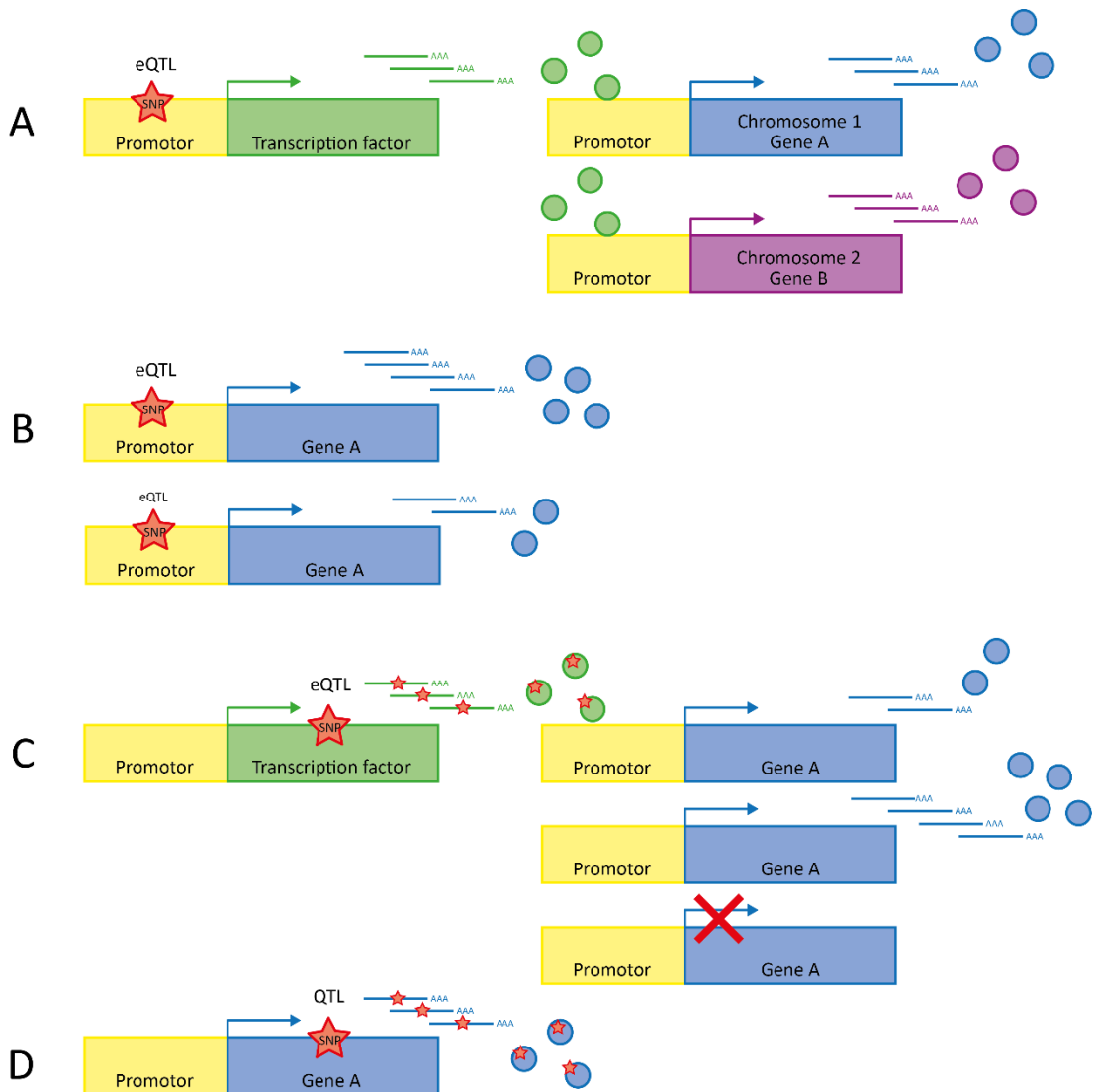
|A| SNP within a promotor of a transcription factor gene, which is near or close the genomic location of the target gene (Local and distant eQTL) |B| SNP within a promotor of a gene. The polymorphism can up- or downregulate transcription of the gene |C| SNP within the transcription factor gene. The altered transcription factor can decrease, increase, or inactivate the transcription of the target gene |D| Standard QTL | information obtained from [108]

BIBLIOGRAPHY

[1]   E.-C. Oerke, "Crop losses to pests," *J. Agric. Sci.*, vol. 144, no. 01, p. 31, Feb. 2006.

[2]   R. Fritsche-Neto and J. C. DoVale, "Root Phenomics," in *Phenomics: how next-generation phenotyping is revolutionazing plant breeding*, 2015, pp. 49–66.

[3]   G. R. Dixon, "Special Issue: Clubroot (Plasmodiophora brassicae Woronin)-an agricultural and biological challenge worldwide," *Can. J. Plant Pathol.*, vol. 36, no. SUPPL. 1, pp. 5–18, 2014.

[4]   H. D. Vanetten, J. W. Mansfield, J. A. Bailey, and E. E. Farmer, "Letter To the Editor," *Phytopathol. Z*, vol. 101, no. September, pp. 106–109, 1981.

[5]   J. D. G. Jones and J. L. Dangl, "The plant immune system.," *Nature*, vol. 444, no. 7117, pp. 323–329, 2006.

[6]   R. Bari and J. D. G. Jones, "Role of plant hormones in plant defence responses," *Plant Mol. Biol.*, vol. 69, no. 4, pp. 473–488, 2009.

[7]   R. E. Niks, X. Qi, and T. C. Marcel, "Quantitative Resistance to Biotrophic Filamentous Plant Pathogens: Concepts, Misconceptions, and Mechanisms," *Annu. Rev. Phytopathol.*, vol. 53, no. 1, pp. 445–470, 2015.

[8]   G. R. Dixon, "The occurrence and economic impact of plasmodiophora brassicae and clubroot disease," *J. Plant Growth Regul.*, vol. 28, no. 3, pp. 194–202, 2009.

[9]   T. Cavalier-Smith, "Protist phylogeny and the high-level classification of Protozoa," *Eur. J. Protistol.*, vol. 39, no. 4, pp. 338–348, 2003.

[10]   F. Burki and P. J. Keeling, "Rhizaria," *Curr. Biol.*, vol. 24, no. 3, pp. 103–107, 2014.

[11]   S.-F. Hwang, S. E. Strelkov, J. Feng, B. D. Gossen, and R. J. Howard, "Plasmodiophora brassicae: a review of an emerging pathogen of the Canadian canola (Brassica napus) crop.," *Mol. Plant Pathol.*, vol. 13, no. 2, pp. 105–13, 2012.

[12]   R. Malinowski, O. Novák, M. H. Borhan, L. Spíchal, M. Strnad, and S. A. Rolfe, "The role of cytokinins in clubroot disease," *Eur. J. Plant Pathol.*, vol. 145, no. 3, pp. 543–557, 2016.

[13]   D. Jones, D. Ingram, and G. Dixon, "Characterisation of isolates derived from single resting spores of Plasmodiosphora brassicae," *Plan Physiol.*, vol. 31, pp. 239–245, 1982.

[14]   D. S. Ingram and I. C. Tommerup, "The Life History of Plasmodiophora brassicae Woron," *Proc. R. Soc. B Biol. Sci.*, vol. 180, no. 1058, pp. 103–112, 1972.

[15]   M. S. Woronin, "Plasmodiophora Brassicae, Urheber der Kohlpflanzenhernie," *Jahrbücher für Wissenschaftliche Bot.*, vol. 11, pp. 548–574, 1878.

[16]   G. W. Ayers, "Studies on the life history of the clubroot organism Plasmodiophora brassicae," *Can. J. Res.*, vol. 22, 1944.

[17]   K. Kageyama and T. Asano, "Life cycle of plasmodiophora brassicae," *J. Plant Growth Regul.*, vol. 28, no. 3, pp. 203–211, 2009.

[18]   A.-C. Wallenhammar, "Prevalence of Plasmodiophora brassicae in a spring oilseed rape growing area in central Sweden and factors influencing soil infestation levels," *Plant Pathol.*, vol. 45, pp. 710–719, 1996.

[19]   K. Suzuki, E. Matsumiya, Y. Ueno, and J. Mizutani, "Some properties of germination-stimulating factor from plants for resting spore of Plasmodiophora beassicae," *Ann. Phytopathol. Soc. Japan*, vol. 58, pp. 699–705, 1992.

[20]   I. Macfarlane, "Germination of resting spores of Plasmodiophora brassicae," *Trans. Br. Mycol. Soc.*, vol. 55, no. 1, pp. 97–112, 1970.

[21]   H. U. Ahmed, S. F. Hwang, S. E. Strelkov, B. D. Gossen, G. Peng, R. J. Howard, and G. D. Turnbull, "Assessment of bait crops to reduce inoculum of clubroot (*Plasmodiophora brassicae*) of canola," *Can. J. Plant Sci.*, vol. 91, no. 3, pp. 545–551, 2011.

[22]   H. Friberg, J. Lagerlöf, and B. Rämert, "Germination of Plasmodiophora brassicae resting spores stimulated by a non-host plant," *Eur. J. Plant Pathol.*, vol. 113, no. 3, pp. 275–281, 2005.

[23]   H. Friberg, J. Lagerlöf, and B. Rämert, "Usefulness of nonhost plants in managing Plasmodiophora brassicae," *Plant Pathol.*, vol. 55, no. 5, pp. 690–695, 2006.

[24]   A. Rashid, H. U. Ahmed, Q. Xiao, S. F. Hwang, and S. E. Strelkov, "Effects of root exudates and pH on Plasmodiophora brassicae resting spore germination and infection of canola (Brassica napus L.) root hairs," *Crop Prot.*, vol. 48, pp. 16–23, 2013.

[25]   J. Feng, R. U. Hwang, S. F. Hwang, S. E. Strelkov, B. D. Gossen, Q. X. Zhou, and G. Peng, "Molecular characterization of a serine protease Pro1 from Plasmodiophora brassicae that stimulates resting spore germination," *Mol. Plant Pathol.*, vol. 11, no. 4, pp. 503–512, 2010.

[26]   J. P. Braselton, "Current status of the plasmodiophorids," *Crit. Rev. Microbiol.*, vol. 21, no. 4, pp. 263–275, 1995.

[27]   T. Naiki, C. Kawaguchi, and H. Ikegami, "Root hair reinfection in Chinese cabbage seedlings by the secondary zoospores of Plasmodiophora brassicae Woronin," *Japanese J. Phytopathol.*, vol. 50, no. 2, pp. 216–220, 1984.

[28]   R. Mithen and R. Magrath, "A contribution to the life history of Plasmodiophora brassicae: secondary plasmodia development in root galls of Arabidopsis thaliana," *Mycol. Res.*, vol. 96, no. 10, pp. 877–885, 1992.

[29]   M. Fähling, H. Graf, and J. Siemens, "Characterization of a Single-Spore Isolate Population of Plasmodiophora brassicae Resulting from a Single Club," *J. Phytopathol.*, vol. 152, no. 7, pp. 438–444, 2004.

[30]   J. S. Karling, "The Plasmodiophorales," *2nd Ed. Hafner*, 1968.

[31]   J. Colhoun, "Clubroot disease of crucifers caused by Plasmodiophora brassicae Woron. A monograph," *Phytopathol. Pap. No.3*, 1958.

[32]   J. Ludwig-Müller, R. N. Bennett, G. Kiddle, S. Ihmig, M. Ruppel, and W. Hilgenberg, "The host range of Plasmodiophora brassicae and its relationship to endogenous glucosinolate content," *New Phytol.*, vol. 141, no. 3, pp. 443–458, 1999.

[33]   J. Feng, Q. Xiao, S. F. Hwang, S. E. Strelkov, and B. D. Gossen, "Infection of canola by secondary zoospores of Plasmodiophora brassicae produced on a nonhost," *Eur. J. Plant Pathol.*, vol. 132, no. 3, pp. 309–315, 2012.

[34]   L. Taiz and E. Zeiger, *Plant Physiology - Chapter 19 - Auxin: The growth hormone*. 2006.

[35]   A. W. Woodward and B. Bartel, "Auxin: Regulation, action, and interaction," *Ann. Bot.*, vol. 95, no. 5, pp. 707–735, 2005.

[36] A. J. Ludwig-müller, U. Bendel, P. Thermann, M. Ruppel, and W. Hilgenberg, "Concentrations of indole-3-acetic acid in plants of of Chinese tolerant cabbage and susceptible infected with varieties Plasmodiophora brassicae Woron," *New Phytol.*, vol. 125, no. 4, pp. 763–769, 1993.

[37] J. Ludwig-Müller and A. Schuller, "What can we learn from clubroots: Alterations in host roots and hormone homeostasis caused by Plasmodiophora brassicae," *Sustain. Dis. Manag. a Eur. Context*, pp. 291–302, 2008.

[38] J. Brumos, J. M. Alonso, and A. N. Stepanova, "Genetic aspects of auxin biosynthesis and its regulation," *Physiol. Plant.*, vol. 151, no. 1, pp. 3–12, 2014.

[39] B. A. Halkier and J. Gershenzon, "Biology and Biochemistry of Glucosinolates," *Annu. Rev. Plant Biol.*, vol. 57, no. 1, pp. 303–333, 2006.

[40] J. Ludwig-Müller, B. Schubert, K. Pieper, S. Ihmig, and W. Hilgenberg, "Glucosinolate content in susceptible and resistant Chinese cabbage varieties during development of clubroot disease," *Phytochemistry*, vol. 44, no. 3, pp. 407–414, 1997.

[41] S. Grsic, B. Kirchheim, K. Pieper, M. Fritsch, W. Hilgenberg, and J. Ludwig-Müller, "Induction of auxin biosynthetic enzymes by jasmonic acid and in clubroot diseased Chinese cabbage plants," *Physiol. Plant.*, vol. 105, no. 3, pp. 521–531, 1999.

[42] S. Devos and E. Prinsen, "Plant hormones: a key inclubroot development," *Proc. 33rd PGRSA Annu. Meet.*, pp. 3–6, 2006.

[43] S. Grsic-Rausch, P. Kobelt, J. M. Siemens, M. Bischoff, and J. Ludwig-Müller, "Expression and Localization of Nitrilase during Symptom Development of the Clubroot Disease in Arabidopsis," *Plant Physiol.*, vol. 122, no. 2, pp. 369–378, 2000.

[44] J. Siemens, E. Glawischnig, and J. Ludwig-Müller, "Indole glucosinolates and camalexin do not influence the development of the clubroot disease in Arabidopsis thaliana," *J. Phytopathol.*, vol. 156, no. 6, pp. 332–337, 2008.

[45] P. E. Staswick, B. Serban, M. Rowe, and I. Tiryaki, "Characterization of an *Arabidopsis* enzyme family that conjugates amino acids to indole-3-acetic acid," *Plant Cell*, vol. 17, no. 2, pp. 616–627, 2005.

[46] J. Ludwig-Müller, E. Epstein, and W. Hilgenberg, "Auxin-conjugate hydrolysis in Chinese cabbage: Characterization of an amidohydrolase and its role during infection with clubroot disease," *Physiol. Plant.*, vol. 97, no. 4, pp. 627–634, 1996.

[47] L. Jahn, S. Mucha, S. Bergmann, C. Horn, P. Staswick, B. Steffens, J. Siemens, and J. Ludwig-Müller, "The Clubroot Pathogen (Plasmodiophora brassicae) Influences Auxin Signaling to Regulate Auxin Homeostasis in Arabidopsis," *Plants*, vol. 2, no. 4, pp. 726–749, 2013.

[48] J. Ludwig-Müller, "Auxin homeostasis, signaling, and interaction with other growth hormones during the clubroot disease of Brassicaceae," *Plant Signal. Behav.*, vol. 9, no. APR, pp. 9–12, 2014.

[49] S. A. Rolfe, S. E. Strelkov, M. G. Links, W. E. Clarke, S. J. Robinson, M. Djavaheri, R. Malinowski, P. Haddadi, S. Kagale, I. A. P. Parkin, A. Taheri, and M. H. Borhan, "The compact genome of the plant pathogen Plasmodiophora brassicae is adapted to intracellular interactions with host Brassica spp," *BMC Genomics*, vol. 17, no. 1, pp. 1–15, 2016.

[50] B. M. Kuhn, T. Nodzyński, S. Errafi, R. Bucher, S. Gupta, B. Aryal, P. Dobrev, L. Bigler, M. Geisler, E. Zažímalová, J. Friml, and C. Ringli, "Flavonol-induced changes in PIN2 polarity

and auxin transport in the Arabidopsis thaliana rol1-2 mutant require phosphatase activity," *Sci. Rep.*, vol. 7, no. January, pp. 1–13, 2017.

[51]   S. Päsold, I. Siegel, C. Seidel, and J. Ludwig-Müller, "Flavonoid accumulation in Arabidopsis thaliana root galls caused by the obligate biotrophic pathogen Plasmodiophora brassicae," *Mol. Plant Pathol.*, vol. 11, no. 4, pp. 545–562, 2010.

[52]   M. Lavy and M. Estelle, "Mechanisms of auxin signaling," *Development*, vol. 143, no. 18, pp. 3226–3229, 2016.

[53]   R. Wang and M. Estelle, "Diversity and specificity: Auxin perception and signaling through the TIR1/AFB pathway," *Curr. Opin. Plant Biol.*, vol. 21, pp. 51–58, 2014.

[54]   J. E. Park, J. Y. Park, Y. S. Kim, P. E. Staswick, J. Jeon, J. Yun, S. Y. Kim, J. Kim, Y. H. Lee, and C. M. Park, "GH3-mediated auxin homeostasis links growth regulation with stress adaptation response in Arabidopsis," *J. Biol. Chem.*, vol. 282, no. 13, pp. 10036–10046, 2007.

[55]   M. Y. Wang, X. T. Liu, Y. Chen, X. J. Xu, B. Yu, S. Q. Zhang, Q. Li, and Z. H. He, "Arabidopsis Acetyl-Amido Synthetase GH3.5 Involvement in Camalexin Biosynthesis through Conjugation of Indole-3-Carboxylic Acid and Cysteine and Upregulation of Camalexin Biosynthesis Genes," *J. Integr. Plant Biol.*, vol. 54, no. 7, pp. 471–485, 2012.

[56]   L. Taiz and E. Zeiger, *Plant Physiology - Chapter 21 - Cytokinins: Regulators of Cell Devision*. 2006.

[57]   J. J. Kieber and G. E. Schaller, "Cytokinins," *Arab. B.*, vol. 12, p. e0168, 2014.

[58]   H. M. Dekhuijzen, "The occurrence of free and bound cytokinins in plasmodia of Plasmodiophora brassicae isolated from tissue cultures of clubroots.," *Plant Cell Rep.*, vol. 1, no. 1, pp. 18–20, 1981.

[59]   S. Devos, K. Vissenberg, J.-P. Verbelen, and E. Prinsen, "Infection of Chinese cabbage by Plasmodiophora brassicae leads to a stimulation of plant growth: impacts on cell wall metabolism and hormone balance," *New Phytol.*, vol. 166, no. 1, pp. 241–250, 2005.

[60]   S. Devos, K. Laukens, P. Deckers, D. Van Der Straeten, T. Beeckman, D. Inzé, H. Van Onckelen, E. Witters, and E. Prinsen, "A Hormone and Proteome Approach to Picturing the Initial Metabolic Events During *Plasmodiophora brassicae* Infection on *Arabidopsis*," *Mol. Plant-Microbe Interact.*, vol. 19, no. 12, pp. 1431–1443, 2006.

[61]   J. Siemens, I. Keller, J. Sarx, S. Kunz, A. Schuller, W. Nagel, T. Schmülling, M. Parniske, and J. Ludwig-Müller, "Transcriptome Analysis of *Arabidopsis* Clubroots Indicate a Key Role for Cytokinins in Disease Development," *Mol. Plant-Microbe Interact.*, vol. 19, no. 5, pp. 480–494, 2006.

[62]   A. Schwelm, J. Fogelqvist, A. Knaust, S. Jülke, T. Lilja, G. Bonilla-Rosso, M. Karlsson, A. Shevchenko, V. Dhandapani, S. R. Choi, H. G. Kim, J. Y. Park, Y. P. Lim, J. Ludwig-Müller, and C. Dixelius, "The Plasmodiophora brassicae genome reveals insights in its life cycle and ancestry of chitin synthases," *Sci. Rep.*, vol. 5, no. May, pp. 1–12, 2015.

[63]   L. Taiz and E. Zeiger, *Plant Physiology - Chapter 8 - Photosynthesis - Carbon Reactions*, 4th ed. Sinauer Associates Inc, 2006.

[64]   L.-Q. Chen, B.-H. Hou, S. Lalonde, H. Takanaga, M. L. Hartung, X.-Q. Qu, W.-J. Guo, J.-G. Kim, W. Underwood, B. Chaudhuri, D. Chermak, G. Antony, F. F. White, S. C. Somerville, M. BethMudgetta, and W. B. Frommer, "Sugar transporters for intercellular exchange and nutrition of pathogens," *Nature*, vol. 468, no. 7323, pp. 527–532, 2010.

[65] K. E. Koch, "Carbohydrate-Modulated Gene Expression in Plants," *Annu. Rev. Plant Physiol. Plant Mol. Biol.*, vol. 47, no. 1, pp. 509–540, 1996.

[66] M. J. Paul and C. H. Foyer, "Sink regulation of photosynthesis," *J. Exp. Bot.*, vol. 52, no. 360, pp. 1383–1400, 2001.

[67] N. T. Keen and P. H. Williams, "Translocation of sugars into infected cabbage tissues during clubroot development," *Plant Physiol.*, vol. 44, pp. 748–754, 1969.

[68] J. Ludwig-Müller, E. Prinsen, S. A. Rolfe, and J. D. Scholes, "Metabolism and plant hormone action during clubroot disease," *J. Plant Growth Regul.*, vol. 28, no. 3, pp. 229–244, 2009.

[69] J. Evans and J. D. Scholes, "How does clubroot alter the regulation of carbohydrate metabolism in its host?," *Asp. Appl. Biol.*, vol. 42, pp. 125–132, 1995.

[70] H. Li, X. Li, Y. Xuan, J. Jiang, Y. Wei, and Z. Piao, "Genome Wide Identification and Expression Profiling of SWEET Genes Family Reveals Its Role During Plasmodiophora brassicae -Induced Formation of Clubroot in Brassica rapa," vol. 9, no. February, pp. 1–16, 2018.

[71] P. Walerowski, A. Gündel, N. Yahaya, W. Truman, M. Olszak, S. Rolfe, L. Borisjuk, and R. Malinowski, "Clubroot Disease Stimulates Early Steps of Phloem Differentiation and Recruits SWEET Sucrose Transporters All Phloem Lineage Cells are Present in Higher Numbers in," vol. 30, no. December, pp. 3058–3073, 2018.

[72] J. Siemens, M. González, S. Wolf, C. Hofmann, S. Greiner, Y. Du, T. Rausch, T. Roitsch, and J. Ludwig-müller, "Extracellular invertase is involved in the regulation of clubroot disease in Arabidopsis thaliana," vol. 12, pp. 247–262, 2011.

[73] R. Malinowski, J. A. Smith, A. J. Fleming, J. D. Scholes, and S. A. Rolfe, "Gall formation in clubroot-infected Arabidopsis results from an increase in existing meristematic activities of the host but is not essential for the completion of the pathogen life cycle," *Plant J.*, vol. 71, no. 2, pp. 226–238, 2012.

[74] D. Brodmann, A. Schuller, J. Ludwig-Müller, R. A. Aeschbacher, A. Wiemken, T. Boller, and A. Wingler, "Induction of Trehalase in *Arabidopsis* Plants Infected With the Trehalose-Producing Pathogen *Plasmodiophora brassicae*," *Mol. Plant-Microbe Interact.*, vol. 15, no. 7, pp. 693–700, 2002.

[75] D. A. Dempsey, A. C. Vlot, M. C. Wildermuth, and D. F. Klessig, "Salicylic Acid Biosynthesis and Metabolism," *Arab. B.*, vol. 9, p. e0156, 2011.

[76] J. C. D'Auria, F. Chen, and E. Pichersky, "The SABATH family of MTS in Arabidopsis Thaliana and other plant species," *Recent Adv. Phytochem.*, vol. 37, pp. 253–283, 2003.

[77] J. Ludwig-Müller, S. Jülke, K. Geiß, F. Richter, A. Mithöfer, I. Šola, G. Rusak, S. Keenan, and S. Bulman, "A novel methyltransferase from the intracellular pathogen Plasmodiophora brassicae methylates salicylic acid," *Mol. Plant Pathol.*, vol. 16, no. 4, pp. 349–364, 2015.

[78] S. Lemarié, A. Robert-Seilaniantz, C. Lariagon, J. Lemoine, N. Marnet, M. Jubault, M. J. Manzanares-Dauleux, and A. Gravot, "Both the Jasmonic Acid and the Salicylic Acid Pathways Contribute to Resistance to the Biotrophic Clubroot Agent Plasmodiophora brassicae in Arabidopsis," *Plant Cell Physiol.*, vol. 56, no. 11, pp. 2158–2168, 2015.

[79] C. Wasternack and B. Hause, "Jasmonates: Biosynthesis, perception, signal transduction and action in plant stress response, growth and development. An update to the 2007 review in Annals of Botany," *Ann. Bot.*, vol. 111, no. 6, pp. 1021–1058, 2013.

[80] P. E. Staswick and I. Tiryaki, "The Oxylipin Signal Jasmonic Acid Is Activated by an Enzyme That Conjugates It to Isoleucine in Arabidopsis," *Plant Cell Online*, vol. 16, no. 8, pp. 2117–2127, 2004.

[81] A. Schuller, J. Kehr, and J. Ludwig-Müller, "Laser microdissection coupled to transcriptional profiling of arabidopsis roots inoculated by plasmodiophora brassicae indicates a role for brassinosteroids in clubroot formation," *Plant Cell Physiol.*, vol. 55, no. 2, pp. 392–411, 2014.

[82] J. Siemens, M. Nagel, J. Ludwig-Müller, and M. D. Sacristán, "The interaction of Plasmodiophora brassicae and Arabidopsis thaliana: Parameters for disease quantification and screening of mutant lines," *J. Phytopathol.*, vol. 150, no. 11–12, pp. 592–605, 2002.

[83] Z. Wei and J. Li, "Brassinosteroids Regulate Root Growth, Development, and Symbiosis," *Mol. Plant*, vol. 9, no. 1, pp. 86–100, 2016.

[84] C. Kühn, "Review: Post-translational cross-talk between brassinosteroid and sucrose signaling," *Plant Sci.*, vol. 248, pp. 75–81, 2016.

[85] Y. Chung and S. Choe, "The Regulation of Brassinosteroid Biosynthesis in Arabidopsis," *CRC. Crit. Rev. Plant Sci.*, vol. 32, no. 6, pp. 396–410, 2013.

[86] M. A. Webster and G. R. Dixon, "Boron, pH and inoculum concentration influencing colonization by Plasmodiophora brassicae," *Mycol. Res.*, vol. 95, no. 1, pp. 74–79, 1991.

[87] M. A. Webster and G. R. Dixon, "Calcium, pH and inoculum concentration influencing colonization by Plasmodiophora brassicae," *Mycol. Res.*, vol. 95, no. 1, pp. 64–73, 1991.

[88] E. C. Donald, L. J. Porter, R. Faggian, and R. A. Lancaster, "An Integrated Approach to the Control of Clubroot in Vegetable Brassica Crops," *Acta Hort.*, vol. 706, pp. 283–300, 2006.

[89] H. Murakamia, S. Tsushima, T. Akimoto, K. Murakami, I. Goto, and Y. Shishido, "Effects of growing leafy daikon (Raphanus sativus) on populations of Plasmodiophora brassicae (clubroot)," *Plant Pathol.*, vol. 49, no. 5, pp. 584–589, 2000.

[90] E. Diederichsen, M. Frauen, E. G. A. Linders, K. Hatakeyama, and M. Hirai, "Status and perspectives of clubroot resistance breeding in crucifer crops," *J. Plant Growth Regul.*, vol. 28, no. 3, pp. 265–281, 2009.

[91] H. Fuchs and M. Sacristán, "Identification of a gene in Arabidopsis thaliana controlling resistance to clubroot (Plasmodiophora brassicae) and characterization of the resistance response.," *Mol. Plant-Microbe Interact.*, vol. 9, no. 2, pp. 91–97, 1996.

[92] M. Jubault, C. Lariagon, M. Simon, R. Delourme, and M. J. Manzanares-Dauleux, "Identification of quantitative trait loci controlling partial clubroot resistance in new mapping populations of Arabidopsis thaliana," *Theor. Appl. Genet.*, vol. 117, no. 2, pp. 191–202, 2008.

[93] J. R. Aist and P. H. Williams, "The cytology and kinetics of cabbage root hair penetration by Plasmodiophora brassicae," *Can. J. Bot.*, vol. 49, pp. 2023–2034, 1971.

[94] U. Nagaharu, "Genome Analysis in Brassica with Special Reference to the Experimental Formation of B. Napus and Peculiar Mode of Fertilization," *Japanese J. Bot.*, vol. 7, pp. 389–452, 1935.

[95] J. Chen, J. Jing, Z. Zhan, T. Zhang, C. Zhang, and Z. Piao, "Identification of novel QTLs for isolate-specific partial resistance to Plasmodiophora brassicae in Brassica rapa," *PLoS*

One, vol. 8, no. 12, pp. 1–11, 2013.

[96] E. Diederichsen, U. Deppe, M. D. Sacristan, F. U. Berlin, and B. Angewandte, "Characterization of Clubroot Resistance in Recent Winter Oilseed Rape Material," *Proc. 11th Int. Rapeseed Congr.*, pp. 68–70, 2003.

[97] E. Diederichsen, J. Beckmann, J. Schondelmeier, and F. Dreyer, "Genetics of clubroot resistance in Brassica napus 'Mendel,'" *Acta Hortic.*, vol. 706, pp. 307–311, 2006.

[98] R. Fredua-Agyeman, S. F. Hwang, S. E. Strelkov, Q. Zhou, and D. Feindel, "Potential loss of clubroot resistance genes from donor parent Brassica rapa subsp. rapifera (ECD 04) during doubled haploid production," *Plant Pathol.*, vol. 67, no. 4, pp. 892–901, 2018.

[99] K. Suwabe, H. Tsukazaki, H. Iketani, K. Hatakeyama, M. Fujimura, T. Nunome, H. Fukuoka, S. Matsumoto, and M. Hirai, "Identification of two loci for resistance to clubroot (Plasmodiophora brassicae Woronin) in Brassica rapa L.," *Theor. Appl. Genet.*, vol. 107, no. 6, pp. 997–1002, 2003.

[100] K. Suwabe, H. Tsukazaki, H. Iketani, K. Hatakeyama, M. Kondo, M. Fujimura, T. Nunome, H. Fukuoka, M. Hirai, and S. Matsumoto, "Simple sequence repeat-based comparative genomics between Brassica rapa and Arabidopsis thaliana: The genetic origin of clubroot resistance," *Genetics*, vol. 173, no. 1, pp. 309–319, 2006.

[101] M. Hirai, T. Harada, N. Kubo, M. Tsukada, K. Suwabe, and S. Matsumoto, "A novel locus for clubroot resistance in Brassica rapa and its linkage markers," *Theor. Appl. Genet.*, vol. 108, no. 4, pp. 639–643, 2004.

[102] E. Matsumoto, C. Yasui, M. Ohi, and M. Tsudaka, "Linkage analysis of RFLP markers for clubroot resistance and pigmentation in Chinese cabbage (Brassica rapa ssp. pekinensis)," *Euphytica*, vol. 104, no. 79, 1998.

[103] W. Pang, P. Fu, X. Li, Z. Zhan, S. Yu, and Z. Piao, "Identification and Mapping of the Clubroot Resistance Gene CRd in Chinese Cabbage (Brassica rapa ssp. pekinensis)," *Front. Plant Sci.*, vol. 9, no. May, pp. 1–9, 2018.

[104] K. Sakamoto, A. Saito, N. Hayashida, G. Taguchi, and E. Matsumoto, "Mapping of isolate-specific QTLs for clubroot resistance in Chinese cabbage (Brassica rapa L. ssp. pekinensis)," *Theor. Appl. Genet.*, vol. 117, no. 5, pp. 759–767, 2008.

[105] F. Yu, X. Zhang, G. Peng, K. C. Falk, S. E. Strelkov, and B. D. Gossen, "Genotyping-by-sequencing reveals three QTL for clubroot resistance to six pathotypes of Plasmodiophora brassicae in Brassica rapa," *Sci. Rep.*, vol. 7, no. 1, pp. 1–11, 2017.

[106] S. T. Buczacki, H. Toxopeus, P. Mattusch, T. D. Johnston, G. R. Dixon, and L. a. Hobolth, "Study of physiologic specialization in Plasmodiophora brassicae: Proposals for attempted rationalization through an international approach," *Trans. Br. Mycol. Soc.*, vol. 65, no. 2, pp. 295–303, 1975.

[107] E. C. Donald, J. M. Lawrence, and I. J. Porter, "Evaluation of a fluorescent staining technique as an indicator of pathogenicity of resting spores of Plasmodiophora brassicae," *Australas. Plant Pathol.*, vol. 31, no. 4, pp. 373–379, 2002.

[108] A. L. Harper, M. Trick, J. Higgins, F. Fraser, L. Clissold, R. Wells, C. Hattori, P. Werner, and I. Bancroft, "Associative transcriptomics of traits in the polyploid crop species Brassica napus," *Nat. Biotechnol.*, vol. 30, no. 8, pp. 798–802, 2012.

[109] Y. Kuginuki, H. Yoshikawa, and M. Hirai, "Variation in virulence of Plasmodiophora brassicae in Japan tested with clubroot-resistant cultivars of Chinese cabbage (Brassica rapa L. ssp. pekinensis)," *Eur. J. Plant Pathol.*, vol. 105, no. 4, pp. 327–332, 1999.

[110] S. K. Sahu, M. Thangaraj, and K. Kathiresan, "DNA Extraction Protocol for Plants with High Levels of Secondary Metabolites and Polysaccharides without Using Liquid Nitrogen and Phenol," *ISRN Mol. Biol.*, vol. 2012, pp. 1–6, 2012.

[111] A. Schwelm and S. Neuhauser, "Letter to the Editor: 'Detection of Ribosomal DNA Sequence Polymorphisms in the Protist Plasmodiophora brassicae for the Identification of Geographical Isolates,'" *Int. J. Mol. Sci.*, vol. 18, no. 1, pp. 1453–1454, 2017.

[112] P. Pétriacq, J. Ton, O. Patrit, G. Tcherkez, and B. Gakière, "NAD acts as an integral regulator of multiple defense layers," *Plant Physiol.*, vol. 172, pp. 1–15, 2016.

[113] C. a Smith, E. J. Want, G. O'Maille, R. Abagyan, G. Siuzdak, and and G. S. CA Smith, J Elizabeth, G O'Maille,Ruben Abagyan, "XCMS: processing mass spectrometry data for metabolite profiling using Nonlinear Peak Alignment,Matching,and Identification," *ACS Publ.*, vol. 78, no. 3, pp. 779–87, 2006.

[114] J. Xia, I. V. Sinelnikov, B. Han, and D. S. Wishart, "MetaboAnalyst 3.0-making metabolomics more meaningful," *Nucleic Acids Res.*, vol. 43, no. W1, pp. W251–W257, 2015.

[115] J. Chong and J. Xia, "MetaboAnalystR: an R package for flexible and reproducible analysis of metabolomics data," *Bioinformatics*, no. June, pp. 1–2, 2018.

[116] M. V. Rockman and L. Kruglyak, "Genetics of global gene expression," *Nat. Rev. Genet.*, vol. 7, no. 11, pp. 862–872, 2006.

[117] T. W. T. C. C. Consortium, "Genome-wide association study of 14 000 cases of seven common diseases and 3 000 shared controls," *Nature*, vol. 447, no. 7145, pp. 661–678, 2007.

[118] D. Houle, D. R. Govindaraju, and S. Omholt, "Phenomics: the next challenge," *Nat. Rev. Genet.*, vol. 11, no. 12, pp. 855–866, 2010.

[119] J. Kumar, A. Pratap, and S. Kumar, "Plant Phenomics: An Overview," in *Phenomics in crop plants: Trends, Opinions, and Limitations*, J. Kumar, A. Pratap, and S. Kumar, Eds. 2015, pp. 1–10.

[120] É. A. Giglioti, C. H. Sumida, and M. G. Canteri, "Disease Phenomics," in *Phenomics: how next-generation phenotyping is revolutionazing plant breeding*, R. Fritsche-Neto and A. Borém, Eds. 2015, pp. 101–123.

[121] F. Zou, Z. Xu, and T. Vision, "Assessing the significance of quantitative trait loci in replicable mapping populations," *Genetics*, vol. 174, no. 2, pp. 1063–1068, 2006.

[122] H. Poorter, F. Fiorani, M. Stitt, U. Schurr, A. Finck, Y. Gibon, B. Usadel, R. Munns, O. K. Atkin, F. Tardieu, and T. L. Pons, "The art of growing plants for experimental purposes: A practical guide for the plant biologist," *Funct. Plant Biol.*, vol. 39, no. 11, pp. 821–838, 2012.

[123] H. Zhang and U. Sonnewald, "Differences and commonalities of plant responses to single and combined stresses," *Plant J.*, vol. 90, no. 5, pp. 839–855, 2017.

[124] S. Ito, T. Maehara, E. Maruno, S. Tanaka, M. Kameya-Iwaki, and F. Kishi, "Development of a PCR-based assay for the detection of Plasmodiophora brassicae in soil," *J. Phytopathol.*, vol. 147, no. 2, pp. 83–88, 1999.

[125] S. Ito, T. Maehara, S. Tanaka, M. Kameya-Iwaki, S. Yano, and F. Kishi, "Cloning of a single-copy DNA sequence unique to Plasmodiophora brassicae," *Physiol. Mol. Plant Pathol.*, vol. 50, no. 5, pp. 289–300, 1997.

[126] R. Faggian, S. R. Bulman, a C. Lawrie, and I. J. Porter, "Specific Polymerase Chain Reaction Primers for the Detection of Plasmodiophora brassicae in Soil and Water.," *Phytopathology*, vol. 89, no. 5, pp. 392–397, 1999.

[127] T. Cao, J. Tewari, S. E. Strelkov, N. Science, and A. B. Tg, "Molecular Detection of Plasmodiophora brassicae,Causal Agent of Clubroot of Crucifers, in Plant and Soil," *Plant Dis.*, vol. 91, no. 1, pp. 5–12, 2007.

[128] R. Laila, A. H. K. Robin, K. Yang, G. Ja Choi, J. I. Park, and I. S. Nou, "Detection of ribosomal DNA sequence polymorphisms in the protist plasmodiophora brassicae for the identification of geographical isolates," *Int. J. Mol. Sci.*, vol. 18, no. 1, 2017.

[129] S. F. Hwang, H. U. Ahmed, Q. Zhou, S. E. Strelkov, B. D. Gossen, G. Peng, and G. D. Turnbull, "Influence of cultivar resistance and inoculum density on root hair infection of canola (Brassica napus) by Plasmodiophora brassicae," *Plant Pathol.*, vol. 60, no. 5, pp. 820–829, 2011.

[130] S. F. Hwang, S. E. Strelkov, H. U. Ahmed, V. P. Manolii, Q. Zhou, H. Fu, G. Turnbull, R. Fredua-Agyeman, and D. Feindel, "Virulence and inoculum density-dependent interactions between clubroot resistant canola (*Brassica napus*) and *Plasmodiophora brassicae*," *Plant Pathol.*, pp. 1–11, 2017.

[131] J. Greaves and J. Roboz, *Mass Spectrometry for the Novice. New York. CRC Press*. 2010.

[132] J. H. Gross, *Mass Spectrometry*. 2011.

[133] A. L. Heuberger, F. M. Robison, S. M. A. Lyons, C. D. Broeckling, and J. E. Prenni, "Evaluating plant immunity using mass spectrometry-based metabolomics workflows," *Front. Plant Sci.*, vol. 5, no. June, pp. 1–11, 2014.

[134] K. N. Yogendra, A. C. Kushalappa, F. Sarmiento, E. Rodriguez, and T. Mosquera, "Metabolomics deciphers quantitative resistance mechanisms in diploid potato clones against late blight," *Funct. Plant Biol.*, vol. 42, no. 3, pp. 284–298, 2015.

[135] D. Parker, M. Beckmann, H. Zubair, D. P. Enot, Z. Caracuel-Rios, D. P. Overy, S. Snowdon, N. J. Talbot, and J. Draper, "Metabolomic analysis reveals a common pattern of metabolic re-programming during invasion of three host plant species by Magnaporthe grisea," *Plant J.*, vol. 59, no. 5, pp. 723–737, 2009.

[136] V. Bollina, A. C. Kushalappa, T. M. Choo, Y. Dion, and S. Rioux, "Identification of metabolites related to mechanisms of resistance in barley against Fusarium graminearum, based on mass spectrometry," *Plant Mol. Biol.*, vol. 77: 355, 2011.

[137] G. Wagner, S. Charton, C. Lariagon, A. Laperche, R. Lugan, J. Hopkins, P. Frendo, A. Bouchereau, R. Delourme, A. Gravot, and M. J. Manzanares-Dauleux, "L.) Genetic Diversity in the Metabolic Response to Clubroot Infection," *Mol. Plant-Microbe Interact.*, vol. 25, no. 11, pp. 1478–1491, 2012.

[138] K. Bi, Z. He, Z. Gao, Y. Zhao, Y. Fu, J. Cheng, J. Xie, D. Jiang, and T. Chen, "Integrated omics study of lipid droplets from Plasmodiophora brassicae," *Sci. Rep.*, vol. 6, no. November, pp. 1–12, 2016.

[139] T. Sundelin, C. B. Christensen, J. Larsen, K. Møller, M. Lübeck, L. Bødker, and B. Jensen, "In planta quantification of Plasmodiophora brassicae using signature fatty acids and real-time PCR," *Plant Dis.*, vol. 94, no. 4, pp. 432–438, 2010.

[140] J. Siemens, E. Glawischnig, and J. Ludwig-Müller, "Indole Glucosinolates and Camalexin do not Influence the Development of the Clubroot Disease in Arabidopsis thaliana," *J. Phytopathol.*, vol. 156, no. 6, pp. 332–337, 2008.

[141] Séverine Lemarié, A. Robert-Seilaniantz, C. Lariagon, J. Lemoine, N. Marnet, A. Levrel, M. Jubault, M. J. Manzanares-Dauleux, and A. Gravot, "Camalexin contributes to the partial resistance of Arabidopsis thaliana to the biotrophic soilborne protist Plasmodiophora brassicae," *Front. Plant Sci.*, vol. 6, no. July, pp. 1–11, 2015.

[142] S. T. Ong, J. Z. Shan Ho, B. Ho, and J. L. Ding, "Iron-withholding strategy in innate immunity," *Immunobiology*, vol. 211, no. 4, pp. 295–314, 2006.

[143] R. C. Hider and X. Kong, "Chemistry and biology of siderophores," *Nat. Prod. Rep.*, vol. 27, no. 5, p. 637, 2010.

[144] J. F. Briat, K. Ravet, N. Arnaud, C. Duc, J. Boucherez, B. Touraine, F. Cellier, and F. Gaymard, "New insights into ferritin synthesis and function highlight a link between iron homeostasis and oxidative stress in plants," *Ann. Bot.*, vol. 105, no. 5, pp. 811–822, 2010.

[145] E. L. Walker and E. L. Connolly, "Time to pump iron: iron-deficiency-signaling mechanisms of higher plants," *Curr. Opin. Plant Biol.*, vol. 11, no. 5, pp. 530–535, 2008.

[146] M. Lou Guerinot and Y. Yi, "Iron: Nutritious, Noxious, and Not Readily Available," *Plant Physiol*, vol. 104, pp. 815–820, 1994.

[147] C. Lucena, F. J. Romera, M. J. García, E. Alcántara, and R. Pérez-Vicente, "Ethylene Participates in the Regulation of Fe Deficiency Responses in Strategy I Plants and in Rice," *Front. Plant Sci.*, vol. 6, no. November, pp. 1–16, 2015.

APPENDIX
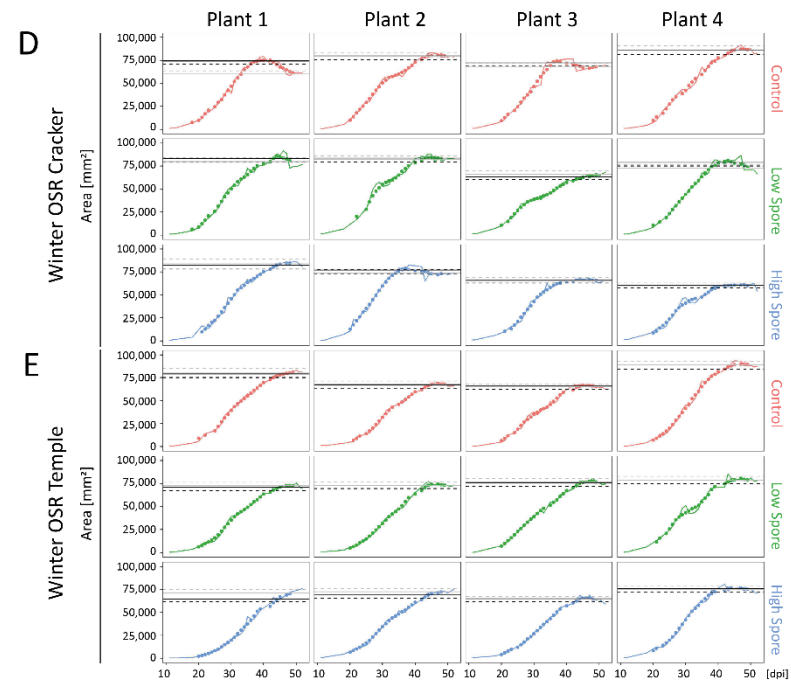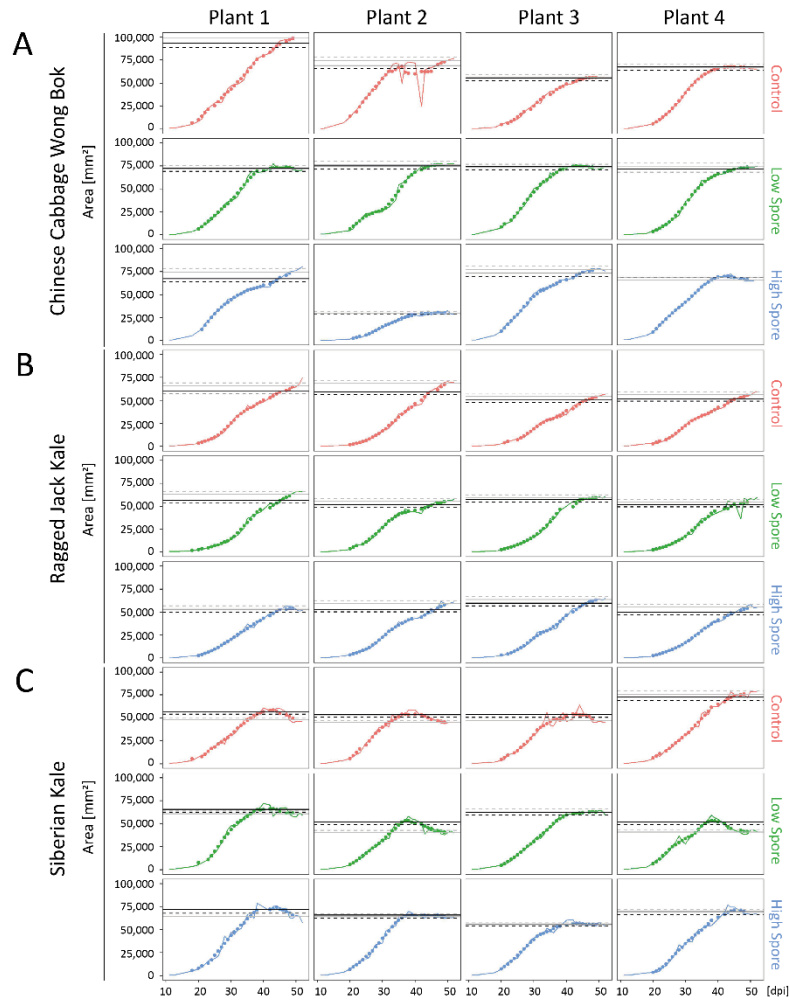
Supplementary figure 1: RAW data of plant area

|A|-|E| Area data of 5 Brassica cultivars (three treatments, 4 biological replicates per treatment) measured using RGB images. RAW data is shown as grey line, a rolling average (central 7 day window) as connected coloured dots. Mock treated cultivars (dH2O) are red, clubroot spore treated cultivars green (low concentration) and blue (high concentration). Final and maximum values are indicated as solid horizontal lines of grey and black colour, respectively. Dashed horizontal lines in black represent the area when values approached 95% of the maximum value. Dashed horizontal lines in grey highlight when plants were still growing at the end of the experiment (= final value + 5%)

|A| Area (mm²) of Chinese Cabbage Wong Bok |B| Area (mm²) of Ragged Jack Kale |C| Area (mm²) of Siberian Kale |D| Area (mm²) of Winter Oilseed Rape Cracker |E| Area (mm²) of Winter Oilseed Rape Temple.
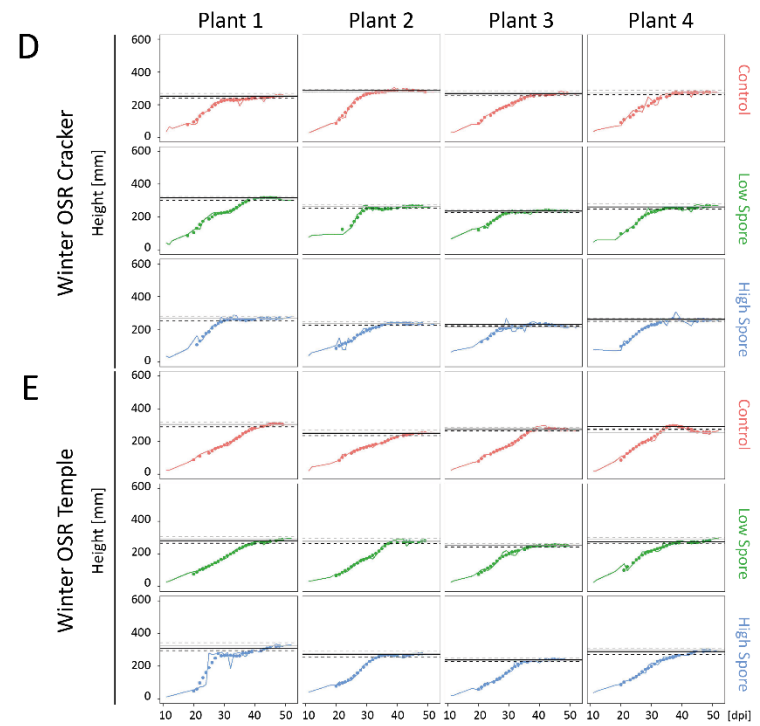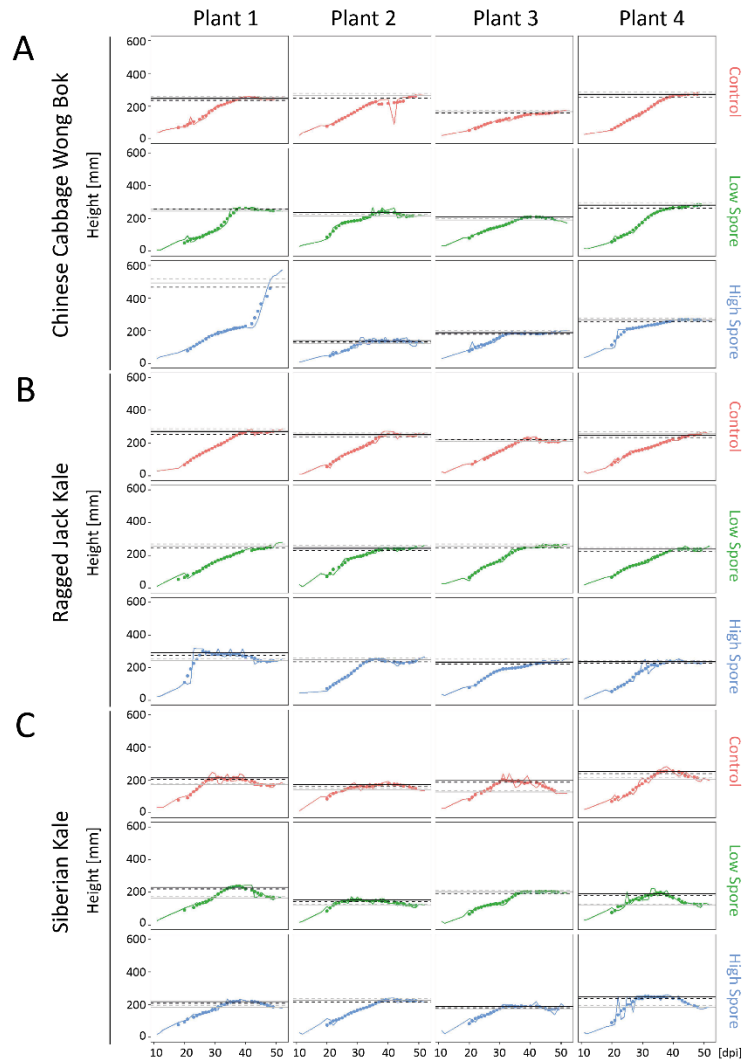
Supplementary figure 2: RAW data of plant height

|A|-|E| Height data of 5 Brassica cultivars (three treatments, 4 biological replicates per treatment) measured using RGB images. RAW data is shown as grey line, a rolling average (central 7 day window) as connected coloured dots. Mock treated cultivars (dH2O) are red, clubroot spore treated cultivars green (low concentration) and blue (high concentration). Final and maximum values are indicated as solid horizontal lines of grey and black colour, respectively. Dashed horizontal lines in black represent the height when values approached 95% of the maximum value. Dashed horizontal lines in grey highlight when plants were still growing at the end of the experiment (= final value + 5%)

|A| Height (mm) of Chinese Cabbage Wong Bok |B| Height (mm) of Ragged Jack Kale |C| Height (mm) of Siberian Kale |D| Height (mm) of Winter Oilseed Rape Cracker |E| Height (mm) of Winter Oilseed Rape Temple.

170
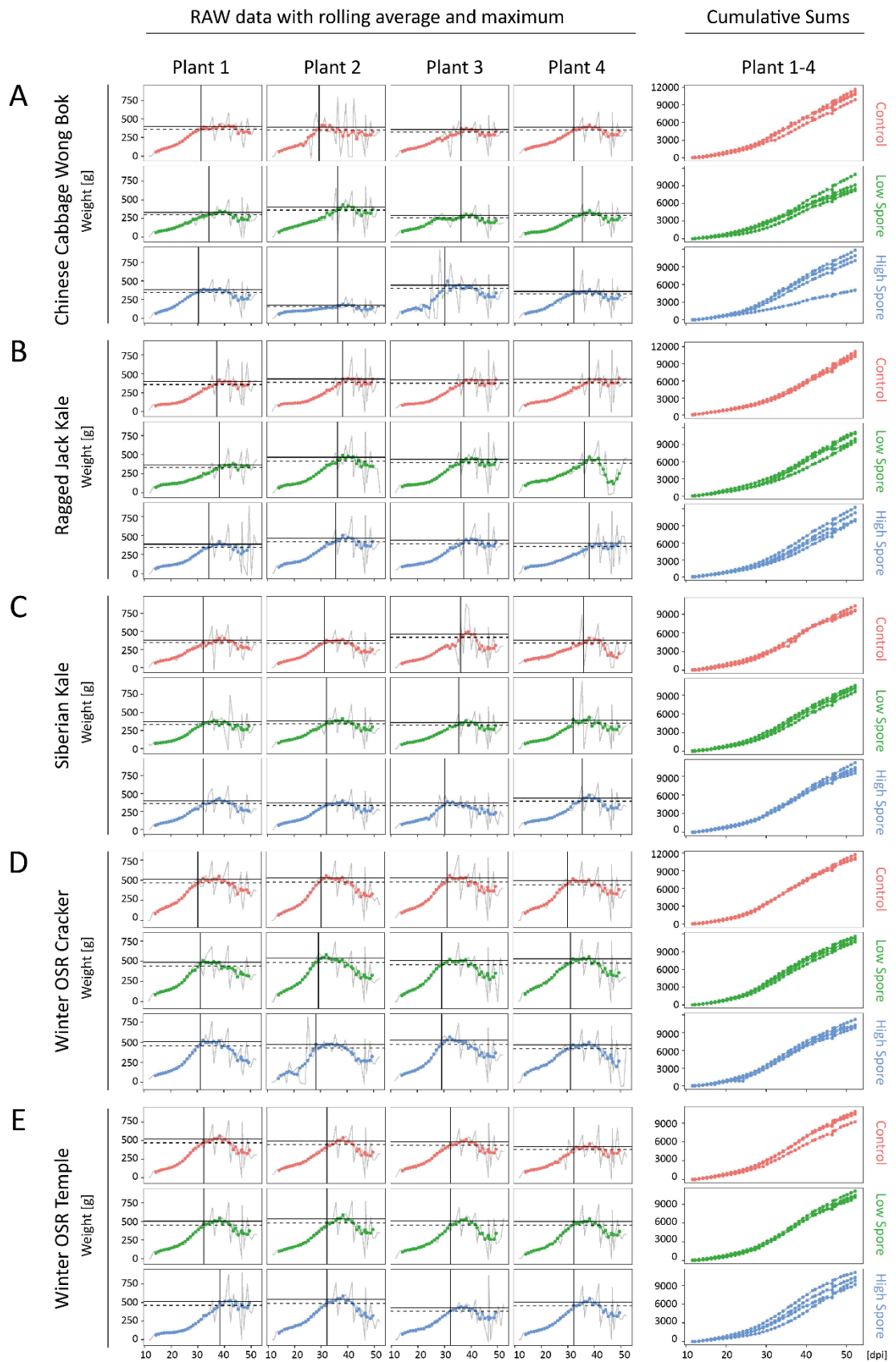
Supplementary figure 3: RAW data for water use and cumulative sums – IBERS Trial 1

[Legend on next page]

[Legend to supplementary figure 4]

|A|-|E| left panel | Water use data for 5 Brassica cultivars (3 treatments, 4 biological replicates per treatment). RAW daily water use is displayed as solid grey line. A rolling average (central 7 day window) is shown as connected dots in red (mock treated cultivars with dH_2O), green (low spore), and blue (high spore). Solid and dashed horizontal lines in black indicate maximum values and the position when values approached 90% of the maximum value, respectively. Vertical solid lines show the day when the maximum is reached

|A|-|E| right panel | Cumulative sums of 5 Brassica cultivars (3 treatments, 4 biological replicates per treatment). Same colour code applies for mock-treated and clubroot inoculated cultivars.

|A| Water use and cumulative sums (g) of Chinese Cabbage Wong Bok

|B| Water use and cumulative sums (g) of Ragged Jack Kale

|C| Water use and cumulative sums (g) of Siberian Kale

|D| Water use and cumulative sums (g) of Winter Oilseed Rape Cracker

|E| Water use and cumulative sums (g) of Winter Oilseed Rape Temple
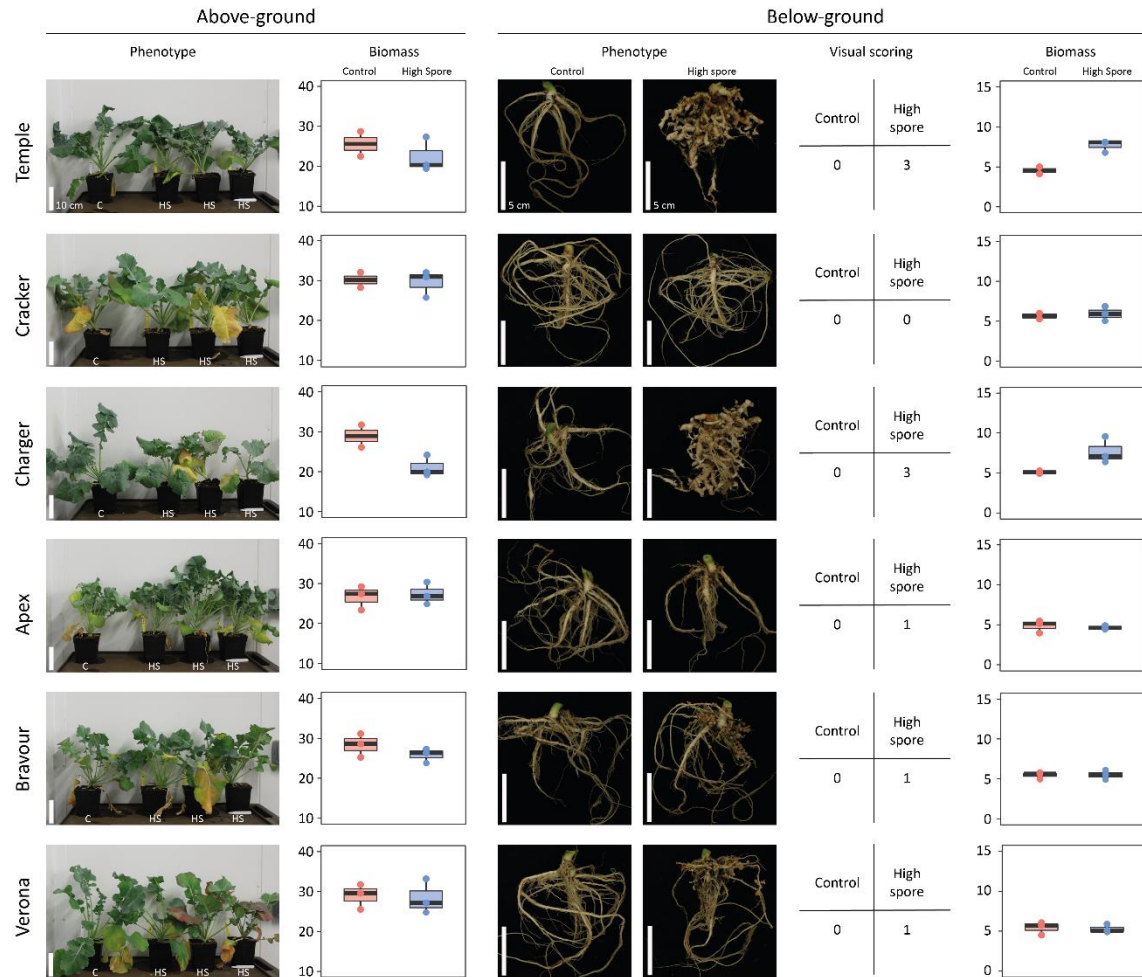
Supplementary figure 4.1: Above- and below-ground phenotypes with biomass (log10) and visual scoring results
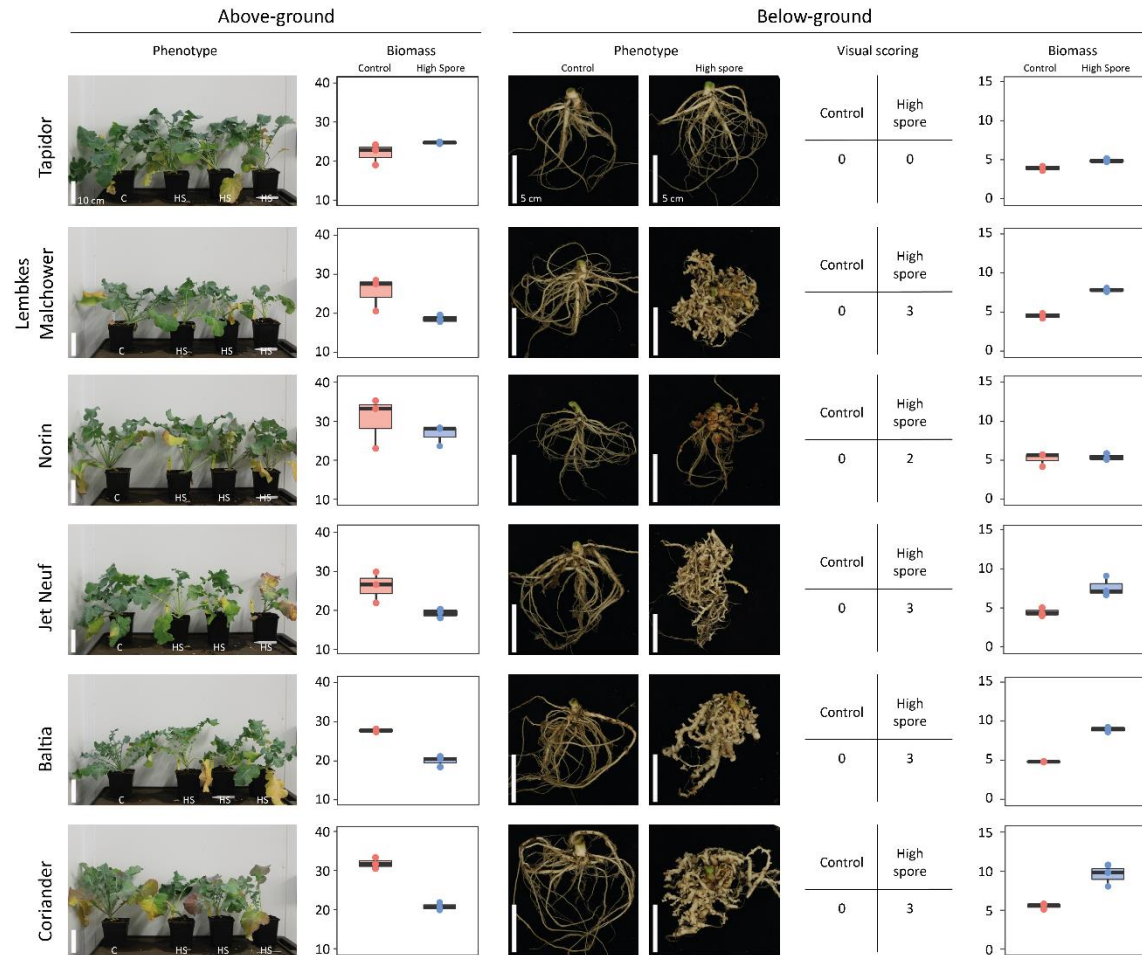
Supplementary figure 4.2: Above- and below-ground phenotypes with biomass (log10) and visual scoring results
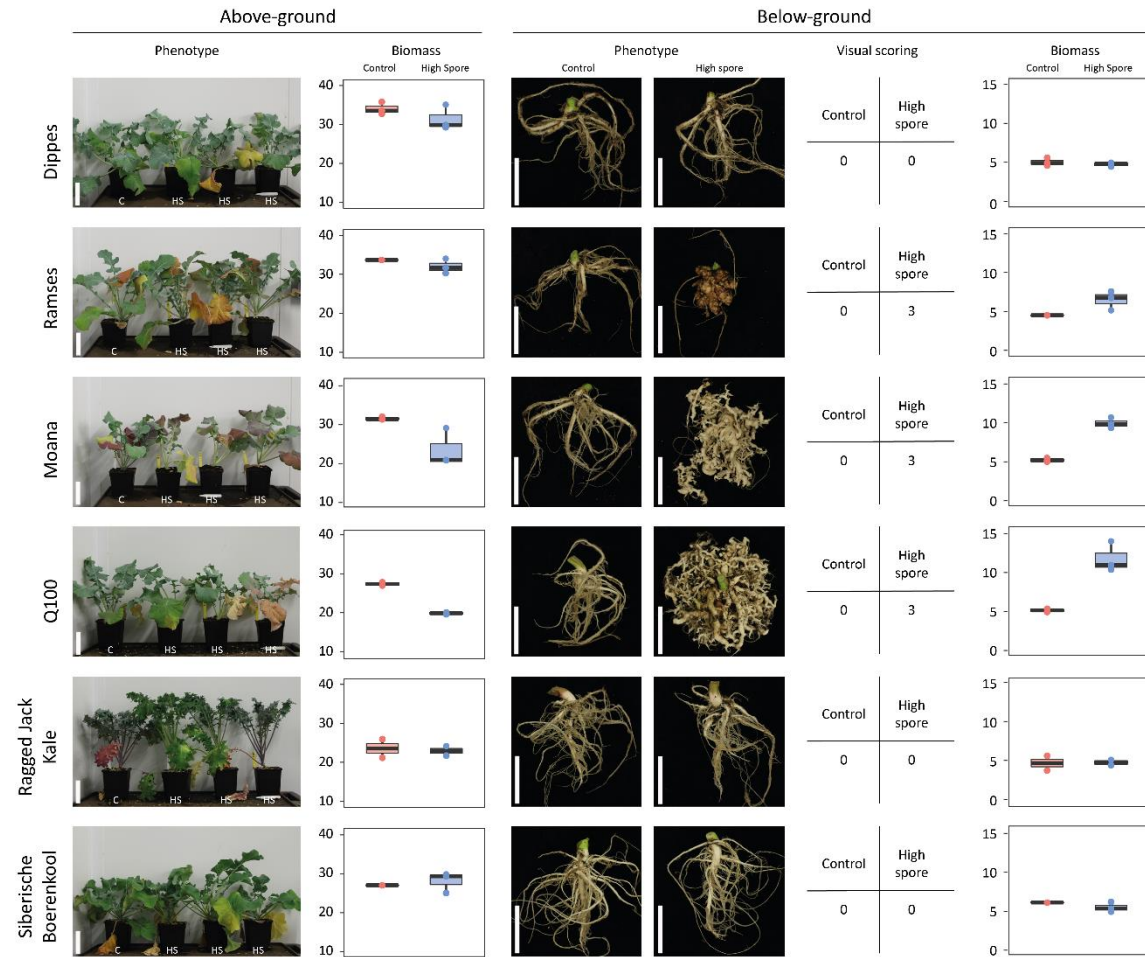
Supplementary figure 4.3: Above- and below-ground phenotypes with biomass (log10) and visual scoring results
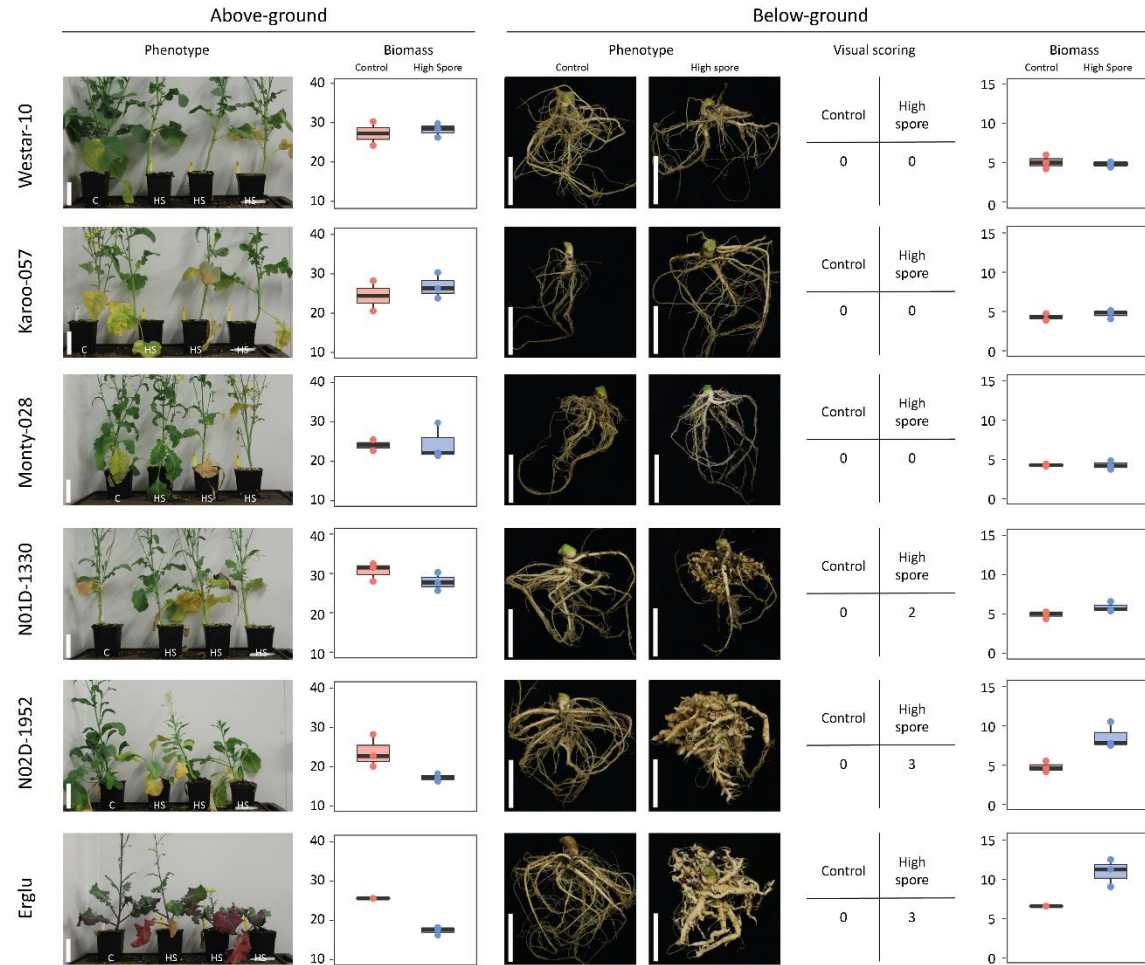
Supplementary figure 4.4: Above- and below-ground phenotypes with biomass (log10) and visual scoring results
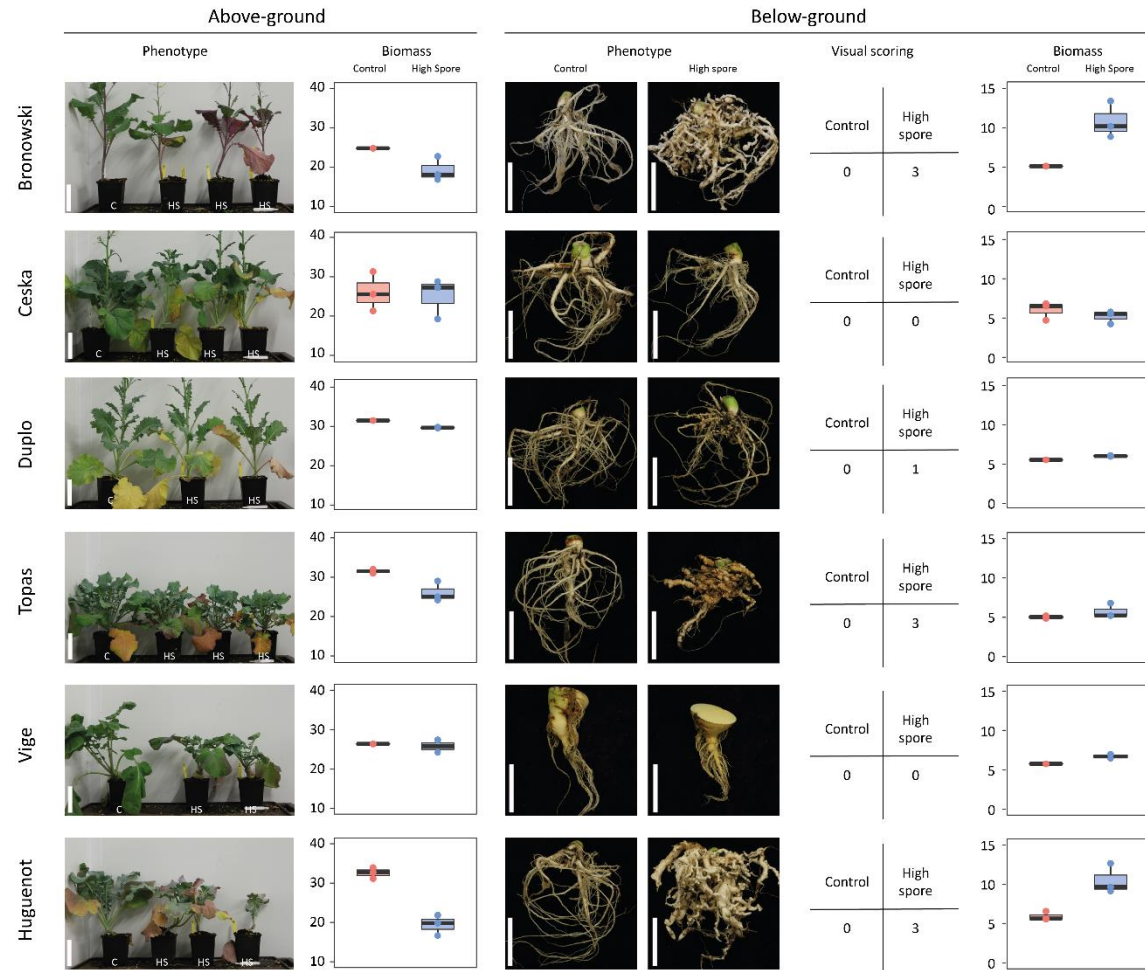
Supplementary figure 4.5: Above- and below-ground phenotypes with biomass (log10) and visual scoring results
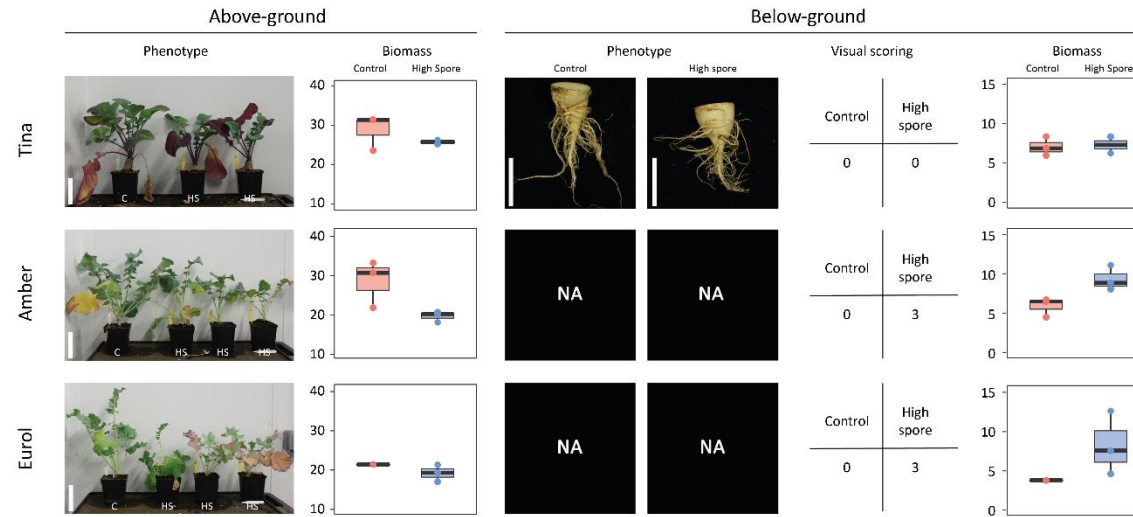
Supplementary figure 4.6: Above- and below-ground phenotypes with biomass (log10) and visual scoring results